



MONASH University
Accident Research Centre

OCCUPANT PROTECTION IN FAR-SIDE CRASHES

Editors:
Brian Fildes
Kennerly Digges

April 2010

Report No. 294

**MONASH UNIVERSITY ACCIDENT RESEARCH CENTRE
REPORT DOCUMENTATION PAGE**

Report No.	Date	ISBN	Pages
294	April 2010	0 7326 2364 2	162

Title and sub-title:

Occupant protection in far-side crashes.

Author(s):

Brian Fildes and Kennerly Digges (Editors)

Each Chapter was compiled by the representatives of the research team and authorship is acknowledged at the start of each Chapter

Sponsoring Organisation(s):

Australian Research Council (Linkage Grant), George Washington University, Virginia, USA, GM_Holden, Australia, and Autoliv Research, Sweden.

Abstract:

Side-impacts involving the far or non-struck-side occupants account for around 30% of side impact occupant Harm and there are no tests or regulations currently that address these crashes. With this in mind, the Monash University Accident Research Centre, in conjunction with a consortium of international research and automotive experts, initiated a collaborative research program to investigate a range of issues involving these crashes and injuries. The research objectives called for a more detailed understanding of far side crash environment, injuries and injury mechanisms, the development of suitable test procedures, computer models, test devices and injury criteria, evaluating the suitability of existing crash test dummies for use in this crash scenario, and to identify a range of generic far side injury countermeasures and estimate their potential safety benefits. The research program was structured into 7 Work Packages that addressed epidemiological, biomechanical, computer programs and the specification of test procedures and injury criteria. The final Work Package set out to identify a range of suitable generic countermeasures and where possible, the likely benefits of these in mitigating far side Harm. The extensive findings from this research are found in the various Chapters of the report. Overall, it shows that addressing far side occupant protection offers substantial improvements for reducing motor vehicle casualties internationally and the research findings provide the technical basis for evaluating and developing far-side countermeasures. Ultimately, minimum safety standards need to be adopted by governments and auto makers and a program of consumer information would help encourage far-side crash protection improvements.

Key Words:

Far-side impact,

Disclaimer

This report is disseminated in the interest of information exchange. The views expressed here are those of the authors, and not necessarily those of the project sponsors or other members of the research team.

Distribution:

Report available from the Monash University Accident Research Centre, Wellington Road, Clayton, Victoria, 3800, Australia. Telephone: +61 3 9905 4381, Fax: +61 3 9905 4363

Reproduction of this page is authorised

PROJECT PARTICIPANTS AND ROLES

This study was a collaborative research effort involving many international organisations and participants. The main sponsor of the work was the Australian Research Council under its Linkage scheme, with additional funds from various industry partners. The research participants and their roles are shown below.

Name	Institute	Role
Brian Fildes	MUARC, Australia	Chief Investigator
Kennerly Digges	George Washington University	Chief Investigator (Partner in Application)
Laurie Sparke	GM_Holden, Australia	Sponsor & Investigator
Stu Smith	GM_Holden, Australia	Sponsor & Investigator
Ola Bostrom	Autoliv Research	Sponsor & Investigator
Cecilia.Sunnevang	Autoliv Research	Sponsor & Investigator
Richard Morgan	George Washington University	Sponsor & Investigator
Frank Pintar	Medical College Wisconsin	Investigator
Narayan Yoganandan	Medical College Wisconsin	Investigator
Brian Stemper	Medical College Wisconsin	Investigator
Hampton Clay Gabler	Virginia Tech (Mech Eng)	Investigator
Stefan Duma	Virginia Tech (CIB)	Investigator
Joel Stitzel	Virginia Tech (CIB)	Investigator
Jeff Augenstein	William Lehman Centre	Investigator
Tom Gibson	Human Impact Engineering	Investigator
Clay Douglas	MUARC, Australia	Graduate Student
Brian Alonso	George Washington University	Graduate Student
Joseph Cuadradro	George Washington University	Graduate Student
Pradeep Mohan	George Washington University	Graduate Student
Stephen Rouhana	Ford (US)	Expert Adelta-Visor
King Yang	Wayne State University	Observer
Keith Seyer	DOTARS, Australia	Observer
Thomas Belcher	DOTARS, Australia	Observer
Craig Newland	DOTARS, Australia	Observer

ACKNOWLEDGMENTS

This study would not have been possible without the help and assistance of a large number of organisations and individuals.

Funders of the program included the Australian Research Council through a Linkage Grant in 2003, General Motors Holden in Australia, Autoliv in Sweden and the George Washington University through a settlement received from the Ford Motor Company.

In respect of the latter, these funds were provided by private partners who selected Dr Kennerly Digges and the FHWA/NHTSA National Crash Analysis Centre at the George Washington University to be an independent solicitor of, and funder for, research in motor vehicle safety, and to be one of the peer reviewers for the research projects and reports. Neither of the private parties have determined the allocation of funds or had any influence on the content of this report.

Many experienced organisations in the forefront of research into occupant protection agreed willingly to participate in the program and are listed above. We thank these organisations for their generous assistance and contribution to the research.

In addition, a number of other parties contributed equipment and advice during the course of the research. In particular, Dr. Astrid Linder (VTI Sweden), Dr. Peter Vulcan (MUARC Retired), Robert Judd (Autoliv Australia), Stephen Ridella, Dr. Peter Martin and Dr. Andrew Kemper, NHTSA USA, Suzanne Tylko, and Danius Dalmotas (Retired) Transport Canada.

We are also thankful to Dr. Melanie Franklyn for her assistance with constructing the Far Side website and assisting with helping to assemble this report.

TABLE OF CONTENTS

INTRODUCTION.....	1
1.0 Background	1
1.0.1 Definition of a far-side crash	1
1.0.2 The far-side collaborative research programme	1
1.0.3 Research Collaborators.....	2
1.0.4 Project Objectives:.....	3
1.0.5 The Research Programme.....	3
1.1 Description of Project Tasks	4
WP 1 – Injury and HARM Analysis	4
WP 2 – Biomechanical Test Programme	4
WP 3 - Soft Tissue Injury to the Neck	4
WP 4 – Dummy Development.....	4
WP 5 – Test Procedures and Injury Criteria	5
WP 6 - Computer Model Development	5
WP 7 – Far Side Countermeasures	5
1.2 Programme Responsibilities.....	5
1.3 Research Outcomes.....	6
1.3.1 Academic Outcomes.....	6
1.3.2 Government Outcomes	6
1.3.3 Commercial Outcomes	7
2 INJURY AND HARM ANALYSIS	9
2.0 Introduction.....	9
2.1 Objective	9
2.2 Approach	9
2.2.1 Data Sources	9
2.2.2 Far-side Impact Dataset	10
2.2.3 Measuring Societal Cost with Harm.....	11
2.3 Results	12
2.3.1 Comparison of Australian and US Far-side Crashes	12
2.3.2 Impact Configuration.....	20
2.3.3 Injury Sources.....	24
2.4 Conclusions.....	26
3 BIOMECHANICAL TEST PROGRAMME	28
3.0 Introduction.....	28
3.1 Methods.....	28
3.2 Results	33
3.3 Discussion.....	38
3.4 Conclusion	40

4	SOFT TISSUE INJURY TO THE NECK.....	41
4.0	Introduction.....	41
4.1	Methods.....	41
4.1.1	Method for Creating the Model.....	41
4.1.2	Initial Model Assessment.....	46
4.1.3	Kinematic Modelling Using THUMS.....	50
4.1.4	Final Model Parameters.....	50
4.2	Results.....	52
4.2.1	Initial Model Assessment.....	52
4.2.2	Kinematic Modelling Using THUMS.....	52
4.2.3	Final Model Parameters.....	54
4.3	Discussion.....	57
4.4	Conclusions.....	57
5	FAR SIDE INJURY CRITERIA.....	58
5.1	Introduction.....	58
5.2	INJURY IN FAR SIDE IMPACTS.....	58
5.2.1	Injury Priorities.....	58
5.3	Specific Injuries in Far Side Crashes.....	61
5.4	Summary.....	63
5.5	AVAILABLE DUMMIES.....	64
5.6	AVAILABLE INJURY RISK FUNCTIONS.....	65
5.6.1	Whole Body Lateral Loading of Restrained Volunteers.....	65
5.6.2	Upper Extremities.....	66
5.6.3	Head and Face.....	66
5.7	Lower Extremities.....	72
5.8	Spine.....	74
5.9	Thorax.....	75
5.10	Abdomen.....	77
5.11	Neck.....	78
5.12	Shoulder.....	79
5.13	Pelvis.....	79
5.14	PROPOSED INJURY RISK CURVES.....	80
5.14.1	Risk Curves for the Head.....	80
5.14.2	Injury Risk for the Neck.....	82
5.14.3	Risk Curves for the Upper Extremities.....	83
5.14.4	Risk Curve for the Chest.....	85
	Chest - V*C.....	86

5.15	Injury Risk Curve for the Abdomen	86
	Abdominal Compression	86
	Abdominal – V*C.....	87
5.16	Injury Risk Curve for the Pelvis	88
5.17	Limits for the Spine.....	89
5.18	Injury Risk for the Lower Extremities	90
6	CRASH SIMULATIONS & TEST CONDITIONS.....	91
6.0	Introduction.....	91
6.0.1	Chapter Organization.....	91
6.02	Results	92
6.03	Conclusions	93
6.1	Crash Test Configurations for the Far-side Environment	93
6.1.1	Introduction	93
6.1.2	FEM Model Simulations	94
6.1.3	IIHS Crash Test Deformations vs. Model Results.....	95
6.1.4	Discussion	96
6.1.5	Conclusions	96
6.2	Human Facet Model Validation and Dummy Evaluation	97
6.2.1	Introduction	97
6.2.2	Results	98
6.2.3	Conclusions	101
6.3	Effect of Sled Test Parameters on Dummy Kinematics.....	102
6.3.1	Introduction	102
6.3.2	Methods	102
6.3.3	Results	102
6.3.4	Conclusions	104
6.4	Variations of Dummies and Countermeasures.....	105
6.4.1	Introduction	105
6.4.2	Methodology.....	105
6.4.3	Discussion	106
6.4.4	Conclusions	108
6.5	Sled Test Configurations for the Far-Side Crash Environment	109
6.5.1	Introduction	109
6.5.2	Background.....	109
6.5.3	Methodology.....	110
6.5.4	Simulations	111
6.5.5	Simulation Results.....	112
6.5.6	Conclusions	113
7	COMPUTER MODEL DEVELOPMENT	114
7.0	Introduction.....	114
7.1	Tests Conducted and Results	115
7.1.1	Quasi-static far-side tests.....	115
7.1.2	Pendulum tests.....	118
7.1.3	Pelvic Offset Sled Tests.....	119
7.1.4	Full Vehicle Crash Test	120

7.1.5	Far-Side Sled Tests.....	122
7.1.6	Parameter Study	125
7.2	Discussion	127
7.3	Conclusion	130
8	COUNTERMEASURES BENEFITS ANALYSIS.....	131
8.0	Far Side Countermeasures.....	131
8.1	Countermeasure Tests	132
8.2	Injury Reduction Analysis.....	134
8.3	Conclusions.....	135
9	GENERAL DISCUSSION & COMMENTS.....	136
9.0	Introduction.....	136
9.1	Definition of the Far-side Injury Environment	137
9.2	Test Conditions and Injury Criteria	138
9.3	Occupant Kinematics and Available Dummies	139
9.4	The Biomechanical Test Program	139
9.5	Crash Tests with Both Near Side and Far Side Dummies	139
9.6	Countermeasures and Injury Reduction Analysis	140
9.7	Conclusions.....	140
10	REFERENCES.....	142
APPENDIX 1 LIST OF REPORTS CREATED DURING THIS PROJECT		150
INTRODUCTION		1
1.0	Background	1
1.0.1	Definition of a far-side crash.....	1
1.0.2	The far-side collaborative research programme	1
1.0.3	Research Collaborators.....	2
1.0.4	Project Objectives:	3
1.0.5	The Research Programme.....	3
1.1	Description of Project Tasks	4
	WP 1 – Injury and HARM Analysis	4
	WP 2 – Biomechanical Test Programme	4
	WP 3 - Soft Tissue Injury to the Neck.....	4
	WP 4 – Dummy Development.....	4
	WP 5 – Test Procedures and Injury Criteria	5

WP 6 - Computer Model Development	5
WP 7 – Far Side Countermeasures	5
1.2 Programme Responsibilities.....	5
1.3 Research Outcomes.....	6
1.3.1 Academic Outcomes.....	6
1.3.2 Government Outcomes	6
1.3.3 Commercial Outcomes	7
2 INJURY AND HARM ANALYSIS	9
2.0 Introduction.....	9
2.1 Objective	9
2.2 Approach	9
2.2.1 Data Sources	9
2.2.2 Far-side Impact Dataset	10
2.2.3 Measuring Societal Cost with Harm.....	11
2.3 Results	12
2.3.1 Comparison of Australian and US Far-side Crashes	12
2.3.2 Impact Configuration.....	20
2.3.3 Injury Sources.....	24
2.4 Conclusions.....	26
3 BIOMECHANICAL TEST PROGRAMME	28
3.0 Introduction.....	28
3.1 Methods.....	28
3.2 Results	33
3.3 Discussion.....	38
3.4 Conclusion	40
4 SOFT TISSUE INJURY TO THE NECK	41
4.0 Introduction.....	41
4.1 Methods.....	41
4.1.1 Method for Creating the Model	41
4.1.2 Initial Model Assessment	46
4.1.3 Kinematic Modelling Using THUMS	50
4.1.4 Final Model Parameters	50
4.2 Results	52
4.2.1 Initial Model Assessment	52
4.2.2 Kinematic Modelling Using THUMS	52
4.2.3 Final Model Parameters	54
4.3 Discussion.....	57

4.4	Conclusions.....	57
5	FAR SIDE INJURY CRITERIA	58
5.1	Introduction.....	58
5.2	INJURY IN FAR SIDE IMPACTS	58
5.2.1	Injury Priorities.....	58
5.3	Specific Injuries in Far Side Crashes	61
5.4	Summary.....	63
5.5	AVAILABLE DUMMIES	64
5.6	AVAILABLE INJURY RISK FUNCTIONS.....	65
5.6.1	Whole Body Lateral Loading of Restrained Volunteers	65
5.6.2	Upper Extremities.....	66
5.6.3	Head and Face	66
5.7	Lower Extremities.....	72
5.8	Spine.....	74
5.9	Thorax.....	75
5.10	Abdomen	77
5.11	Neck.....	78
5.12	Shoulder	79
5.13	Pelvis.....	79
5.14	PROPOSED INJURY RISK CURVES.....	80
5.14.1	Risk Curves for the Head.....	80
5.14.2	Injury Risk for the Neck	82
5.14.3	Risk Curves for the Upper Extremities	83
5.14.4	Risk Curve for the Chest.....	85
	Chest - $V \cdot C$	86
5.15	Injury Risk Curve for the Abdomen	86
	Abdominal Compression	86
	Abdominal – $V \cdot C$	87
5.16	Injury Risk Curve for the Pelvis	88
5.17	Limits for the Spine.....	89
5.18	Injury Risk for the Lower Extremities.....	90
6	CRASH SIMULATIONS & TEST CONDITIONS	91
6.0	Introduction.....	91
6.0.1	Chapter Organization	91
6.02	Results	92
6.03	Conclusions	93

6.1	Crash Test Configurations for the Far-side Environment	93
6.1.1	Introduction	93
6.1.2	FEM Model Simulations	94
6.1.3	IIHS Crash Test Deformations vs. Model Results	95
6.1.4	Discussion	96
6.1.5	Conclusions	96
6.2	Human Facet Model Validation and Dummy Evaluation	97
6.2.1	Introduction	97
6.2.2	Results	98
6.2.3	Conclusions	101
6.3	Effect of Sled Test Parameters on Dummy Kinematics	102
6.3.1	Introduction	102
6.3.2	Methods	102
6.3.3	Results	102
6.3.4	Conclusions	104
6.4	Variations of Dummies and Countermeasures	105
6.4.1	Introduction	105
6.4.2	Methodology.....	105
6.4.3	Discussion	106
6.4.4	Conclusions	108
6.5	Sled Test Configurations for the Far-Side Crash Environment	109
6.5.1	Introduction	109
6.5.2	Background.....	109
6.5.3	Methodology.....	110
6.5.4	Simulations	111
6.5.5	Simulation Results	112
6.5.6	Conclusions	113
7	COMPUTER MODEL DEVELOPMENT	114
7.0	Introduction.....	114
7.1	Tests Conducted and Results	115
7.1.1	Quasi-static far-side tests	115
7.1.2	Pendulum tests.....	118
7.1.3	Pelvic Offset Sled Tests.....	119
7.1.4	Full Vehicle Crash Test	120
7.1.5	Far-Side Sled Tests	122
7.1.6	Parameter Study.....	125
7.2	Discussion.....	127
7.3	Conclusion	130
8	COUNTERMEASURES BENEFITS ANALYSIS	131
8.0	Far Side Countermeasures	131
8.1	Countermeasure Tests	132
8.2	Injury Reduction Analysis.....	134
8.3	Conclusions	135

9	GENERAL DISCUSSION & COMMENTS.....	136
9.0	Introduction.....	136
9.1	Definition of the Far-side Injury Environment	137
9.2	Test Conditions and Injury Criteria	138
9.3	Occupant Kinematics and Available Dummies	139
9.4	The Biomechanical Test Program	139
9.5	Crash Tests with Both Near Side and Far Side Dummies.....	139
9.6	Countermeasures and Injury Reduction Analysis	140
9.7	Conclusions.....	140
10	REFERENCES.....	142
	APPENDIX 1 LIST OF REPORTS CREATED DURING THIS PROJECT	150

INTRODUCTION

AUTHORS: Brian Fildes and Kennerly Digges

1.0 BACKGROUND

Vehicle and road design has quite rightly placed considerable emphasis on preventing head-on crashes and injuries over recent years, given the predominance of these crashes in statistical data (Fildes et al., 1994; Thomas and Frampton 1999). Consequently, the proportion of fatal frontal crashes has fallen while the proportion of these severe side impact outcomes has increased (Figure 1.1). This is further evidenced in the numbers of these crashes where those in fatal head-on collisions in Australia have actually fallen while the number of side impact fatal crashes has remained relatively stable over that time period (Fildes, Fitzharris, Gabler and Logan 2005).

Side impacts account for approx one-third of all vehicle occupant Harm in Australia (Gibson et al., 2001a; Chipman 2004). They are a particularly severe type of crash as the vehicle structure does not allow the same degree of energy absorbing capability as that offered in a frontal crash, due to the limited structure available between the occupant and the impacting object. Hence, given a crash, the likelihood of severe intrusion into the passenger compartment increases the risk of severe injury to the occupants (Cessari et al., 1988). Frontal structure offers more opportunities to absorb crash energy by its greater structure, thereby minimizing intrusion in lower speed impacts

Side-impact regulation has focussed on protecting the near or struck-side occupant, as they make up approximately 70% of the Harm in side impact crashes. However, 30% of side impact Harm occurs to occupants seated on the far side of the vehicle in both Australia and North America (Gabler, Digges, Fildes and Sparke, 2005). Moreover, these crashes are not currently focussed on in side-impact regulations and as a consequence, there are very few countermeasures available that specifically aim to improve far side occupant protection. Understanding the mechanisms of far side impact injuries and potential countermeasures to address these is urgently required to address this neglected vehicle safety problem.

1.0.1 Definition of a far-side crash

For the purpose of this study, a far-side crash is defined as a side impact collision where the striking vehicle or object impacts on the opposite side of the vehicle to where the occupant is sitting. In Figure 1.2 for example, where there is only a driver seated on the left side of the vehicle, the far-side crash involves an impact to the right or passenger side of the vehicle.

By contrast, an occupant seated on the impacted side of the vehicle in a side impact collision is referred to as the near side occupant. The near and far-side occupants have also be referred to as the struck and non-struck side occupants in side-impact collisions. However, in this report, the near and far side nomenclature will be used.

1.0.2 The far-side collaborative research programme

The Australian Research Council encourages collaborative research efforts involving partners from universities, industries and governments to address high-risk but significant community problems through their “Linkage” research programme. This programme provides funds to universities for research in addition to those provided by industry and government partners.

Dr. Kennerly Digges of the FHWA/NHTSA National Crash Analysis Centre at the George Washington University was selected as an independent research agent in motor vehicle safety to administer funds provided by private parties and he agreed to help fund the partnership. In addition, General Motors Holden Innovation in Australia and Autoliv Research in Sweden also agreed to part fund the research effort.

Consequently, the Monash University Accident Research Centre in Melbourne, Australia was appointed as the Host organisation for a collaborative ARC Linkage research programme into far-side occupant protection, funded through these various funding sources.

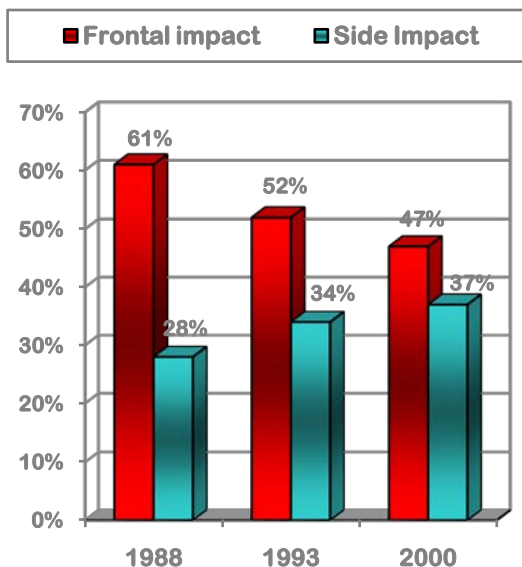


Fig 1.1. Proportion of frontal and side fatal crashes in Australia (1988 to 2000).

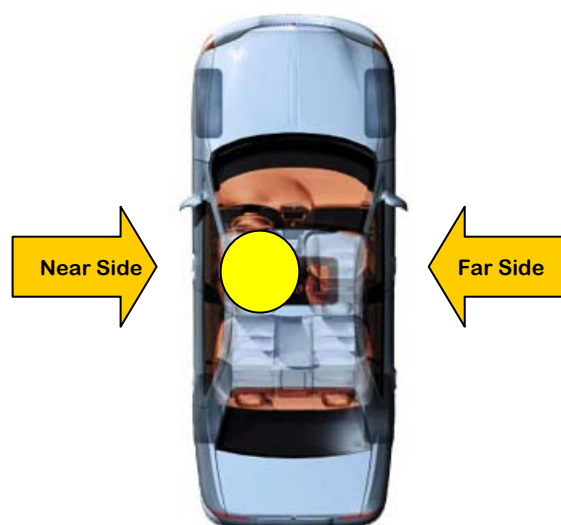


Fig 1.2 Definition of near and far-side impact for a driver on the left side of the vehicle.

1.0.3 Research Collaborators

The research team was a collaboration of 12 universities, industry and government partners across three continents with 20 individual participants as listed in Table 1.

Table 1: Participating organisations and individuals in the ARC Far-side Project.

<i>Participating Organisation</i>	<i>Participants</i>
Monash University Accident Research Centre, Australia (Host Organisation)	Brian Fildes, PhD (Chief Investigator), Clay Douglas
George Washington University, USA	Kennerly Digges PhD (Co-Chief Investigator), Richard Morgan, Brian Alonso, Joseph Cuadradro, Pradeep Mohan
General Motors Holden, Australia	Laurie Sparke, PhD, Stu Smith
Autoliv Sweden	Ola Bostrom PhD
Dept. Transport and Regional Services, Australia	Craig Newland
Medical College Wisconsin, USA	Frank Pintar PhD, Narayan Yoganandan, PhD
Va. Tech (Centre Injury Biomechanics), USA	Stefan Duma, PhD, Joel Stitzel, PhD
Virginia Tech (Mech. Eng.), USA	Hampton Clay Gabler, PhD
Human Impact Engineering, Australia	Tom Gibson, PhD
Wayne State University, USA	King Yang, PhD
William Lehman Research Centre, USA	Jeffery Augenstein, MBBS
Ford Motor Company, USA (Expert Advisor)	Stephen Rouhana, PhD

1.0.4 Project Objectives:

The ARC far-side programme nominated four objectives for the research effort:

- A more detailed understanding of far side crash environment, injuries and injury mechanisms
- Develop suitable test procedures, computer models, test devices and injury criteria
- Evaluate suitability of current side impact test dummies for far side crash configurations in comparison with PMHS
- Identify a range of generic far side injury countermeasures and estimate their potential safety benefits.

1.0.5 The Research Programme

To address the objectives, the research program nominated 8-topic areas of interest, which were assigned Work Package task descriptions, Task leaders and Task participants within the research collaborators. The seven topic areas of interest were:

WP1: A more detailed understanding of far-side injuries and Harm in real-world crashes

WP2: A more detailed laboratory biomechanical test programme using PMHS (post mortem human subjects) i.e. cadavers and Anthropomorphic Test Devices (ATDs)

WP3: Injury criteria for soft tissue neck injury

WP4: Revisit ATD (test ATD) suitability

WP5: Test procedures and injury criteria specification

WP6: Computer models for far-side occupants

WP7: Countermeasure benefits analysis

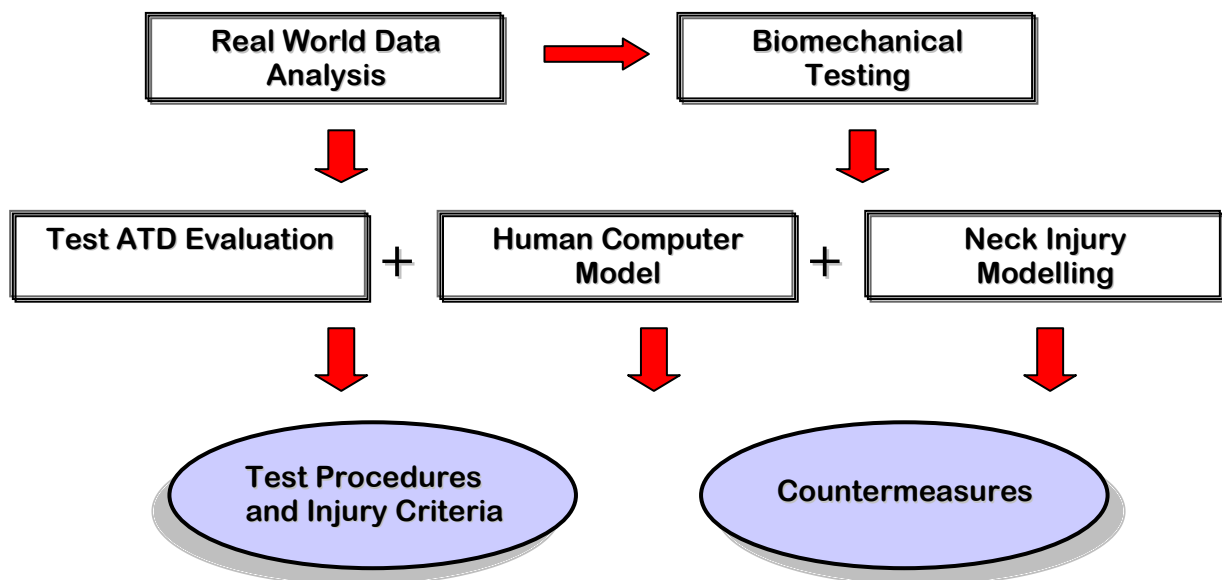


Figure 3. Diagram of task breakdown in the ARC Far-side Project.

More details of the seven Work Packages are listed below.

1.1 DESCRIPTION OF PROJECT TASKS

WP 1 – Injury and HARM Analysis

Research Team – GW and Virginia Tech. Mech. Eng. leadership (Digges & Gabler) with support from MUARC, WLIRC, MCW, GMH and Ford.

The major tasks of this Work Package were to:

- Analyse occupant injury and HARM by contacts, body region, crash direction, crash severity, intrusion extent, crash partner, occupant characteristics, injury lesions, to provide a comprehensive account of crashes and injuries;
- Conduct HARM benefits analysis of generic countermeasures, based on model and sled test results of the far-side ATD.

WP 2 – Biomechanical Test Programme

Research Team – MCW leadership (Pintar), with support from MUARC, GWU, GMH, Autoliv Research and Ford Motor Company.

The major tasks of this Work Package were to undertake:

- Pre-modelling of ATD/cadaver performance in a far-side crash (validation from existing tests)
- Design and undertake a comprehensive sled test programme using post-mortem human surrogates (PMHS) to measure kinematics and loadings for countermeasures across the range of different crash types and severities.
- Conduct tests to validate WorldSID and THOR ATD responses against cadaver kinematics and restraint loading (6 restraint combinations)

WP 3 - Soft Tissue Injury to the Neck

Research Team – Virginia Tech. CIB leadership (Duma & Stitzel), with support from MCW, Autoliv and GWU.

The major tasks of this Work Package were to:

- Conduct tests of neck soft tissue and determine constitutive properties and failure conditions
- Model carotid artery and validate
- Incorporate the carotid model into a head/neck model
- Exercise model determine injury criteria, risk functions, and propose surrogate injury measurements for use on ATD

WP 4 – Dummy Development

Research Team – MUARC Leadership (Fildes), with support from MCW, GW, Autoliv Research, DOARS and Ford Motor Company.

The major tasks of this Work Package were to:

- Identify restraint conditions from injury data and cadaver tests
- ATD selection (WorldSID and THOR)
- Conduct tests to validate ATD responses against cadaver kinematics and restraint loading (6 restraint combinations)
- Determine need for any ATD modifications
- Conduct any additional tests and simulations required for far side countermeasure evaluation

WP 5 – Test Procedures and Injury Criteria

Research Team – GWU leadership (Digges & Morgan), with support from HIE Australia and WLIRC.

The major tasks of this Work Package were to:

- Identify suitable test conditions for specifying improved far side impact protection.
- Develop acceptable injury criteria for use in far-side testing.
- Continue to evaluate the suitability of these tests and injury criteria throughout the research programme.

WP 6 - Computer Model Development

Research Team – MUARC Leadership (Fildes), with support from a new PhD Student Douglas (MUARC) funded as a Australian Postgraduate Award Industry (APAI) scholar through the research program.

The major tasks of this Work Package were to:

- Develop a model of a vehicle/HIII ATD to study intrusion, crash pulse, and kinematics in far side crashes.
- Develop & validate the model of human in a far side crash configuration.
- Use the model to examine two occupant interactions.
- Exercise the model to evaluate countermeasure performance in sled tests and car crash configurations.
- Exercise the model to predict injury reduction of generic countermeasures in real world crashes for HARM benefits analysis.

WP 7 – Far Side Countermeasures

Research Team – Autoliv leadership (Bostrom), with support from Virginia Tech MechEng., GWU, and MUARC.

The major tasks of this Work Package were to:

- Identify a range of potential beneficial far side protection strategies and countermeasures.
- Conduct a generic countermeasure test and modelling program to demonstrate likely kinematic and injury benefits.
- Conduct HARM benefits analysis of generic constraint options.

During the course of the research, it was found that reporting the results would be more concise if Tasks WP 2 and WP 4 were reported together. The results of both Tasks are summarized in Chapter 3 of this report. For reporting purposes, Task 5 was split. The Injury Criteria portion is reported in Chapter 5. The Test Procedures are reported in Chapter 6.

1.2 PROGRAMME RESPONSIBILITIES

The overall responsibility for the ARC Far-side research programme was with the Monash University Accident Research Centre (MUARC) in Melbourne, Australia. Professor Brian Fildes was responsible for the overall management and administration of the research programme, a requirement of the Australian Research Council in issuing the grant. In addition, Dr. Kennerly Digges took responsibility for the administration of the USA private funds in the programme. Both these individuals were nominated as Chief Investigators.

A number of the senior research partners agreed to take responsibility for the leadership and conduct of each of the Working Groups for which the Chief Investigators of the programme are particularly grateful. In addition, all participants were assigned to work on various tasks in the program and to be responsible for their research to the WP Leader and ultimately, the Chief Investigators¹.

The coordination and success of the program is clearly a sign of the commitment and caliber of the researchers involved in this program and an indication of what can be achieved in terms of high quality research outcomes from these collaborative research programs with appropriate structure and funding.

1.3 RESEARCH OUTCOMES

Prior to this research project there was virtually no technology base for evaluating far-side countermeasures. There were no qualified dummies, no validated computer models, no qualification test conditions or no benefits studies. This research provided the technology for all these missing attributes and removed the major impediments to the development of life saving technology to protect occupants in far-side crashes.

A number of academic and commercial outcomes have also emanated from the programme.

1.3.1 Academic Outcomes

The findings from the research have been presented at a number of important Australian and international conferences in Europe and the USA. These have included:

- Enhanced Safety of Vehicles (ESV) conferences from 2005 to 2009;
- Society of Engineers (SAE) Meetings, 2005 to 2008;
- International Research Conference On the Biomechanics of Injury (IRCOBI), 2005 to 2008;
- STAPP Car Conferences, 2008 and 2008; and
- The Association for the Advancement of Automotive Medicine (AAAM) annual conferences from 2006 to 2008.

The paper presented by Hampton Clay Gabler on behalf of his co-workers at the SAE International Congress in April 2005 was judged to be the best vehicle safety paper at the meeting. The authors (Gabler, Digges, Fildes and Sparke) were awarded the Ralph H. Isbrandt Automotive Safety Engineering Award for the most outstanding paper in the year 2005 on the subject of automotive safety engineering.

In addition, there have been 25 papers prepared and published in international journals or major conference proceedings. A listing of these is provided in Appendix 1 of this report.

1.3.2 Government Outcomes

It was noted earlier that the subject of far side occupant protection has received practically no attention in terms of new safety initiatives or regulations in side impact collisions. Yet, more than 30% of side impact Harm occurs to the far side occupant (those seated on the opposite side of the vehicle in a side impact crash). Needless to say, the governments of the USA and Australia were particularly interested in the outcomes of this research program as noted below.

The National Highway Traffic Safety Administration in the USA cooperated in providing access to test dummies (especially THOR) for the use of the consortium for comparative purposes in Task 2, Biomechanics. In addition, in 2008, they requested a briefing from the research staff at their headquarters in Washington on the results and potential regulation implications of the findings.

The Department Of Transport And Regional Services in Australia, responsible for the Australian Design Rule system, participated in the research program and made available local resources as

¹ The high degree of cooperation that was achieved throughout the full duration of the research program was especially noteworthy and tantamount to the level of professionalism and the quality of the individuals, their organisations and the outputs achieved.

required. Moreover, as a result of their involvement in this research program, they separately commissioned a series of side impact crash tests with two test dummies positioned in the front seat compartment to evaluate the effects of multiple occupants (a near and a far side occupant) in a side impact collision.

Both these two government bodies, responsible for regulating vehicle standards in the USA and Australia are presently considering the need for additional requirements to ensure that both near and far side occupants are protected in these severe types of collisions.

1.3.3 Commercial Outcomes

The inclusion of two auto makers (GMH and Ford) and a Level 1 supplier of vehicle restraints (Autoliv) was critical, both for the success of the research in providing access to world-class facilities, as well as for conducting additional tests to answer specific questions that arose during the course of the program. These industry partners collaborated effectively with the researchers, ensuring the research was of maximum value for the community at large.

There is absolutely no doubt that the results emanating from this project will be considered by the industry partners to provide improved far side impact protection and with Autoliv's involvement, new restraint mechanisms will become available to help far side occupant protection systems in future vehicles.

It should be noted that a website was established for this project. URL for the website is: <http://www.monash.edu.au/muarc/far-side>. This was to ensure that the findings from the study would be available for the use of all auto manufacturers and part suppliers to maximise the inclusion of the finding in improved crashworthiness of all future vehicles on the road.

2 INJURY AND HARM ANALYSIS

AUTHORS: H. Clay Gabler, Kennerly Digges, Brian Fildes, Michael Fitzharris and Melanie Franklyn

2.0 INTRODUCTION

To date, the primary objective of side-impact research and regulation has been to protect occupants located on the struck side of a passenger vehicle. However, occupants of the non-struck side (or the far side) of the vehicle are also at considerable risk of injury (Digges and Dalmotas, 2001). The mechanisms behind far-side impact injuries are believed to be significantly different from those in near-side impact injuries, consequently, far-side impact protection may require the development of different countermeasures than those which are currently implemented for near-side impacts.

In this report, the risk of crash injury for far-side occupants in Australia and the United States is evaluated. The study was based on the analysis of Australian data drawn from the Monash In-depth Data System (MIDS) from the Monash University Accident Research Centre (MUARC) and from US data derived from the National Automotive Sampling System Crashworthiness Data System (NASS CDS). Over 100 cases of Australian far-side struck occupants were examined from the MIDS database and over 4,500 cases of US far-side struck occupants were investigated from the NASS/CDS. For both datasets, the analysis was restricted to three-point belted occupants of passenger vehicles, light trucks and vans.

In early 2004, an international consortium of universities and crashworthiness research groups led by MUARC instigated the project herein to examine the far-side impact injury risk problem (Fildes et al., 2005). The overall goal of the research programme was to investigate far-side impact injury to occupants of passenger cars, light trucks and vans. The specific objectives of the project were to establish an improved understanding of occupant injury biomechanics in far-side impacts, to develop a test procedure for evaluating the potential of injury in a far-side impact, and to explore new countermeasure approaches for far-side impact injury prevention.

2.1 OBJECTIVE

The overall goal of this task was to determine the risk of injury from far-side impact crashes in Australia and the US. The specific objectives were to firstly, to characterise the type of impact conditions which lead to a far-side impact injuries and secondly, to determine the priorities for injury countermeasure development, subsequently assisting in the development of a far-side impact test procedure.

2.2 APPROACH

The analysis presented in this report was based on the examination of Australian data drawn from the MIDS (from 1989 to 2004 inclusive) and US data extracted from the NASS CDS (using data from 1993 to 2002 inclusive).

2.2.1 Data Sources

The MUARC MIDS is comprised of in-depth accident investigation data from four crashed vehicle studies conducted by MUARC: (1) the Crashed Vehicle File (CVF) collected from 1989 to 1993 inclusive; (2) the study conducted from 1995 to 2000 inclusive funded by FORS (now the Australian Transport Safety Bureau, ATSB) to evaluate ADR 69; (3) the Holden Crash Investigation project (data from 1993 onwards) and the current (4) Australian National Crash In-Depth Study (ANCIS), with data from 2000 to onwards being used.

The MIDS database contains weighing factors which, when applied to individual cases, permitted national estimates of traffic crash injury in Australia. The MIDS weighting system uses key crash parameters which, when used in combination, result in 4,032 possible covariate patterns, captures crash and injury characteristics. Principal variables for the weighting system are: the year of vehicle manufacture (pre/post 1990), impact direction (e.g. front, left, or right side of vehicle), seating position of the occupant, single vehicle crash or multiple vehicle crash; speed zone (categories: ≤ 60 , 80-90, 100+ km/h); head injury AIS ≥ 3 , chest or abdominal injury AIS ≥ 3 ; lower extremity injury AIS ≥ 3 , where the AIS refers to the Abbreviated Injury Scale. The severity is measured using the Abbreviated Injury Scale (AIS) 1990 (Revision 1998), which describes the relative threat-to-life of a single injury. The AIS severity levels range from 1 for a minor injury to 6 for maximal injuries, with AIS 0 meaning that there was no injury sustained.

The weighting system used relies on key crash parameters, which, when used in combination, result in 4032 possible covariate patterns. The year of manufacture was included in the crash parameters in order to capture the differences in safety features as well as vehicular structural changes which occurred after 1990. In addition, it was used as an indicator of the general age of the vehicle i.e. the Australian fleet is, on average, 10-12 years of age, hence using 1989 as a crude cut-off point was aimed at including a more uniform sample of vehicles in relation to structure and safety features. Although it would have been preferable to categorise the years further e.g. pre-1985, 1986–1990, 1990-1994, 1995-2000 and 2000 onwards, there was not enough data to make this distinction.

The expected number of crashes in each of the 4,032 covariate patterns was calculated for all fatality crashes in Australia for a three-year period (1999-2001), with Victorian crashes adjusted and multiplied to approximate and equal, respectively, the Australian serious, minor and non-injury crashes. Weights were determined by expressing expected number of occupants per covariate pattern divided by the number of matching occupants in MIDS. The analysis was conducted with and without weighting factors applied.

NASS CDS is a sample of 4,000 to 5,000 crashes investigated each year by NHTSA at up to 28 locations throughout the US. Employing a tow-away criterion, for a crash to be included in NASS CDS at least one of the vehicles involved in the crash must have been towed from the scene. Each case in NASS CDS has corresponding weights which allow national estimates of traffic crash injury outcome to be computed.

2.2.2 Far-side Impact Dataset

The following analysis focuses exclusively on occupants involved in a far-side impact, and was limited to occupants of passenger vehicles, light trucks, and vans. For this study, a side-impact crash was defined to be an impact where the general area of damage in the most harmful event was to the left or right side of the vehicle. Any rollover cases were excluded.

A far-side occupant was defined to be either an outboard occupant on the opposite side of a crash or a centrally-seated occupant. For impacts to the driver's side of the vehicle, a front seat passenger would be an example of a far-side occupant. Likewise, for impacts to the front passenger side of the vehicle, the driver would be an example of a far-side occupant. Only occupants who were restrained by a three-point safety belt were included in the study.

As shown in 2.1, the final sample of occupants in far-side impacts consisted of 108 Australian cases and 4,518 US cases. Using a definition of seriously injured occupants having their most severe injury as an AIS 3 severity level or greater, there were 10 Australian cases and 281 US cases with seriously injured occupants. Both Australian and US data files included data on a small number of fatally injured occupants which were included in the Harm calculation but not analysed separately. In addition to the unweighted number of cases, Tables 2.1 also presents weighted counts of the number of occupants in each injury severity category. The weighted numbers were developed using the

multipliers included in both MIDS and NASS to permit national estimates of injury in their corresponding countries. All analyses which follow were performed with weighed crash data.

Table 2.1. Number of Australian and US belted far-side struck occupants from MIDS (1989-2004 inclusive) and NASS CDS (1993-2002 inclusive)

Number	Australia		US	
	Unweighted	Weighted	Unweighted	Weighted
Occupants	108	5,894	4,518	2,386,633
Seriously injured occupants (AIS 3+)	10	39	281	21,982
Fatalities	1	4	80	5,185

One analytical challenge of this study was the problem of how to combine the Australian and US data. The US far-side impact dataset is numerous times larger than the corresponding Australian dataset. The approach employed in the current study was to firstly, use both Australian and US data to compare and contrast the higher level characteristics of the far-side impact problem i.e. to determine the body region priorities for injury reduction, then secondly, use the larger US dataset analyse the detailed injury mechanisms in far-side impacts.

2.2.3 Measuring Societal Cost with Harm

In this study, the Harm metric to measure the societal cost of traffic accidents. The Harm metric was first developed by Malliaris et al. (1982) as a means of balancing the number of injuries with the severity or cost of an injury. Using the Malliaris Harm metric, each AIS level has a prescribed social cost. This societal cost includes both medical costs and indirect costs such as loss of wages. For each injured person, the Harm is the social cost which corresponds to their maximum AIS injury level.

This original Harm metric was a remarkable new method of injury assessment but had two weaknesses. Firstly, societal cost is not a function exclusively of AIS level, as the societal cost of injury varies by body region as well as by injury severity. For example, an AIS 3 head injury has a higher societal cost than an AIS 3 arm injury. Secondly, in the original Harm metric, a cost was assigned to the injury of highest severity only. This approach can underestimate the total societal cost when considering an individual who sustains multiple injuries, as multiple injuries generally increase a patient's threat-to-life.

Fildes et al. (1994) developed an improved Harm metric which addressed the two limitations in the original measure. In the revised method, a societal cost is assigned to each injury, then these costs are summed to estimate a total societal cost of injury:

$$Harm = \sum_{i=1}^{NumInjuries} Cost_i(bodyregion, AIS)$$

where $Cost_i$, which is a function of the AIS injury severity and the body region injured, is the societal cost of an injury, and i , as defined by Fildes et al. (1994), was used as a measure of societal cost. The cost component not only includes treatment and rehabilitation costs, but also all other costs to society such as loss of wages and productivity, medical and emergency service infrastructure costs, legal and insurance costs, legal and insurance charges, family and associated losses and allowances for pain and suffering.

In the current study, a variation of the Fildes method for computation of Harm was employed. Although in some cases, there may be multiple injuries to a single body region, the maximum injury severity to a single body region was used when assigning costs, as costs are typically assigned to treat a single body region, not individual injuries to that body region. The number of seriously injured persons (AIS 3 or greater) and the Malliaris Harm Metric will also be presented in this study. The costs used for the Fildes Harm metric were normalised to cost of a fatality and are presented in Table 2.2.

As another measure of injury outcome, the number of serious injuries was also computed in the analysis. Like the Harm metric, the use of serious injuries as a metric avoids the biases associated with the use of fatality or total injury counts. Both Harm and number of serious injuries are frequently set as targets for reduction through countermeasure development.

Table 2.2. Average cost per injury (normalised to the cost of a fatal injury).

Body Region	INJURY SEVERITY					Maximum AIS = 6	Unknown
	Minor AIS = 1	Moderate AIS = 2	Serious AIS = 3	Severe AIS = 4	Critical AIS = 5		
External	0.0045	0.0250	0.0698	0.1135	0.1646	1.0000	0.0045
Head	0.0063	0.0295	0.1213	0.2896	0.9888	1.0000	0.0045
Face	0.0063	0.0295	0.1213	0.1601	0.3288	1.0000	0.0045
Neck	0.0063	0.0295	0.1213	0.1601	0.3288	1.0000	0.0045
Chest	0.0045	0.0250	0.0698	0.1135	0.1646	1.0000	0.0045
Abdomen	0.0045	0.0250	0.0698	0.1135	0.1646	1.0000	0.0045
Pelvis	0.0045	0.0250	0.0698	0.1135	0.1646	1.0000	0.0045
Spine	0.0045	0.0250	0.1631	1.4054	1.6804	1.0000	0.0045
Upper extremity	0.0063	0.0433	0.1026	N/A	N/A	N/A	0.0045
Lower extremity	0.0045	0.0433	0.1303	0.1926	0.3288	N/A	0.0045

2.3 RESULTS

2.3.1 Comparison of Australian and US Far-side Crashes

Although the traffic safety environment in Australia and the US share some common vehicle types and similar safety regulations, they also differ in several important aspects. These differences relate to the overall fleet composition, the driver's seating position, and the rural-to-urban driving mix, all of which may have an influence on the priorities for countermeasure development. The initial step in the analysis was to compare and contrast the risk of far-side impact injuries in Australia and the US.

Figure 2.1 and 2.2 present the relative injury risk in side impacts for Australia and the US respectively. According to the MIDS database, the percentages of near-side to far-side occupants involved in crashes were 60% and 40% respectively (Figure 2.1). On the other hand, in the US, the NASS CDS data showed that there was approximately equal probability that a side-impact occupant was on the either side of the vehicle, as the percentages for near-side and far-side impacts were similar (Figure 2.2).

Despite the fact that in Australia, there were more occupants involved in near-side crashes than in the US, the percentage of occupants with serious injuries and the Harm were similar for both countries. It was apparent that a near-side impact carries a significantly higher injury risk than a far-side impact,

with near-side crashes accounting for approximately 80% of the serious injuries, while far-side impacts were only responsible for about 20% of these injuries. Similarly, near-side impacts resulted in about three-quarters of all Harm, while the remaining quarter could be attributed to far-side impacts.

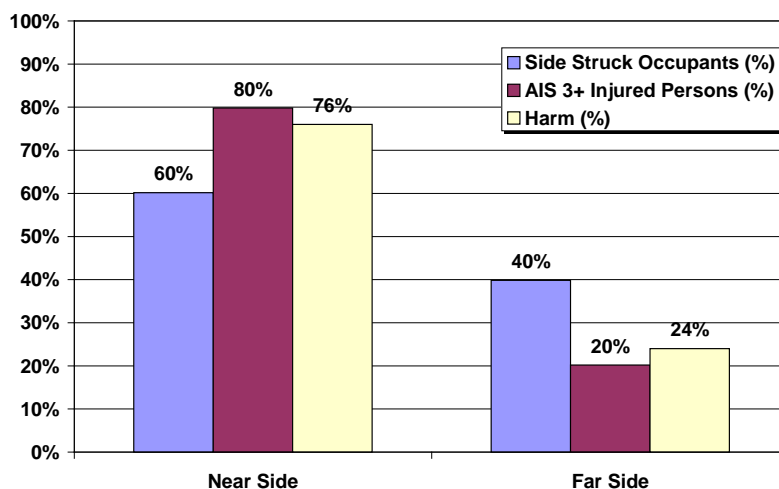


Figure 2.1. Distribution of Australian near-side versus far-side impact injuries for 3-point belted occupants.

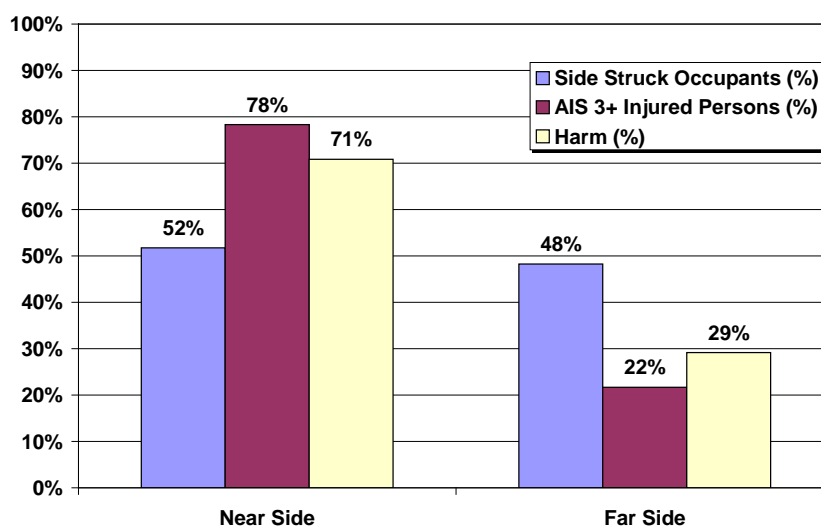


Figure 2.2. Comparison of US near-side and far-side impact injuries for 3-point belted occupants.

Excluding the chest and spine, the distribution of far-side impact injury by body region is similar in both Australia and the US (Figure 2.3). In both countries, head injuries accounted for nearly one-quarter of all Harm, and were the largest fraction of total Harm. This was followed by the upper extremities, which accounted for over 20% of all overall Harm, then the lower extremities, which accounted for approximately 18 % of all overall Harm. These findings suggest that developing countermeasures for the head, then the extremities, would result in the highest reduction of overall Harm. However, developing new countermeasures for the extremities is difficult as there is little knowledge in this area of countermeasure development. On the other hand, there has been some previous work on countermeasures for spine and chest, and as Figure 2.3 shows, these body regions also comprise a significant proportion of the total Harm. Hence, the best compromise between reducing the maximum amount of Harm and the potential for developing improved countermeasures was to focus on countermeasure development for the head, chest and spine. In total, these three body

regions comprise of approximately 45% of the overall Harm, thus countermeasures for these body regions have the capacity to reduce a considerable percentage of the total Harm.

One limitation in this data which should be highlighted is that in the MIDS database, pelvic injuries are grouped with the abdominal injuries while in NASS/CDS database, pelvic injuries are grouped with lower extremity injuries. Consequently, the percentages for these body regions may have a slight variation as a result of this grouping. Nevertheless, this will not influence the analysis which follows, since the body regions for analysis were the head, spine and chest, not the abdomen or lower extremities.

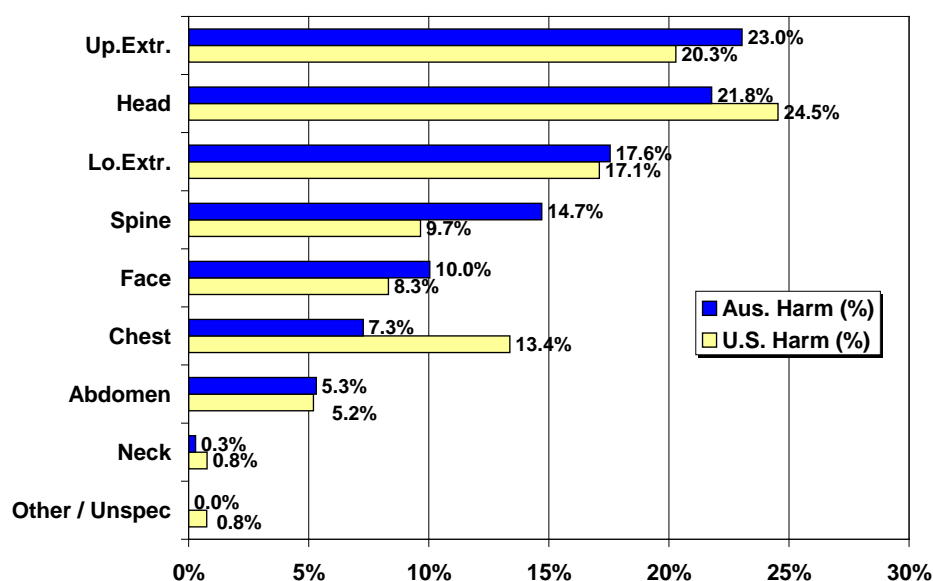


Figure 2.3. Distribution of far-side impact harm by body region: Australia versus the US.

A comparison of the distribution of US far-side serious impact injuries and Harm by body region is demonstrated in Figure 2.4 (a similar analysis using Australian data was not possible because the serious injury dataset was too small). According to the US data, the body region most likely to have sustained a serious injury was the chest (33.8%), yet it only accounted for approximately 13% of all Harm. This was followed by the head, where the likelihood of sustaining an injury was approximately 28% and its contribution to Harm was about 24%. In the extremities, the reverse situation was true than for the chest: in the lower extremities, the quantity of Harm was a significantly greater than the number of serious injuries. Thus, in the chest, a large percentage of serious injuries account for a lower proportion of all Harm, while in the extremities, it was the converse. The distribution of Harm by seating position was similar in Australia and the US.

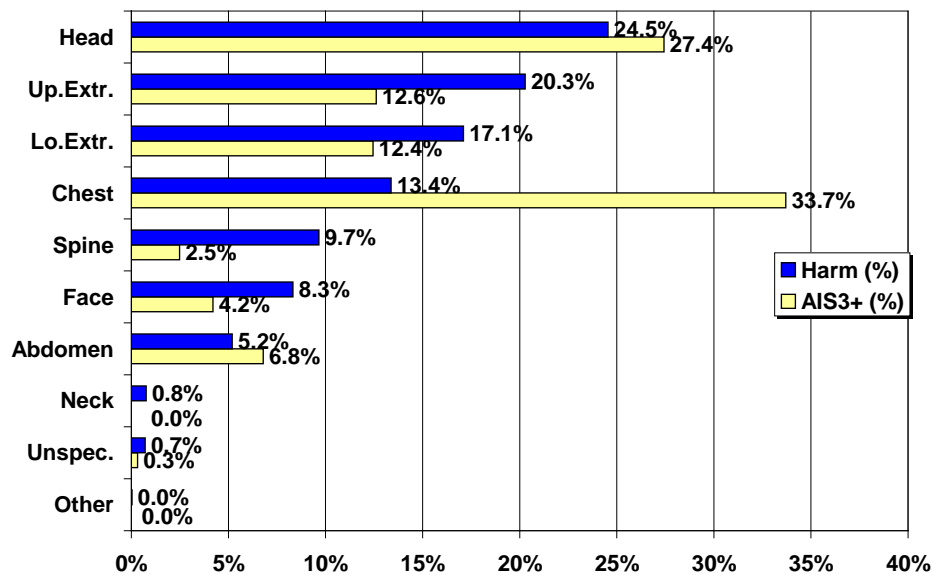


Figure 2.4. Distribution of injuries by body region using the US data.

As shown in Figures 2.5 and 2.6, in both countries, drivers comprised approximately three-quarters of the far-side struck occupants and marginally over three-quarters of the total Harm. Front seat passengers accounted for approximately 20% of the far-side struck occupants and 14-20% of the Harm, while rear passengers comprised only 8% of the total far-side struck occupants and only 3-6% of the Harm. Consequently, a test procedure which targets on the front seat occupants would capture over 90% of the total Harm.

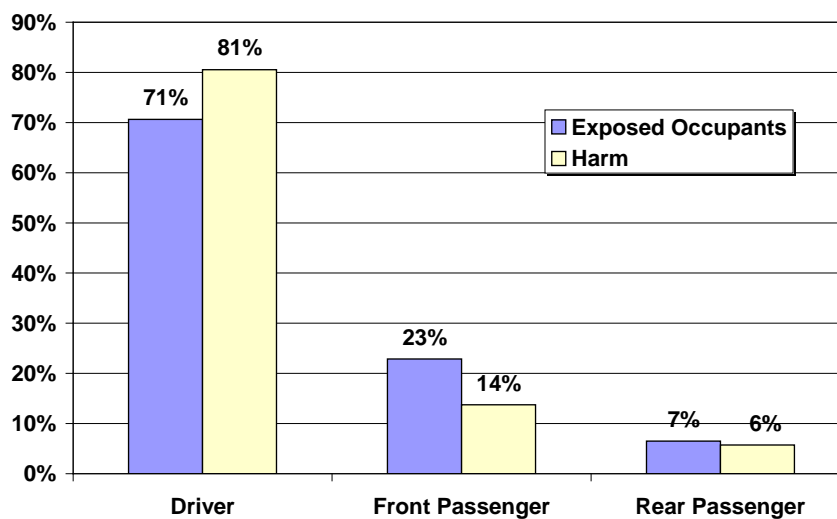


Figure 2.5. Australian far-side injuries to belted occupants by seating position.

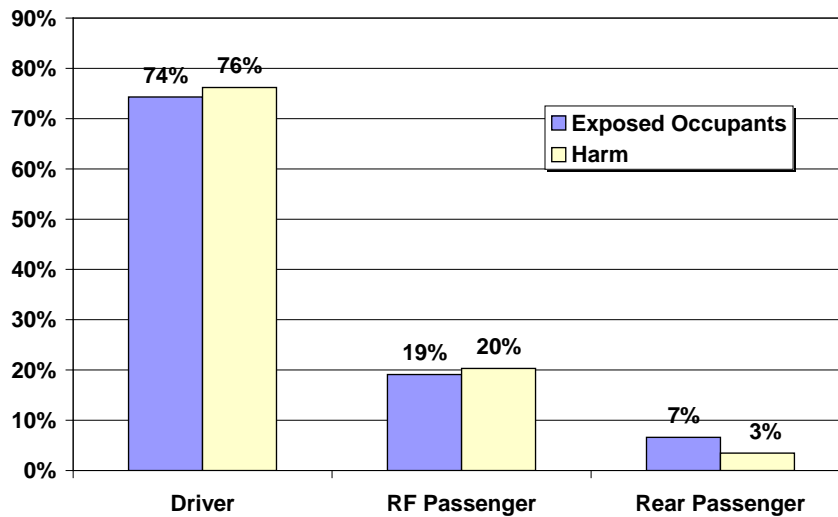


Figure 2.6. US far-side injuries to belted occupants by seating position.

There are some significant differences in the composition of the Australian and US passenger vehicle. While the Australian fleet is primarily composed on passenger cars, the US fleet is characterised by a growing segment of light trucks and vans (LTVs), where the LTV category includes pickup trucks, sport utility vehicles, vans, and minivans and is currently estimated to account for 40% of registered light vehicles and 50% of all light vehicle sales in the US.

An analysis of the fleet composition shows that the Australian dataset contained only passenger vehicle data, while the US dataset contained cases of both passenger vehicle and LTVs. Figure 2.7 presents the distribution of injuries in the US by the body type of the struck vehicle. Approximately three-quarters (86%) of the side-struck occupants in the US were in a passenger vehicle, while the remaining occupants were in a LTV. The data shows that a far-side impact is considerably more precarious for an occupant of a passenger vehicle than an occupant of a LTV: although passenger vehicle occupants comprised of 86% of side-struck occupants in the US, they also accounted for 83% of the seriously injured persons and 84% of the Harm.

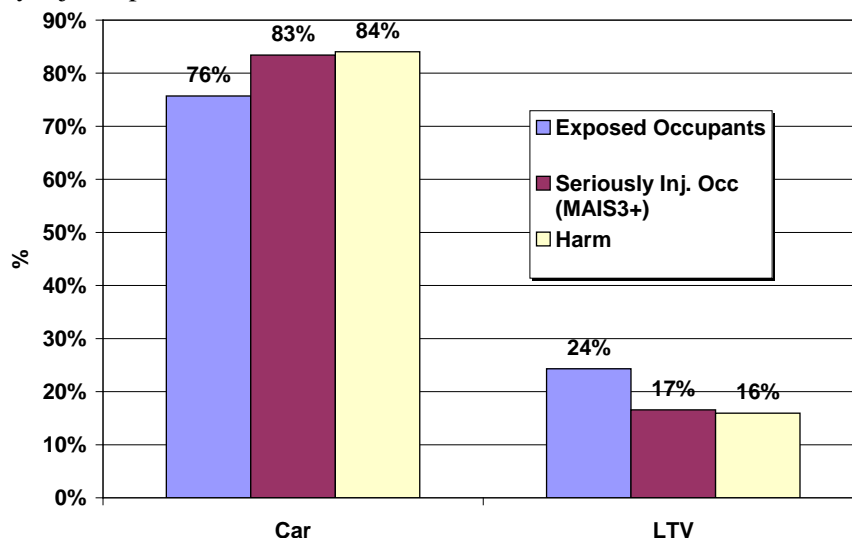


Figure 2.7. Far-side impact injuries by body type of struck vehicle (US data).

It was apparent that a substantial proportion of the far-side harm in the US is incurred by LTV occupants, thus a further examination of the data involved investigating whether passenger vehicle occupants require different injury countermeasures to occupants of LTVs (Figure 2.8). An examination of the head, chest and spine body regions shows that, although there are differences in the

Harm which can be attributed to passenger vehicles and Harm as a result of LTV's e.g. chest injuries resulted in more Harm for car occupants (14%) than for LTV occupants (10%), this difference is not great. More importantly, the distribution of Harm by body region in the amalgamated vehicle data (Figure 2.3) was similar to the distribution when separated by vehicle type (Figure 2.8). Consequently, the head, chest and spine, regardless of impacting partner, remain the focus of countermeasure development in this study.

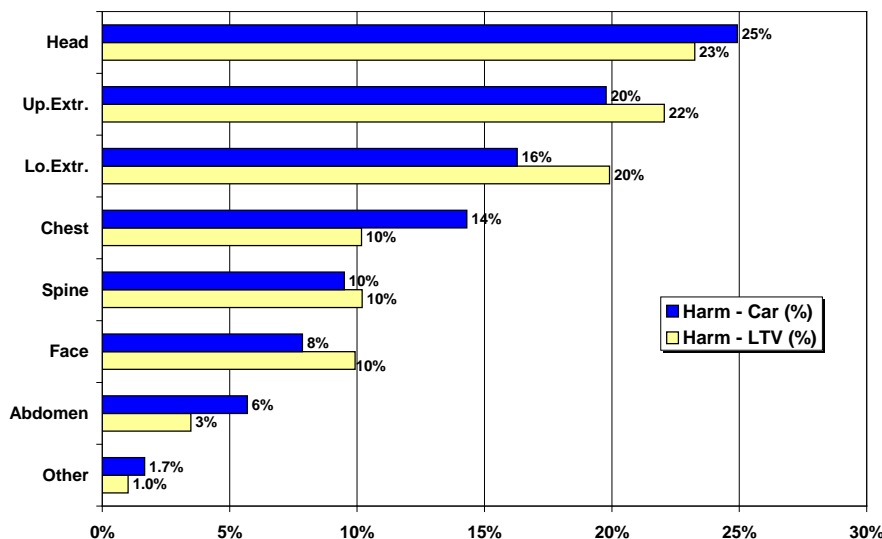


Figure 2.8. Distribution of serious injuries by type of struck vehicle type and body region injured in the US.

As shown in Figure 2.9, the serious injuries sustained by motor vehicle occupants were most likely to be chest (35%) and head (29%) injuries, followed by the upper and lower extremities (11% each) and lastly, by the remaining body regions. By contrast, serious injuries to LTV occupants were either fairly evenly distributed among the head, chest, upper extremity and lower extremity injuries, or distributed somewhat uniformly between the remaining body regions. The variations in the injury distribution by body region between passenger vehicle and LTV's suggest that the countermeasures implemented for occupants in vehicles of varying body styles may also need to differ.

The distribution of Australian and US far-side injuries by striking vehicle were next evaluated in order to determine the influence of the differences in fleet composition. However, as shown in Table 2.3, there were too few cases in the Australian data to disaggregate the data to the level of fleet composition. Nevertheless, there was enough data to show that the primary striking vehicle was either a passenger vehicle, or a derivative of a passenger vehicle (e.g. a Ute).

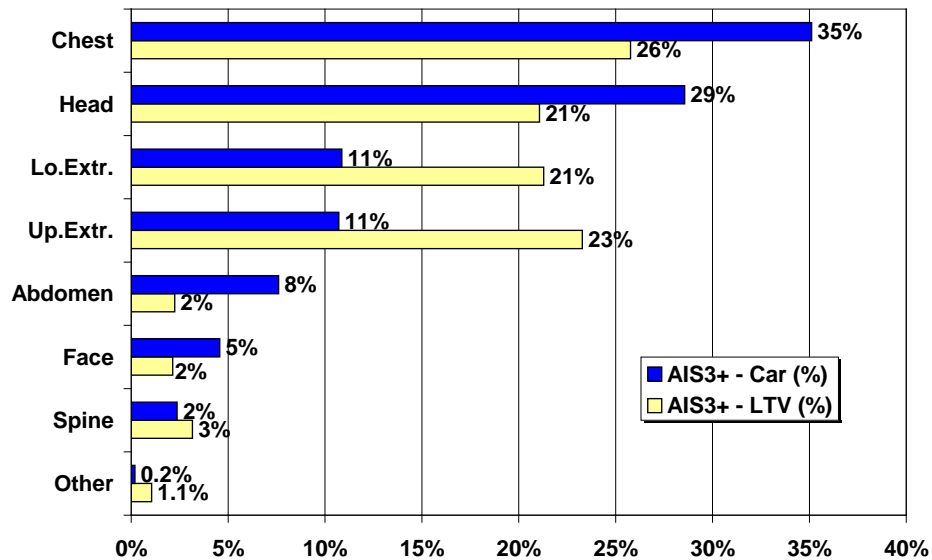


Figure 2.9. Distribution of Serious Injuries by Type of Struck Type and Body Region Injured.

Table 2.3. Distribution of Serious Injuries by Striking Vehicle Type in Australia.

Striking vehicle or object	Weighted		Unweighted	
	Occupants	AIS3+	Occupants	AIS3+
Passenger vehicle/UTE	3,892	28	63	5
4WD	264	0	5	0
Van	91	0	3	0
Heavy truck/bus	169	0	4	0
Other vehicle	1,063	0	6	0
Pole	139	2	11	2
Tree	251	9	14	3
Other object	26	0	1	0
Total	5,894	39	108	10

Figure 2.10 depicts the distribution of far-side injuries as a function of the striking vehicle type. In several previous studies, it has been shown that there are incompatibility problems between passenger vehicles and either light trucks or vans in a crash (Summers et al, 2001; Gabler and Hollowell, 1998; IIHS, 1998), particularly when the striking vehicle is an LTV and the struck vehicle is a passenger vehicle. Similar results were found in the current study (Figure 2.10): the striking object for over half of the side-struck occupants was a passenger vehicle, yet this collision partner accounted for only 31% of the Harm and 38% of the fatalities, whereas 28% of the occupants were struck by an LTV, but these collisions resulted in 35% of the Harm and 35% of the fatalities. Collisions with fixed objects, e.g. trees and poles, accounted for 16% of the side struck occupants, 19% of the fatalities and 18% of the Harm. Lastly, although rare, collisions with other vehicles (a category which includes heavy trucks, buses, and motorcycles) were especially precarious.

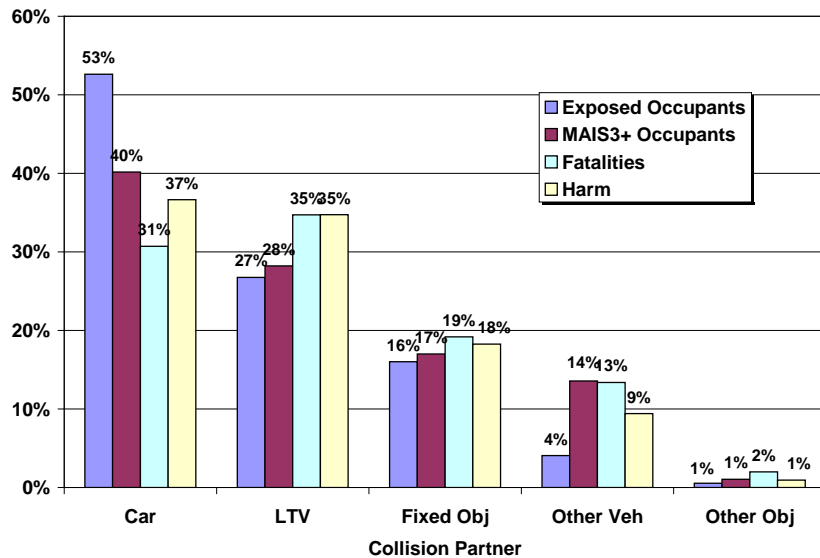


Figure 2.10. Distribution of Injuries by Striking Vehicle Type in the US.

As shown in Figure 2.11, the injury patterns to the head and chest differ by collision partner: when the collision partner was another vehicle, LTV's accounted for more Harm than passenger vehicles. The percentage of combined head and chest Harm for occupants struck by LTVs was 41%, while the percentage resulting from passenger vehicles was 33%. For occupants involved in a far-side impact with a fixed object, 45% of the Harm is a result of head and face injuries. There are several potential reasons for the greater amount of Harm from LTV's and fixed objects than from passenger vehicles: it may be due to the greater intrusion associated with LTV and fixed object collisions or simply to differences in impacting geometry between these three categories of collision partners. However, this cannot be concluded from the present data.

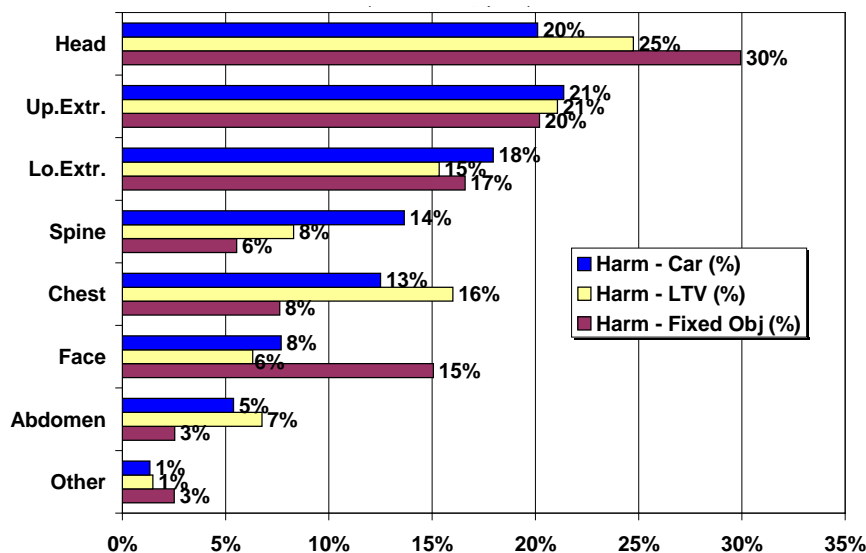


Figure 2.11. Distribution of Injuries by Striking Vehicle Type and Injured Body Region

In many instances, a crash involves not just one, but several impacts. In these cases, the crash is considered to be the most harmful event, as judged by the crash investigators. Figure 2.11 presents US data for distribution of injury by the number of events in which the side-struck vehicle was involved. Of the side-struck occupants, 62% were involved in only a single event collision, which were responsible for 52% of the seriously injured occupants and 54% of all Harm. The remaining 38% of

the side-struck occupants incurred approximately half of the serious injuries, and about half of all Harm. Thus, as might be expected, the data demonstrated that multiple collisions carry a higher risk of serious injury than do single event collisions.

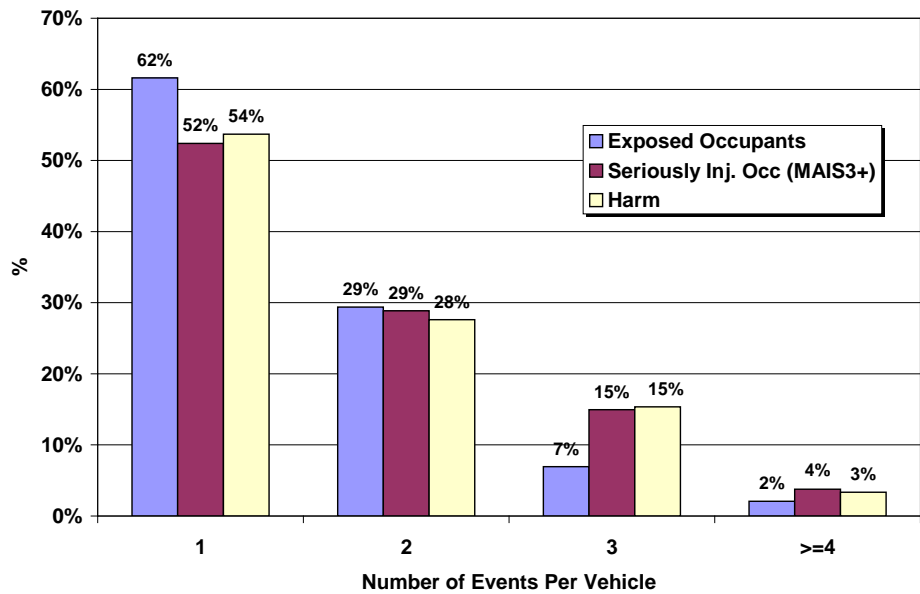


Figure 2.11. Distribution of injuries by number of events in the US.

2.3.2 Impact Configuration

Impact speed, angle, and position on the vehicle are all potential factors which may influence the injury outcome to the occupant, and hence need to be examined before a test procedure can be designed for far-side impacts. Because of the small number of Australian cases, the following analysis which follows is based exclusively on US data.

Figure 2.13 presents the distribution of far-side injuries by total delta-V of the struck vehicle. The delta-V, which is the resultant change in velocity upon impact, is comprised of both lateral and longitudinal components. The median total delta-V for all far-side struck occupants was 15 km/hr, while half of the Harm occurred for total delta-V less than or equal to 24 km/hr. The median total delta-V for occupants with a maximum AIS injury level of 3 or higher was 32 km/hr.

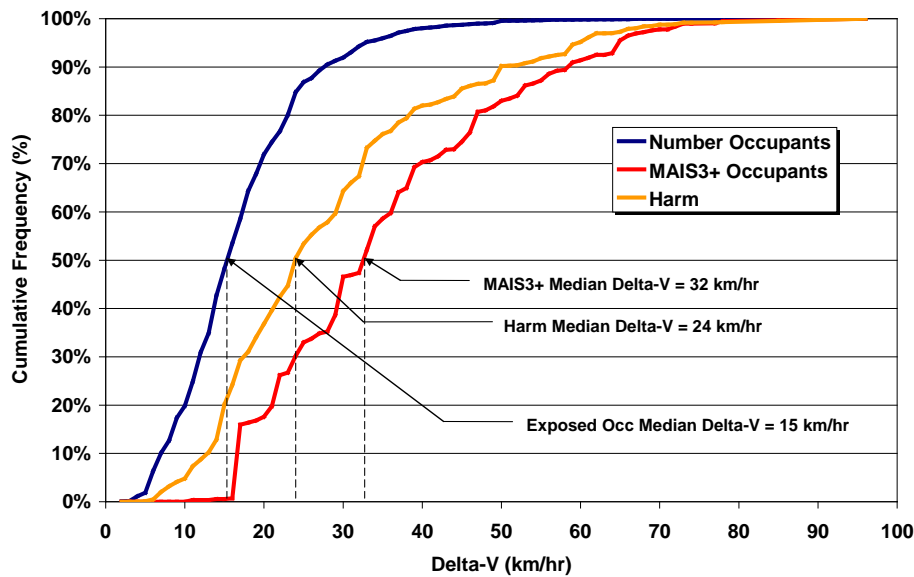


Figure 2.12. Distribution of far-side impact injuries by total delta-V.

The distribution of far-side injuries by lateral delta-V of the struck vehicle is demonstrated in Figure 2.14. The median lateral delta-V for all far-side struck occupants was 12 km/hr and half of the Harm occurred for total delta-V less than or equal to 22 km/hr. The median lateral delta-V for occupants with a maximum injury level of AIS 3 or higher was 28 km/hr.

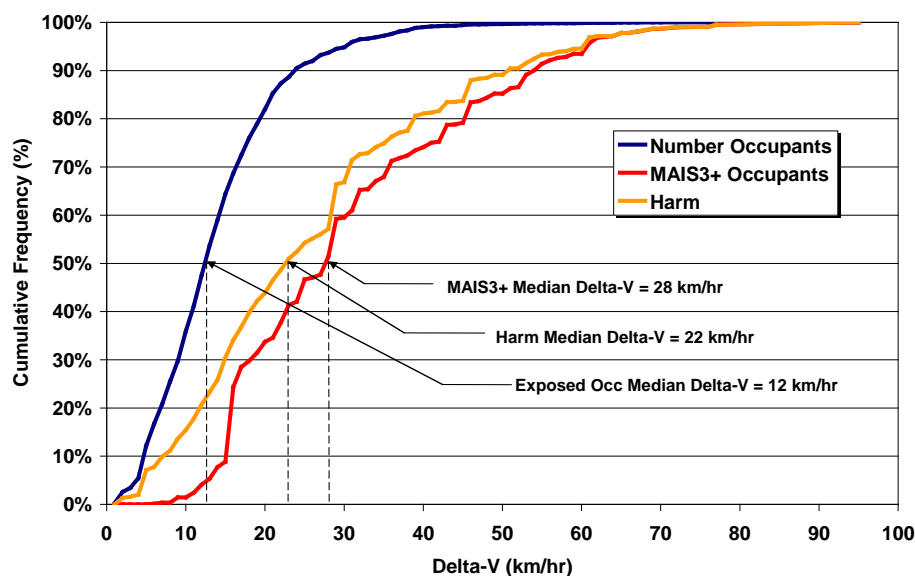


Figure 2.13. Distribution of far-side impact injuries by lateral delta-V.

For near-side struck occupants, intrusion into the occupant compartment is known to increase the severity of impact injury, but the effect of cabin intrusion on injury outcome are not as evident for far-side struck occupants as in near-side struck occupants. Using the SAE (Society of Automotive Engineers) Collision Deformation Classification (CDC) as a measure of the amount of crush, the data was analysed to find the relationship between the intrusion and the severity of injuries. As shown in Figure 2.14, the vehicle is divided into nine zones for the CDC, where the boundary between the fifth and sixth zones corresponds to the centreline of the vehicle. In Figure 2.15, the far-side intrusion is shown relative to a US front seat passenger

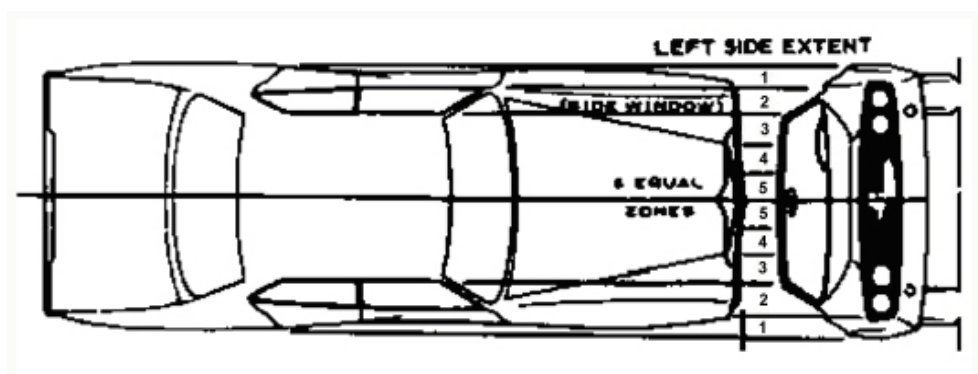


Figure 2.14. The divisions used in the CDC to specify the extent of crush.

As shown in Figure 2.5, 60% of all far-side struck occupants were exposed to crashes with a damage extent involving only the first and second zones. This figure shows that serious injuries are strongly correlated with damage extent. Almost no serious injuries were observed for damage extent limited to

the first two zones. On the other hand, 60% of the serious injuries were incurred by occupants of a vehicle with a damage extent to zones 3 or 4. However, as damage extent is also correlated with delta-V, it is unclear if the injury was a result of intrusion or simply a higher impact force.

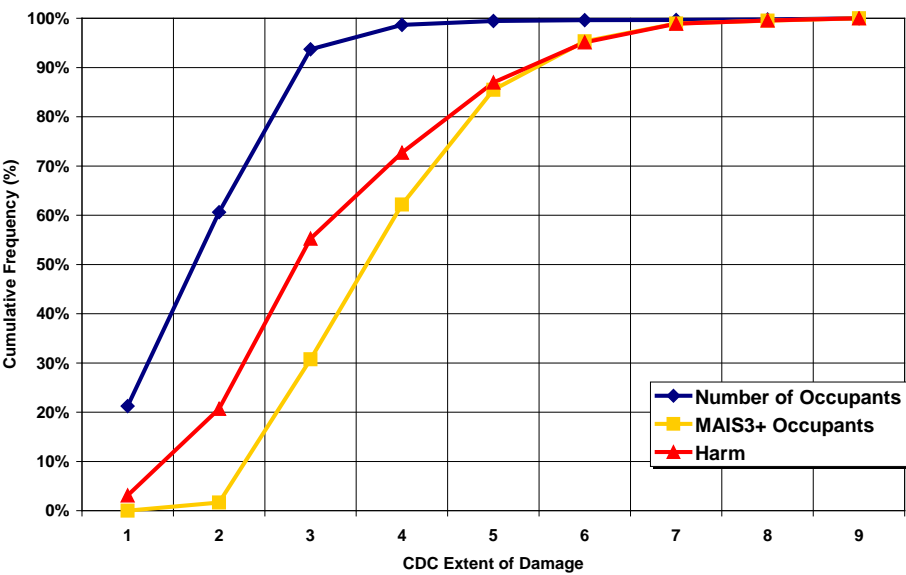


Figure 2.15. Distribution of injuries by damage extent.

Figure 2.16 presents the distribution of injuries by Principal Direction of Force (PDoF), where the PDoF is defined to be 0 degrees at the front of the vehicle, 180 degrees at the rear and 90 degrees normal to the side of the struck car (either left or right). Note that this differs to the standard definition of PDoF (where a PDoF from 0 to 180 degrees corresponds to a right side impact and a PDOF ranging from 180 to 360 degrees correspond to a left side impact). Thus for the current analysis, the PDOF for both left and right side impacts have been collapsed into a set of values ranging from 0 to 180 degrees. Hence, a direction of force perpendicular to the side of either the left or right side of the vehicle would correspond to an angle of 90 degrees, as the aim was to analyse side impacts rather than just find the PDoF.

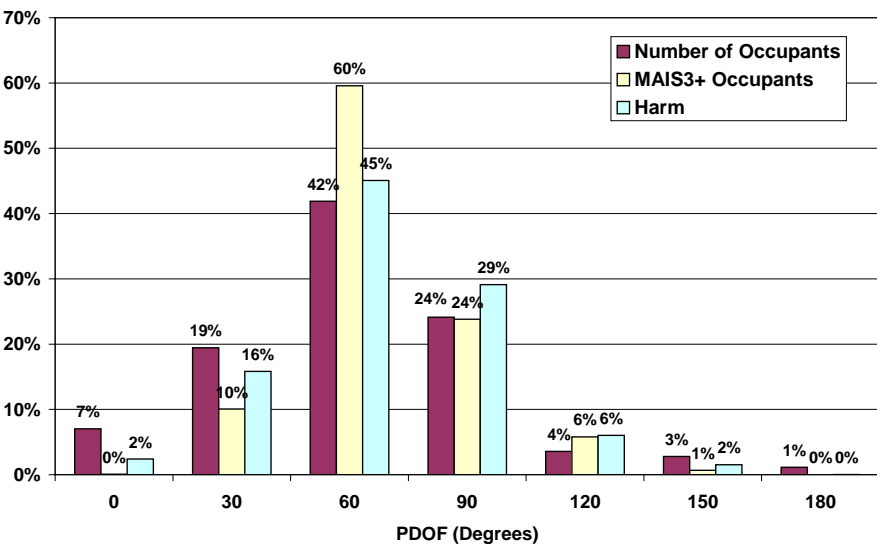


Figure 2.14. Distribution of far-side impact injuries by Principal Direction of Force.

As shown in Figure 2.15,, a principal direction of force of 60 degrees +/- 15 degrees accounted for 60% of the seriously injured occupants and 45% of the Harm. There were few injuries for either a PDoF less than 30 degrees or a PDoF which was greater than 90 degrees. Hence, the PDoF which accounted for the majority of serious injuries and the greatest percentage of Harm was 60 degrees.

The data was next analysed by impact region: these regions, which are the same as those used by NASS, were categorised according to the divisions depicted in Figure 2.18. The six regions analysed in the current study were those pertaining to the sides of the vehicle (i.e. Y, F, Z, P, D and B), four categories (Y, P, Z and D) of which the initial impact point engages the occupant compartment.

As shown in Figure 2.16, the front two-thirds of the vehicle (Y) was associated with the greatest number of crash-involved occupants (42%) in addition to the highest number of seriously injured occupants (28%) and the greatest Harm (39%). Analysis of occupants, serious injuries and Harm by impact regions involving initial impact to the vehicular cabin versus regions not involving an initial impact to the cabin revealed that although only 66% of the side-struck occupants were involved in impacts with cabin intrusion, they accounted for 86% of both the seriously injured occupants and 88% of the total Harm.

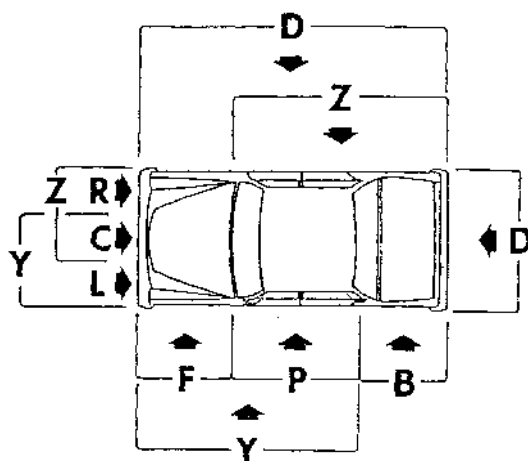


Figure 2.15. NASS impact region categories.

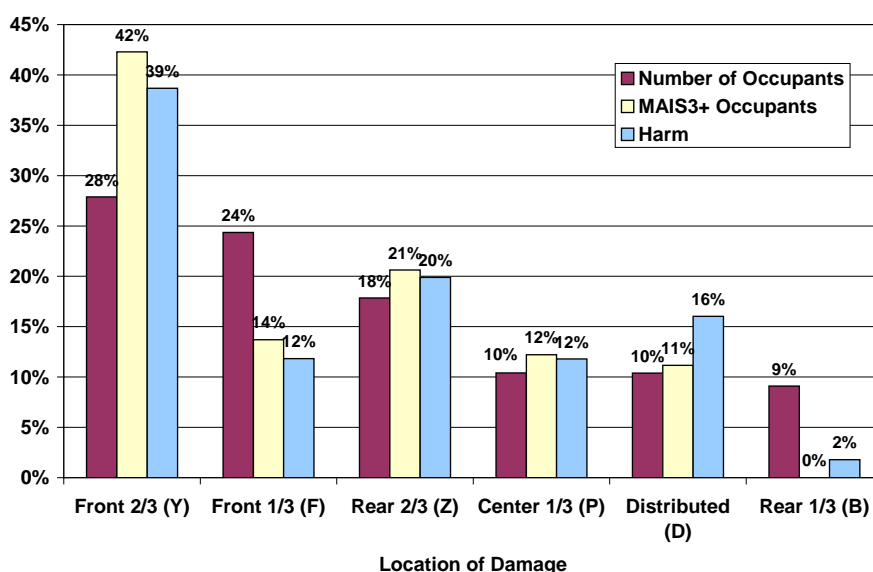


Figure 2.16. Distribution of far-side impact injuries by initial engagement point of impact.

2.3.3 Injury Sources

The following analysis involves examining the distribution of injuries by contact points. The number of serious (AIS 3+) cases from each injury source was too low for statistical analysis, hence database was expanded to include moderate injuries (AIS 2 injuries) in addition to the AIS 3+ injuries, then the Harm was calculated.

As shown in Figure 2.17, the four leading sources of head injuries were contact with the right interior, roof, centre panel, and right roof rail (note that the ‘Other’ category constitutes less than 2% of the injury contact sources). Approximately 20% of the Harm to the head was a result of contact with the right interior surfaces of the vehicle. It is possible that the head is subjected to impacts involving a large range of potential contact sources (compared to other body regions, as shown later) as the head is not restrained like other body regions such as the chest.

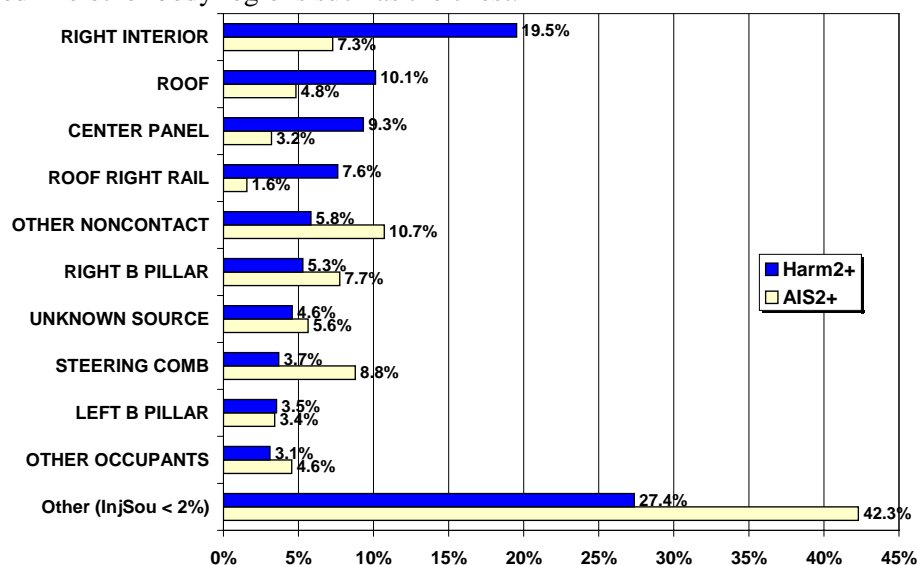


Figure 2.17. Distribution of head injuries by injury source.

Figure 2.18 shows that the four leading sources of chest injuries were contact with the seat back, the belt webbing or buckle, the right interior, and with other occupants, where almost half of the AIS 2+ injuries resulted from contact with the seat back. Analysis of videos available of high-speed side-impact crashes (results not included in this report) revealed that in a side-impact crash, the near side seat is frequently deformed out of position and into the trajectory of a far-side occupant. According to the data in Figure 2.20, injuries induced by the safety belt or buckle accounted for approximately 25% of AIS 2+ injuries. An analysis of the serious chest injuries only (i.e. AIS 3 + injuries, excluding the AIS 2 injuries in this instance) reveals that the majority occurred as a result of impacts with a PDoF of 60 degrees.

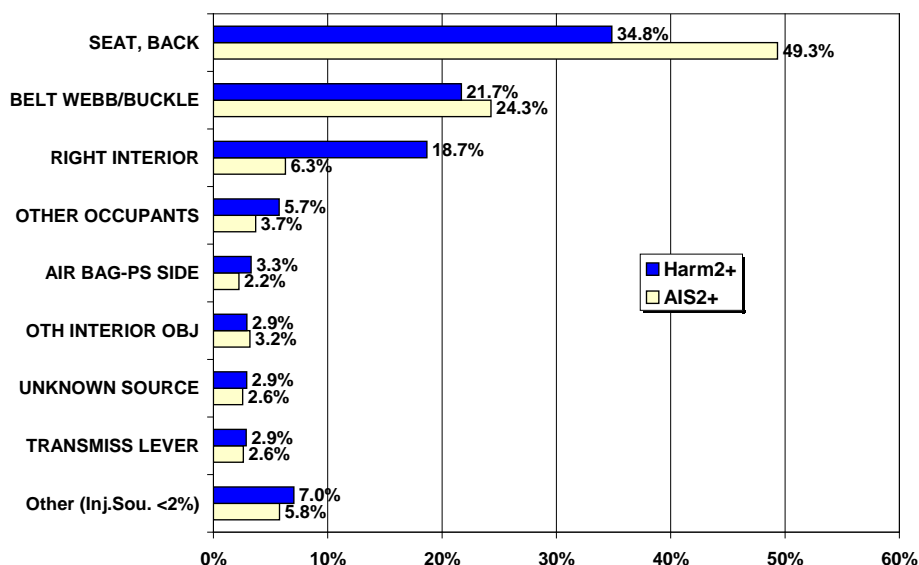


Figure 2.18. Distribution of chest injuries by injury source.

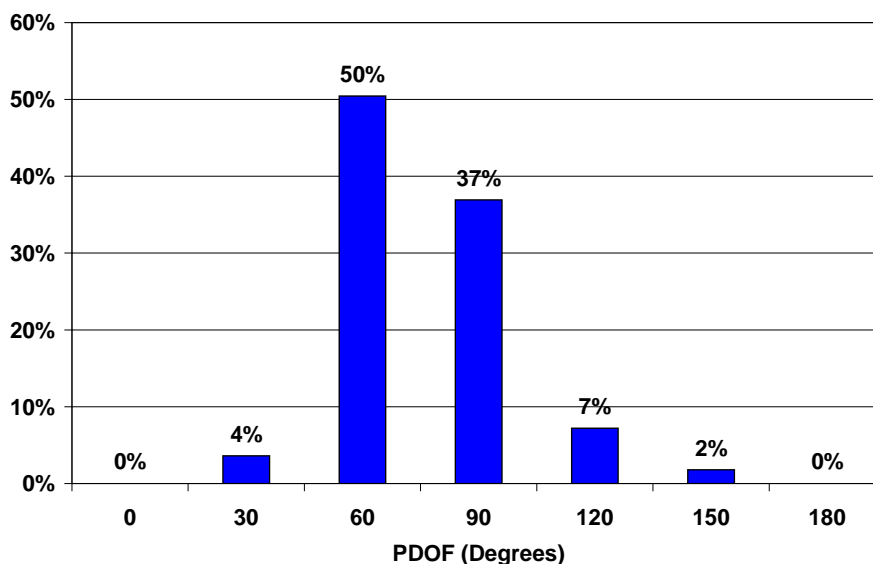


Figure 2.19. Distribution of Serious Chest Injuries (AIS 3+) by PDOF.

As shown in Figure 2.20, approximately 86% of the AIS 2+ injuries and about 83% of the Harm were the result of abdominal contact with either the safety belt or buckle. As shown in Figure 2.21, most of the serious abdominal injuries occurred at a PDOF of 90 degrees. These data suggest that current safety belt designs appear perform poorly in containing the abdomen of far-side struck occupants. Analysis of high speed video of side-impact crashes (results not shown) suggests that abdominal injuries often result from contact with the centre console. It is possible that impacts to the centre console are not always apparent to vehicle inspectors because the centre console is considerably stiffer than the abdomen. Consequently, there is often no evidence of contact in this type of scenario.

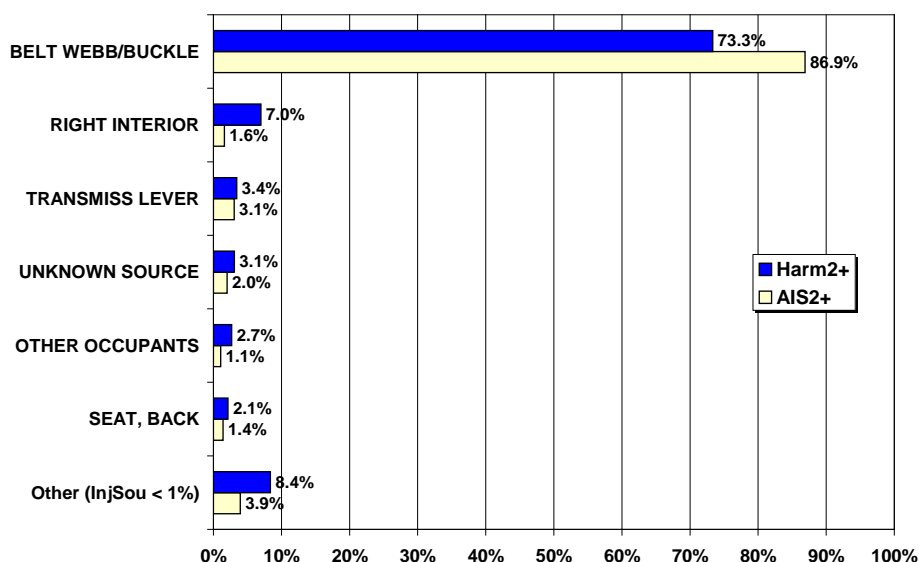


Figure 2.20. Distribution of abdominal injuries by injury source.

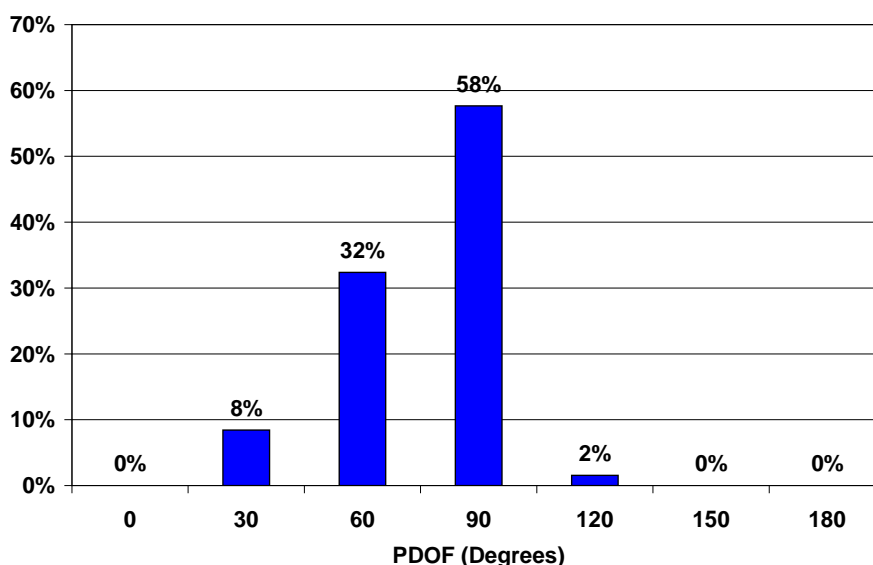


Figure 2.21. Distribution of serious abdominal injuries (AIS 3+) by PDOF.

2.4 CONCLUSIONS

In this report, the risk of injury from far-side impact crashes in Australia and the United States has been evaluated. The analysis was based upon an examination of injury outcomes of 108 occupants drawn from the Australian MIDS database, and over 4,500 occupant data extracted from the US NASS/CDS 1993-2002 crash investigations database. All cases involved three-point belt restrained occupants of passenger cars, light trucks and vans who were exposed to a far-side impact.

The goal of this study was to establish priorities for injury countermeasure development. Specific conclusions are as follows:

- Far-side struck occupants have a significant risk of injury in both Australia and the US. As a percentage of all occupants who experienced a side impact, far-side struck occupants accounted for approximately 20% of the seriously injured persons in both Australia and the US and 24-29% of the Harm.

- Injuries to the upper and lower extremities combined for approximately 40% of the far-side impact Harm in both countries. Along with the head, the extremities accounted for the largest amount of Harm.
- Developing injury countermeasures for the head, then the extremities, would result in the greatest reduction of overall Harm. However, there is limited knowledge in countermeasure development for the extremities, whereas there is previous work on countermeasure development for some other body regions. Hence, the results showed that the best compromise between reducing the maximum amount of Harm and the potential for developing improved countermeasures would be to focus on the head, chest and spine. In total, these body regions accounted for approximately 45% of the overall Harm.
- Nearly half of all AIS 2+ injuries to the chest were the result of contact with the seat back. Analysis of high-speed video footage of side-impact crashes (not included in the report) revealed that in a side impact the near side seat is frequently deformed out of position and into the trajectory of a far side occupant.
- The accident data suggest that improvement of safety belt loading should be a priority for both abdominal and chest injury reduction. Injuries induced by the safety belt or buckle accounted for approximately one-fourth of AIS 2+ chest injuries. Particularly surprising was the finding that 86% of the AIS 2+ abdominal injuries were the result of contact with either the safety belt or buckle. Future studies will investigate whether some of these abdominal injuries may be the result of undetected contact with the centre console.

To assist in the development of a far side impact test procedure, the analysis used US data to investigate the impact conditions which lead to far-side impact injury. Specific findings are as follows:

- The median lateral delta-V for occupants exposed to far side impact was 12 km/hr. The median lateral delta-V for Harm was 22 km/hr while the median lateral delta-V for serious injuries was 28 km/hr.
- A PDoF of 60 degrees was most likely to be associated with serious injury (where the PDoF was not the conventional definition, but was represented by 0 degrees at the front of the vehicle and 90 degrees for both left and right-sided perpendicular impacts). A PDoF of 60° +/- 15° was experienced by 60% of the seriously injured persons and resulted in 45% of the Harm. (It should be noted that a PDoF of 60° degrees does not translate to a test with a sled angle of 60°, as discussed in Section 6.5.)
- A vehicle or fixed object striking the occupant compartment of a subject vehicle was most likely to produce far side injuries. Impacts involving the occupant compartment accounted for 86% of the seriously injured persons and 86% of the Harm.

3 BIOMECHANICAL TEST PROGRAMME

AUTHORS: Frank Pintar and Jason Moore²

3.0 INTRODUCTION

Side-impact crashes are second only to frontal impacts in frequency. In general, the severity of injury for side impacts, however, is greater than for frontal impacts (Banglmaier et al., 2003; Frampton et al., 1998; Franklyn et al., 2002; Haland et al., 1990; Yoganandan et al., 2000). When a side impact occurs to the opposite side of an occupant's seating location, it is termed a far-side crash or a non-struck side crash. In a study using NASS/CDS data from 1993-2002, far-side impact AIS=3+ trauma was found to be 43% of the total trauma in side impacts (Gabler et al., 2005). The chest (33%), followed by the head (28%), were the most likely body regions to suffer serious injury in far-side crashes. In another study of US far-side crashes, chest and abdominal injuries tended to occur in lower severity crashes while head injuries predominated in higher severity crashes (Augenstein et al. 2000). Adding fatalities and MAIS=3+ injuries, Digges et al. (2005) attributed 42% Harm (Malliaris et al. 1982) to the head and 41% Harm to the trunk for belted far-side impact occupants and 55% head and 30% trunk Harm for unbelted far-side occupants.

A distribution of far-side crash injury by Principal Direction of Force (PDOF) was collapsed down to every clock direction; both 60 +/- 15 degrees and 90 +/- 15 degrees were prominent crash directions (Gabler et al. 2005). In a preliminary experimental investigation using a vehicle test, it was determined that a common cause for head injury is contact with the opposite side door or B-pillar (Fildes et al., 2002). Torso trauma occurs commonly to the internal organs such as the liver and spleen and has been largely attributed to belt loading (Augenstein et al., 2000; Yoganandan et al., 2000). Current belt systems were not designed for protection in far side crashes and observations from real-world crashes indicate that the occupants slipped out of the shoulder belt approximately 35% of the time (Mackay et al., 1991).

There are few countermeasures designed specifically for far-side impacts. Belt positioning and belt geometry, in addition to limiting thoracic excursion, may be techniques of enhancing the protection to far-side crash occupants. Newer belt technologies such as pre-tensioners and belt positioning systems may provide some inherent protection to far-side crash occupants if these belt systems reduce the potential for belt slip and limit head excursion.

Before specific countermeasures can be designed or tested, an appropriate Anthropomorphic Test Device (ATD) should be identified for the far side impact mode. Since there is currently no ATD specifically designed for far-side impacts, and since the biofidelity requirements for far side impact have not been established, the current investigation was conducted as a first step. The objectives of the present study, therefore, were to determine responses of Post Mortem Human Subjects (PMHS) in far-side impact configurations, with and without generic countermeasures and to compare responses with two possible candidate ATDs.

3.1 METHODS

A far-side impact buck was designed for a sled test system that included, as a standard configuration, a centre console and outboard three-point belt system. This configuration assumed a left side driver with a right side impact. The geometry and dimensions are shown in Figure 1. The buck allowed for additional options of generic (not linked to any manufacturer's product) restraints including shoulder or thorax restraint or an inboard shoulder belt. The entire buck could be mounted on the sled in either a 90-degree (3-o'clock PDOF) or a 60-degree (2-o'clock PDOF) orientation. The centre console was composed of a vertically oriented pelvis plate and a horizontally oriented centre console plate. The

² The authors recognise the valuable contributions of Narayan Yoganandan, Brian D. Stemper, Kennerly Digges, Ola Bostrom, Stephen W. Rouhana and Brian Fildes to this Chapter.

pelvis plate was designed such that the entire hip engaged the plate; the top of the plate was slightly higher than the lateral iliac crest of a 50th percentile male. The fore-aft dimension for the centre console plate was determined as the dividing point on the Hybrid-III ATD between the hip and thigh junction when the ATD sat in the seat. The lower belt anchor point was determined using the Hybrid-III 50th male ATD and positioning the lap belt such that the belt traversed a 45-degree angle from pelvis to anchor point. Upper belt anchor points were adjustable as described later. The console plate was padded with 25 mm of 208 kPa (30 psi) paper honeycomb. If either a thorax restraint plate or shoulder restraint plate was used, the padding was 25 mm of 103 kPa (15 psi) paper honeycomb. The dimensions of the shoulder or thorax plates were 100 mm in height and 460 mm in length.

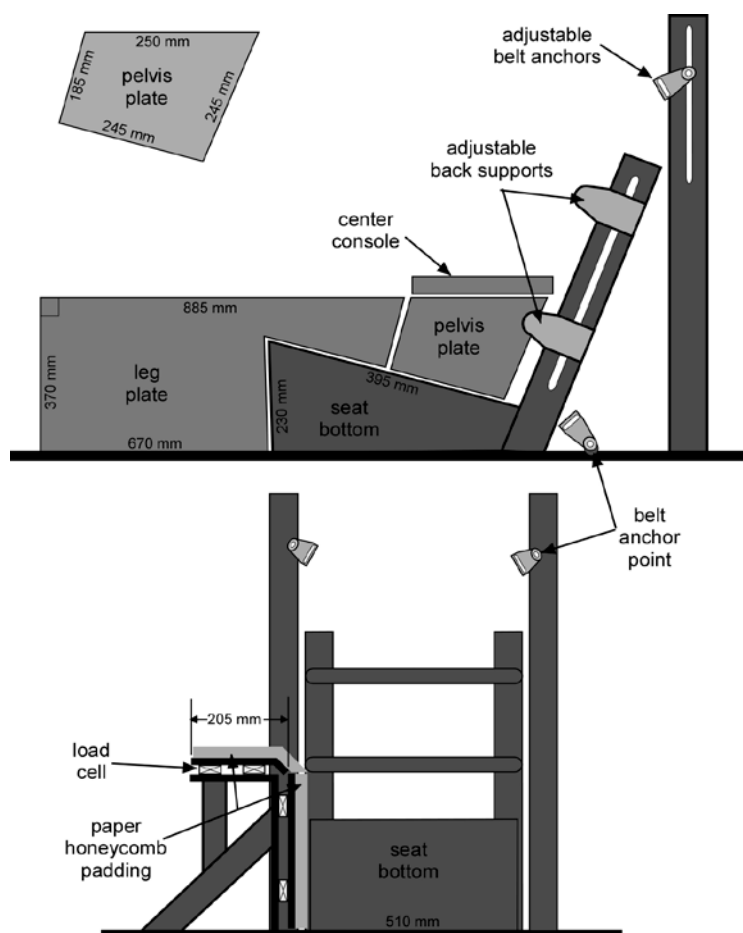


Figure 3.1. Schematic diagram, with dimensions, of far side sled buck viewed from the side (top) and from the front (bottom). The seat bottom angle with respect to horizontal was 15 degrees. Optional thorax or shoulder plates (100 mm X 460 mm not shown) were adjustable up/down/in/out.

As listed in Table 3.1, eighteen different far side test conditions were evaluated including inboard belt geometry, and shoulder or thorax restraints. Some configuration ID's are missing because these tests were part of a larger series; configurations that were not tested with a PMHS are not included. A larger WorldSID test series has been previously published (Pintar et al. 2006). To aid in the presentation of results, a figurine unique to each test configuration is presented (Figure 3.2). Each figurine depicts test velocity, test angle, if a thorax or shoulder plate was used, and position of shoulder belt (high, low, inboard, outboard) and if pre-tension was applied.

Table 3.1. Test configurations and test identifiers.

Config ID	Delta-V	Impact Angle	Plate	Shoulder belt	Belt Configuration	PMHS test (PMHS No.)	WorldSID test	THOR test
1	High	90	None	outboard	Mid, tension	HS104 (1)	WS119	TH155
2	Low	60	None	outboard	Mid	HS105 (2)	WS129	TH180
3	High	60	None	outboard	Mid	HS106 (2)	WS130	TH181
4	Low	90	Shoulder	inboard	Low	HS134 (3)	WS108	TH149
5	High	90	Shoulder	inboard	Low	HS135 (3)	WS108	TH150
6	Low	90	Thorax	inboard	Low	HS136 (3)	WS110	TH152
8	High	90	Thorax	inboard	Low	HS138 (3)	WS113	TH180
8	Low	90	None	inboard	High	HS140 (4)	WS115	TH156
9	High	90	None	inboard	High	HS141 (4)	WS118	TH188
10	Low	90	None	outboard	D-ring forward	HS138 (4)	WS132	TH184
11	High	90	None	outboard	D-ring forward	HS139 (4)	WS133	TH185
14	Low	60	None	inboard	High	HS166 (6)	WS124	TH168
15	High	60	None	inboard	High	HS168 (6)	WS126	TH169
16	High	90	Shoulder	outboard	Mid, tension	HS161 (5)	WS109	TH188
18	High	90	None	inboard	Low, tension	HS162 (5)	WS121	TH158
20	Low	60	None	outboard	Mid, tension	HS164 (6)	---	TH182
21	High	60	None	outboard	Mid, tension	HS165 (6)	---	TH183
22	High	90	None	outboard	Mid	HS163 (5)	---	TH186

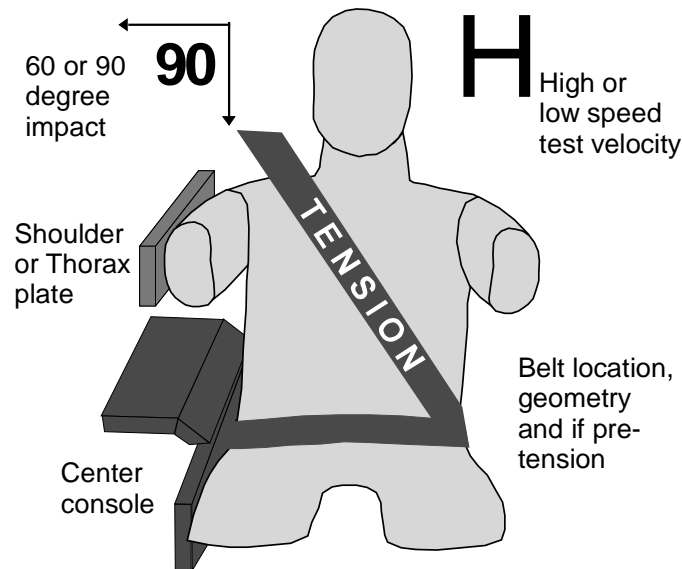


Figure 3.2. Explanation of figurines used as a visual code to clarify configurations depicted in tables and figures.

All tests were conducted with a lap belt, a centre console, and either an inboard or outboard shoulder belt. The shoulder and lap belts were low-elongation standard belts (6% elongation at 11.1 kN). The shoulder belt could be configured such that the D-ring anchor point was horizontal with the top of the shoulder (low position), 90 mm above the shoulder (mid position), or 150 mm above the shoulder (high position). All of these D-ring locations were approximately 120 mm behind the mid point of the shoulder. As a realistic worst-case configuration, the shoulder belt D-ring could be positioned in the mid position vertically, and forward (30 mm behind shoulder instead of 120 mm behind) of the usual anchor location (Configurations 10-11). Tests were conducted at either a direct 90 degree impact or an oblique 60 degree direction and low speed (11 km/h) or high speed (30 km/h) delta-V. The test speeds were chosen based upon real-world data from Gabler et al. (2005) that indicated at 11 km/h less than 5% of the cumulative serious injuries occurred, and at 30 km/h just over 50% of the cumulative serious injuries occurred. Thus, low speed tests were designed to provide low-level response data without injuries and high speed tests were designed to provide responses where countermeasures would be designed. The high speed test condition was a 100 ms square wave sled pulse with 8.8 g average acceleration using a bungee cord propelled rebound sled (MTS Systems, Minneapolis, MN). The low speed test was approximately a 60 ms pulse with 5.6 g average acceleration.

The load wall was instrumented with tri-axial load cells: three for the leg plate, two for the pelvis plate, two for the centre console plate, and two for the thorax or abdomen plates, if used. Seat belt force transducers were used and sled acceleration was recorded. A nine-camera, 1000 f/s motion tracking system (Vicon Motion Systems, Centennial, CO) was used to quantify occupant kinematics in three dimensions (3D). Reflective targets were placed on the head, at T1, T12, and pelvis. Multiple targets on the head were digitized with respect to anatomical landmarks which facilitated measurements with respect to head centre of gravity (CG). Reference targets were fixed to the sled and buck. Thus, head excursion measures are head CG movement with respect to the seat buck reference frame. All coordinate systems followed the SAE-j211 (version DEC 2003) standard sign convention.

The series of 18 tests were conducted with six PMHS (Table 3.2). All studies with PMHS were reviewed and approved by the Institutional Review Board of the Milwaukee VA Medical Centre Research Service. The PMHS were instrumented with triaxial accelerometer arrays at T1, T12, and sacrum. A custom-designed Pyramid Nine Accelerometer Package (PNAP) was used to derive head linear and angular accelerations (Yoganandan et al. 2006). Using inverse dynamics formulae, the PNAP was also used to derive occipital condyle (OC) forces and moments (Pintar et al. 2005).

A single 59-channel chestband (Denton, Inc. Rochester Hills, MI) was used at an appropriate location on the chest depending on the test configuration. For example, for a test with a thorax plate the

chestband was placed around the level of the rib cage immediately adjacent to the plate; for an inboard belt test the chestband was placed lower on the rib cage to assess belt-induced deformations. Chest deflections were recorded in all PMHS tests except for configurations where a shoulder plate was used or in the 90-degree test where there was a “high” inboard shoulder belt orientation. Chest deflections for PMHS tests were taken at the point along the chestband that yielded the maximum value. For each PMHS run, placement in the seating buck consisted of arms outstretched (driving position), head Frankfort plane horizontal, and right hip just touching the pelvis centre console plate. Immediately post-test, PMHS were palpated for bony fractures. After all tests were conducted, a complete X-ray examination and an autopsy identified injuries. The head was isolated and measured for centre of gravity (CG) and moment of inertia (MOI). The head of the PMHS was isolated by dissecting the skin along the inferior mandible, continuing through the occipital condyles, and through the skin along a line just inferior to the posterior base of the skull. The head CG was obtained by suspending the head from a cable along multiple points in the mid-sagittal plane and obtaining the intersection of plumb lines. The MOI about the primary anatomical axes was obtained using a standard three-cord torsional pendulum.

Table 3.2. PMHS specifications and tests.

Config ID	PMHS Test	PMHS	Age	Sex	Height (m)	Weight (kg)
1	HS104	1	80	M	1.83	68
2	HS105	2	81	M	1.85	80
3	HS106					
4	HS134	3	59	M	1.88	58
5	HS135					
6	HS136					
8	HS138					
10	HS138	4	84	F	1.55	80
11	HS139					
8	HS140					
9	HS141					
16	HS161	5	84	M	1.83	65
18	HS162					
22	HS163					
20	HS164	6	65	M	1.85	81
21	HS165					
14	HS166					
15	HS168					

For each test that was conducted with a PMHS, duplicate ATD tests were also conducted (Figure 3.3). Except for the last three configurations (Configurations 20-22), a 50th percentile WorldSID production model was used in one ATD series (Table 3.1). The placement of the WorldSID in the seat buck mimicked the PMHS seating position with the half arms in the horizontal position and the pelvis touching the pelvis plate. The WorldSID instrumentation included head linear and angular accelerations, upper/lower neck loads, chest deflections (IR-TRACC), T1, T12 spine accelerations and pelvic accelerations.

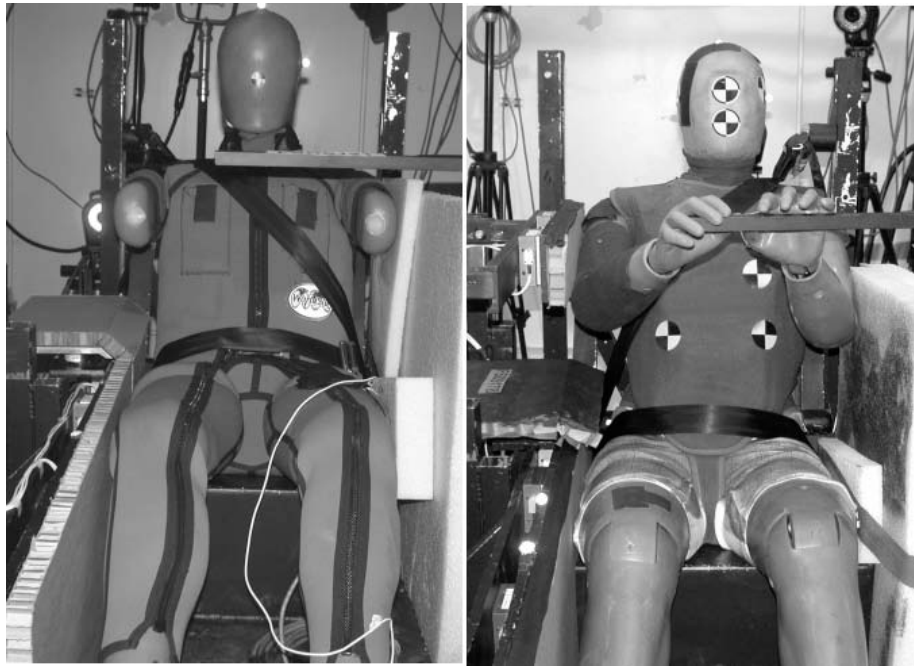




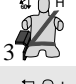






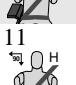







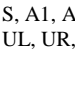
Figure 3.3. Pre-test photos of WorldSID (left) with inboard belt in low position (Config-18) and THOR-NT (right) with outboard belt and shoulder plate (Config-16).

A THOR (NT model, Gesac, Inc) was used in another ATD test series. Its arms, like the PMHS, were in the driving position attached loosely to a bar that simulated the location of the steering wheel. The THOR pelvis was positioned in the seat just touching the load wall. The THOR was modified by the manufacturer for side impact use by inserting additional foam padding over the lateral rib cage and moving the upper-right CRUX-pot to the direct-lateral position. Besides the CRUX-pots, the instrumentation was not altered for head (linear and angular), spine and pelvis accelerometers and the upper neck load cell.

3.2 RESULTS

Each PMHS test was compared to the corresponding ATD test by over-plotting the resulting responses (See Pintar 2008, Task 2 Final Report; Appendix). The minimum and/or maximum values of responses were obtained for comparison (Tables 3.3 and 3.4). In general, low-speed tests (Configurations 2, 4, 6, 8, 10, 14, 20) produced much lower magnitude responses than equivalent high speed test configurations (Table 3.3). Low-speed tests were conducted to evaluate ATD biofidelity at lower delta-V and to ensure that all measurement systems were functioning together. Maximum head CG linear accelerations for low speed PMHS tests were 3-9 g, and 1-18 g for ATD tests. Maximum T1 and T12 spine accelerations were 3-16 g for PMHS low speed tests and 5-15 g for ATD low speed tests. Low-speed test shoulder belt maximum loads were 42-996 N and lap belt loads were 40-656 N. Examination of high-speed video and deformed PMHS chest contour shapes showed that the shoulder belt was responsible for the maximum chest deflection for Configurations 1, 2, 3, 10, 11, 20, 21, 22; the centre console was responsible for maximum chest deflections for Configurations 14 and 15 and the thorax plate induced maximum deflections for Configurations 6 and 8.

Table 3.3. Maximum values from transducer data and calculated responses.










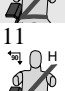








Config ID	Test Code	OCC FZ (N)	OCC FY (N)	OCC MX (Nm)	Y head excursion (mm)	Shoulder Belt Load (N)	Lap Belt Load (N)	Pelvic Load Y (N)	Thorax / Shoulder Load Y(N)	Chest Deflection (mm)
 1	HS104	1012	-844	-58	483	2950	855	-4162	---	62
	WS119	1468	-648	-42	512	2800	894	-5055	---	23 (A2)
	TH155	1802	-860	-98	538	2935	998	-4863	---	45 (LR)
 2	HS105	169	-184	-11	394	884	336	-1855	---	24
	WS129	228	-295	-22	300	996	343	-2418	---	8 (A1)
	TH180	291	-209	-15	330	895	368	-1981	---	9 (LR)
 3	HS106	1314	-898	-53	536	3818	998	-3881	---	49
	WS130	1182	-560	-36	428	3014	1182	-4380	---	15 (T3)
	TH181	1280	-458	-61	489	3585	1302	-3425	---	38 (LR)
 4	HS134	233	-181	-31	164	88	108	-1846	-1958	---
	WS108	205	-228	-18	198	42	49	-2860	-1894	22 (s)
	TH149	305	-340	-30	166	86	83	-1880	-3030	8 (UL)
 5	HS135	1085	-1500	-126	332	464	513	-3218	-3828	---
	WS108	888	-451	-64	383	326	261	-4884	-3228	43 (s)
	TH150	981	-595	-60	312	341	220	-3268	-6886	20 (UL)
 6	HS136	208	-184	-18	218	160	160	-1688	-2093	46
	WS110	210	-241	-24	203	168	266	-2044	-2511	32 (T2)
	TH152	198	-266	-19	195	89	102	-2040	-2021	18 (UR)
 8	HS138	1412	-804	-61	406	895	810	-4115	-3851	68
	WS113	805	-498	-43	428	1235	603	-4248	-3491	64 (T2)
	TH180	1344	-498	-88	430	1300	855	-3925	-4228	39 (UR)
 8	HS140	103	-128*	-8	269	188	92	-1340	---	---
	WS115	314	-343	-29	330	541	382	-2951	---	12 (A2)
	TH156	252	-145	-28	284	688	329	-2361	---	15 (UL)
 9	HS141	1639*	-1168*	-41	465	2093	539	-3833	---	---
	WS118	1895	-945	-58	463	2895	1849	-5663	---	28 (A2)
	TH188	334	-159	-38	388	3380	2348	-3980	---	40 (UL)
 10	HS138	138	-169	-12	301	858	238	-1889	---	31
	WS132	306	-386	-28	351	610	318	-3143	---	12 (A2)
	TH184	306	-358	-28	383	852	299	-2193	---	9 (LR)
 11	HS139	1185	-661	-48	509	2406	622	-4380	---	48
	WS133	1149	-606	-42	496	1693	815	-5008	---	20 (T3)
	TH185	1538	-642	-88	583	3566	865	-4688	---	58 (LR)
 14	HS166	306*	-186	-11	369	886	662	-1885	---	69
	WS124	288	-259	-22	269	864	469	-2388	---	8 (A2)
	TH168	188	-130	-18	282	809	333	-1534	---	13 (UL)
 15	HS168	898	-860	-32	440	2939	1842	-4000	---	83
	WS126	1420	-683	-39	358	2846	1846	-4089	---	20 (A2)
	TH169	689	-528	-45	388	4058	2588	-2443	---	34 (UL)
 16	HS161	1502*	-900*	-59	318	1123	298	-3044	-3219	---
	WS109	1048	-354	-84	355	695	382*	-4638	-2844	30 (S)
	TH188	1108	-531	-58	288	598	268	-3448	-5842	13 (UL)
 18	HS162	2165*	-1845*	-48	465	1351	1010	-2956	---	---
	WS121	1959	-842	-53	466	2244	1515	-5041	---	28 (A2)
	TH158	1139	-508	-108	499	3588	1883	-5589	---	31 (UL)
 20	HS164	105	-105	-6	420	816	516	-1943	---	40
	---	---	---	---	---	---	---	---	---	---
	TH182	163	-208	-15	321	865	356	-1814	---	9 (UL)
 21	HS165	861	-480	-29	538	3508	1142	-4586	---	84
	---	---	---	---	---	---	---	---	---	---
	TH183	1159	-584	-58	484	3348	1400	-3455	---	34 (LR)
 22	HS163	1980*	-995	-38	469	2236	498	-3593	---	80
	---	---	---	---	---	---	---	---	---	---
	TH186	1652	-634	-96	568	3212	835	-4394	---	44 (LR)

* Denotes peak value located at spike in data set.

S, A1, A2, T1, T2, T3 denote peak value recorded from WorldSID shoulder abdomen or thorax rib 1, 2, 3.

UL, UR, LR denotes peak value recorded from THOR crux upper left, upper right, or lower right

Table 3.4. Maximum/minimum values from transducers and calculated data.

Config ID	Test Code	Head CG Linear Accel.		Head Angular Acceleration				T1 Accel.	T12 Accel.	Sacrum/Pelvis Accel.
		YL (G'S)	ZL (G'S)	XL-Max (Rad/s/s)	XL-Min (Rad/s/s)	ZL-Max (Rad/s/s)	ZL-Min (Rad/s/s)	YL (G'S)	YL (G'S)	YL (G'S)
	HS104	-22	31	1982	-1803	345	-1158	-25	-16	-22
	WS119	-15	35	2425	-2840	685	-889	-21	-18	-19
	TH155	-35	49	1521	-3528	1921	-2122	-18	-16	-19
	HS105	-6	4	459	-462	188	-180	-8	-8	-12
	WS129	-8	6	1164	-889	188	-148	-8	-8	-11
	TH180	-5	6	436	-324	295	-458	-6	-9	-11
	HS106	-21	35	2416	-1680	1264	-1393	-38	-19	-18
	WS130	-14	29	2084	-1966	588	-490	-14	-16	-18
	TH181	-24	32	2204	-2482	1342	-3991	-16	-23	-31
	HS134	-4	6	1001	-1088	351	-425	-12	-16	-12
	WS108	-6	5	812	-422	233	-191	-10	-12	-13
	TH149	-8	8	889	-884	225	-195	-15	-11	-11
	HS135	-36	26	2364	-2042	1158	-1608	-42	-24	-19
	WS108	-36	19	2138	-3992	963	-2454	-21	-25	-20
	TH150	-25	24	2524	-1552	532	-816	-68	-21	-16
	HS136	-5	5	885	-542	310	-264	-11	-15	-11
	WS110	-8	5	862	-1213	305	-568	-11	-10	-15
	TH152	-6	5	408	-458	141	-231	-10	-12	-11
	HS138	-19	34	2458	-1129	1189	-616	-34	-40	-21
	WS113	-13	20	963	-1688	362	-424	-18	-18	-19
	TH180	-30	32	1058	-1995	898	-2818	-18	-19	-20
	HS140	-4	3	482	-408	282	-419	-6	-10	-10
	WS115	-9	8	1280	-1151	393	-825	-8	-11	-13
	TH156	-8	6	742	-475	846	-656	-8	-10	-13
	HS141	-32	46	3902	-6088	1914	-1019	-23	-21	-22
	WS118	-19	43	2994	-2939	843	-808	-29	-15	-20
	TH188	-40	9	1364	-2222	5158	-2686	-29	-16	-20
	HS138	-5	4	484	-318	191	-125	-5	-9	-10
	WS132	-10	8	1389	-1600	342	-269	-9	-8	-13
	TH184	-8	8	413	-520	188	-202	-6	-9	-11
	HS139	-18	44	5151	-5102	4334	-6003	-16	-24	-24
	WS133	-13	28	2013	-2185	808	-512	-15	-118	-18
	TH185	-25	36	1088	-2283	1116	-2906	-16	-18	-23
	HS166	-8	9	506	-394	442	-488	-4	-8	-9
	WS124	-8	8	1384	-808	384	-259	-9	-9	-12
	TH168	-18	6	1836	-952	3503	-1521	-5	-9	-11
	HS168	-23	24	1619	-1325	1209	-2428	-23	-16	-19
	WS126	-16	34	2524	-1869	634	-804	-22	-13	-19
	TH169	-14	22	1534	-690	1861	-1632	-25	-19	-26
	HS161	-25	41	2646	-4185	1928	-2616	-44	-25	-19
	WS109	-33	26	5081	-4593	1130	-2219	-19	-22	-20
	TH188	-24	22	2229	-1498	623	-1508	-82	-22	-19
	HS162	-51	69	4344	-4988	2928	-1988	-89	-20	-18
	WS121	-22	46	2839	-3684	816	-884	-28	-68	-20
	TH158	-28	43	2130	-2738	1819	-4408	-28	-18	-26
	HS164	-3	3	230	-202	282	-283	-3	-8	-9
	---	---	---	---	---	---	---	---	---	---
	TH182	-5	5	400	-290	232	-188	-6	-9	-11
	HS165	-13	23	1380	-909	838	-1684	-13	-16	-15
	---	---	---	---	---	---	---	---	---	---
	TH183	-23	30	2548	-2304	1268	-4406	-15	-20	-23
	HS163	-30	58	3089	-3262	1246	-2144	-19	-18	-18
	---	---	---	---	---	---	---	---	---	---
	TH186	-32	38	963	-3822	1362	-3494	-18	-19	-25

Note: XL, YL, ZL denote values are given in local anatomical reference frame.

Maximum Y-direction head CG excursions (Figure 3.4) were examined as a function of restraint for high speed 90-degree tests (Table 3.2). The shoulder belt outboard with a forward D-ring position (Configuration 11) generally produced the most lateral head excursion. When the D-ring position was lowered and more rearward (Configuration 22) or when the belt system had pre-tension (Configuration

1), there was only a slight decrease in lateral head excursion. Only when there was a restraining plate (Configurations 5, 8, 16) were the head excursions appreciably reduced. There were not as many 60-degree tests to make the same comparisons, but the same general trend was apparent for the three high-speed tests (Configurations 3, 15, 21). The head CG excursion plots in three planes are shown in the Final Task Report for Task 2 (Pintar 2008, Task 2 Final Report; Appendix). The starting point for each ATD head excursion in the Y-direction was normalized to the initial location of the PMHS head (approximately 300 mm from the seat left corner reference point). The difference in the starting point for the ATD's with respect to the X and Z directions was not normalised with respect to PMHS. In other words, the offsets in the plots are representative of how each ATD sits in the seat in its initial location. In general, the WorldSID head begins in a more forward position than the THOR head. The PMHS head starting position varied depending on individual anthropometry. From these plots, it can also be seen that the WorldSID follows the PMHS head excursion well for 90-degree tests, and the THOR follows the PMHS head excursions well for the 60-degree tests.

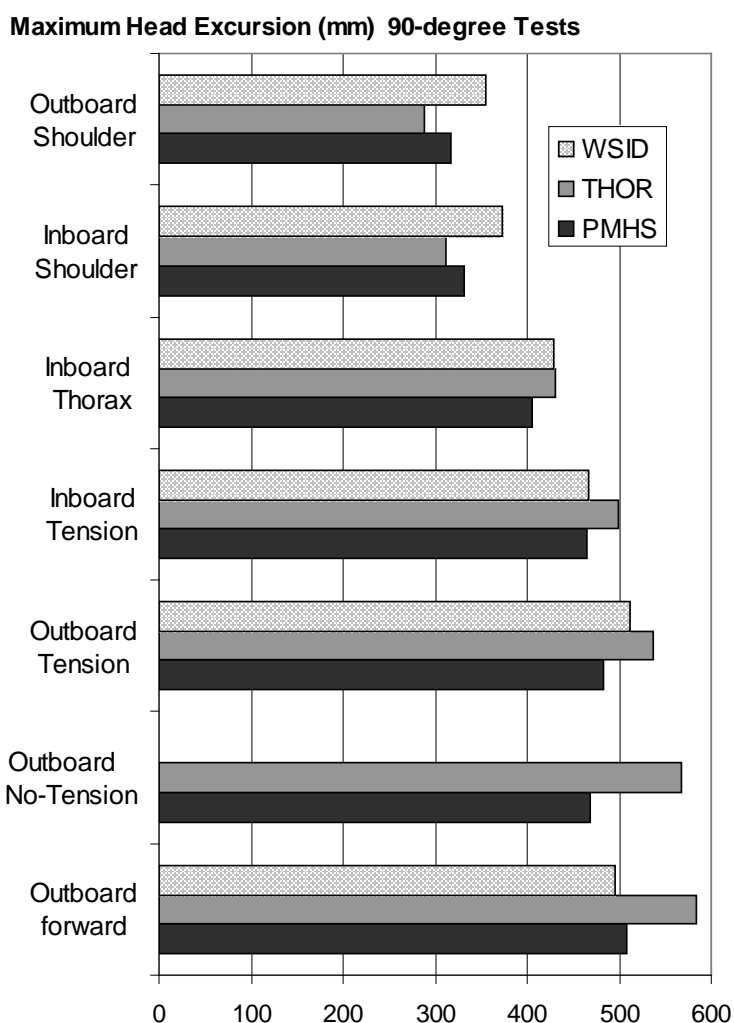

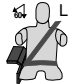

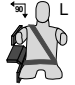
















Figure 3.4. Bar graph representation of maximum head excursions in the Y-direction as a function of restraint.

The loads derived for the occipital condyles (OC), Fx, Fz, and Mx, (Pintar 2008, Task 2 Final Report; Appendix) were not always of the same magnitude between ATD and PMHS, but almost always followed the same curve morphology. The exception to this was when the inboard belt was placed in the “high” position (Configurations 8, 9, 14, 15) over the neck to evaluate worst-case belt loading. The lateral shear load especially was often of opposite sign between PMHS and either ATD. Comparing load wall responses between dummies and PMHS, there was often the same response pattern and timing. WorldSID maximum load wall forces, however, were always greater than PMHS and often significantly (more than 500 N) greater. THOR pelvic forces were sometimes greater and sometimes less than PMHS. When a thorax plate was in place (Configuration 6, 8) both ATD's reproduced

PMHS response fairly well. With a shoulder plate (Configurations 4, 5, 16), but the THOR produced significantly higher shoulder plate loads than PMHS or WorldSID.

Table 3.5. PMHS Injuries.

PMHS	Testing Sequence	Injury Description	AIS
1		1 left rib fx: rib 8; 5 right rib fxs: ribs 3, 8-9 C8 fracture from degeneration	3 2
2	 	6 right rib fxs: ribs 3-8	3
3	   	5 right rib fxs: ribs 4, 8-9	3
4	   	Abrasion, contusion right side of neck Left external carotid artery intimal tear 2 left rib fxs on rib 3 T4-T5 separation with T4 fx; possible cord contusion	1 2 2 3
5	  	Multiple rib fxs: right 1-10, left 1-8; with pneumothorax and flail chest Liver laceration Spleen laceration Stomach laceration Right Clavicle fracture through acromio-clavicular joint Right Scapula fracture Right shoulder dislocation and fracture through glenoid	5 2 2 3 2 2 2
6	   	5 right rib fxs: ribs 3-8; 2 left rib fxs: ribs 5-6 Sternum fracture at rib 4 Fracture/separation right acromio-clavicular joint Left humerus head fracture	3 2 2 2

Injuries sustained by each PMHS are provided in Table 3.5. For the first three PMHS the major injury was rib fracture. For the first and second PMHS the rib fractures were caused by shoulder belt loading seen as direct compression to the lower right rib cage. The third PMHS experienced shoulder plate loading in the first two configurations, and thorax plate loading in the last two configurations. The rib fractures were in the vicinity of where the thorax plate loaded the rib cage. The fourth PMHS experienced a ‘worst-case’ outboard belt configuration where the anchor point was forward of the mid, or ‘normal,’ position. This caused the shoulder of the PMHS to slip out of the belt and resulted in maximal head excursion. There were only two rib fractures in this PMHS. There was however, a fairly serious T4-T5 separation which was unstable enough to imply some type of cord contusion. This PMHS also experienced a ‘worst-case’ inboard belt loading condition where the shoulder belt anchor point was placed high across the mid portion of the neck on the right side. This configuration resulted in abrasions and even contusions in the subcutaneous fat seen upon dissection of the area. The belt location is likely responsible for the intimal tear in the left carotid artery on the opposite side of belt loading due to stretching of the carotid artery.

The fifth PMHS experienced three high-speed tests which resulted in several injuries. The first of these three tests was with a shoulder plate and an outboard belt; the shoulder belt load was the lowest (1123 N) of the three tests. The shoulder plate likely caused the shoulder dislocation and fracture, as well as the clavicle and scapula fractures. The inboard belt configuration produced moderate belt loads (1351 N); the outboard belt configuration produced higher belt loads (2236 N). It was noted from the high speed video that the belt did not slip off the shoulder for this last test (Configuration 22). There were spleen, liver, and a significant stomach laceration; it is unknown which of the three tests produced each of these internal injuries. After the second of the three test runs, it was noted that

palpable rib fractures were present on the right side. The chestband data for test HS163 showed 80 mm of displacement to the right lateral rib cage. For the sixth PMHS, again, right sided rib fractures were present with two left rib fractures. This PMHS experienced all 60-degree tests. The outboard belt produced 84 mm of deformation and the interaction with the centre console on the inboard belt test produced 83 mm of chest compression. The fracture-separation of the right acromioclavicular joint was probably due to arm fling.

3.3 DISCUSSION

Despite contributing to a significant portion of the injuries and Harm (Malliaris et al. 1982) in vehicle crashes far side impacts have received little attention in the literature. It has been noted that because many of the counter-measures that may be effective for reducing head injuries in far side crashes (e.g. inflatable curtains) may also be effective for roll-over crashes, safety systems could have greater protection capability (Digges and Gabler, 2006). The ability to assess vehicle crashworthiness for far side occupants however, depends on the biofidelity of the ATD in the far side loading condition. Since there is currently no ATD that is designed specifically for far side collisions, the primary goal in the current series of tests was to perform a preliminary investigation of the biofidelity of THOR and WorldSID in far side impacts. A secondary goal was to evaluate the efficacy and trade-offs of generic countermeasures.

A sled buck was designed to specifically evaluate the far side impact event in a controlled laboratory environment. This buck was designed with moveable plates and adjustable restraint systems so that PMHS of different sizes would load the generic restraint systems in the same manner as the dummies. For example, a shoulder plate could be moved to optimally load the shoulder of any sized PMHS in the same manner as it would in a 50th percentile sized ATD, and a seat belt anchor point could be aligned with respect to subject anthropometry. This facilitated direct ATD biofidelity evaluation because restraint systems loaded the same location on the body for PMHS and ATD. The buck consisted of a rigid seat design with easy-to-obtain paper honeycomb where padding was needed. The two adjustable rigid cylinders provided back support and maintained visualization for body target movements in three dimensions. The centre console remained in place for all tests as this was considered a standard configuration in late-model vehicles. The seat belt anchor points could be moved such that locations could be made with respect to body landmarks (e.g., horizontal to top of shoulder). All of these adjustments were built-in to ensure robustness in biofidelity evaluations.

Previous epidemiological studies implicated the far side interior as a causative agent for head injuries (Gabler et al., 2005). One of the main purposes therefore, of the generic countermeasures was to reduce head excursion in the direction of the crash vector. This was accomplished in the generic countermeasures using belt system geometry and placement, as well as thorax or shoulder support in the form of padded plates. It was observed in the thorax plate countermeasure that rib fractures resulted from plate loading. A similar observation was noted by Melvin and Gideon (2004) in the design of racing vehicles for side impact protection that a “rib protector” was less desirable than shoulder protection. This is not to imply that a “thorax-type” countermeasure, could not work in the real vehicle environment. An example of the implementation of a thorax or shoulder support for far side impacts has been proposed using an airbag system (Bostrom, 2003). Because the WorldSID response in the thorax plate test in the current study mimicked PMHS response well, this ATD could be used to evaluate thorax loading by countermeasures.

Existing outboard belt restraint systems may have a D-ring position that allows the torso of the occupant to slip out of the shoulder belt in a far side-impact collision. In a previous examination of real-world crashes Mackay et al. (1991) estimated that the torso slipped out of the shoulder belt approximately 35% of the time. Recent real-world data for restrained occupants in far side crashes indicate that 28% of the AIS=3+ injuries occur to the head (Gabler et al. 2005). When AIS=3+ injuries and all fatalities are considered, 42% of the Harm for belted occupants occurs to the head (Digges et al. 2005). Results of the present test series indicated head excursions can still be greater than 400 mm even when the occupant does not slip out of the belt. The addition of pre-tension and belt placement directly over the shoulder reduced head excursion by about 50 mm. Only when shoulder or thorax restraining plates were used, did head excursion reduce by more than 150 mm compared to the

condition where belt slip occurred. These data indicate that even without slipping out of the belt the head can still move quite extensively within the vehicle during a far side crash.

Countermeasures that reduce head excursions must be designed to not increase the likelihood of injury to other body regions. The thorax restraint used in the present study increased lateral chest displacements to injurious levels. An inboard shoulder belt also reduced head excursions, but proper belt placement is critical. Specific placement directly over the shoulder is easier to control in a ATD than it would be in a real human. A mispositioned shoulder belt, such as the high position for the inboard belt (Configurations 8-9, 14-15) may cause high loads and neck lateral bending, placing the internal structures such as the vascular system and spinal column at risk for trauma (Sinson et al. 2003). Rouhana et al. (2006) tested a four-point belt system using PMHS in a far side impact mode and demonstrated no carotid artery injury with optimal “low” belt positioning. In the PMHS test for configuration-9 with a “high” belt position a carotid artery intimal tear was found after histological sectioning was done. This injury did not occur on the “pinching” (right) side, but rather on the “stretching” (left) side. The tension mechanism for carotid artery intimal tears has been well documented (Stemper et al. 2008) and appears to be the cause in this case. The PMHS test instrumentation did not allow for deriving lower neck loads in the present test series, but the WorldSID lower neck lateral shear load (F_y) reported previously (Pintar et al. 2006) demonstrated greater magnitudes and opposite sign compared to tests with optimal belt positions. This lower neck lateral shear load in ATD tests may be a good indicator of sub-optimal belt positioning when using inboard belts.

Two delta-Vanced dummies were evaluated for biofidelity in the current test series: the THOR-NT and the WorldSID. The WorldSID production version ATD provides extensive instrumentation to evaluate near side impacts. The WorldSID ATD used in the present test series was not modified in any way except to move the chest deflection sensors to the right side when they are usually placed on the left. It has a self-contained data acquisition system that allows for complete internal wiring of accelerometers, load cells, and deflection sensors. The WorldSID has direct lateral shoulder deflection measurement capability and mimicked the PMHS shoulder responses well. This is delta-Vantageous for shoulder-type countermeasure design. The WorldSID has a unique design of the lumbar spine that looks like an inverted “U” which allows for lateral motion of the torso relative to the pelvis. This lateral torso motion has been shown to be unique in PMHS testing and may be the reason the head can contact the opposite side door in far side crashes (Fildes et al. 2002). There are some limitations of this ATD for use in far side impact crashes, a mode that it was not originally designed for. Each of the ribs has an internally mounted IR-TRACC (Rouhana et al. 1998) that measures deflection best when impacted in a purely lateral direction. These sensor locations worked well when the plate-type countermeasures were included in the test configuration. With belt-like countermeasures these locations were sub-optimal. The interaction of the outboard shoulder belt with the oblique portion of the right lower rib cage demonstrated in the PMHS test was not fully recorded by the laterally-placed IR-TRACC sensors. Thus belt-like countermeasure tests evaluated by the WorldSID would require relocation of existing sensors or use of other types of sensors. Given the design of the WorldSID chest and rib cage, relocation of sensors should be possible.

The THOR-NT was initially designed as a frontal impact ATD. With some modifications, the manufacturer does also recommend it for use in limited side impact applications. The THOR-NT used for the current test series had extra foam padding over the lateral rib cage and the right antero-lateral CRUX pot was moved to a direct lateral position. The THOR-NT has an articulated spine which appeared to aid more biofidelic lateral torso movement. During outboard belt loading cases the CRUX pot system of the THOR in the lower right rib cage sensed a majority of the maximum deformation caused by the shoulder belt in this area. Given the complex nature of the belt loading in the far side impact environment however, the THOR lower right CRUX pot is still not optimally placed for all configurations. In general the THOR-NT responded with biofidelic chest loads when the belt was the primary restraint, and was particularly better in the 60-degree orientation tests. It was not as good at reproducing human-like shoulder response when a plate-type restraint was present. Again, the design of the THOR-NT shoulder was not intended for direct lateral impact.

Limitations of this study include a limited test series. Six PMHS were used to conduct eighteen tests. In general, low velocity tests (11 km/h) were designed such that no injuries would occur. This was readily apparent given that all tests were conducted with some type of belt restraint and the maximum values recorded by sensors were at sub-injurious levels. For the PMHS that experienced more than one high speed impact, the configurations were designed to produce distinct injury patterns. For example, test HS135 was a shoulder-plate restraint and produced no shoulder injuries, and test HS138 was a thorax-plate restraint and produced some rib fractures adjacent to the plate. Also, test HS139 was an outboard belt test where the PMHS slipped out of the belt and the second high speed test that this PMHS experienced was a mis-positioned inboard belt test. The PMHS experienced a serious thoracic spine injury, which can be assumed to be due to the outboard belt test, and a carotid artery tear, which can be assumed to be due to the inboard belt test. The exception to this pattern was PMHS-5 wherein three high speed tests were conducted. The extensive and multiple injuries this PMHS experienced are difficult to assign to particular test configurations. The resulting response curves including head excursion and chest deflection however, do not demonstrate a pattern indicative of increasing extent of injury, and therefore the responses for biofidelity evaluation should be adequate.

Another limitation is that the biofidelity assessments are based upon a single PMHS response test. To conduct a more complete biofidelity evaluation multiple tests should be conducted at each configuration and response corridors should be derived as has been done in previous studies (Hardy et al. 2001; Maltese et al. 2002; Kent et al. 2004). The decision early in the planning stages of this project was to conduct single tests with many configurations rather than to conduct multiple repeated tests under a small number of configurations. Since the main objective was to compare responses between PMHS and current dummies with and without generic countermeasures, the greater number of configurations was deemed to be ultimately more helpful to cover the potential realm of future countermeasure design.

3.4 CONCLUSION

PMHS testing in the far-side impact crash mode demonstrated inboard shoulder belts that were positioned directly over the shoulder, as well as countermeasures that promoted alternate load paths such as shoulder or thorax restraints, reduced head excursion and helped contain the occupant. The specific design characteristics of these counter-measures must be such that local chest deflections are not injurious. Both the WorldSID and THOR-NT response in far side impact compared favorably to PMHS response, considering that these dummies were not designed for this crash mode. The WorldSID performed better in plate-like countermeasure tests and in general, for 90-degree tests. The THOR-NT performed better in belt-like countermeasure tests and in general, for 60-degree tests. Although both dummies appear to have biofidelic rib cages, the individual location of chest deflection measurement may not be optimal. The far side impact environment is complex with multiple potential sources of injury to the human occupant. The THOR and the WorldSID dummies demonstrate adequate biofidelity to develop countermeasures in this crash mode and would be enhanced by specific instrumentation changes to detect trade-offs in countermeasure design.

4 SOFT TISSUE INJURY TO THE NECK

AUTHORS: Stefan Duma, Joel Stitzel and Ola Bostrom

4.0 INTRODUCTION

Carotid artery injury has been attributed to direct impact to the neck as well as stretching of the artery as a result of extension of the neck (Rozycki et al., 2002; Sinson et al., 2003). Injury to the carotid artery can be life threatening because these vessels, combined with the vertebral arteries, provide all of the blood supply to the brain. These injuries can begin with intimal tears that create a disruption to the vessel. From an intimal disruption, the vessel can become injured through occlusion through platelet aggregation, dissection of the intima, aneurysm, and intramural hematoma (Biffi et al., 2001; Haneline and Lewkovick, 2005; Schievink, 2001). Approximately 8,000 cases of internal artery dissection occur in the US per year (Haneline et al., 2003; Schievink et al., 1994). In a far-side crash, a common mechanism of injury is significant movement of the occupant due to the three point restraint system (Gabler et al., 2005). There is significant interest in the protective capabilities of a four point belt system and other torso restraint systems using PMHS and FE models. However, there are few FE models presented in the literature where attempts have been made to model this method of injury to these important vessels. To test these mechanisms of injury, this study correlated a regional model of the neck and carotid arteries to the results of PMHS impact tests.

4.1 METHODS

This study focused on the development of a regional head, neck and carotid model to examine the response of the carotid artery given lateral impact loading conditions. The methodology for this study can be broken into three components. The first component is an initial model assessment, where the separate parts of the model were examined and initially combined. The second step was establishing boundary conditions of the model by using the Total Human Model for Safety (THUMS) to establish a realistic kinematic given a crash impulse. The last step was integrating these boundary conditions into the existing model and completing the model to assess the response of the model under four different load conditions. These steps will be examined in further detail in the following paragraphs.

4.1.1 Method for Creating the Model

The geometric data was derived from scans of a patient at Wake Forest University Baptist Medical Centre. All protocols pertaining to confidentiality of patient information, confidentiality, and de-identification of patient data, etc were strictly followed. The protocol for use of geometry from clinical medical images was reviewed by Wake Forest's Internal Review Board and approved prior to commencement of work. Images were obtained from Computed Tomography (CT) scans of a patient's left carotid from the level of the base of the jaw to the insertion of the carotid artery into the aorta. In Figure 4.1, the lower bound is readily visible as the insertion of the two carotid arteries into the u shaped aorta at the bottom of the picture. The upper bound would be just above the arrow showing the left internal carotid artery. Scans were obtained using a General Electric (GE) LightSpeed Pro 16, a clinical CT scanner in common use throughout the United States.

Scans were obtained from a 58-year-old male. This patient had a history of CAD/CVA or coronary artery disease with cerebrovascular accident (usually stroke). This was a perfusion study using contrast agent ISOVUE 380 to check perfusion throughout the carotid and cerebral arteries. As the carotids were assessed to be normal by a qualified radiologist, this image was assumed to be representative of an average male. A total of 280 slices were obtained, with a slice thickness of 0.625 mm and a resolution of 160 mm x 160 mm with 512x512 image size for a resolution of 3.2 pixels/mm or 0.3125 mm per pixel. The images had a grayscale depth of resolution of 16 bits per pixel.

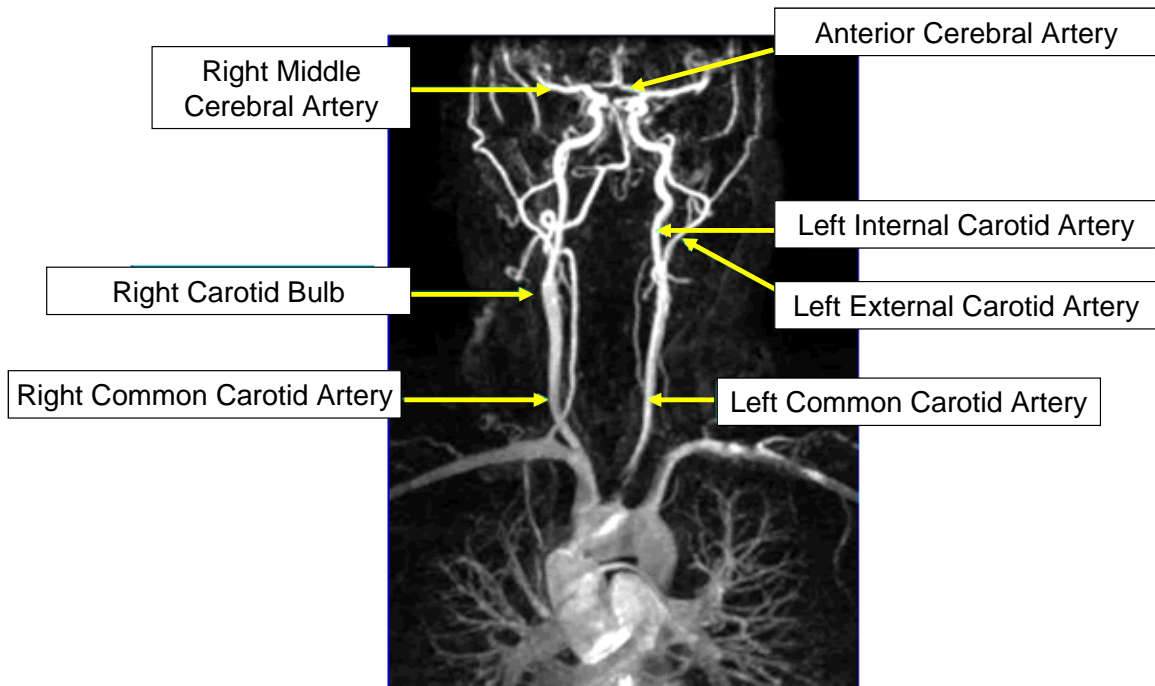


Figure 4.1. Carotid Artery Anatomy
 (adapted from <http://www.cme.wisc.edu/online/radiology/carotid/anatomy.htm>).

The carotid artery was segmented using a GE Adelta-Vantage Workstation to simplify reconstruction of the carotid. The carotid artery was segmented using a marching cubes algorithm such that the internal surface of the carotid formed a three dimensional surface of finite element trias, or three sided elements. The element geometry was imported into Engineering Technology Associates FEMB (Finite Element Model Builder), Version 28.0, to form the input deck for LS-DYNA, Version 9.80. For preliminary analysis, a blunt impactor of tip radius 1.5 mm was constructed and impacted into the carotid. The purpose of this exercise was to check contact algorithms and create a preliminary impactor surface, motion constraints, and a profile that can be altered with relevant crash data characteristics. The resulting geometry is shown in Figure 4.2.

The initial finite element runs included an initial velocity of 1 m/s for the impactor head, which was placed within a few millimeters of the exterior surface of the carotid. Material properties were approximated to be similar to soft tissues and there was no material filling the carotid to represent blood for these preliminary runs. The resulting von Mises stress distributions demonstrate stable behaviour of the model; however, the model still needs more material data for final validation. Global and local views of stress distribution on the model surface are shown in Figure 4.3.

Only local validations have been executed. The model was validated using force-displacement curves provided by Medical College of Wisconsin. Test specimens were cut longitudinally, along the axis of the artery. Specimens were preconditioned for five cycles, re-positioned back to the in vitro length, and then the failure test was run. Data was collected at an acquisition rate of 1000 Hz for 50 seconds, for a total of 50,000 datapoints.

For matching model performance to experimental results, the experimental data was filtered using a 1 Hz CFC filter. The reason for this low sampling rate was the large number of samples taken and an essentially static test. The 50,000 sample dataset was then padded symmetrically by replicating the first and last 3000 elements of the dataset array. This was done to eliminate resampling filter startup and finishing irregularities. The data was then resampled at 1/100 of its original sampling rate to obtain 500 datapoints. Padded data was then removed. The force and displacement traces were zeroed (recall that specimens were positioned to in vitro length, assumed to be zero force) to result in the final data for local model validation, shown below.

For these curves, which have a strain-stiffening toe region, a 2-parameter Mooney-Rivlin model is probably appropriate. This model at the current time is preferred to a more specialized soft tissue model which includes transversely orthotropic or fully orthotropic assumptions. At the current time, the test specimens are being modeled using Belytchko-Tsay shell elements with a resolution of element size that gives approximately cubic elements based on the element thickness assumption.

The LCCA arterial segment model dimensions at initial configuration and stress at maximum extension are shown in Figure 4.5. Force-displacement curve fitting and matching of model response by altering material data and material type are ongoing. The goal is to obtain the best possible match for both local and global response of the model. This model uses a Mooney-Rivlin representation and its material properties are inferred directly from the LCCA force curves from Figure 4.4.



Figure 4.2. Carotid Artery Geometry from CT Data.

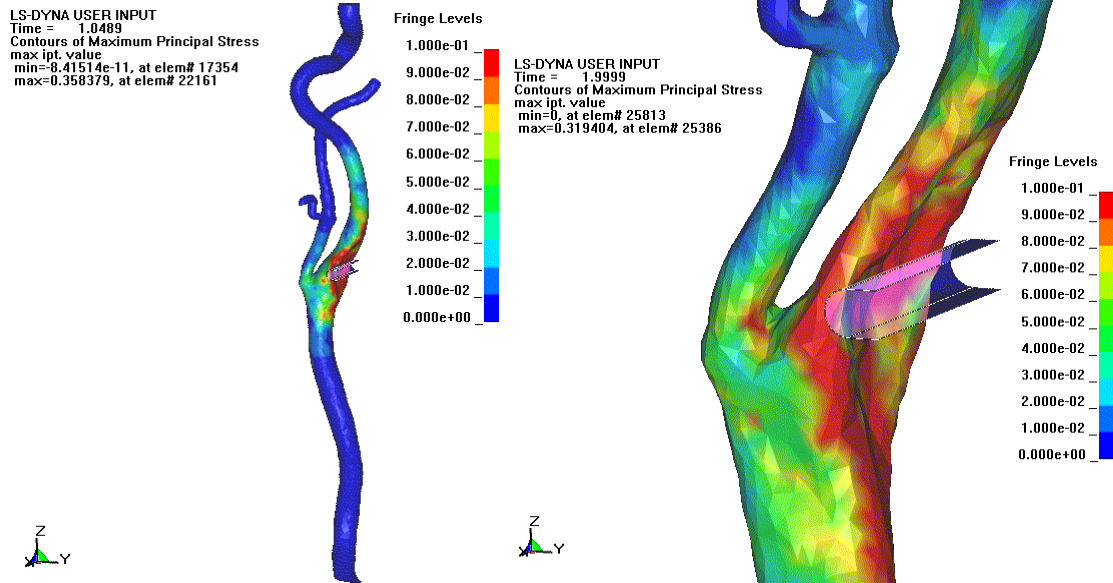
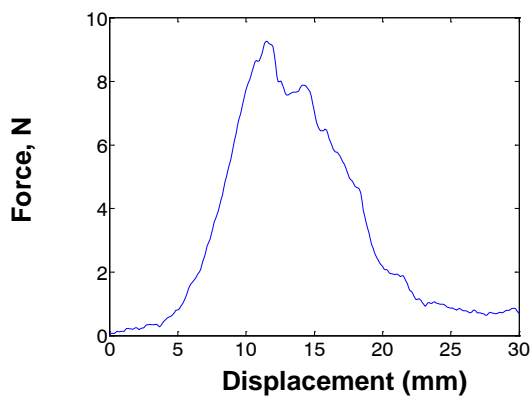
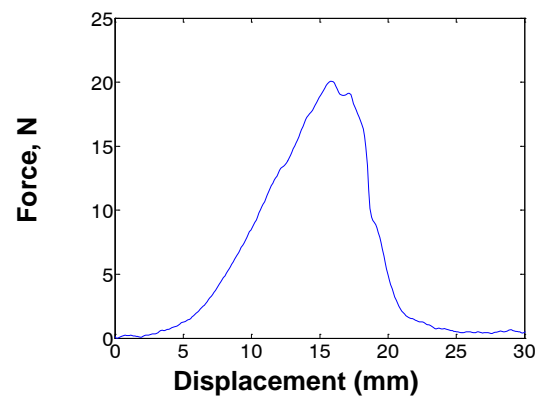


Figure 4.3. Global and localized view of impactor striking carotid just above level of bifurcation.



Force vs. displacement, LICA –
Left internal carotid artery

Specimen dimensions:
length: 18 mm
thickness: 0.89 mm
width: 9.5 mm



Force vs. displacement LCCA –
Left common carotid artery

Specimen dimensions:
length: 22 mm
thickness: 1.88 mm
width: 9.5 mm

Figure 4.4. LICA and LCCA force-displacement curves obtained from Medical College of Wisconsin.

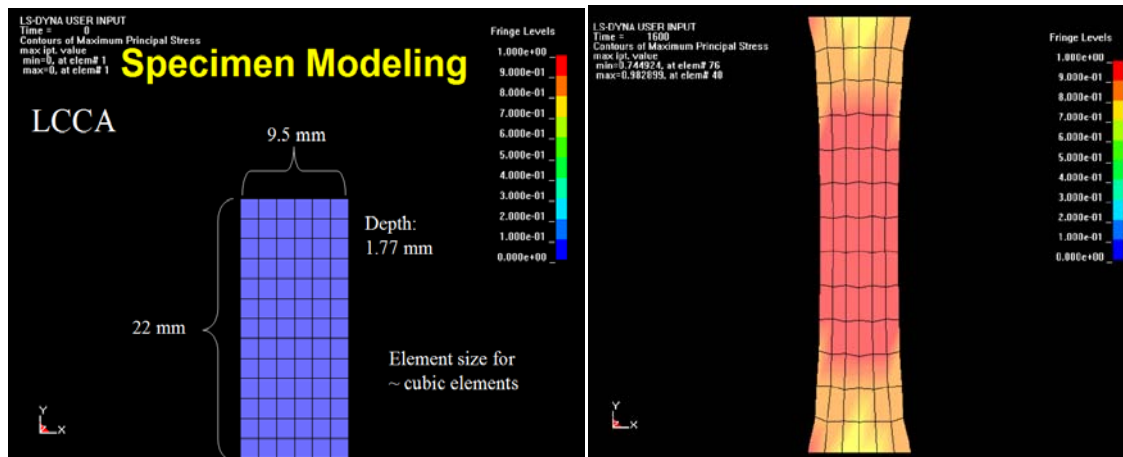


Figure 4.5. Specimen model for LCCA and peak displacement corresponding to failure. Force-displacement response of this model will be matched with experimental tests to incorporate local material properties into the global model of the carotid.

Geometry representing the bony structure of the neck from above the top portion of the carotid model to below the bottom portion will be incorporated. The purpose of this geometry should be that its displacement and motion can be controlled such that it will interact with the arterial structure (through soft tissues) if needed. This structure will not be intended to accurately interpret forces, or to model neck motion in response to an applied acceleration field. Instead, established neck models that have been widely validated will be used to obtain resulting vertebral body motions. Our approach will be to take the kinematics from the kinematically validated neck models and apply them to our model to predict injury. Soft tissues surrounding the carotid such as muscle, fat, other arterial structures, and skin will be incorporated. However, most of these structures were not independently modelled. While some effort was made to incorporate different properties for the skin, the plan was to fill in the void space surrounding the carotid up to the surface of bony structures, with a homogenous, isotropic medium. This volume will be filled with tetrahedral elements so that the interaction of the carotid with the hard structures of the neck and any impacting structures (seat belt, vehicle intrusions, etc) will be more realistic. However, it is beyond the scope of the proposed work to model all of the individual muscles, muscle tensions, etc to predict the arterial damage.

Additional material data should include data from circumferential testing of carotid segments, as well as additional tests so that some data averaging may be performed. It is well known that the properties of arteries are different in the circumferential vs. longitudinal directions. Modelling this difference may be important. Because it adds a level of complexity to the meshing and material assignment, it may not be feasible. Thus, we would at least like to test what the difference in mechanical behavior between the circumferential and longitudinal directions is, and decide whether some material property averaging is warranted. If it is not, it must be determined which direction of loading dominates the failure response by comparing experimental tests.

The carotid has a three-layered structure consisting of the intima, media, and adelta-Ventitia. The intima consists of basal lamina and endothelial cells, and is very thin and contributes little mechanical strength to the arterial wall. The media is comprised primarily of smooth muscle cells and is responsible for the material behavior of the arteries in the physiological range of strain, and particularly in a living environment where vascular tone is present. The adelta-Ventitia contains a layer of collagen with a wavy orientation that will straighten out and contribute strongly to mechanics as the artery reaches peak distension. So, before macroscopic failure of the tissue, this full range of mechanics must be considered. However, intimal damage is a serious biochemical concern because it tends to initiate clotting and can cause stroke and can, over long term, result in intimal hyperplasia. Medial damage is a contributing factor to dissection, where blood can get behind the media, but still be contained by the adelta-Ventitia, resulting in the closing off of the artery. Adelta-Ventitial damage in arteries, which are under high pressure from the blood, can result in internal damage and may

represent the most imminent danger. Hence, each mechanism has a different mechanical cause and may be worthy of an independent layer in the model for prediction. The only alternative to trying to predict failure layer-by-layer is trying to predict each injury indirectly by a strain assumption in a single-layered representation. Either way, mechanical testing was required in order to analyse failure of each layer independently.

4.1.2 Initial Model Assessment

The first step in the regional model creation was assessing the components of the model that were going to be used and completing an initial compilation of these components. The finite element software selected for this study was LSDYNA (LSTC, Livermore, CA). This regional model of the carotid integrates an existing head and spine model developed by Kleinburger (1993) with the carotid material model and geometry developed by Gayzik et al. (2006). Before all of the necessary components were added to fully model a cadaver impact study, the model had to be examined step by step.

The first step was to integrate the geometry of the carotid into a neck composed solely of fascia to demonstrate the response of the carotid given the correct geometry and the validated material model from Gayzik et al. (2006). This model had neck fascia that was the same material and the same geometry as the THUMS neck fascia. The carotid artery was created from a CT scan of a 58-year-old male subject (Gayzik et al., 2006). The crash scenario was modeled as a bent indenter that impacted the side of the neck at the level of the carotid bifurcation. This structure approximated a roped seatbelt. The indenter had a boundary condition of sinusoidal motion while there were locked nodes on the inferior aspect of the neck model and the medial space in the neck that approximated the vertebral column. The key components of this model are highlighted in Table 4.1 and illustrated in Figure 4.6 and Figure 4.8.

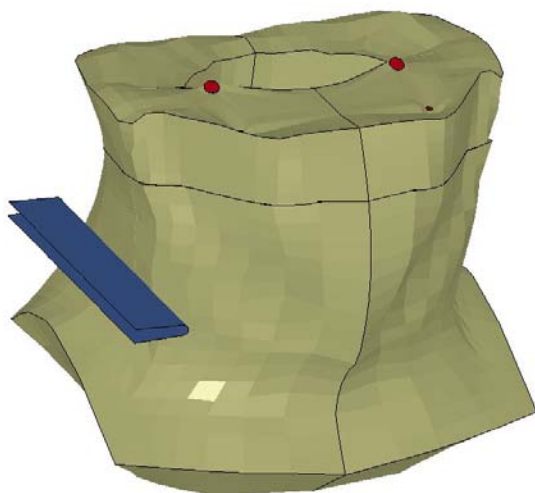


Figure 4.6. Initial neck regional model with neck fascia, carotid arteries and a seatbelt indenter.

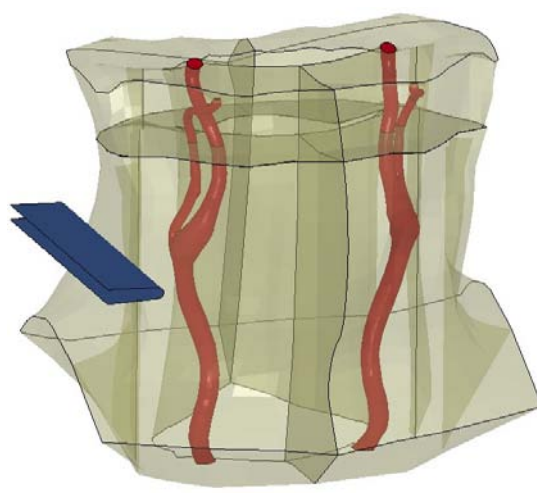


Figure 4.8. Initial neck regional model, transparent fascia for visualisation of the carotid artery placement.

Table 4.1: Summary of key model properties, initial regional model.

Model Parameter	Anatomical feature	LS-DYNA Cards
Materials	Neck Fascia and musculature	*Mat_Viscoelastic
	Carotid	*Mat_Simplified_Rubber
	Indenter	*Mat_Rigid
Contacts	Neck to Carotid	Auto_Surface_to_Surface
	Neck top to neck bottom	Tied Nodes
Boundary	Locked nodes	Inferior plane, medial vert body space
	Indenter	Sinusoidal Motion

This model was run and the resulting strains in the shells around the carotid artery were evaluated. This model did not incorporate the bony structures of the neck, the inertial response of the head and the corresponding response of the opposite side of the neck. Due to these limitations, it was determined that a model that incorporates these aspects needed to be developed to evaluate the carotid response on both sides of the neck. This model could study the compression of the carotid on the ipsilateral side and the extension of the carotid on the contralateral side.

To more accurately model an impact scenario, there were several modifications to the existing model. The first was the addition of the Kleinberger neck model. This model was developed to study cervical spine mechanics in frontal impact scenarios. The first step in this integration was translating this model into current Dyna code. From that point, the unit system was translated to m-N-kg-s. This model is pictured below in Figure 4.8 and Figure 4.9.

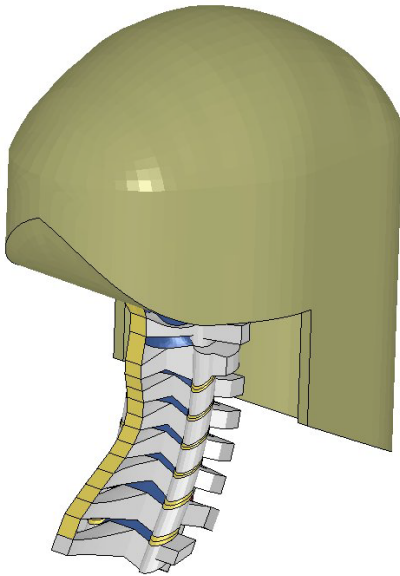


Figure 4.8. Rear oblique view of the Kleinberger neck model.

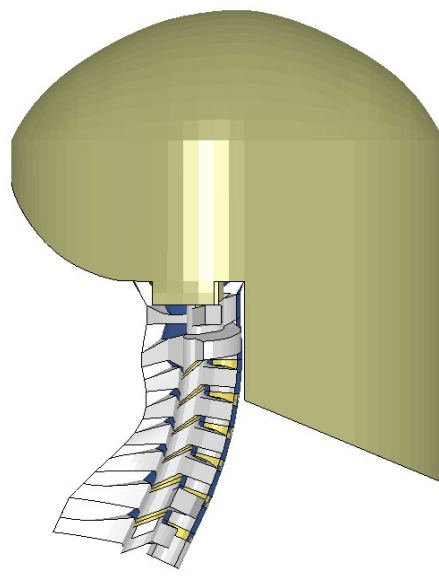


Figure 4.9. Right side view of the Kleinberger neck model.

As shown by these figures, the main cervical anatomy modeled are the vertebral bodies from C1 to T1, a head mass that has the geometry of an anthropometric test device (ATD), the primary ligaments that connect the vertebral bodies, and the facet joints. When this model was combined with the existing neck regional model, the neck fascia was too wide for the Kleinberger head, as illustrated in Figure 4.10 and Figure 4.11.

To make a more anatomically accurate model, a new neck fascia was created to have the same contours as the head in the spine model. Additionally, measurements taken from CT were used to properly place the carotid arteries in relation to the vertebral bodies (Lambert et al., 2008). Figure 4.12

and Figure 4.13 illustrate the new neck fascia integrated with the Kleinberger neck. The locations of the carotid arteries, in relation to the vertebral bodies, are shown in Figure 4.14 and Figure 4.15. The important model characteristics are shown in Table 4.2.

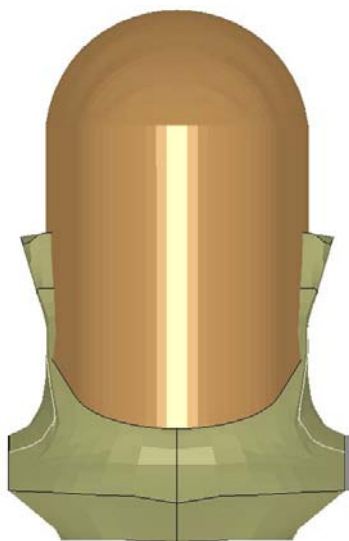


Figure 4.10. Front view of the initial neck model with the head and spine.

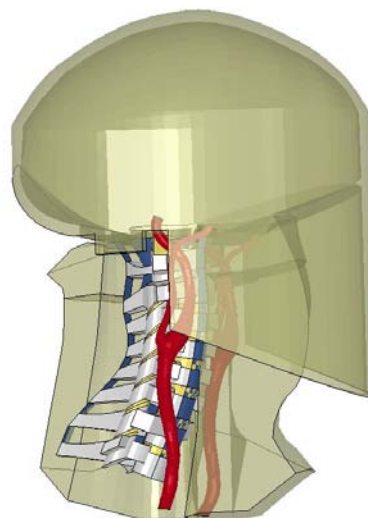


Figure 4.11. Oblique view with the right neck fascia removed and transparent head and fascia to illustrate the spine and carotid placement.

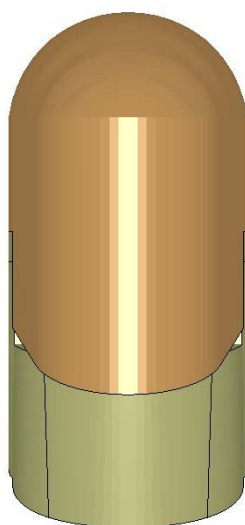


Figure 4.12. Kleinberger neck integrated with revised neck fascia.

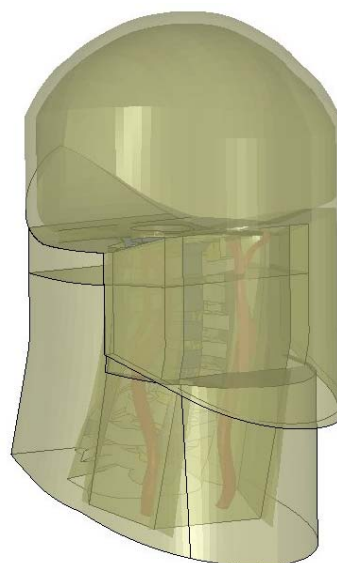


Figure 4.13. Oblique view of the Kleinberger neck integrated with the revised neck fascia, fascia and head are transparent.

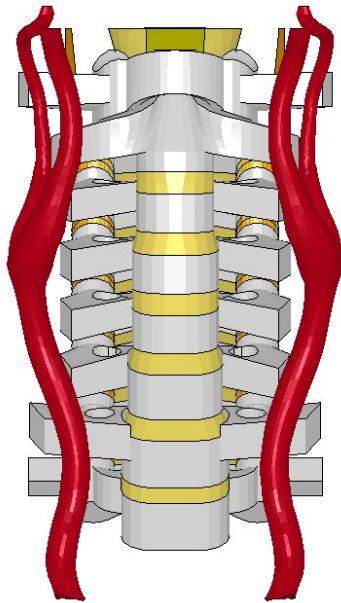


Figure 4.14. Front view of carotid placement, with select ligaments removed for clarity.

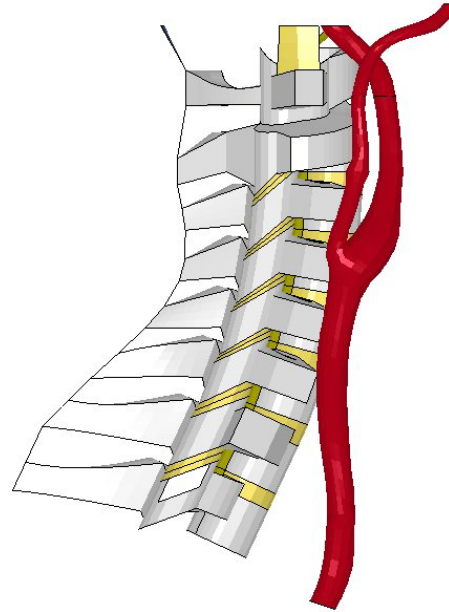


Figure 4.15. Right view of carotid placement, with select ligaments removed for clarity.

Table 4.2. Model parameters for the first version of the integrated head, spine, and neck model.

Materials	Neck fascia and musculature	*Mat_Elastic
	Carotid	*Mat_Simplified_Rubber
	Ligaments, Disks	*Mat_Elastic
	Vertebral bodies, Head	*Mat_Rigid
Contacts	NHTSA neck	Preserve contacts
	Top of neck to head	Constrained extra nodes
	Neck to carotid	Tied surf to surf
	Vertebral bodies to neck	Auto surf to surf
Boundaries	Locked nodes	Bottom of neck to T1
	T1	Prescribed motion

Once this step was complete, initial runs of the model were conducted to evaluate the response of the spine model in a side impact loading scenario. For these impacts, acceleration data from MCW far side PMHS tests were used as the boundary conditions. Figure 4.16 shows all the plots of the initial load configurations for the four load conditions of low belt and low delta-V, low belt and high delta-V, high belt and low delta-v, and high belt and high delta-V.

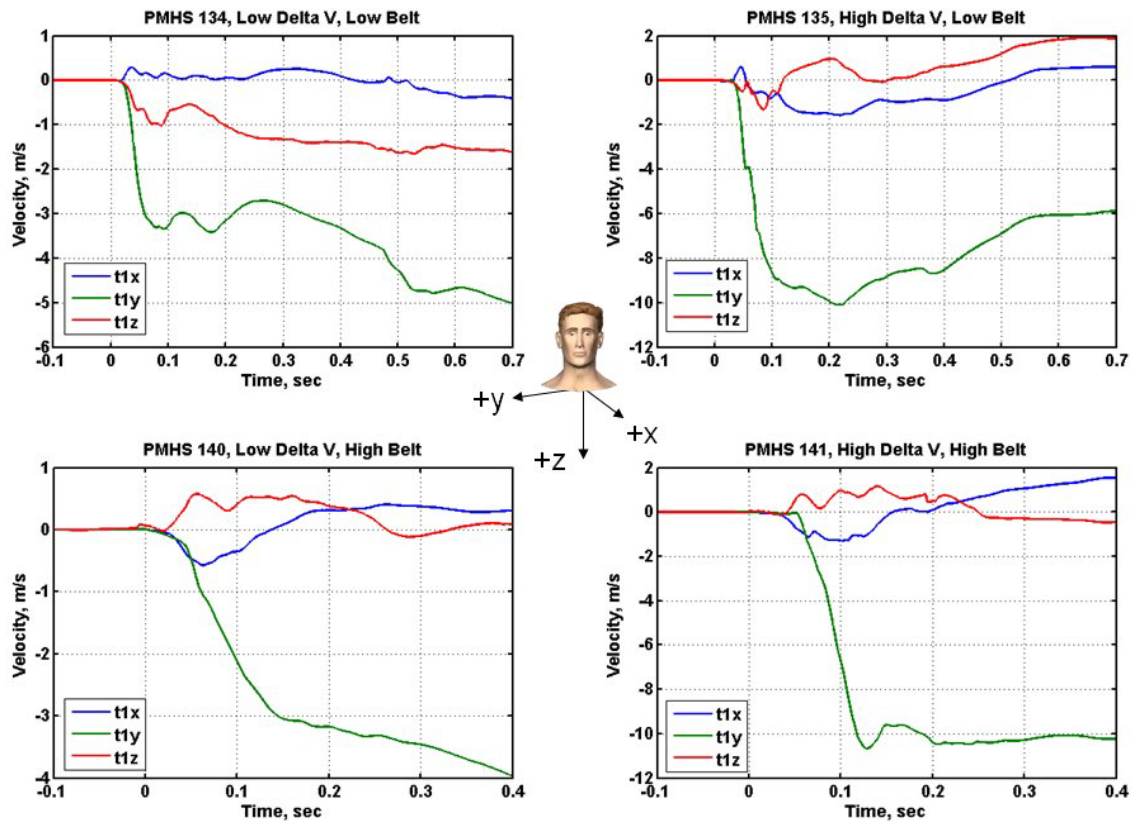


Figure 4.16. Boundary conditions for T1 from the MCW tests. The blue line is T1 x velocity (m/s), the green line is T1 y velocity (m/s), and the red line is T1 z velocity (m/s).

The T1 velocity data from the tests was applied as a velocity to T1 in the model. The bottom of the neck was constrained to move in the same manner as T1. The top of the neck was coupled to the bottom of the head. During this phase of the model development, different versions of the material models used for the neck fascia and ligaments were evaluated over a range of load conditions.

4.1.3 Kinematic Modelling Using THUMS

Given the response of the Kleinberger neck at high delta-V, the initial model configuration was determined to be unstable and without a biofidelic response of the head and neck. To address this issue, the boundary conditions to be modelled were used as inputs to the Total Human Model for Safety (THUMS). The acceleration recorded for the seat in the MCW tests was applied to the seat as the boundary condition for the THUMS model. The THUMS model was placed in a similar sled configuration as the test configuration. This configuration was reconstructed from diagrams and descriptions in Pintar et al. (2008). In the THUMS model, there were nodes selected on each of the cervical vertebral bodies, the first thoracic vertebral body, the shoulder attachment of the modelled seatbelt, and a node on the seatbelt located at the sternum. The displacements of these nodes were recorded for each test configuration. These displacement files were then used as inputs for the final model.

4.1.4 Final Model Parameters

The final model used the neck fascia contoured to the head of the neck model as described as the final configuration for the first version of the regional model. The ligaments and the intervertebral discs were removed because each vertebral body was constrained. A shoulder structure that was modified from the THUMS shoulder geometry was added to the model with the same material properties as the neck fascia. This addition was to prevent the seatbelt from slipping under the neck. A seatbelt

segment was also added to the final model. This belt went from an upper attachment point, just like the full THUMS model, and terminated at the approximate level of the sternum. The location of the upper attachment point was measured from the level of T1 and comparable to the location of the anchor point in the PMHS tests. The sternum attachment point was also estimated based on the similar location on the THUMS model. Figure 4.18 and Figure 4.18 show the complete model given a high belt configuration and Table 4.3 shows the model parameters.

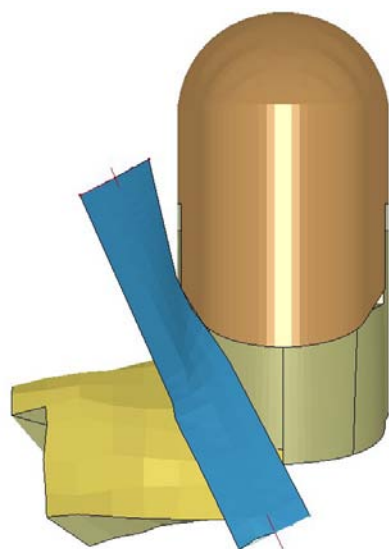


Figure 4.18. Front view of the final version of the neck regional model.

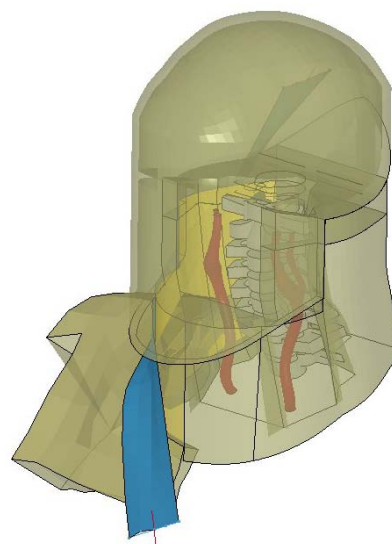


Figure 4.18. Oblique view with the fascia removed and transparent head and fascia.

Table 4.3. Model parameters for the final version of the integrated head, spine and neck model.

Materials	Neck fascia and musculature	*Mat_Elastic
	Carotid	*Mat_Simplified_Rubber
	Ligaments, Disks	REMOVED
	Vertebral bodies, head	*Mat_Rigid
	Seatbelt	*Mat_seatbelt
Contacts	NHTSA neck	Remove all existing
	Top of neck to head	Constrained extra nodes
	Neck to Carotid	Shared nodes
	Vertebral bodies to Neck	Auto surf to surf
	Seatbelt to neck	Auto surf to surf
	Bottom of neck to T1	Constrained extra nodes
Boundaries	All Vertebral bodies, Seatbelt	Displacement from THUMS

The model was run given 4 conditions based on PMHS test configurations as shown in the test matrix in Table 4.4. From Pintar et al. (2008), an intimal tear occurred in the PMHS test that experienced high belt loading at both high and low speeds. Since multiple tests were conducted on the same PMHS, the time of the carotid artery injury is unknown.

Table 4.4. Test Matrix for the model.

PMHS Test No.	Belt Position	Delta-V
134	Low	Low
135	Low	High
140	High	Low
141	High	High

4.2 RESULTS

There were several steps before the final version of the model; therefore, there were several intermediate results that will be discussed in this section. The first segment was an initial model assessment to determine the response of the Kleinberger neck (Kleinberger, 1993). The second was kinematic modelling of the neck using the THUMS model.

4.2.1 Initial Model Assessment

The initial model assessment demonstrated instability of the Kleinberger neck in a lateral impact scenario. Also, the Kleinberger neck demonstrated a lack of biofidelic response of the spinal column. Finally, the neck had no shoulder; therefore, the low belt configuration did not properly interact with the model. Figure 4.19 and Figure 4.20 demonstrate the failure of the spinal column due to interaction between the vertebral bodies and the low belt configuration.

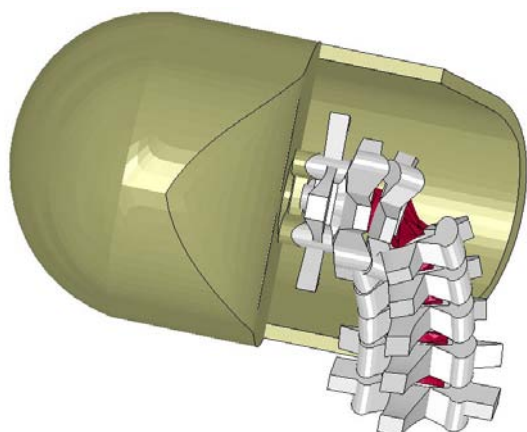


Figure 4.19. The response of the Kleinberger neck given a lateral impact scenario.

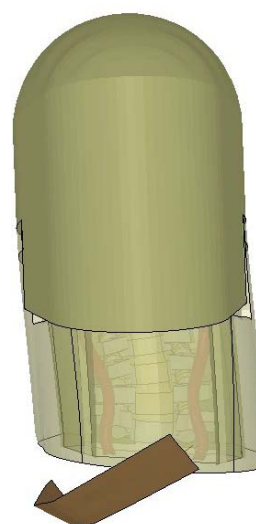


Figure 4.20. Low belt missing the first version of the combined model.

These problems were a result of the geometry of the existing head and neck model. Specifically, the vertebral bodies had significant interaction between the lateral edges which prevented reasonable lateral flexion. Additionally, the ligament structures in the model were more efficient at constraining anterior to posterior motion rather than lateral motion. Given these results, it was determined that the motion of the vertebral bodies would have to be determined in another manner. The existing THUMS finite element model was selected as a method of obtaining displacement data for each vertebral body.

4.2.2 Kinematic Modelling Using THUMS

The THUMS model was taken and seated in the same sled configuration as the PMHS subjects used in data collection. All of the loading scenarios ran to completion with qualitative improvements of the model response. Figure 4.21 and Figure 4.22 illustrate the THUMS model in the high and low belt configurations. The model response at the time of maximum extension is shown in Figure 4.23 to Figure 4.26 for each test configuration. This response qualitatively matched the PMHS test results.

The time at maximum extension of the THUMS model was noted in Table 4.5 for comparison with the regional carotid artery models.

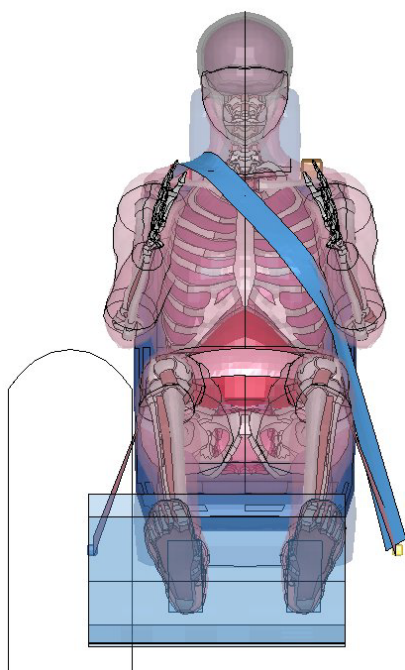


Figure 4.21. THUMS model with the low belt configuration.

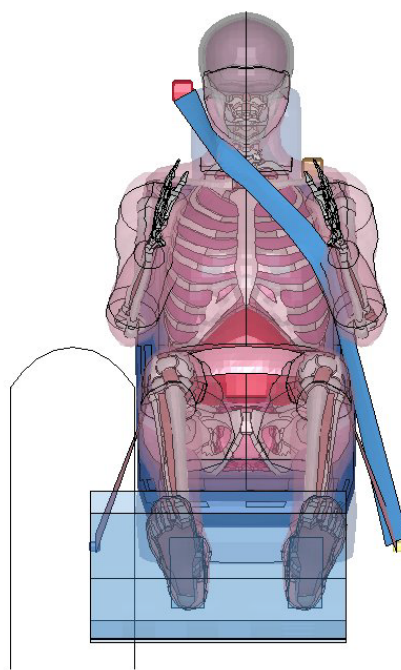


Figure 4.22. THUMS model with the high belt configuration.

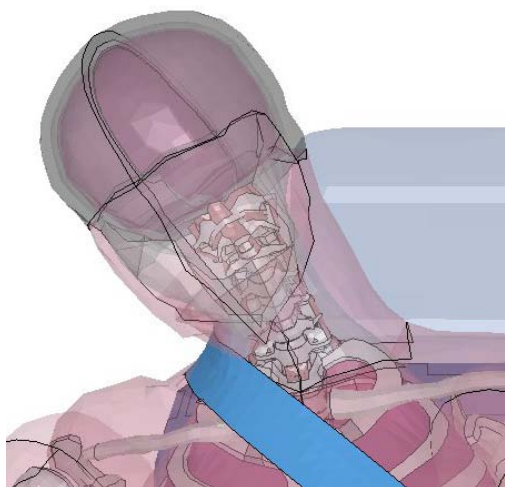


Figure 4.23 THUMS model at maximum neck extension, low belt and low delta-v

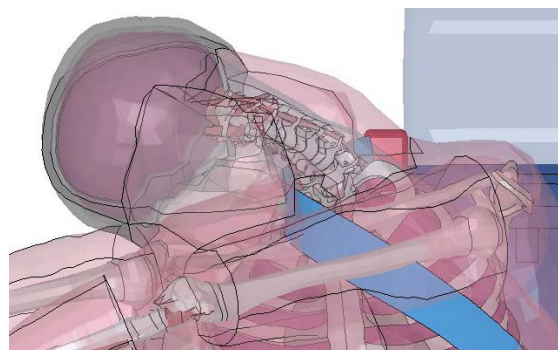


Figure 4.24. THUMS model at maximum neck extension, low belt and high delta-v

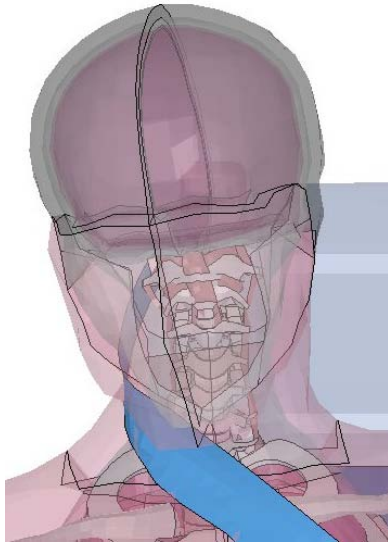


Figure 4.25. THUMS model at maximum neck extension, high belt and low delta-v

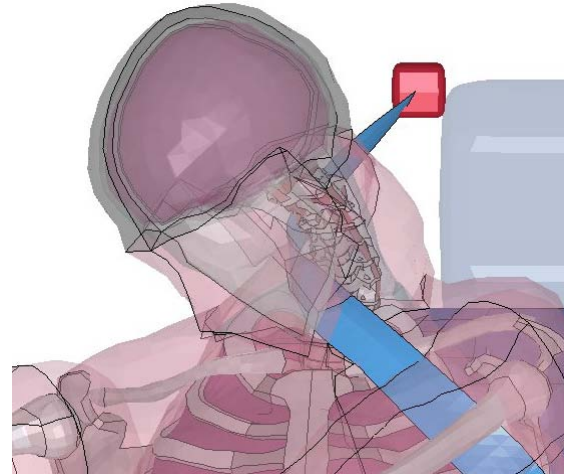


Figure 4.26. THUMS model at maximum neck extension, high belt and high delta-v

Table 4.5. Time of maximum neck extension of the THUMS model.

Test Configuration	Time of Maximum extension
Low Belt, Low Delta-V	140 ms
Low Belt, High Delta-V	135 ms
High Belt, Low Delta-V	110 ms
High Belt, High Delta-V	120 ms

4.2.3 Final Model Parameters

Using the THUMS model results as inputs for the final version of the combined neck and carotid model, the 4 load configurations were examined. The first measure of the possibility of injury to the carotid was the largest maximum principal strain value measured in any element of the carotid artery shells. These values are listed in Table 4.6. As this table illustrates, the highest strain value out of the models that ran to completion was in the low belt, high delta-V configuration. There is a trend between the low belt configurations in that as the delta-V increases, the maximum stain value increases. This trend was also postulated to apply to the high belt configurations.

Table 4.6. Maximum principal strain values for each test configuration.

Test Configuration	Maximum Principal Strain	Time of Maximum Strain
Low Belt, Low Delta-V	0.3182	136.5 ms
Low Belt, High Delta-V	1.5884	126.0 ms
High Belt, Low Delta-V	1.2884	136.5 ms
High Belt, High Delta-V	Error Termination	Error Termination

To examine the location of the higher strain values in the carotid artery, the fringe plot function in LS-Prepost (LSTC, Livermore, CA) was used to graphically illustrate the location of high strain values. The areas of red, orange and yellow have higher strain. Areas in blue and green have a lower strain value. To have these fringe plots reflect the same relative scale, the maximum strain value (illustrated by dark red) was set as 1.3. This was based on the maximum value of 1.5884 recorded for the Low Belt, High Delta-V configuration. The minimum value (illustrated by darker blue) was set as 0.

These figures illustrate the low levels of strain in the low delta-V configurations, especially the low delta-V, low belt configuration shown in Figure 4.28 and Figure 4.28.

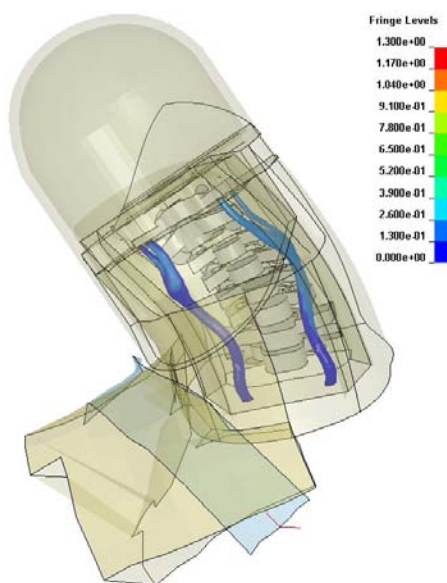


Figure 4.28. Fringe plot of the Low Delta-V, Low Belt impact configuration. This is at the time of the maximum strain, 125 ms.

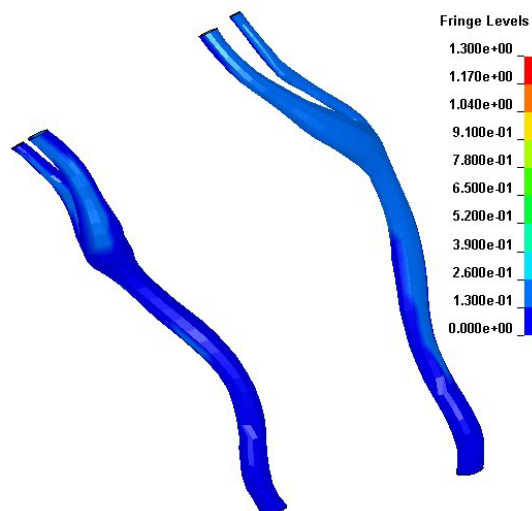


Figure 4.28. Close up of the same time point and the same approximate orientation with the carotid arteries isolated.

The high belt, low delta-V plot, Figure 4.29 and Figure 4.30, showed higher strains than the low delta-V, low belt plot, but lower strains than the low belt, high delta-V plot, Figure 4.31 and Figure 4.32. These figures also show that even though there were isolated elements in the high belt, low delta-v configuration that achieved a fairly high strain, there were not many elements that experienced higher strains.

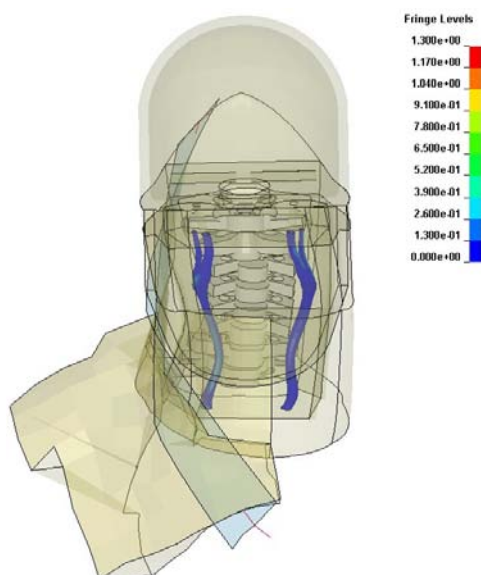


Figure 4.29. Fringe plot of the Low Delta-V, High Belt impact configuration. This is at the time of the maximum strain, 125 ms.

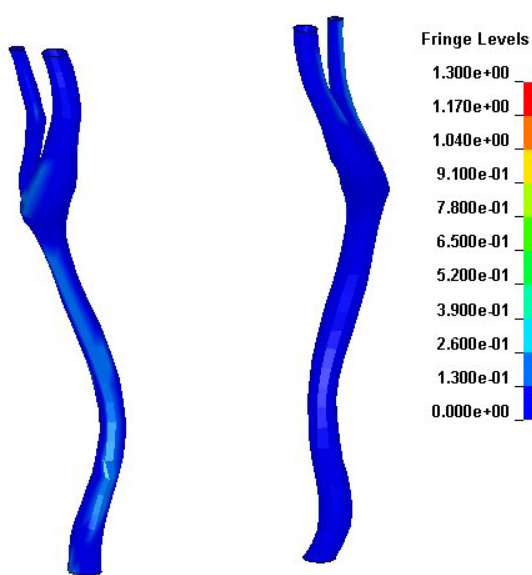


Figure 4.30. Close up of the same time point and the same approximate orientation with the carotid arteries isolated.

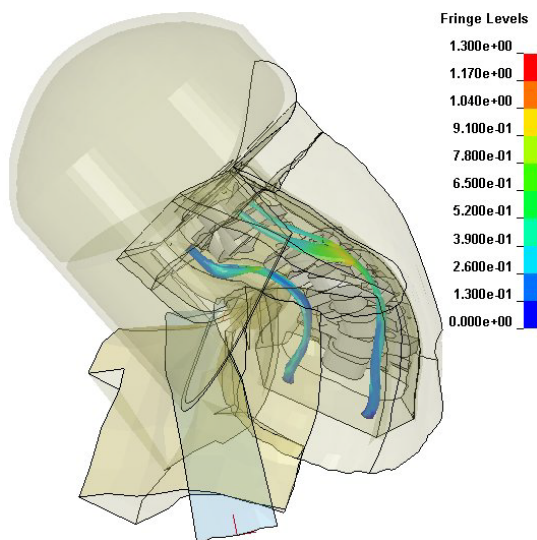


Figure 4.31. Fringe plot of the High Delta-V, Low Belt impact configuration. This is at the time of the maximum strain, 125 ms.

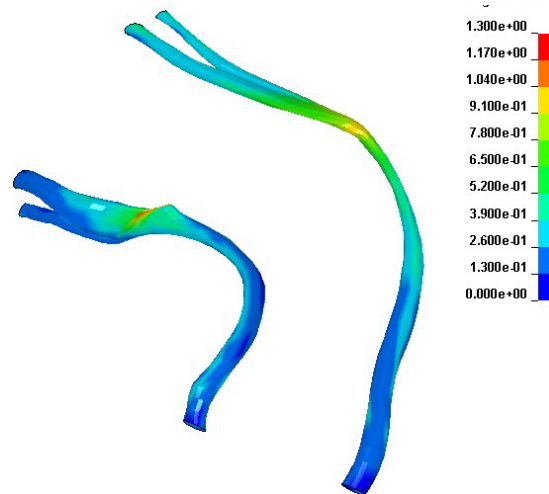


Figure 4.32. Close up of the same time point and the same approximate orientation with the carotid arteries isolated.

Next, to hypothesize the potential outcome for the high belt, high delta-v configuration the results from the THUMS model were compared between the belt configurations and given a high delta-V. Figure 4.33 and Figure 4.34 illustrate the loading scenario that the regional model failed to run to completion in the THUMS model. When compared to Figure 4.35 and Figure 4.36 there is significantly less extension of the spine in the high belt configuration. From these results it can be concluded that the high belt, high delta-V configuration will have less neck extension on the side contralateral to the belt than the low belt, high delta-V configuration. However, the high delta-V, high belt neck configuration will have more compression of the neck fascia and carotids between the belt and the vertebral bodies.

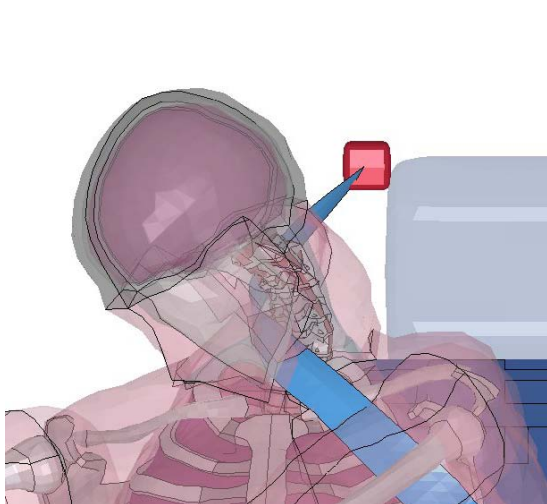


Figure 4.33. THUMS results, High delta-V, High belt configuration.

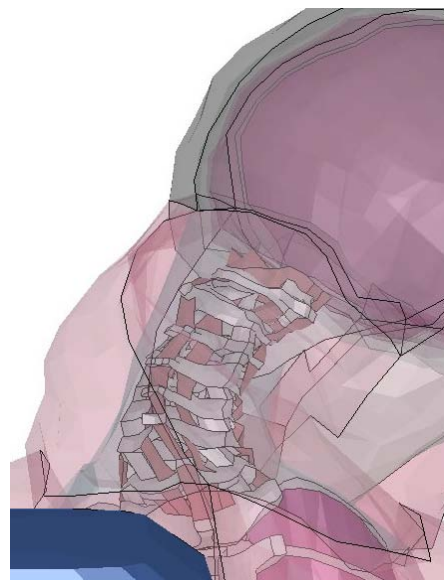


Figure 4.34. Close up view of the High Delta-V, high belt THUMS results.

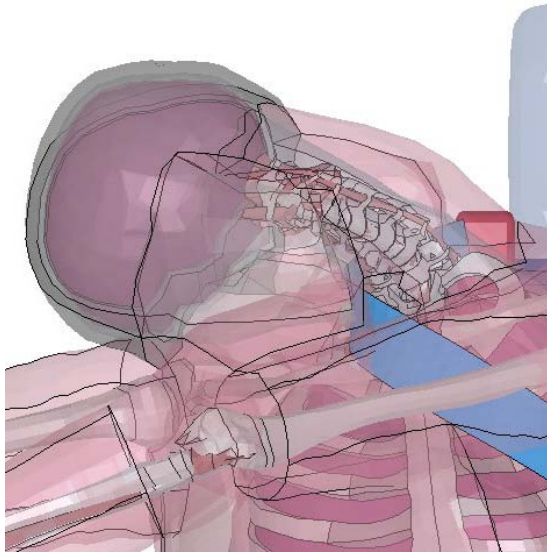


Figure 4.35. THUMS results, high delta-V, low belt configuration.

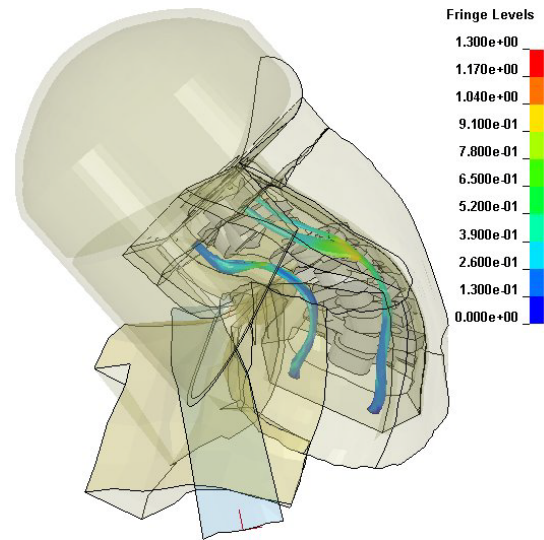


Figure 4.36. Version 2 model results, high delta-V, low belt.

4.3 DISCUSSION

The resulting neck model illustrated several trends in the response of the carotid artery given a lateral impact and variable speeds and belt positions. The primary trend seen in the results was the compression of the ipsilateral vessel, with respect to the belt, and stretching of the vessel on the contralateral side. Based on Stemper et al, the strain to failure for the intima is approximately 0.40 strain and to total vessel failure it is 0.60 strain (Stemper et al., 2005). Based on these values, at least one element in the high belt and low delta-v, and low belt and high delta-v cases exceeded this limit. Based on the THUMS modelling results, it is estimated that the high belt, high delta-v configuration would also have at least one element exceeding this value.

This model also demonstrated the need for continued development of neck models for lateral impact scenarios. The base neck model used for model development was validated solely in frontal flexion; therefore, it was unstable given a lateral impact. The THUMS model was then used to determine a more biofidelic neck response for the regional neck model. Another limitation of the regional model is the basic geometry used in the model. The head and vertebral bodies are relatively square and lack true anatomical detail. The THUMS model, which was more anatomically accurate, had a more accurate model response given the loading scenario. Another limitation introduced with the geometry of the model used was the angular interfaces between structures. Again, this limited the ability of the model to replicate a biofidelic response.

4.4 CONCLUSIONS

To determine the possible effect of a four point style restraint in a farside crash configuration, a regional model of the neck and carotid artery was created. This model determined the strain in the carotid arteries given a range of impact severities and seatbelt configurations. Given the model response and the hypothesized strain to failure of the carotid artery, the carotid artery would have been injured in all of the tests except the low belt, low delta-v configuration. More importantly, the model illustrated that given a low belt configuration, the occupant was more likely to injure the contralateral vessel via an extension type injury. Given a high belt configuration, the occupant was more likely to injure the ipsilateral vessel via compression of the vessel between the seatbelt and the vertebral bodies.

5 FAR SIDE INJURY CRITERIA

AUTHORS: Richard Morgan, Tom Gibson

5.1 INTRODUCTION

The aim of this phase of the research (Task 5) was to conduct a literature investigation into injury mechanisms in both lateral and frontal oblique directions in order to either identify or to develop injury risk functions for far-side occupants. Before undertaking the subsequent investigations (Task 6 and Task 8), the object was for the Far-Side Impact Team to complete Task 5, as it was envisioned that the Task 5 Final Report would act as a handbook to support and guide Task 7 (computer modelling) and Task 8 (Countermeasure Development).

The task objectives were as follow:

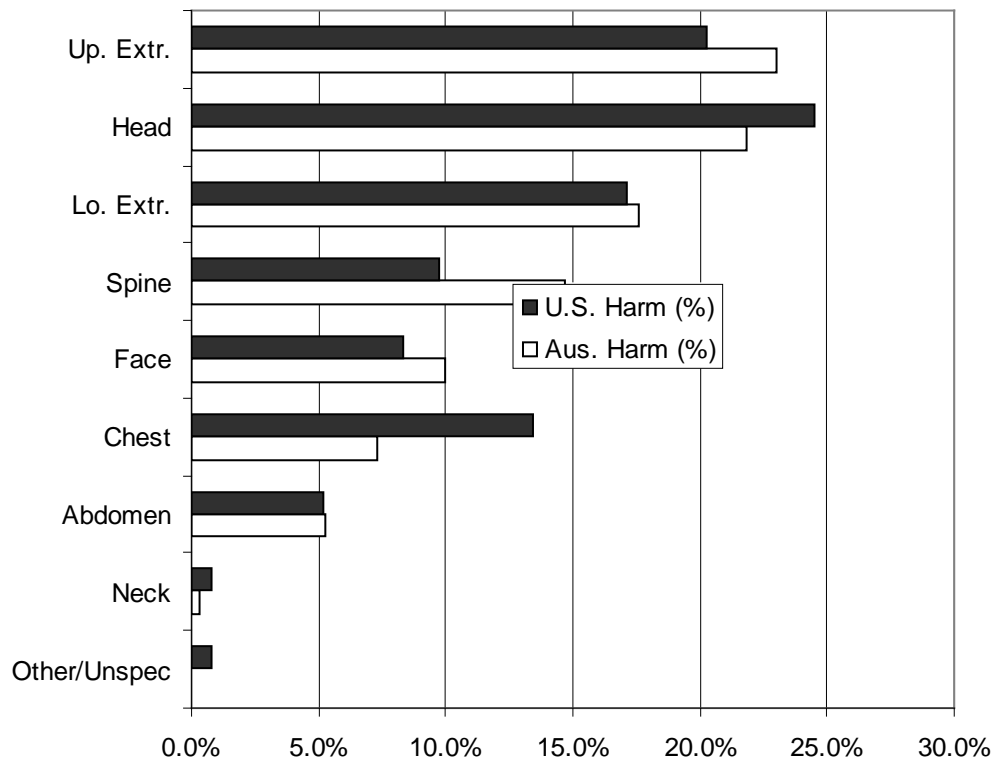
- To quantify injuries and identify mechanisms of injury in far side impact;
- To identify attributes that may affect injury risk;
- To help develop probability of trauma functions for measuring injury risk in this crash mode. At a minimum the functions were to include:
 1. a head injury criteria,
 2. a trauma metric for hard-structure neck injury,
 3. the best construction of a metric for carotid artery dissection, and
 4. an abdominal criteria for far-side impact.
- To help develop and quantify injury risk parameters (for both soft tissue and bone fracture) for use in assessment of potential safety countermeasures.

This document reports on the work carried out in part fulfilment of the requirements for Task 5, the investigation of injury criteria suitable for use with occupants in far side impacts. The report includes both the identification of existing risk functions and the development of new functions as appropriate for use in dummy development, establishing injury criteria, and in modelling and countermeasure programs.

5.2 INJURY IN FAR SIDE IMPACTS

5.2.1 Injury Priorities

In a recent paper, Gabler et al. (2005a) evaluated the risk of side impact injury for far side impact. This analysis was based on NASS/CDS 1993-2002 and examined injury outcomes for over 4500 three-point belted occupants of cars, light trucks and vans involved in a far side impact. This analysis is used in this report to characterise the impact conditions that lead to far side injury and to set the priorities for the development of a comprehensive set of injury risk functions. In a second paper, Gabler et al. (2005b) compared the situation in Australia and the USA. The injury priorities for the body regions as a result of far-side impacts from Gabler et al. (2005b) are shown in Figure 5.1 and listed in Table 5.1 for both the USA and Australia. The injured body regions with the highest priority in terms of HARM were found to be the upper extremities, the head, the lower extremities followed by the spine, face, chest and abdomen.



**Figure 5.1 Injury priorities of body regions as a result of far-side impacts
(from Gabler et al. 2005b)**

**Table 5.1 Injury priorities of body regions as a result of far-side impacts
(based on Gabler et al. 2005b)**

PRIORITY	BODY REGION	% HARM	
		AUS	USA
1	UPPER EXTR	23.0	20.3
2	HEAD	21.8	24.5
3	LOWER EXTR	17.6	17.1
4	SPINE	14.7	9.7
5	FACE	10.0	8.3
6	THX (+HLSK)	7.3	13.4
7	ABD (-LSK)	6.3	5.2
8	NECK	0.3	0.8
9	OTHER	0.0	0.8

In Figure 5.2, the distribution of injuries by the principal direction of force (PDoF) in the crash is presented, where zero degrees is the front of the car. The testing and modelling must be capable of reproducing the impacts with a PDoF between 30° and 90° (please note that a PDoF between 30° and 90° is quite different from an angle between 30° and 90°).

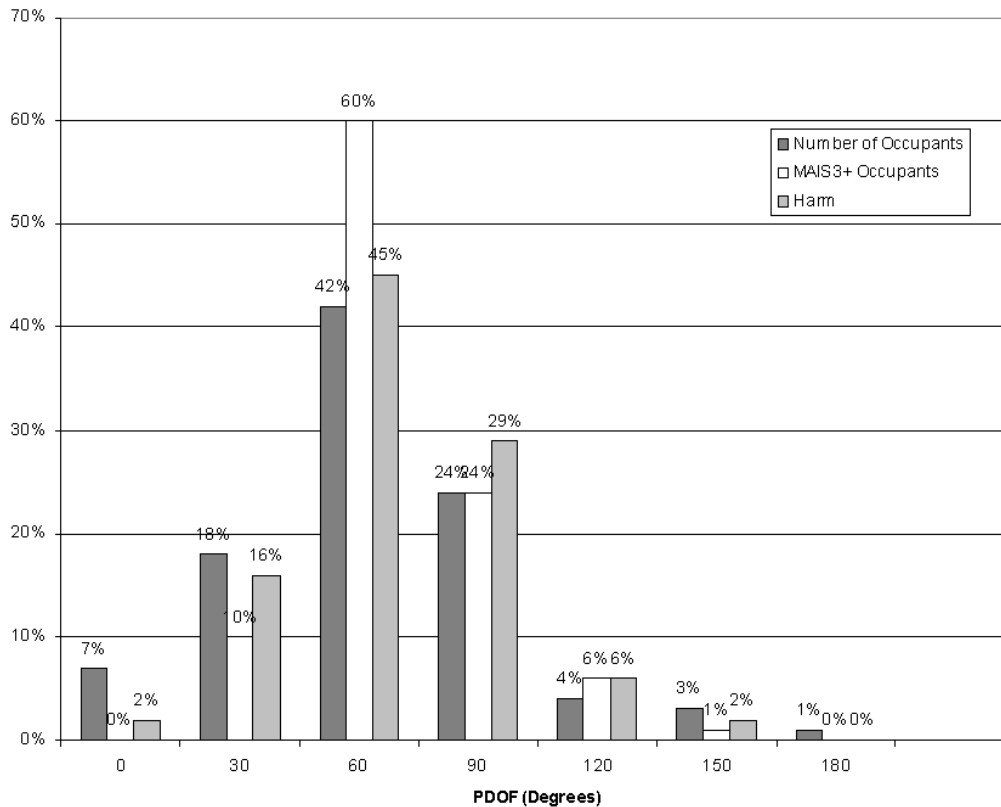


Figure 5.2 Injury by PDoF as a result of far side impacts from Gabler et al. (2005a)

The most common vehicle interior contacts found by these researchers for the occupants in far side impacts are listed in Table 5.2.

Table 5.2 AIS 3+ injuries to belted front seat occupants in far side impact by injuring contacts, NASS/CDS 1988-1998 Gabler et al.

INJURY SOURCE	ALL OCCUPANTS (%)	DRIVERS (%)	RF PASSENGERS (%)
R/S Interior	26.7	30.5	0
Seatbelt	20.8	22.6	8.5
Roof	12.2	13.1	5.9
All other	8.7	8.2	12.4
Seat	7.5	3.5	35.4
L/S interior	7.2	8	1.7
Non contact	6.4	6	9
Dashboard	5.2	4.3	11.4
Other occupant	2.9	1.4	13.2
Steering system	2.4	2.4	2.5

These are the source of injury and are important both in getting the injury risk function correct and in the design of counter-measures. The contact will be dealt with in more detail in the following section along with the body regions injured.

Based on the far side accident data in Gibson et al. (2001b), the injury priorities for far side collisions were assessed by body region total Harm. The priority for the body regions with the three highest priority AIS injury severities are listed in Table 5.3. These priorities guided the risk function development.

Table 5.3 The injury priorities for far side are listed, based on the individual body region Harm along with the three highest priority AIS injury severities for each region (the darker the shading the higher priority), Gibson et al. (2001b).

Body Region	AIS 1	AIS 2	AIS 3	AIS 4	AIS 5	AIS 6
Upper Extremities						
Head						
Lower Extremities						
Spine						
Face						
Thorax (inc HLSK)						
Abdomen (-LSK)						
Neck						
Shoulder						
Pelvis						

5.3 SPECIFIC INJURIES IN FAR SIDE CRASHES

A brief case review was undertaken of the actual injuries suffered in be belted drivers in far side impacts in NASS for the years 2002 (n = 27 cases) and 2003 (n = 32 cases), Digges (2006). The aim of this review was to assist in understanding the specific injury types and the typical contacts causing these injuries. The injury types by body region for these belted drivers are given in Figure 5.3 for the upper and lower extremities and pelvis, Figure 5.4 for the head, Figure 5.5 for the neck and spine, Figure 5.6 for the thorax and Figure 5.7 for the abdomen.

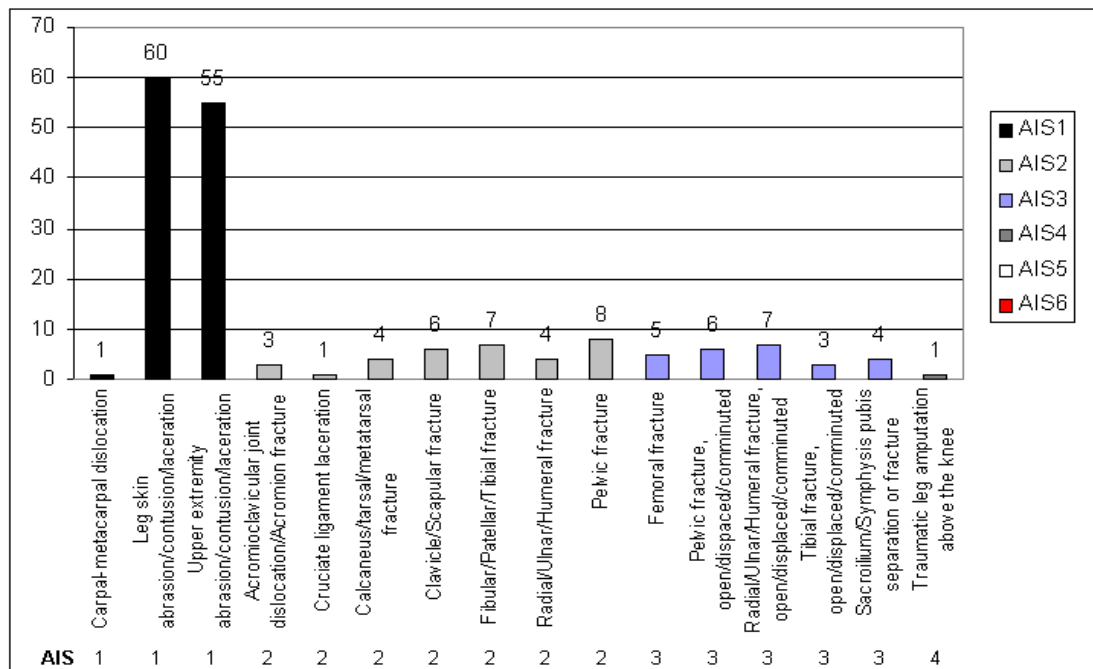


Figure 5.3 Injury to the upper and lower extremities and pelvis of belted drivers in far side impacts in NASS for the years 2002 (n=27) and 2003 (n=32).

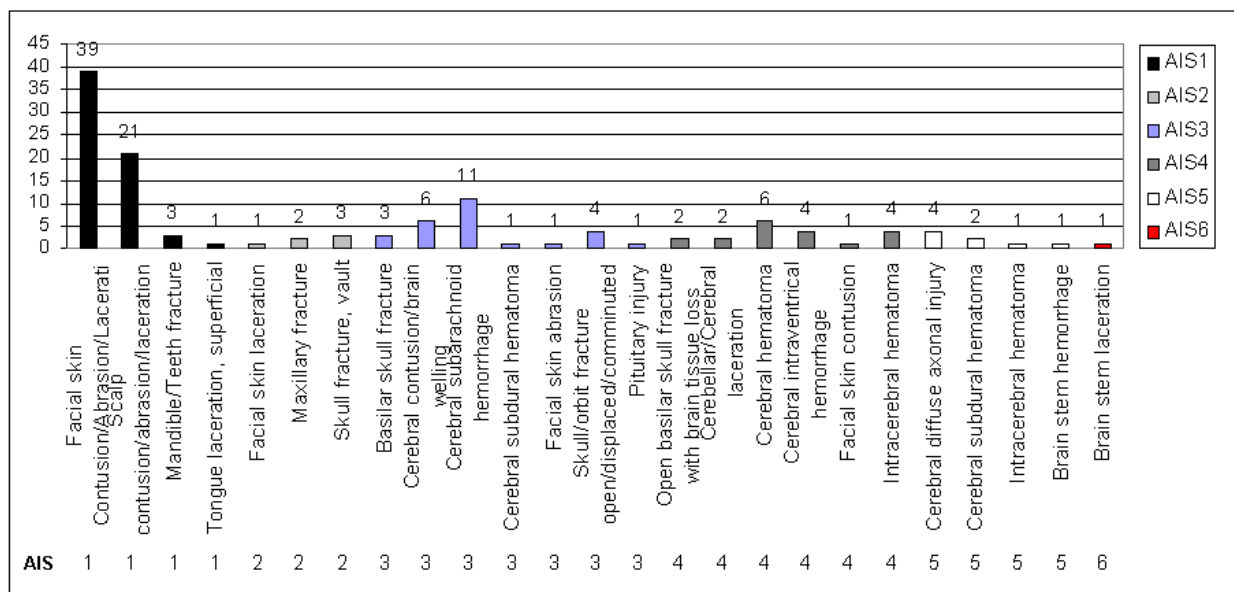


Figure 5.4 Injury to the head and face of belted drivers in far side impacts in NASS for the years 2002 (n=27) and 2003 (n=32).

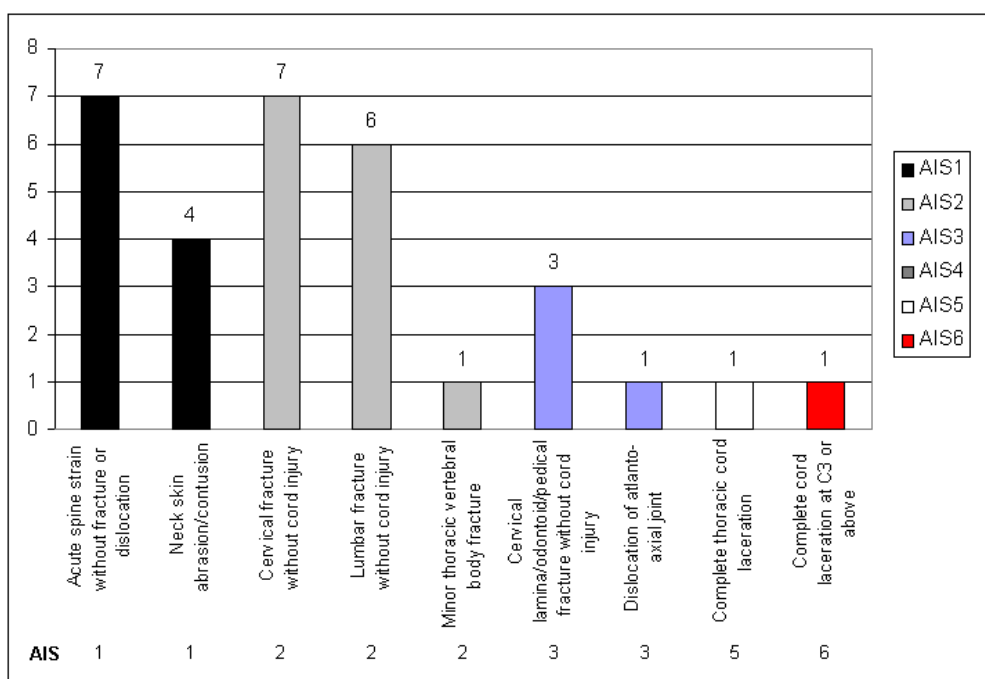


Figure 5.5 Injury to the neck and spine, belted drivers in far side impacts in NASS for the years 2002 (n=27) and 2003 (n=32).

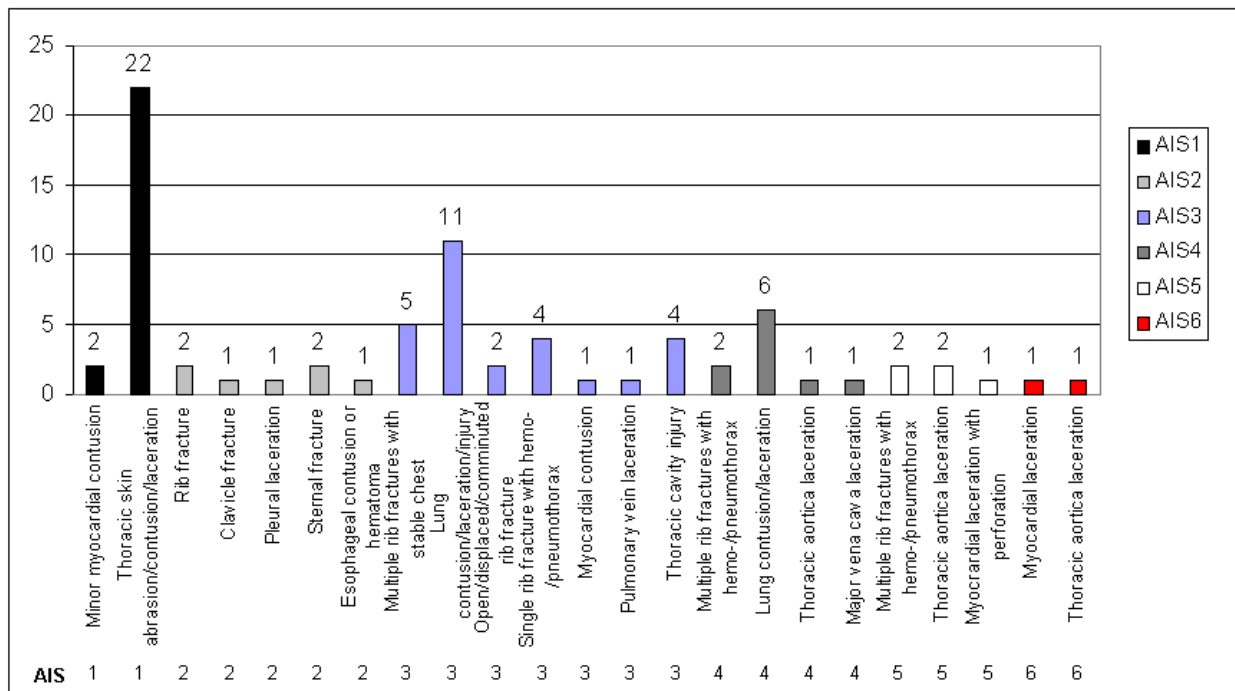


Figure 5.6 Injury to the thorax, belted drivers in far side impacts in NASS for the years 2002 (n=27) and 2003 (n=32).

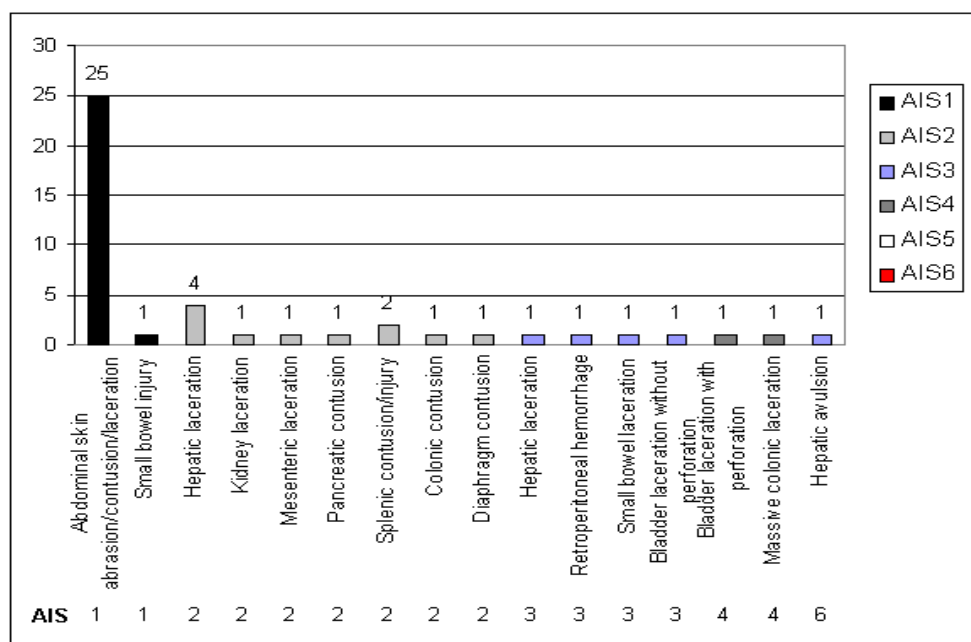


Figure 5.7 Injury to the abdomen, belted drivers in far side impacts in NASS for the years 2002 (n=27) and 2003 (n=32).

5.4 SUMMARY

In summary, the priorities for the capabilities required for the test dummy and the associated injury risk functions for injury in far side impacts have to deal with the following for current restraint systems:

- The highest priority injuries in far side crashes are to the head and face, spine, thorax, upper and lower limbs.
- The impact direction (crash PDoF) is between 30° and 90°.
- The most common vehicle components involved are: the vehicle interior, restraint system, roof, seat, dashboard and steering wheel.

5.5 AVAILABLE DUMMIES

Of utmost importance in a project based on the use of a dummy to predict impact injury, is that the dummy have high levels of biofidelity in its responses. The available test data indicates that the most biofidelic side impact dummy is the WorldSID, Hautmann et al. (2003) and Scherer et al. (2001). The biofidelity of the WorldSID pictured in Figure 5.8 was the most recent side impact dummy and found to be potentially suitable for use as a regulatory dummy in far side testing (Fildes et al 2002).

The sign conventions used with the dummy are indicated in Figure 5.9 and the instrumentation fitted to the WorldSID in the tests at WMC, Pintar et al. (2006), for this project is summarised in Table 5.4. The injury risk functions developed in this report need to be supported by the available instrumentation fitted to the WorldSID. Instrumented upper and lower extremities are available for use in the WorldSID, Scherer et al. (2001), but are not shown here.



Figure 5.8 The WorldSID prototype dummy

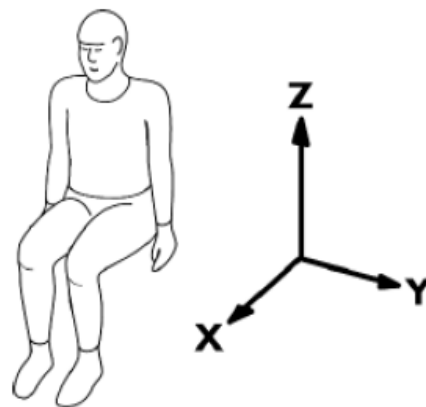


Figure 5.9 Sign convention used in the report

Table 5.4 WorldSID instrumentation used by WMC in testing for this project.

Channel Description	Axes	Filter	Units
Head CG Acceleration	X,Y,Z	CFC1000	G
Head Angular Acceleration	X,Z	CFC1000	RSS
Upper Neck Force	X,Y,Z	CFC1000	N
Upper Neck Moment	X,Y,Z	CFC600	Nm
Lower Neck Force	X,Y,Z	CFC1000	N
Lower Neck Moment	X,Y,Z	CFC600	Nm
T1 Acceleration	X,Y,Z	CFC1000	G
T4 Acceleration	X,Y,Z	CFC180	G
T12 Acceleration	X,Y,Z	CFC180	G
Pelvis Acceleration	X,Y,Z	CFC180	G
Shoulder Acceleration	X,Y,Z	CFC600	G
Thorax Rib 1 Acceleration	X,Y,Z	CFC1000	G
Thorax Rib 2 Acceleration	X,Y	CFC1000	G
Thorax Rib 3 Acceleration	X,Y,Z	CFC1000	G
Abdomen Rib 1 Acceleration	X,Y,Z	CFC1000	G
Abdomen Rib 2 Acceleration	X,Y,Z	CFC1000	G
Shoulder Displacement	Y	CFC600	mm
Thorax Rib 1 Displacement	X,Y,Z	CFC600	mm
Abdomen Rib 1 Displacement	X,Y	CFC600	mm
Shoulder Force	X,Y,Z	CFC600	N
Lumbar Force	X,Y,Z	CFC1000	N
Lumbar Moment	X,Y,Z	CFC1000	Nm
Pubic Force	Y	CFC1000	N

The THOR is an adelta-Vanced frontal test dummy sponsored by the NHTSA, as explained in Haffner et al. (2001). The research presented in Chapter 3 concluded that both the WorldSID and THOR had adequate biofidelity to permit their use in developing far side countermeasures. However, only the WorldSID has calibration procedures and injury measures for the side impact crash mode. For this reason, this task addressed the injury measures required by WorldSID in order to specifically address far side issues.

5.6 AVAILABLE INJURY RISK FUNCTIONS

The available injury risk functions for the individual body regions for injury causation and prediction and match with dummy capability, following the priority order:

5.6.1 Whole Body Lateral Loading of Restrained Volunteers

Zaborowski (1966) tested young male volunteers (n=52) to determine human tolerance to lateral impacts when wearing a restraint. The seatbelt used was a harness with two straps over the shoulders attached to a lap belt. The subjects were exposed to a total of 87 impacts at average accelerations from 4.5 to 11.6 g with no permanent physiological changes noted. The subject complaints (to 60%) increased above 8.8 g exposure. The experiments were halted for medical reasons after two subjects were subjected to the 11.6 g acceleration pulse. One of the subjects showed a marked cardiovascular response with rapid decrease in blood pressure and heart rate (bradycardia). Approximately 60 seconds post test the subject fainted in the seat. The author reported other similar results following lateral testing of volunteers.

5.6.2 Upper Extremities

In Chapter 2, it was found that the most common AIS3+ upper extremity injury were displaced and open fractures to the ulna (62%), to the radius (30%) and to the humerus (8%). Figure 5.3 gives the actual injuries to the upper extremities in far side crashes. There are instrumented upper limbs available for the WorldSID, but these do not include instrumentation for the hand.

The most obvious injury criteria to use are long bone lateral fracture force and bending moment. Lund (2003) suggested the following criteria for upper extremity injury based on work performed by Begeman & Pratima (1999) and Pintar et al (1998) for the radius and ulna and by Kirkish et al (1996) for the humerus:

- Bending moment for the 50th male humerus (upper arm) is 214 Nm.
- Bending moment for fracture of the 50th male ulna (forearm) is 90 Nm.

These values have been scaled by Mertz and Irwin (2003) for a range of occupants. Duma et al. (1999) used a dynamic three point bending test with a 9.48 kg impactor, released from a drop height of 2.0 m to give an impact velocity of 4.42 m/s. This velocity was chosen to match radius and ulna strain rates as measured in cadaver tests with driver side air bags (Bass et al., 1997). Three matched pairs of female forearms were tested with one forearm supinated and the other pronated to compare the differences. Within the three matched pair tests, the supinated position was significantly stronger ($p = .02$) than the pronated position with a 21% higher average peak moment of 92 ± 5 Nm versus 75 ± 7 Nm respectively.

Duma et al. (2003) developed injury risk functions for the 5th female dummy. They presented equations for bending of the humerus and forearm and axial loading of the wrist and elbow.

$$\text{Forearm Moment} = \sqrt{(MX)^2 + (MY)^2}$$

$$\text{Humerus Moment} = \sqrt{(MX)^2 + (MY)^2}$$

$$\text{Wrist Load} = -FZ - (0.47) \cdot AZ$$

$$\text{Elbow Load} = \sqrt{(-FZ + (0.74) \cdot AZ)^2 + (FX + (0.74) \cdot AX)^2}$$

The risk functions predicted a 50% risk of injury at 128 Nm bending of the humerus, 58 Nm bending of the forearm, 1700 N axial loading of the wrist, and 1780 N axial loading of the elbow. Subsequently, Duma et al. (1997) developed injury risk functions for the humerus and forearm of the 50th male.

5.6.3 Head and Face

Injury priorities of body regions as a result of far-side impacts based on Gabler et al. (2005b) show the head and face as each individually having high priority. Head injuries were the most frequent injuries, caused the most Harm and were the most debilitating and life threatening injuries that occurred. The analysis also identified that head injuries of AIS 3 and greater severity caused the most Harm, and hence warranted priority in occupant protection considerations. Gabler et al. (2005a) found that the leading source of injury to the head were contacts with the right interior (occupants in study were mainly drivers of left hand drive vehicles), roof, centre panel and right roof rail, shown in Figure 5.10.

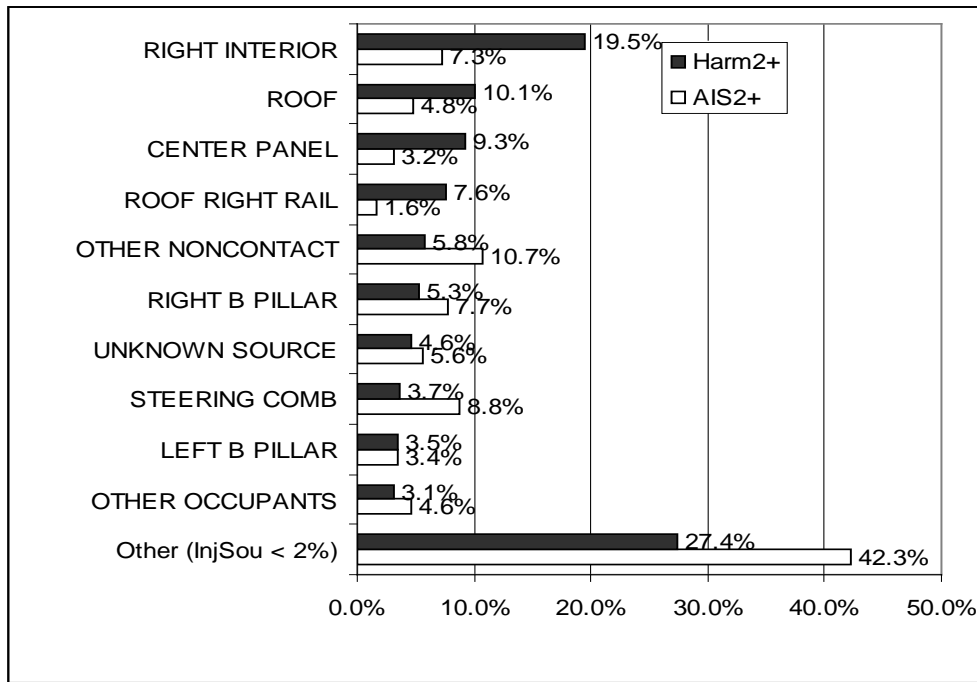


Figure 5.10 Source of AIS2+ head injury as a result of far-side impacts from Gabler et al. (2005a)

The direction of impact to the head and face in far-side collisions is not known at present. McLean et al. (1997) showed the location of fatal head injuries to vehicle occupants to be spread over the forehead, face, laterally and the crown in frontal crashes, see Figure 5.11.

Even though these contacts were from frontal crashes, real-world crash analysis suggests that, for the occupant on the non stuck side, the occupant will see lateral impacts to the head and also frontal and crown impacts. This suggests we want risk curves for the front and side or one set of curves that are sufficient to handle both conditions.

- The WorldSID head is only calibrated for lateral impacts on a rigid surface. It is presumed the head is also valid for impacts to the forehead, as for HIII dummy.
- The WorldSID head has both translational and rotational acceleration measurement capability.



Figure 5.11 Location of fatal head injuries to car occupants, MacLean et al. (1997)

The most commonly used indicator of head injury based on the acceleration of the head resulting from an impact, HIC (Head Injury Criterion) is defined as:

$$HIC = \max \left[\frac{1}{(t_2 - t_1)} \int_{t_1}^{t_2} a(t) dt \right]^{2.5} (t_2 - t_1)$$

where: $a(t)$ = resultant acceleration of the head's centre of gravity during the $t_2 - t_1$ time interval (G)

$t_2 - t_1$ = time interval during the acceleration pulse in which $a(t)$ attains a maximum value (ms)

HIC is based on the Wayne State University Concussion Tolerance Curve (Figure 5.12). This curve plots the effective translational acceleration of the head, which is an average anterior-posterior acceleration of the skull measured at the occipital bone, in impacts of the forehead with a rigid planar surface, against effective duration of the pulse (SAE 1980). The latter part of the curve with the asymptotic value of 42G is based on volunteer whole body data, which did not involve direct blows to the head. Patrick et al. (1965) recommended that this asymptotic value be raised to 80G. This revised level has been used as the basis of the U.S. Federal Motor Vehicle Safety Standards (FMVSS 208).

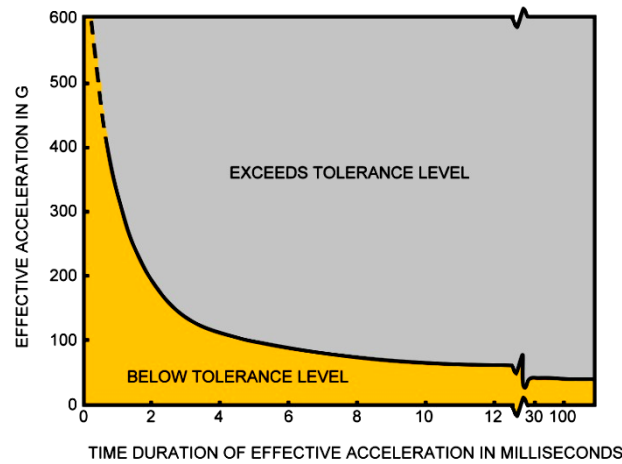


Figure 5.12 The Wayne State University Concussion Tolerance Curve, after SAE (1980).

Mertz et al. (2003) published a skull fracture risk curve with peak resultant acceleration of the head centre of gravity (CG) for the adult population, based on published cadaver head impact data. Using this, a 180G limit for the head acceleration as a result of direct impact for the 50th-percentile male Hybrid III dummy was proposed. This value is based on a 5% risk of skull fracture for the adult population, and represents a less than 5% risk for the mid-sized male (see Figure 5.13).

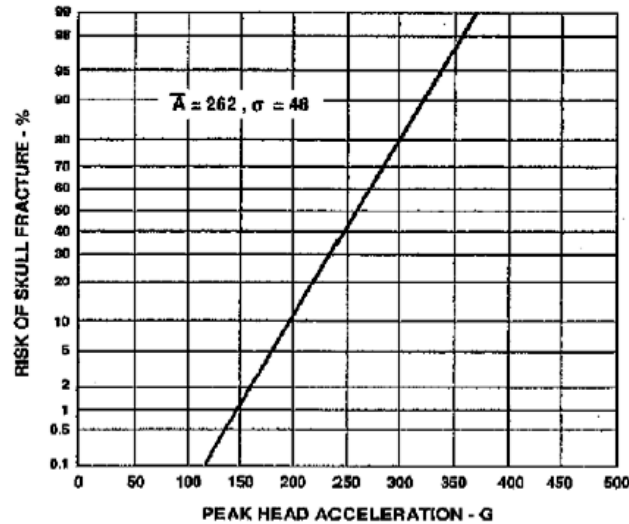


Figure 5.13 Skull fracture risk curve for the adult population based on peak head acceleration, from Mertz, Irwin, and Prasad (2003)

The recommended Injury Reference Values for HIC are the same as given in the Alliance (1999) recommendation to NHTSA for the OOP assessment of frontal airbags. For the average sized adult male, HIC of 700 corresponds approximately to a 5 percent risk of an AIS 4 or greater injury (Mertz et al., 1997). This value was scaled to give the Injury Reference Values for other sizes of occupants. The scaling method used takes into account size and brain tissue strength variation with age as described by Mertz et al. (1997). For all dummy sizes, the time interval of the search for the maximum HIC value was not to exceed 15 ms.

The curves proposed by NHTSA expanded from the Mertz/Prasad AIS 4+ brain injury curve go from AIS1 (concussion) through to fatal head injury form an appropriate method for assessing the risk of head injury (see formulae below and Figure 5.14 for a plot of the risk curves). These curves have reasonable matches with the other risk functions based on HIC available for comparison, such as for lateral head impact derived by Gibson et al. (2001) and the AIS 4+ brain injury risk curves derived by Mertz et al. (2003) for frontal impacts.

$$\text{MAIS 1: } [1 + \exp((1.54 + 200/\text{HIC}) - 0.0065 \times \text{HIC})]^{-1}$$

$$\text{MAIS 1: } [1 + \exp((2.49 + 200/\text{HIC}) - 0.00483 \times \text{HIC})]^{-1}$$

$$\text{MAIS 1: } [1 + \exp((3.39 + 200/\text{HIC}) - 0.00372 \times \text{HIC})]^{-1}$$

$$\text{MAIS 1: } [1 + \exp((4.9 + 200/\text{HIC}) - 0.00351 \times \text{HIC})]^{-1}$$

$$\text{MAIS 1: } [1 + \exp((7.82 + 200/\text{HIC}) - 0.00429 \times \text{HIC})]^{-1}$$

$$\text{Fatal: } [1 + \exp((12.24 + 200/\text{HIC}) - 0.00565 \times \text{HIC})]^{-1}$$

Figure 5.14 Formulae for the expanded Prasad/Mertz curves derived by NHTSA (1995).

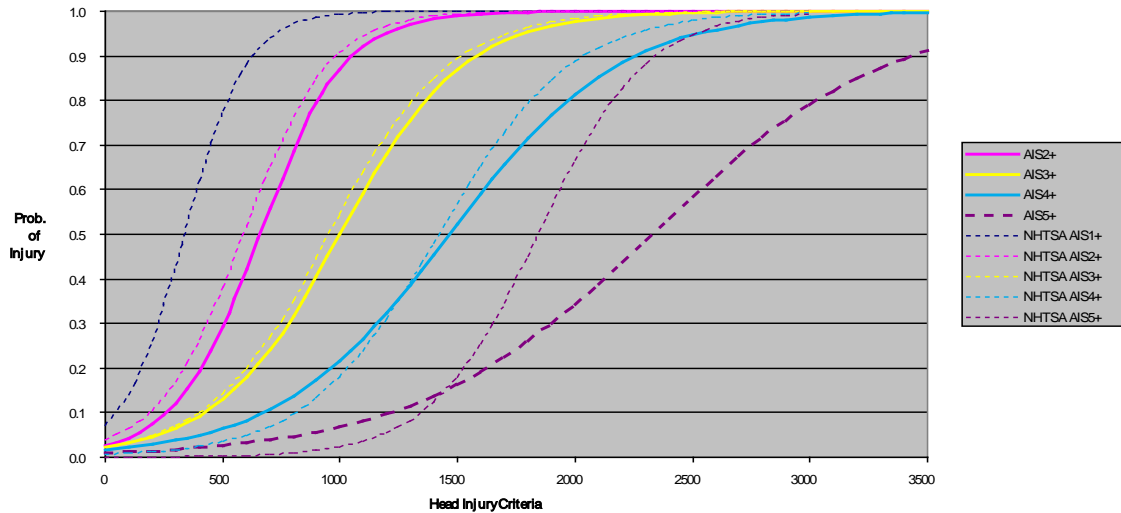


Figure 5.15 A comparison of the various risk of probability of head injury versus HIC curves the expanded Mertz/Prasad curves derived by NHTSA (1995) for frontal impacts to the head and AIS 2, 3, 4 and 5 curves derived by Gibson et al. (2001) for lateral impacts to the head.

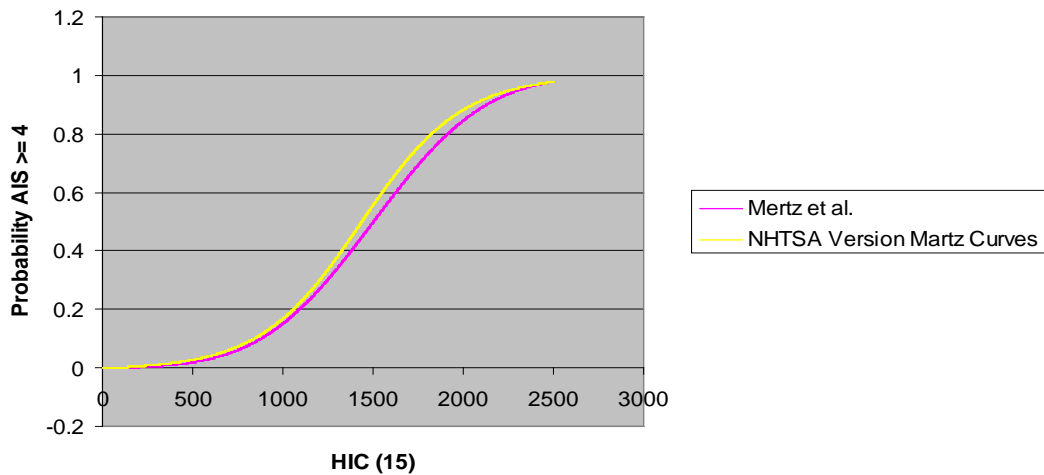


Figure 5.16 Comparison of the Mertz (2003) AIS4+ injury risk curve and AIS 4 NHTSA (1995) expanded curves for frontal impact.

At the low severity end, the AIS 1 curve for 15 ms impact durations Newman et al. (2000) reconstructed helmeted head impacts leading to MTBI in footballers. These researchers found that a 50% probability of concussion was found for a HIC of 240 and observed that the head was less sensitive to anterior posterior impacts than lateral.

The JARI Human Head Tolerance Curves, JHTC, were developed to overcome some of the deficiencies with the Wayne State curve. They generally supported the shape and values suggested in the WSTC. The frontal impact JHTC data show that the threshold for human skull fracture is slightly higher than that for cerebral concussion. The lateral head impact work at JARI was discussed in more detail by Kikuchi et al. (1982) and it was found that the tolerance for skull fracture as a result of lateral impacts was lower than for sagittal and occipital impacts, but that the threshold for concussion was higher. Ono (1998) suggests, “. . . *The concussion threshold against lateral impact . . . is located twice as high above the curve of sagittal [frontal] impact.*”

Ommaya (1988) summarized the many experimental animal studies with which he had been involved, and extrapolated from the experimental data, proposing limits for allowable rotational acceleration for the human head. These limits are given in Table 5.6. He went further and suggested that a combined

criteria was necessary for the prediction of head injury, and that such a criteria must link both rotational and translation effects.

Table 5.6 The allowable limits for rotational acceleration and velocity measured about the centre of gravity of the head (Ommaya 1988)

Rotational Velocity Change rad/s	Rotational Acceleration rad/s ²	AIS
>30	<1700	2
	<3000	3
	<3900	4
	<4500	5
<30	<4500	0 or 1
	<4500	5

Margulies and Thibault (1992) proposed human tolerance criterion for diffuse axonal injury specifically for lateral rotational loads to the head. This criterion was based on a combination of animal studies, physical models and analytical models. The animal data was scaled to human brain geometry and several different brain masses were used to derive threshold curves for the onset of moderate to severe diffuse axonal injury (DAI), see Figure 5.17.

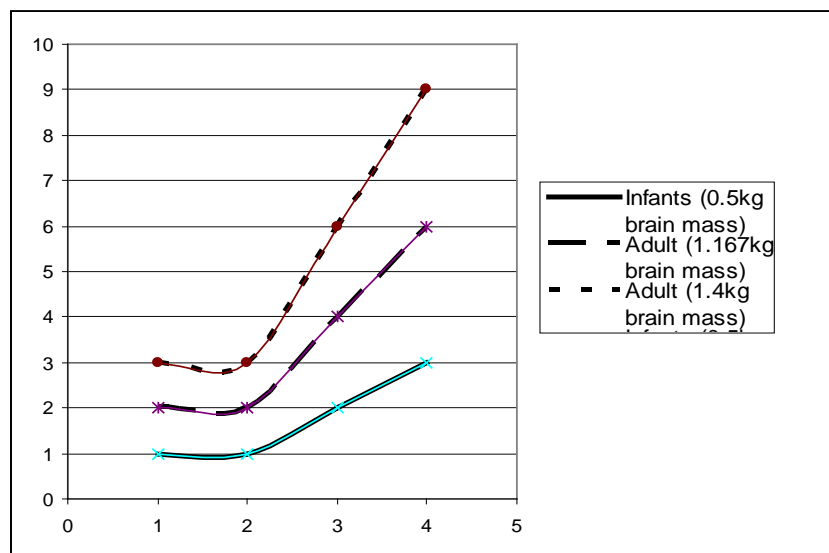


Figure 5.17 Moderate to severe diffuse axonal injury (DAI), thresholds for a range of human brain masses, for infant (500g brain mass, heavy solid line) and adult (1067g, solid line and 1400g, dashed line), Margulies and Thibault (1992)

Gennarelli and co-workers studied the effects of pure angular acceleration, i.e., without direct impact to the head, on brain injuries. Their exhaustive research using subhuman primates and physical models led to the development of rotational acceleration thresholds for varying levels of brain injury including concussion, diffuse axonal injury (DAI), and subdural hematoma. More recently, Gennarelli et al. (2003) synthesized these data and proposed angular acceleration thresholds for diffuse brain injuries as a linear function of varying severities (equation 3, $R^2 = 0.99$), described by the Abbreviated Injury Scale,

$$\dot{\omega} = 2.88 * AIS$$

where, $\dot{\omega}$ is the rotational acceleration (krad/sec²) and AIS represents the injury severity values in the length of unconsciousness section according to AIS 1998 version.

Rotational acceleration thresholds have been established from non contact experiments, Margulies and Thibault (1992). Other studies have examined angular acceleration magnitudes resulting from head contact. Meaney et al. (1994) used computer models of head contact to develop inertial loading conditions for diffuse brain injuries in minor to moderate collisions. A ΔV of 74 km/h was found to be needed to exceed the tolerance for concussion and “yet higher velocities for mild to severe DAI”. These researchers’ conclusions on the significance of head contact had support from real-world epidemiological studies, for example Morris et al.(1993). McLean found no cases with brain injury in the absence of evidence of head impact in an analysis of 414 fatal cases of road users in Australia.

5.7 LOWER EXTREMITIES

In Chapter 2, it was reported that the leading source of AIS3 lower extremity injury in far side cases were the result of contacts with the centre panel, the transmission lever followed by the right interior of the vehicle. The most common injury was found to be fractures of the long bones, the femur, tibia and fibula. Injury to the knee and ankle joints also needs to be considered.

There are existing injury risk curves for the lower extremities but these mainly relate to frontal impacts, Mertz (2003). The use of the injury criteria for long bone bending for pedestrian impacts based on Ivarsson et al. (2004) and others is a good approach. This is supported by the IIHS side impact requirements, IIHS (2004). The IIHS (2004) report on side impact test program rating specifies a degree of acceptability for distal femur A-P and L-M moment (3 msec clip) of an M_{femur} of 255 – 305 Nm.

Konosu et al. (2005) of the Japan Automobile Research Institute (JARI) reviewed recent lower leg injury tolerance, which are summarized in Table 5.7 below.

Table 5.7 Recent lower leg injury tolerance values for pedestrian leg impacts selected by Konosu et al. (2005).

Body regions		50% injury risk level for 50 percentile American male (tentative)	References
Leg		BM (312 - 350 Nm)	BM (312 Nm): Kerrigan et al., 2004 BM (350 Nm): INF GR/PS/82
Knee	MCL	EL (18 - 20 mm)**	BA (18 deg.): Ivarsson et al., 2004 BA (20 deg.): INF GR/PS/82
	ACL	EL (10 mm)***	SD (10 mm): IHRA/PS/309
	PCL	EL (10 mm)***	SD (10 mm): IHRA/PS/309
Thigh		BM (372-447 Nm)	BM (372 - 447 Nm): Kerrigan et al., 2004 BM (390 - 395 Nm): Kennedy et al., 2004

* BM: Bending moment, EL: Elongation, BA: Bending angle, SD: Shearing displacement.

** Estimated from BA (18-20 deg.), *** Estimated from SD (10 mm)

Kerrigan et al. (2004) found the risk function for femur fractures (see Figure 5.18) to be:

$$p(\text{femur fracture}) = 1 - \text{EXP} [-\text{EXP}(6.24242 \ln(M_{\max}) - 38.45762)] .$$

Kennedy et al. (2004) did 45 experiments on the femur of PMHS using a dynamic three-point drop test. They found no significant difference between the lateral-medial bending experiments and the posterior-anterior bending experiments. These investigators determined

$$p(\text{femur fracture}) = 1 - \text{EXP} \{-\text{EXP}[7.1613 \ln (M_{\max}) - 42.987]\}$$

as the risk of femur fracture for the 50th male.

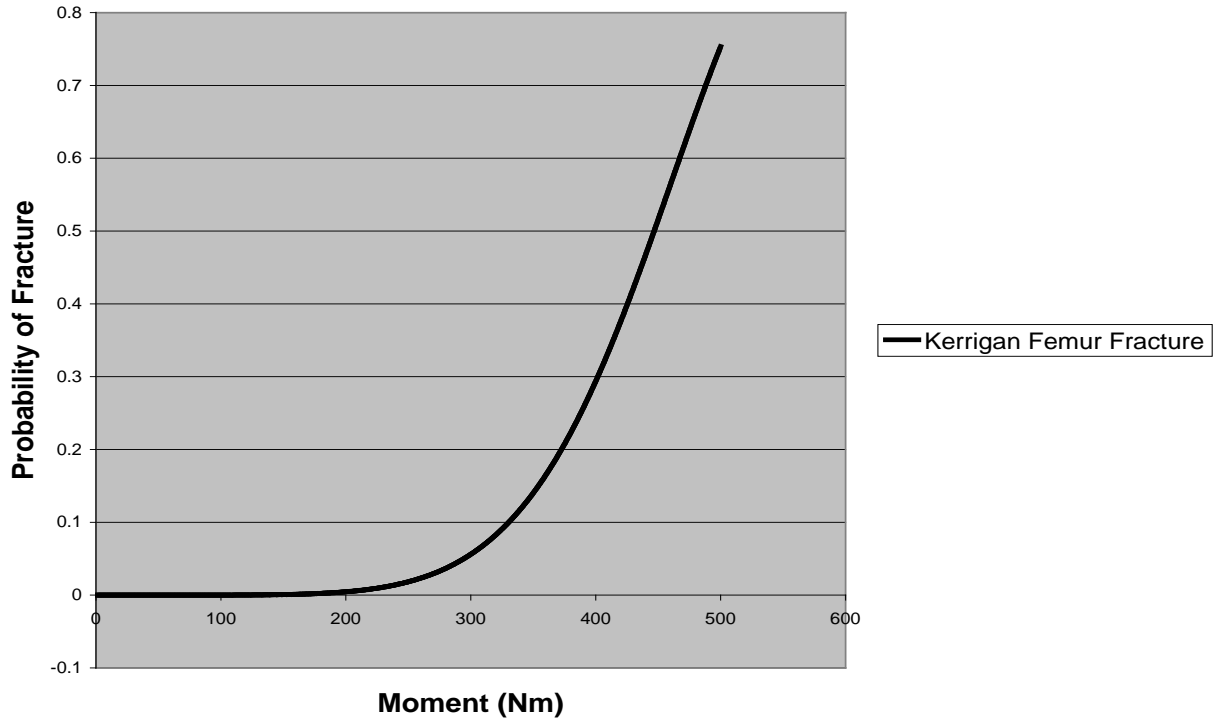


Figure 5.18 Femur fracture risk function from Kerrigan et al. (2004).

Kerrigan et al. (2004) also found a risk function for tibia fractures:

$$p(\text{tibia fracture}) = 1 - \text{EXP}[-\text{EXP}(5.69112 \ln(M_{\max}) - 33.05211)]$$

Mertz et al. (2003) proposed a tibia shaft fracture risk curve for the adult male population based on maximum bending moment:

$$\text{Probability density function} = \text{EXP}[-((M - 317)^2)/(15,488)]/(220.5833)$$

$$p(\text{tibia fracture}) = \int_0^M (\text{probability density function}) dM$$

The two functions by Kerrigan et al (2004) and Mertz et al. (2003) give very similar results (see Figure 5.19).

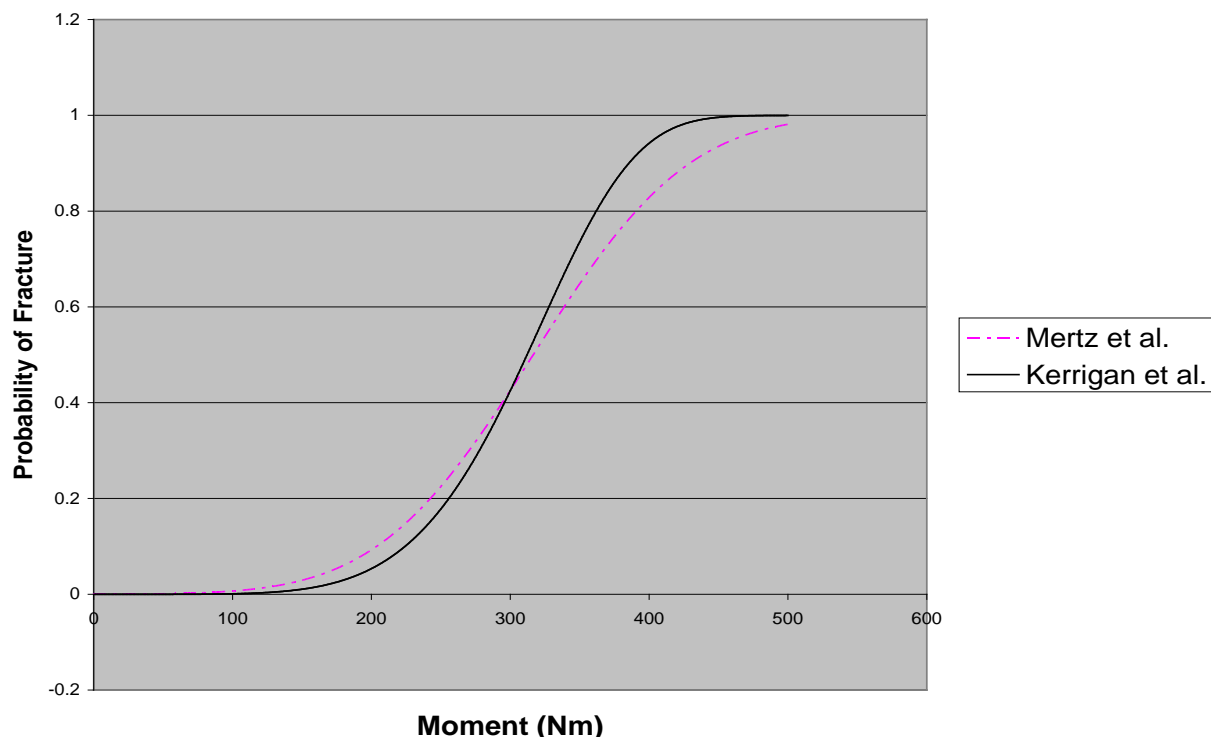


Figure 5.19. Comparison of the tibia fracture risk functions proposed by Mertz et al. (2003) and Kerrigan et al. (2004)

5.8 SPINE

The most representative testing for real crashes of the strength of regions of the spine is of complete spines. The discussion here will only be on the literature concerning the failure properties of multiple vertebral body spinal segments of the thoracolumbar spine, which is the most limited of the three main areas of spinal failure property research. However, there are a few studies that provide valuable insight into the failure properties and failure mechanisms of multiple thoracolumbar vertebral body spinal segments (Yoganandan, et al. 1988; Myklebust, 1989; Duma et al, 2006). The testing type, failure properties, and failure modes of these studies have been summarized by Kemper and Duma (2006), see Table 5.8.

There have been no studies that have investigated the failure properties of multiple thoracolumbar vertebral body spinal segments in lateral bending. However, Demetropoulos (1988) conducted sub-failure stiffness testing on 10 multiple lumbar vertebral body spinal segments, T12-L5, in compression, tension, flexion, extension, lateral bending, anterior shear, posterior shear, and lateral shear. The average maximum sub failure moment in lateral bending was reported to be 113 Nm. The average maximum sub failure load in anterior shear, posterior shear, and lateral shear was reported to be 830 N, 1760 N, and 150 N respectively.

Chandler and Gaudy (1983) developed a lumbar spine injury criteria for the HII dummy based on injuries occurring during ejections from military aircraft of a 5% risk of injury for a compression load of 6.7 kN. This is used by the Federal Aviation Authority (FAA) for testing aircraft seats, FAA (1996).

Table 5.8. Failure properties of multiple vertebral body spinal segments

Reference	Spinal Level	Experiment	Loading Rate	Average Failure Load (N)	Average Failure Moment (N-m)	Failure Mode
Yoganandan (1988)	T3-L5 (9) T2-L5 (4) T4-L5 (1) C2-L5 (2) T6-L5 (2)	compression-flexion	2.5 mm/s	2344 1192 444 679 5418	177 99 289 84 284	Spinal column fracture due to wedging (T10-L2)
	T2-L3 T3-L2 T8-L3	Three-point Bending (flexion)	2.5 mm/s	1681 2170 1432	201 326 129	Center of spine at point of maximum flexural moment
	T12-L5 T4-L4 T10-L2	Four-point Bending (flexion)	2.5 mm/s	4893 1712 1544	245 86 77	Center of spine at point of pure flexural moment and no shear
Myklebust (1989)	T2-T9 T10-L1 (n=14)	compression (neck flexed)	ranged from 10-1200 mm/s	1223 2680	N/R	Wedge fractures from T9-L1
	intact cadaver (n=4)	Compressive load applied to T1	10 mm/s	1788	N/R	wedge /compression fractures at thoracolumbar junction
Duma (2006)	T12-L5 (n=2)	Axial compression (anatomically oriented in seated position)	1000 mm/s	5460	201	wedge /compression fractures of T12
FAA (1996)	Compressive lumbar load limit during restraint system testing POD in line with spinal column		dynamic	6672	-	N/A

5.9 THORAX

Gabler et al. (2005a) found that the leading source of AIS2+ chest injury were contacts with the seat back, the belt webbing or buckle, the right interior (occupants in study were mainly drivers of left hand drive vehicles) and other occupants. The most serious chest injury occurred as a result of impacts resulting in a PDOF of 60°.

Chest IARVs for acceleration of the chest spine (at the T4 vertebra) were proposed by the General Motors Corporation for the 50th-percentile male Hybrid III dummy, Mertz (1984). A 60G limit was imposed based on human volunteer rocket tests (Stapp, 1970) and stunt diver tests (Mertz & Gadd, 1971). A resultant T4 acceleration less than 60G (3 ms criterion) represents a less than 5% risk of significant thoracic organ injury ($\text{AIS} \geq 3$) due to gross chest acceleration. Note that significant injury may still be produced by other means such as chest compression or sternal loading.

Kuppa et al. (2004) suggested an injury assessment curve based on lateral chest deformation based on 34 side impact tests using PMHS, see Figure 5.20.

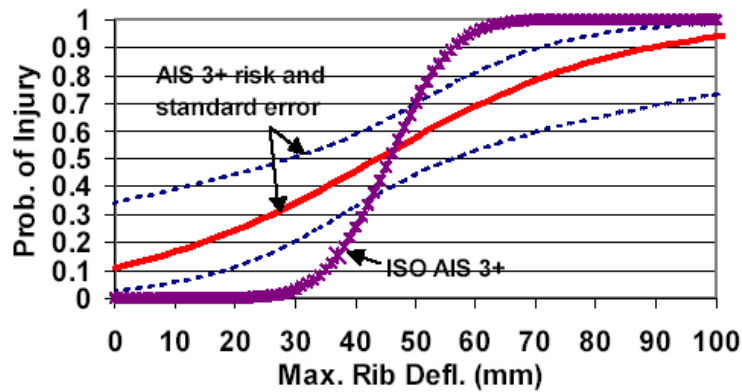


Figure 5.20. Comparison of the AIS 3+ probability of thoracic injury suggested by Kuppala et al. (2004) for with the ISO (2004) risk curve for the EuroSID 1 for rib deflection.

Viano et al. (1995) suggested that it was necessary to use a viscous criterion as well. A $V \cdot C$ value of 1.0 m/s, represents approximately a 5 percent risk of AIS 4+ thoracic injury.

The IIHS (2004) guidelines suggested that a peak deflection 50 mm and a peak $V \cdot C$ of 1.01-1.2 was acceptable.

The ISO (2005) injury risk curves for the chest responses of the WorldSID dummy were developed based on selected PMHS test data, see Figure 5.21 and Figure 5.22.

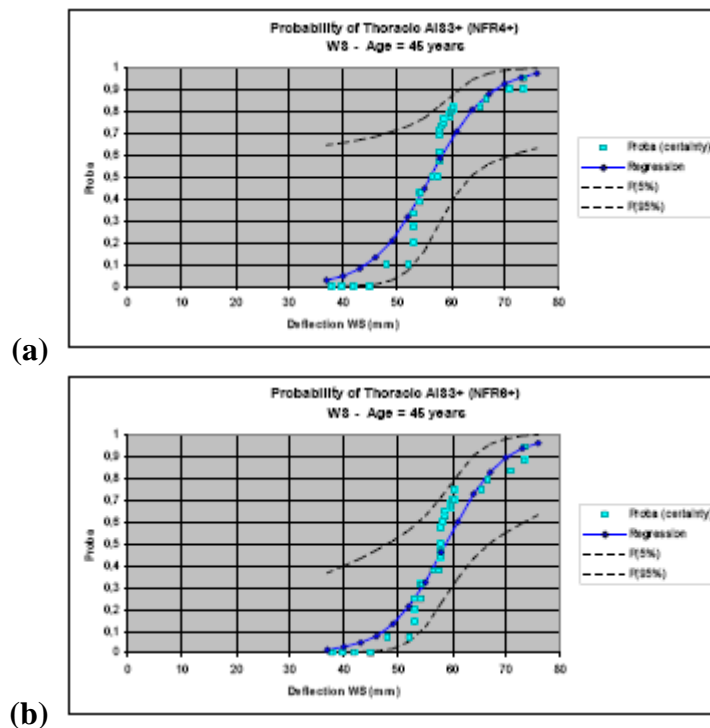


Figure 5.21 Injury risk functions for lateral chest deflection of the WorldSID dummy, from ISO (2005).

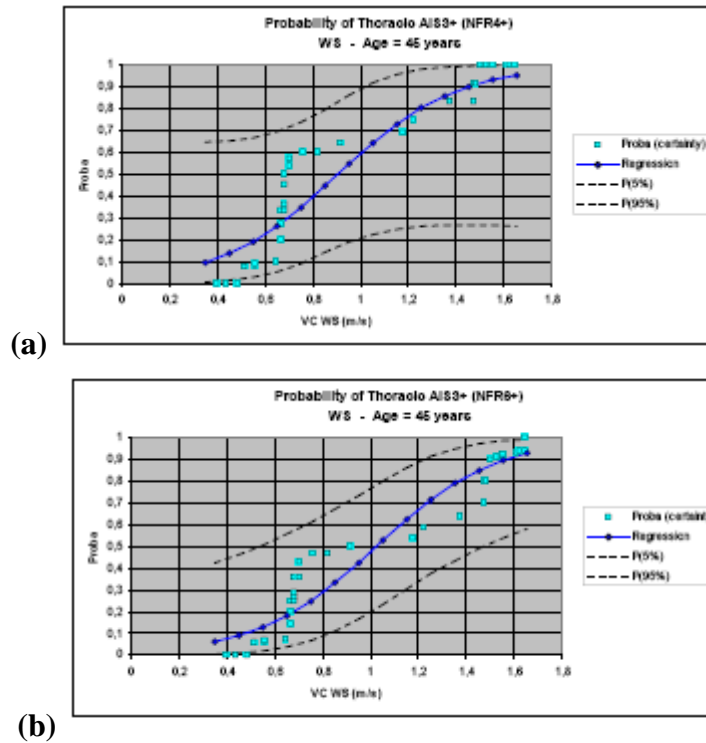


Figure 5.22 Injury risk functions for lateral chest V*C of the WorldSID dummy, from ISO (2005).

5.10 ABDOMEN

Gabler et al. (2005a) found that the leading source of AIS2+ abdominal injury were the result of contacts with the safety belt webbing or buckle (86%), followed by the right interior (7%). For the AIS 3+ injuries the seat belt and buckle were still the most common source of injury (37%), but contacts with the other occupant (10%) transmission lever (9%) and right interior (8%) were significant sources. The most serious abdominal injury occurred as a result of impacts with a PDoF of 90°.

Kuppa (2004) suggested an abdominal injury assessment curve based on total internal abdominal force for the ES 2re, see Figure 5.23.

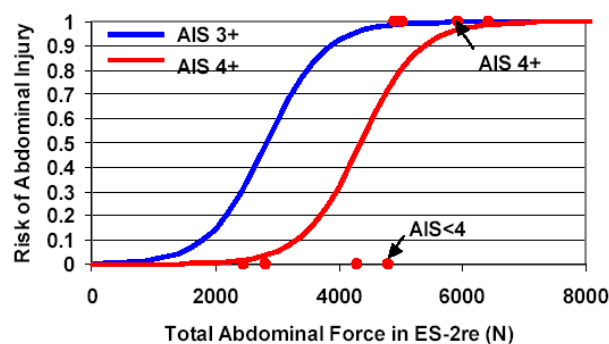


Figure 5.23 Injury assessment curve based on total internal abdominal force for the ES 2re, Kuppa (2004).

Mertz et al. (2003) suggested a limit on internal abdominal load of 2,500 Newton. Rouhana et al. (1985) based on testing with rabbits, found abdominal trauma correlates with V*C.

The IIHS (2004) report sets side impact testing guidelines and rates a V*C of 1.01 – 1.2 as acceptable for the abdomen in lateral crashes.

In ISO (2005) injury risk curves for abdominal responses of the WorldSID dummy were developed based on selected PMHS test data, see Figure 5.24. These functions were based on lower spine acceleration, abdominal deflection and V*C for the dummy.

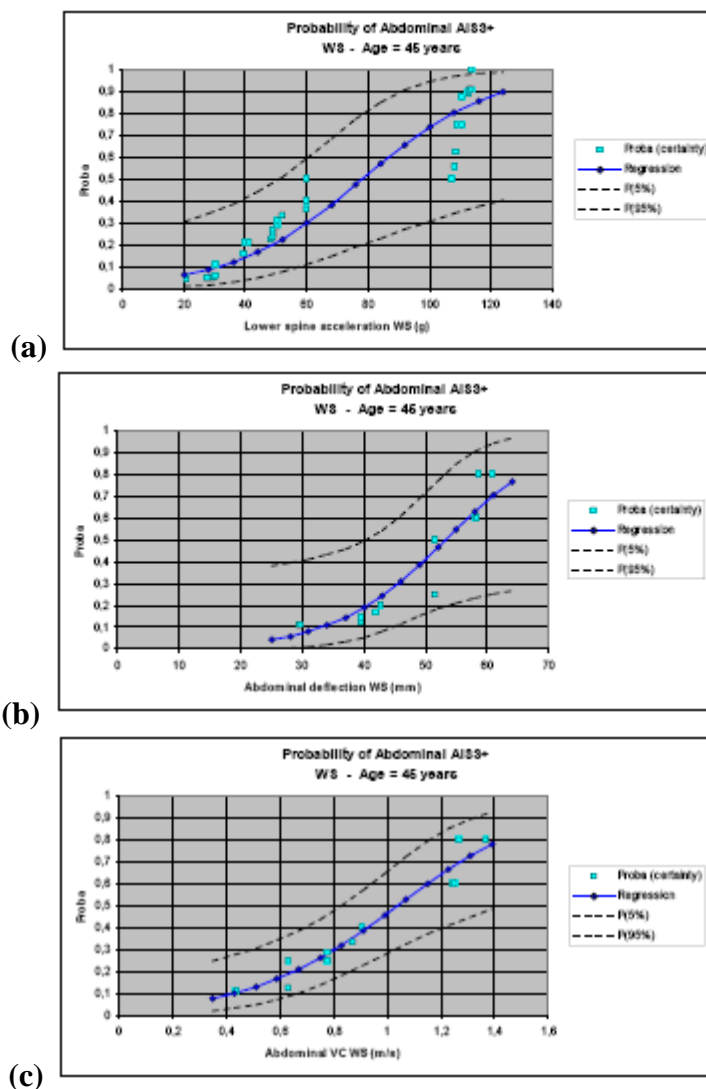


Figure 5.24 Injury risk functions for lateral abdominal responses of the WorldSID dummy, from ISO (2005).

5.11 NECK

The conundrum for the choosing a neck injury criterion is that the only existing combined load neck injury risk function is based on N_{ij} . It was developed and validated based on axial loading, flexion and extension of the neck in frontal impacts, in the mid-sagittal plane. Most likely loading is going to be tension compression with lateral bending and axial twisting. We have no neck injury risk functions for the lateral direction. If we follow the IIHS (2004) approach of using the values developed for the frontal direction, then we need to develop an interpretation that gives a reason for going forward.

An alternative approach used by WTG and IIHS, Lund (2003) for side impact neck injuries is to use a risk function for axial force and monitor the magnitude of the x axis moment (lateral bending) and the z axis moment or neck twist.

Mertz et al. (2003) propose a risk of $AIS \geq 3$ neck injury based on normalized tension, $F_{\text{tension}} / F_{\text{critical}}$, where $F_{\text{critical}} = 3,290$ Newtons. This is based on no muscle tone for the neck. The resulting risk curve for neck tensile loading is plotted in Figure 5.25.

Probability density function = $\text{EXP} [-(F_{\text{tension}} / F_{\text{critical}} - 1.250)^2 / (0.034848)] / (0.330875)$

$$p(\text{AIS} \geq 3) = \int_0^{F_{\text{normalized}}} (\text{probability density function}) dF$$

Mertz et al. Neck Tension

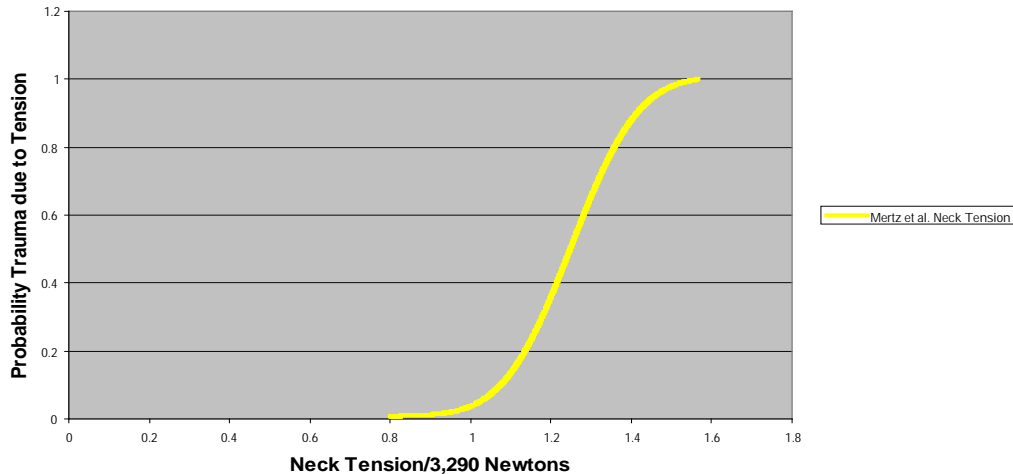


Figure 5.25. Injury risk curve for neck tensile loading Mertz et al. (2003)

Lund (2003) noted that lateral bending of the neck should be monitored. Based on the judgment of the biomechanical engineers assisting Lund, the lateral bending moment injury assessment reference value (IARV) was set midway between the flexion and the extension IARV. The biomechanical engineers followed the logic that “. . . the amount of muscle and connective tissue that resists lateral bending is greater than the amount that resists extension bending, but not greater than the amount that resists flexion, the necks strongest bending mode.” For the 50th male, Mertz et al. (2003) list the flexion IARV as 190 Nm and the extension IARV as 96 Nm. Following this suggestion of using the midway point as the IARV for lateral bending, the upper neck of the dummy should be under 143 Nm.

5.12 SHOULDER

Bolte et al. (2000) used pneumatic impacting ram was employed in carrying out twenty two lateral impacts to eleven unembalmed human cadavers at the level of the glenohumeral joint. The objective of this study was to determine response characteristics and injury of the shoulder due to lateral impacts, at a ram velocity of 3.5 to 7.0 m/s. The most common result was a loosened acromio-clavicular joint and a distal fracture of the clavicle occurred in 9 cases, approximately 1-2 cm from the acromio-clavicular joint. A maximum deflection of 47 mm between the impacted acromion and the sternum lead to approximately half of the impacts resulting in an AIS2 injury. The peak force varied with the velocity from 1550 to 4130N. Mertz et al. (2003) suggest several shoulder injury criteria:

- Limiting the peak lateral shoulder force to 4000 N or less; and,
- Limiting the peak lateral deflection to 75 mm or less.

5.13 PELVIS

Kuppa (2004) suggests a pelvic injury assessment curve based on pubic symphysis force of the ES-2re dummy, see Figure 5.26.

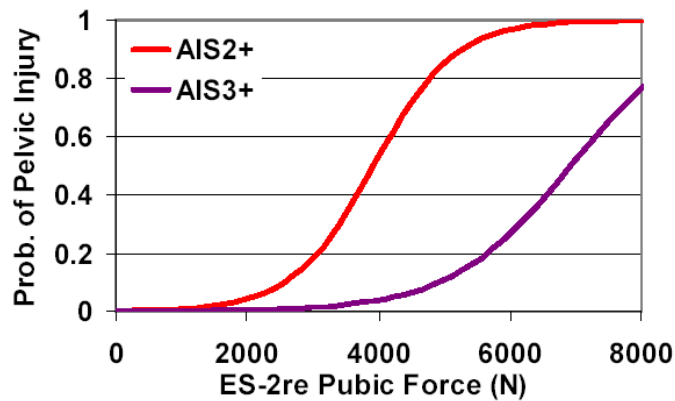


Figure 5.26. Pelvic injury assessment curve based on pubic symphysis force of the ES-2re dummy, Kuppia (2004)

The IIHS (2004) report sets side impact testing guidelines and rates a F_{pelvis} of 4100 – 4800 N to be acceptable. IIHS also uses combined acetabulum and ilium forces of less than 4.8 kN for either or 6.1 kN combined and pelvic acceleration.

In an ISO (2005) document, pelvic fracture risk curves for the WorldSID dummy were developed based on selected PMHS test data, see Figure 5.27. These functions were based on pubic force and pelvic acceleration.

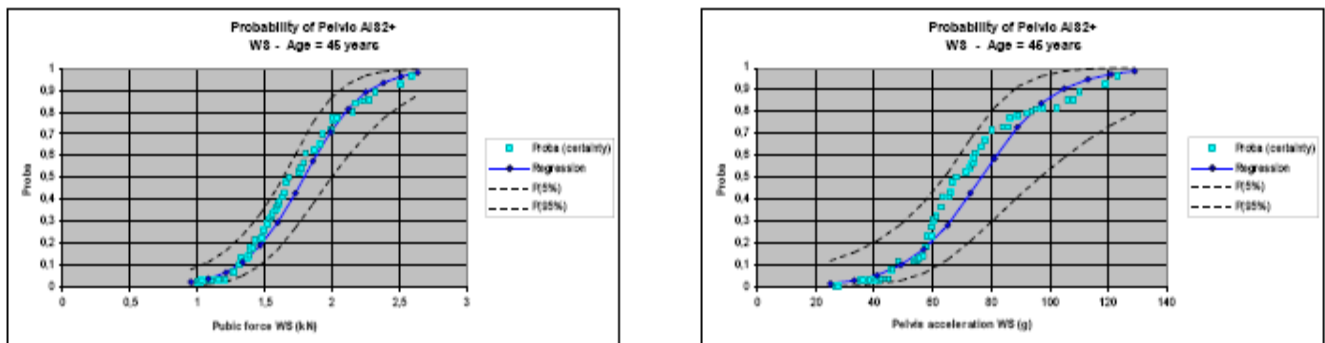


Figure 5.27 Pelvic fracture risk curves for the WorldSID dummy, ISO (2005)

In an ISO (2005) document, pelvic fracture risk curves for the WorldSID dummy were developed based on selected PMHS test data, see Figure 5.27. These functions were based on pubic force and pelvic acceleration. Mertz et al. (2003) suggested limiting the iliac crest, pubic, and sacrum loading to:

- Peak iliac crest load to 6000 Newton.
- Peak pubic load to 6000 Newton.
- Peak sacrum load to 6000 Newton.

Kuppia (2004) says 6,000 Newtons is about a 25% probability of an $\text{AIS} \geq 3$ injury in the abdominal region. The ISO says 6,000 Newtons is about a 52% probability of a pelvic fracture.

5.14 PROPOSED INJURY RISK CURVES

5.14.1 Risk Curves for the Head

Recall that the aim of Task 5 — Test Procedures and Injury Criteria of the ARC Far Side Collaborative Research Program described in Chapter 1 was to conduct a literature investigation into

injury mechanisms in the lateral and frontal oblique direction to identify or develop injury risk functions for far side occupants involved in side impact collisions. Sections 1 through 4 addressed herein the literature investigation. Recall that, in addition, the Team envisioned the Task 5 Report as a handbook to support and guide Task 7, *Computer Modelling* and Task 8, *Countermeasure Development*. This section and the following sections address the injury function guide, or recommended approach, part of the object of Task 5. The first of these guides to an injury function addresses the head.

Ono (1998) discusses the fracture threshold for front and side and the concussion threshold for front and side impact to the head.

“However, the temporal fracture threshold shows a value ... approximately 50 percent of the fracture threshold on frontal and occipital impact

... the concussion threshold curve of lateral impact. The entire curve is located twice as high above the curve of sagittal impact.”

In other words, the Ono study suggests using the frontal curve for the side would give more fractures and fewer concussions. In animal tests, Dixon (1998) studied the presence or absence of a summed neurological score after 50 minutes and discussed his findings.

“... central and lateral impacts .. illustrates similar functions in regard to the acute neurological responses.”

Using HIC as the dependent variable, Gibson et al (2001c) analyzed 55 (after dropping 3 outliers) lateral impacts to PMHS heads. The analysis suggests that the lateral risk curves are similar to frontal risk curves for the head.

In writing the support document for a Notice of Proposed Rulemaking for Federal Motor Vehicle Safety Standard, Kuppa (2004) equated the lateral HIC criterion to the frontal HIC criterion.

The real-world crash analysis suggests that, for the occupant on the non stuck side, the occupant will see lateral impacts to the head and also frontal and crown impacts. This suggests we want risk curves for the front and side or one set of curves that are sufficient—given the present stage of biomechanical research—to handle both conditions.

The injury risk curve proposed for use with the WorldSID is the Mertz et al. curve published in 2003. The curve assumes a normal distribution with mean and standard deviation, shown in Table 5.9 and Figure 5.28.

Table 5.9. Probability of Brain Injury

Body Region	Independent Variable	Mean Value	Standard Deviation
Head	HIC (15)	1,434	430

Mertz (2003) Probability of Brain Injury

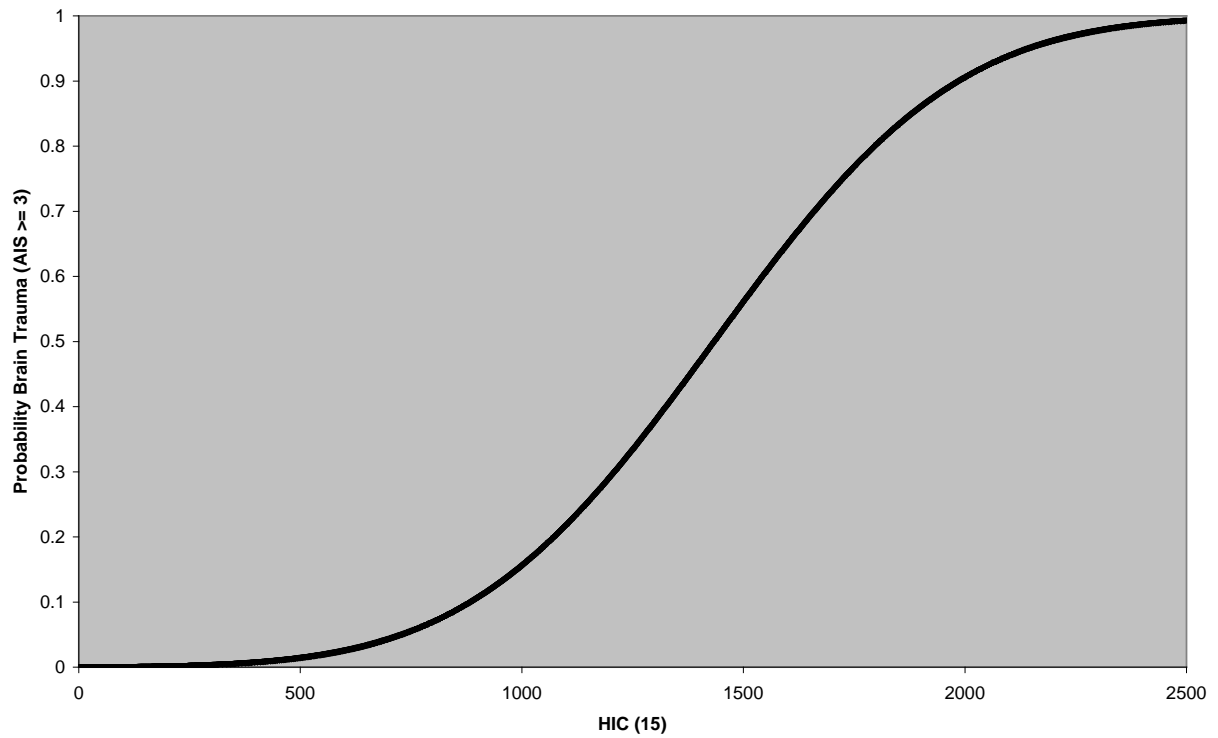


Figure 5.28. Probability of brain injury

5.14.2 Injury Risk for the Neck

AIS ≥ 3 neck injury risk is based on normalized tension, $F_{\text{tension}} / F_{\text{critical}}$, where $F_{\text{critical}} = 3,290$ Newtons. The resulting risk curve for neck tensile loading is

$$\text{Probability density function} = \text{EXP} [-((F_{\text{tension}} / F_{\text{critical}} - 1.250)^2) / (0.034848)] / (0.330875)$$

$$p(\text{AIS} \geq 3) = \int_0^{F_{\text{normalized}}} (\text{probability density function}) dF$$

0

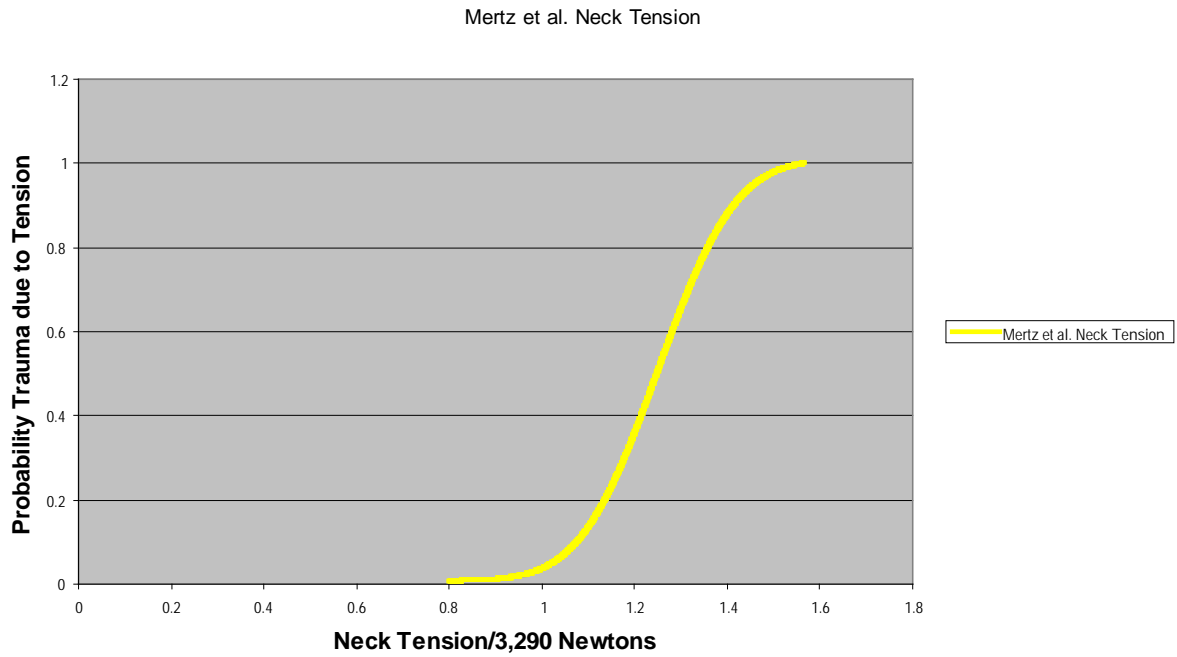


Figure 5.29 Injury risk curve for neck tensile loading Mertz et al. (2003)

An allowable upper cutoff point on neck shear is specified.

Body Region	Independent Variable	Mean Limit
Neck	Shear (N)	3100

In addition, a limit on the bending moment of the upper load cell of the neck is recommended. The bending moment of the neck should be at or below 143 Nm.

5.14.3 Risk Curves for the Upper Extremities

Following Duma et al. (2006), the risk function for the humerus is in terms of bending moment, and is given by:

$$\text{Risk of humerus fracture} = 1 - e^{-(0.0036 * x)^{4.871}}$$

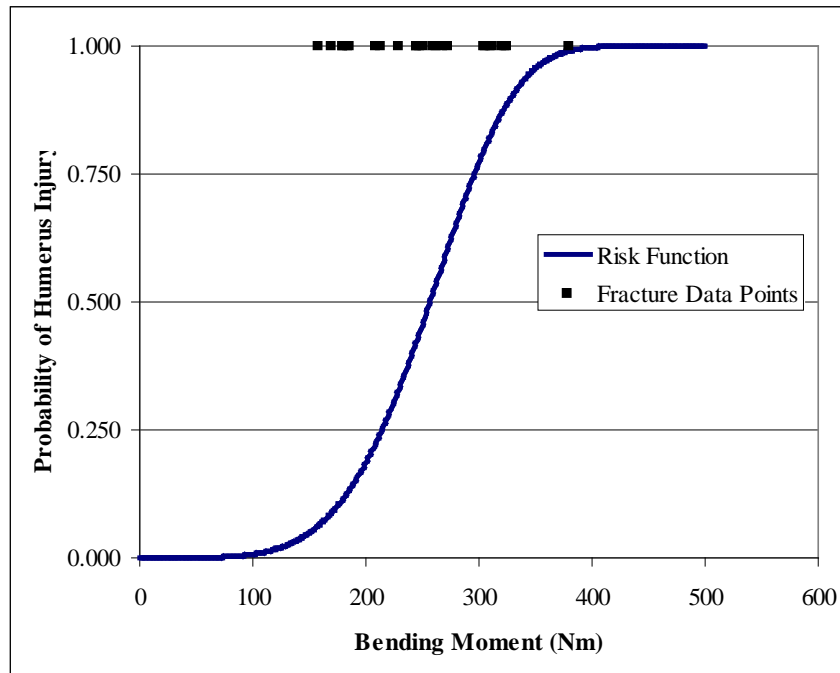


Figure 5.30 Humerus fracture risk function for the 50th percentile male

Following Duma et al. (2006), the risk function for the forearm is in terms of bending moment, and is given by:

$$\text{Risk of forearm fracture} = 1 - e^{-(0.0092 * x)^{4.409}}$$

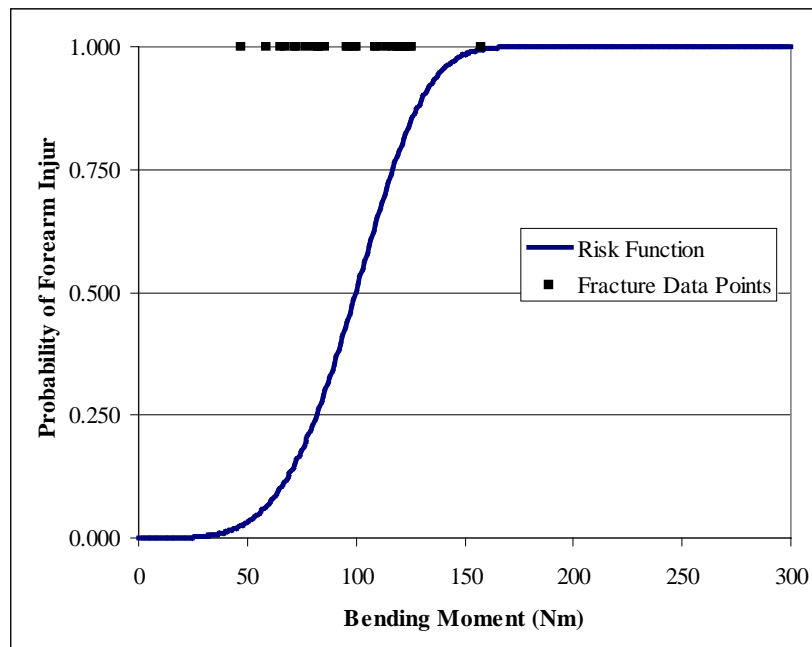


Figure 5.31 Forearm fracture risk function for the 50th percentile male

5.14.4 Risk Curve for the Chest

Chest Deflection) Body Region	Independent Variable	Mean Value	Standard Deviation
Chest	Maximum Chest Deflection (mm)	56.1	9.1

WorldSID Thorax (nFR 4+)

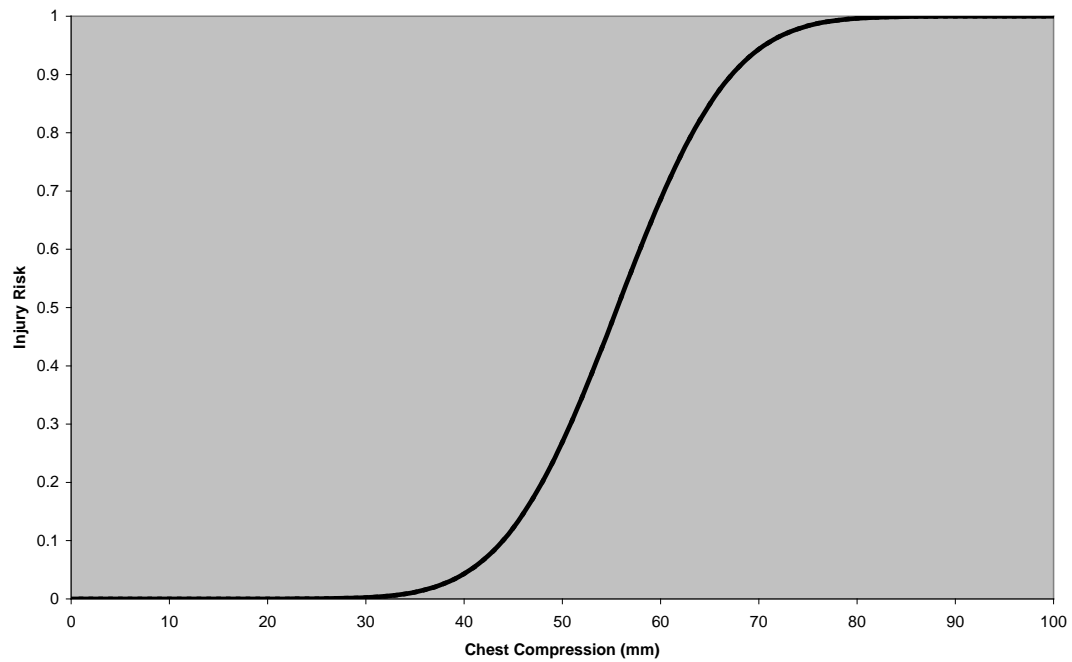


Figure 5.32 Risk curve for the chest deflection

Chest - V*C

Body Region	Independent Variable	Mean Value	Standard Deviation
Chest	V*C (m/s)	0.9	0.41

Risk of Chest Injury using V*C

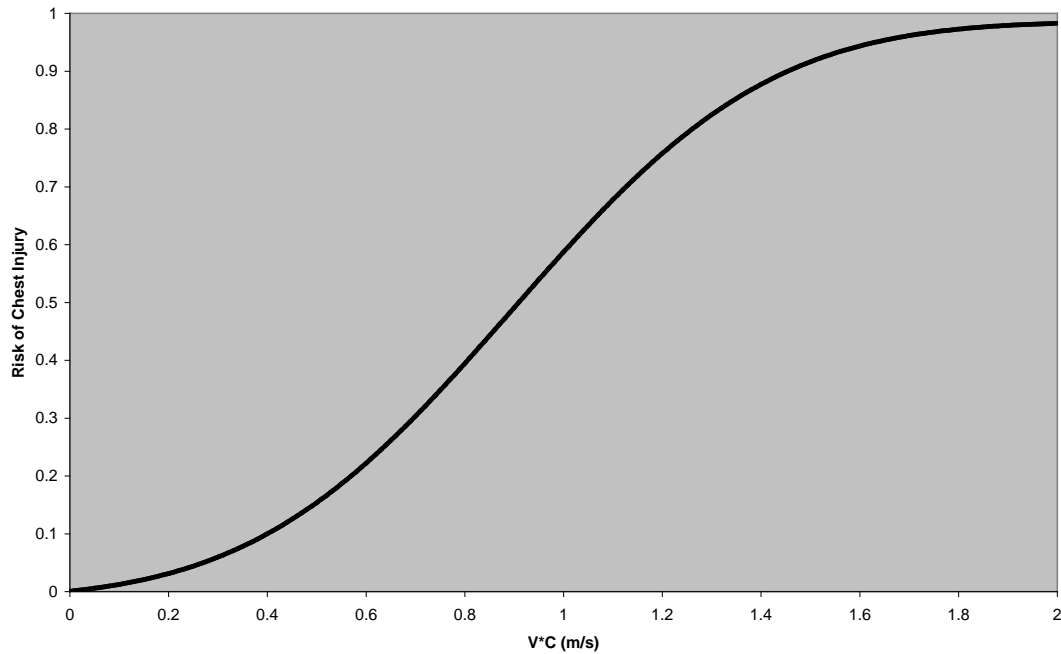


Figure 5.33 Risk curve for the V * C

5.15 INJURY RISK CURVE FOR THE ABDOMEN

Kuppa (2004) suggested an injury assessment curve based on internal abdominal force. The ISO suggested an injury assessment curve based on internal abdominal force. Mertz et al. (2003) suggested a limit on internal abdominal force. Based on testing with rabbits, Rouhana et al. (1996; 1998) found abdominal trauma correlates with V*C.

Abdominal Compression

Body Region	Independent Variable	Mean Value	Standard Deviation
Abdomen	Maximum Abdomen Compression (mm)	53.2	15.1

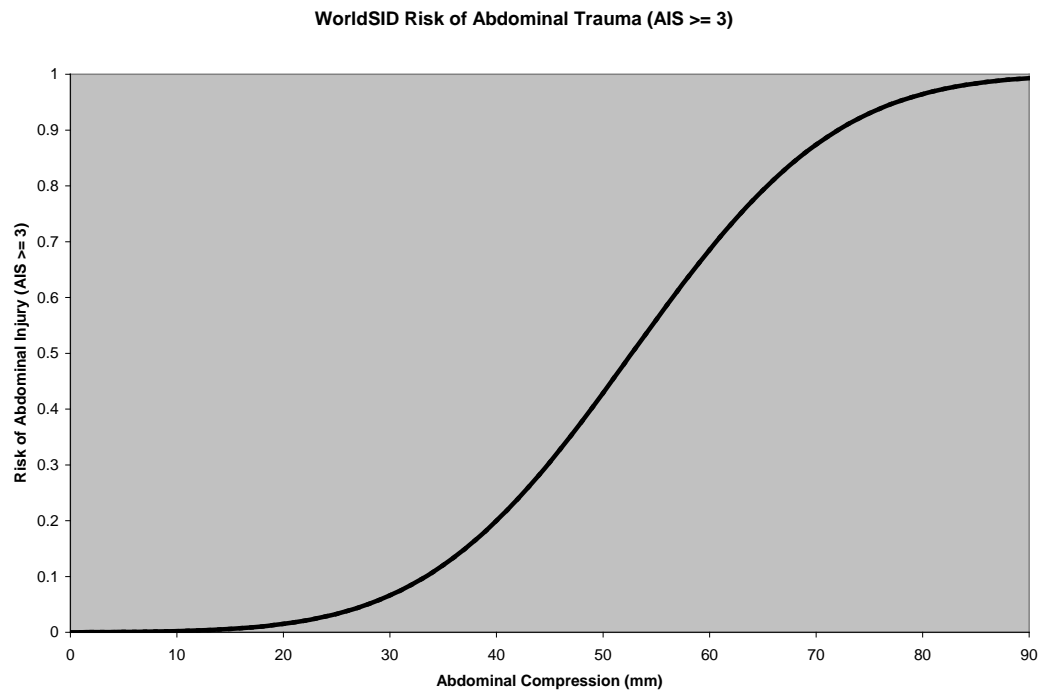


Figure 5.34 Risk curve for the abdomen deflection

Abdominal – $V \cdot C$

Body Region	Independent Variable	Mean Value	Standard Deviation
Abdomen	$V \cdot C$ (m/s)	1.03	0.46

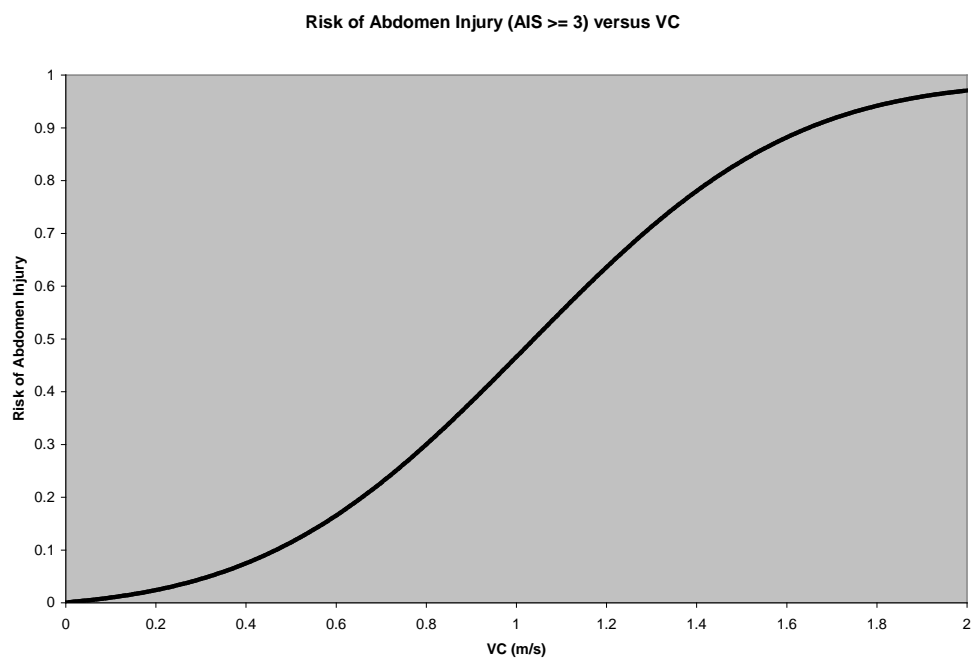


Figure 5.35 Risk Curve for the abdomen $V \cdot C$

5.16 INJURY RISK CURVE FOR THE PELVIS

Kuppa (2004) suggested an injury assessment curve based on pubic symphysis force. The ISO (2005) suggested an injury assessment curve based on pelvic force. Mertz et al. (2003) suggested a limit on iliac crest, pubic, and sacrum load.

The WorldSID pelvis is very different from that of other dummies. "The pelvis consists of a conical shaped polyurethane pelvic bone that mimics the human pelvic bone. The major landmarks of the WorldSID dummy are close to the anatomical data. A vinyl skin surrounds the pelvic bone and this skin is filled with an elastomer. The hip joint of the WorldSID dummy consists of a ball and socket joint, this is a different configuration from the existing side impact dummies which all have hyme joint construction." In contrast, the EuroSID2, SID, and BioSID all have a fairly rigid metal pelvis surrounded by simulated flesh. This may lead to a different response than what researchers are currently expecting of a dummy pelvic response.

As a consequence of this design direction, the risk curves for pelvic trauma are two in number. The first risk curve, for external pelvic loading, is based on the independent variable acceleration. The second risk, for loading going through the pubic symphysis, is based on the independent variable pubic force.

Body Region	Independent Variable	Mean Value	Standard Deviation
Overall Pelvis	Acceleration (G)	76.6	21.2

WorldSID Risk of Pelvic Trauma - Acceleration

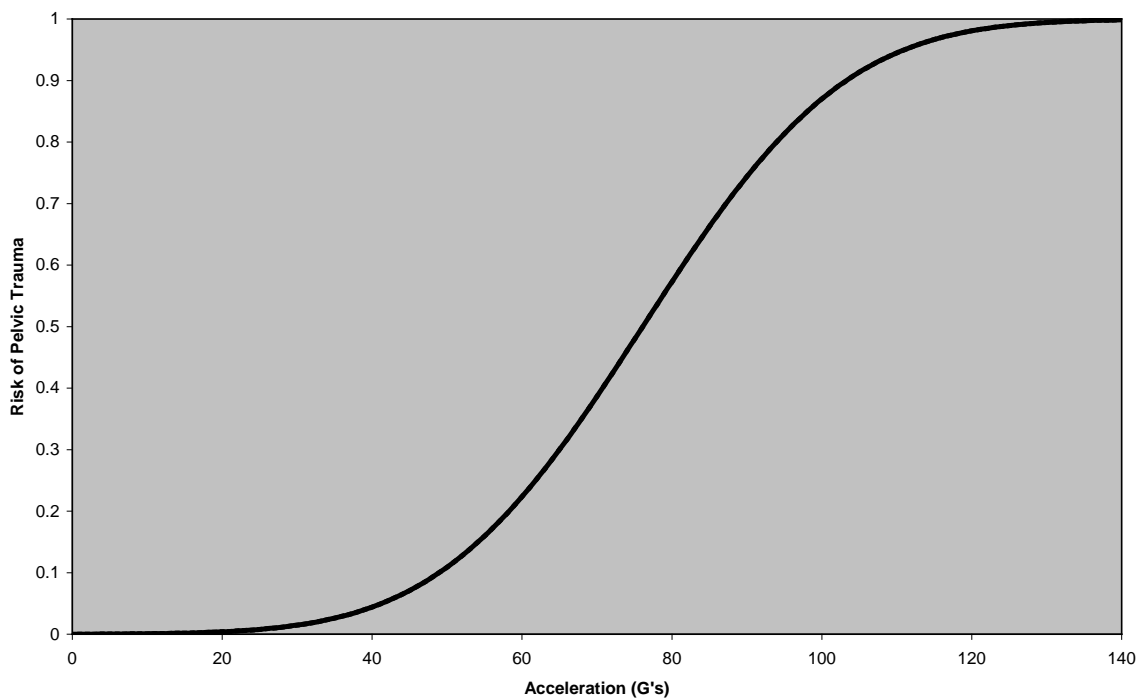


Figure 5.36 Risk curve for the pelvis acceleration

Body Region	Independent Variable	Mean Value	Standard Deviation
Pelvis Symphysis	Pubic Force (N)	1,800	400

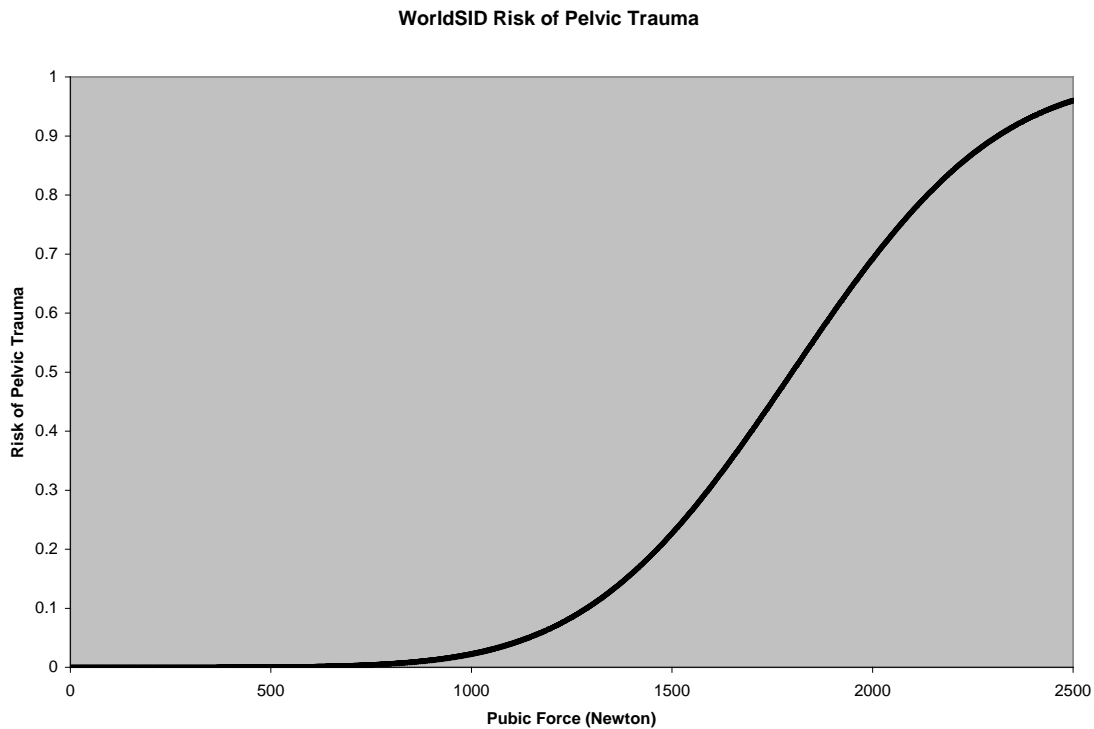


Figure 5.37 Risk Curve for the pubic symphysis force

5.17 LIMITS FOR THE SPINE

While all is not known with respect to the failure properties of the spine and there are many methods of testing, the following provides a first order approximation for thoracolumbar injury criteria (Table 5.10).

Allowable limits for the thoracolumbar spine in pure compression, tension, and shear were developed based on the failure properties reported from the two primary areas of spinal failure property research: isolated vertebral bodies; and functional spinal units (Sonoda, 1962; Messerer, 1880; Hanssen et al 1979; Hutton et al. 1979; Pintar, 1986; Kazarian, 1977; Brown, 1957; Perry, 1957; Yoganandan, 1989; Duma et al, 2006; Sundararajan, 2005). Allowable limits for the thoracolumbar spine in combined compression and moment loading were developed based on the failure properties reported from failure property research using multiple vertebral body spinal segments (refer Table 5.8).

The suggested criteria were determined by averaging the failure data, rounded to the nearest hundredth, of predominantly young male cadavers tested at static to semi dynamic rates. Therefore, the suggested criteria can be used for testing with the 50th Percentile Hybrid III dummy. If there were insufficient data for certain regions in a specific testing mode, then the criteria was scaled based on the averages reported for compression testing because it was the most complete data set. Allowable limits are suggested for the upper thorax, middle thorax, and lumbar regions because these regions correspond to the locations of spinal load cells in the 50th Percentile Hybrid III dummy.

Table 5.10 Allowable limits to be closely monitored for the spine

Site in Spine	Pure Compression (N)	Pure Tension (N)	Pure Shear (N)	Combined Compression/ Moment
Upper Thoracic	3100	800	900	100 N-m (@ 1400 N)
Middle Thoracic	4500	1600	1300	146 N-m (@ 2000 N)
Lumbar	6200	2200	1800	200 N-m (@ 2430 N)

5.18 INJURY RISK FOR THE LOWER EXTREMITIES

Following Kerrigan et al. (2004), the suggested risk function for femur fractures (see **Error! Reference source not found.**) is approximately:

$$p(\text{femur fracture}) = 1 - \text{EXP} [-\text{EXP}(6.24242 \ln(M_{\max}) - 38.45762)] .$$

Following Kerrigan et al. (2004), the suggested risk function for tibia fractures is approximately:

$$p(\text{tibia fracture}) = 1 - \text{EXP}[-\text{EXP}(5.69112 \ln(M_{\max}) - 33.05211)]$$

Mertz et al. (2003) proposed a tibia shaft fracture risk curve for the adult male population based on maximum bending moment:

$$\text{Probability density function} = \text{EXP}[-((M - 317)^2)/(15,488)]/(220.5833)$$

$$p(\text{tibia fracture}) = \int_0^M (\text{probability density function}) dM$$

These two functions (Kerrigan et al. and Mertz et al.) give very similar results when plotted, as shown earlier in Figure 5.19.

6 CRASH SIMULATIONS & TEST CONDITIONS

AUTHORS: Kennerly Digges, Pradeep Mohan, Brian Alonso & Joseph Cuadradro

6.0 INTRODUCTION

6.0.1 Chapter Organization

An objective of this task was to study issues associated with far-side sled testing and crash testing using computer simulation.

Section 6.1 reports studies of finite element simulations of vehicle and moving barrier crashes into a Ford Taurus. A principal purpose was to determine the degree to which the moving barriers produced damage patterns that were similar in shape and extent to those produced by vehicle impacts. A secondary purpose was to determine the damage patterns for a frequently occurring crashes at 60 degrees and crashes that impact the front wheels, producing Y-damage (See Figure 2.16 for definition of Y-damage).

Section 6.2 reports studies of MADYMO simulations to determine a dummy or human model that best matched the kinematics of a cadaver that was tested in a far-side crash. A principal purpose was to establish a validated model for use in evaluation occupant response in the far-side crash environment. A second objective was to compare existing dummy models to the cadaver kinematics.

Section 6.3 applied the MADYMO human facet model to explore centre console configuration and crash pulse issues associated with sled testing in far-side crashes. The cadaver test program summarized in Chapter 3 required a console to provide restraint to the pelvic region. The height of the console should be sufficient to provide pelvic restraint without causing excessive loading of the abdomen. The modelling effort in Section 6.3 explored the occupant kinematics when subjected to consoles of varying heights. In addition, the MADYMO human facet model was used to explore a crash pulse issue associated with sled testing in far-side crashes. The cadaver test program summarized in Chapter 3 required a crash pulse that was representative of a vehicle-to-vehicle crash. However, the test sled had limited capability to duplicate the highest accelerations that were observed in a crash test. The MADYMO model was used to determine an appropriate sled crash pulse.

Section 6.4 applied MADYMO models to explore the interaction between five different dummy models and five different countermeasures. The dummy models were:

- (1) Hybrid III; (2) BioSID; (3) EuroSID I; (4) EuroSID II, and (5) SID2s.

With these dummy models, five restraint configurations were simulated:

- (1) Baseline (standard 3-point belt); (2) Reverse belts; (3) Base with chest airbag; (4) Base with shoulder airbag, and (5) Base with chest and shoulder airbag.

Section 6.5 used data from crash tests and MADYMO occupant modelling to explore the relationship between the crash PDOF as documented in the accident data and the test sled configuration required to simulate the same far-side crash environment.

Although not part of the far-side project, a complementary series of six crash tests with both near-side and far-side dummies was conducted by The Australian Department of Infrastructure [Newland, 2008 Stapp Car Crash Conference]. One purpose of the tests was to examine dummy to dummy interaction.

6.02 Results

The Finite Element Models used in Section 6.1 indicate that the IIHS barrier produced similar damage on a Taurus patterns to those produced by a full size pickup truck. The NHTSA barrier and the Y damage test produced less damage to the Taurus front door than the IIHS barrier.

The average CDC extent of damage produced in actual IIHS crash tests is considerably less than the average extent of damage to vehicles with far-side occupants injured at the AIS 3+ severity level (see Figures 2.15 and 2.16.). This result suggests that the barrier test speed of a far-side test should be higher than the speed used by IIHS in their side impact tests for consumer ratings.

The MADYMO modelling effort summarized in Section 6.2 found that the human facet model matched the cadaver kinematics very well and it was considered suitable for evaluation of occupant motion in the far-side crash that was simulated. The MADYMO dummy models (Hybrid III, BioSID, EuroSID 1, EuroSID2 and SID2s) did not accurately reflect the motion of a human cadaver under the same impact configurations as the cadaver test.

The conclusion of Section 6.3 was that the force exerted by the occupant on the centre console increased as the height of the centre console increased. As the centre console height increased above 8 inches, it loaded the occupant's abdomen and ribs.

The modelling research documented in Section 6.4 shows that a square wave sled test pulse can produce similar occupant kinematics to the desired car-to-car pulse. It also showed that the side-impact dummies, designed primarily to test for occupant injuries on the near-side are limited in their ability to emulate occupant kinematics for a far-side impact. However, models for the WorldSID and THOR were not available and, therefore, not evaluated. Also, modelling indicated that the Hybrid III dummy, designed primarily for frontal impacts, is limited in its ability to test for far-side impacts. Although the five anthropomorphic test devices (ATDs) simulated in MADYMO for far-side impacts failed to produce desired kinematics, the human faceted MADYMO model did show promise by properly reproducing occupant kinematics.

Despite the short-comings of the dummies for reproducing far-side kinematics, the reaction of these dummies in MADYMO to certain countermeasures offers some insight into future studies. A reverse 3-point seatbelt effectively restrained the occupant. However, this belt configuration significantly increased neck force levels, almost crossing injury threshold levels. Chest and shoulder airbags on the inside of the occupant contained the occupant and prevented excursion. However, these configurations left the head and neck unrestrained and showed awkward movement of the head. In addition, the use of a petite dummy indicated some vulnerability of small sized occupants to airbags.

The results from the study reported in Section 6.5 show that a sled test can effectively mimic the kinematic response of a far-side occupant in the side and corner impacts for which there was crash test data. It is important to understand that a side impact with a 60 degree PDOF does not translate to a sled test with a sled angle of 60 degrees! For example, the SNCAP test has a direction of force of 63 degrees but an appropriate sled angle of 87 degrees. The difference is due to the rapid rotation of the struck vehicle to align with the striking vehicle.

The impact angle, initial vehicle velocities, delta-V, and impact location are all important factors in developing a proper sled test configuration. However, no direct correlations were able to be determined between a single variable and the sled pulse or correct sled or instrument panel angle to be used in the test configuration. The use of the approach documented by this study can provide a basis for determining the best sled configuration to mimic any far-side crash condition.

Tests conducted in Australia have shown that the presence of a far-side dummy does not interfere with the side protection measurements made by the near-side dummy. However, there was interaction between the near-side and far-side dummies during the rebound of the near-side dummy. The interaction occurred well after the far-side dummy slipped out of the shoulder belt [Newland, 2008

Stapp Car Crash Conference]. These test results indicate that it may be feasible to incorporate a far-side dummy in the vehicles used in consumer information tests. Such a proposal was presented at the ESV meeting in June, 2009 [Digges, 2009 ESV Conference]. This paper presents simulations of safety belt geometry and pretensioning that indicate relatively simple countermeasures can improve far-side protection.

6.03 Conclusions

The following conclusions are based on computer modelling:

1. The IIHS barrier and test procedure produces vehicle damage patterns on a Ford Taurus that are generally similar to an occupant compartment impact by a pickup truck with a principal direction of force (PDOF) in the range of 60 to 90 degrees. However, the damage severity produced by the IIHS test procedure is less than that reported in the majority of real world crashes with MAIS 3+ injuries to far-side occupants.
2. The MADYMO human facet model can be used to simulate human kinematics in a far-side crash. The MADYMO dummy models (Hybrid III, BioSID, EuroSID 1, EuroSID2 and SID2s) did not accurately reflect the motion of a human cadaver under the same impact configurations as the cadaver test. However, these dummy models provide useful insights.
3. The presence of a console higher than 8 inches causes undesirable chest loading.
4. A square sled pulse can be adjusted to adequately simulate a far-side car-to-car impact environment.
5. A side crash with a PDOF of 60 degrees is not accurately simulated by a sled test with an angle of 60 degrees. Vehicle rotation has a large influence on the kinematics of the far-side occupant relative to the vehicle. Computer modelling is useful in determining the appropriate sled configuration to develop countermeasures for far-side crashes.

6.1 CRASH TEST CONFIGURATIONS FOR THE FAR-SIDE ENVIRONMENT

6.1.1 Introduction

In Chapter 2, the crash environment associated with injury producing far-side crashes was defined using US Accident data and confirmed from Australian data. The analysis indicated that for belted occupants with MAIS 3+ injuries, the 50% median crash severity was a lateral delta-V of 28 km/h and an extent of damage of 3.6 as measured by the CDC scale [SAE Standard J224, Collision Deformation Classification]. The most frequent damage area for seriously injured belted occupants was the front 2/3 of the vehicle (42%), followed by the rear 2/3 (21%). The most frequent principal direction of force (PDOF) was 60° (60%), followed by 90° (24%). The head and chest were the most frequently injured body regions, each at about 40% [Gabler 2008]. The injuring contacts that most frequently caused chest injury were the struck-side interior (23.6%), the belt or buckle (21.4%) and the seat back (20.9%) [Fildes 2007].

This task applied finite element models of vehicles and barriers to determine the degree to which the NHTSA and IIHS barriers produced the extent of damage that would be expected in a far-side crash that is representative of the 50 percentile injury producing crash. The research is documented in more detail in reports listed in the Reference section [Mohan, 2005].

The baseline test for this study was the impact of a full size pickup truck into the side of a Taurus. For a delta-V of 28 km/h and a 90 degree impact with the occupant compartment, the extent of damage was approximately 3.6.

This test formed the basis for comparing the deformation produced by the NHTSA and IIHS barriers. Other crash conditions were conducted to determine the crash severity that produced deformation that was similar in extent to the 90 degree test.

6.1.2 FEM Model Simulations

FE Model of the Ford Taurus was chosen as a representative mid-size sedan for this study. The model is one of the most detailed models developed and validated at the National Crash Analysis Centre. The model consists of 850K elements (Guerra, 2006). The Taurus FE model is target vehicle in this study.

The US-LNCAP and the IIHS side impact barriers were used as the bullet vehicles in this study. Both of these barriers were recently developed at the National Crash Analysis Centre (Kildare 2005). The barriers have been validated for the available load cell wall tests. The third bullet vehicle used was a GM C-1500 pick up truck that was developed and validated by the NCAC.

The five different impact configurations and the measured lateral delta-V for each of the configuration are shown in Figure 6.1.1. The first two configurations were based on the US-LNCAP and IIHS test protocols respectively. The remaining three impact configuration was with a GM C-1500 pickup truck. In the first case the impact point was at the mid of the front door and the impact angle was 60° . The next case was set-up similar to the IIHS side impact protocol except that the bullet vehicle was a pick-up truck instead of the barrier. In the third case the impact point was at the front body hinge pillar.

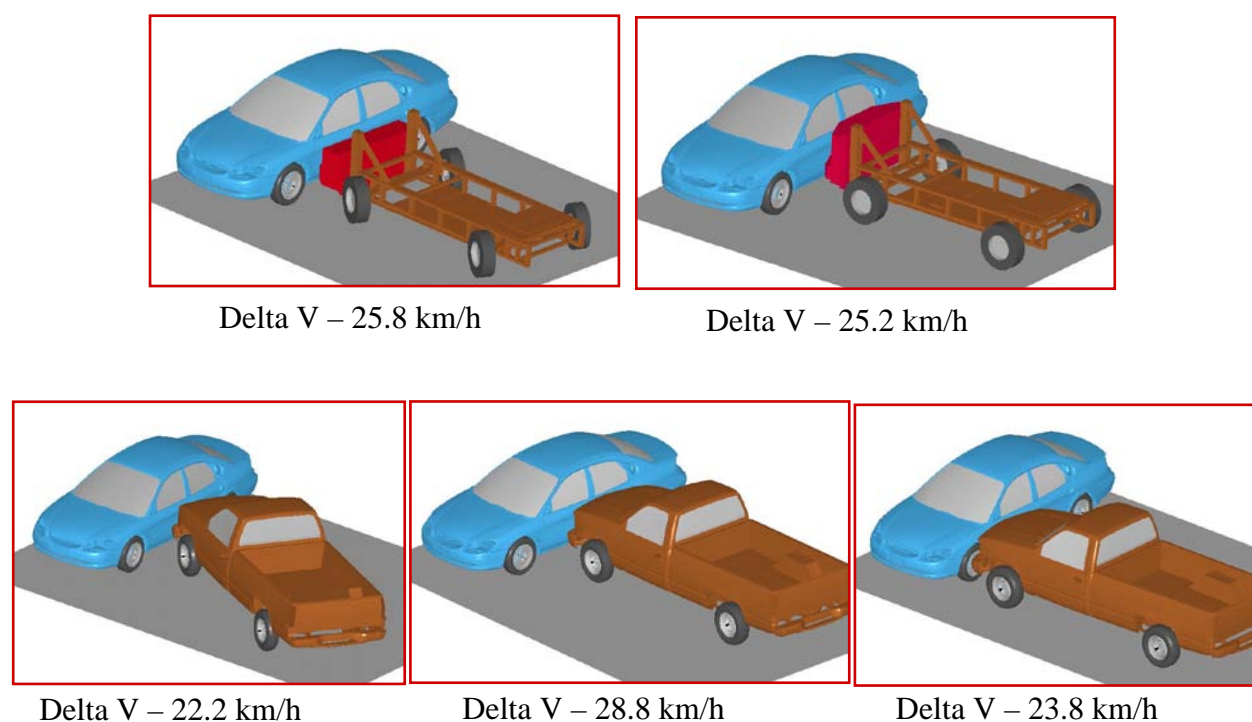


Figure 6.1.1: Crash Configurations Simulated with FEM Models

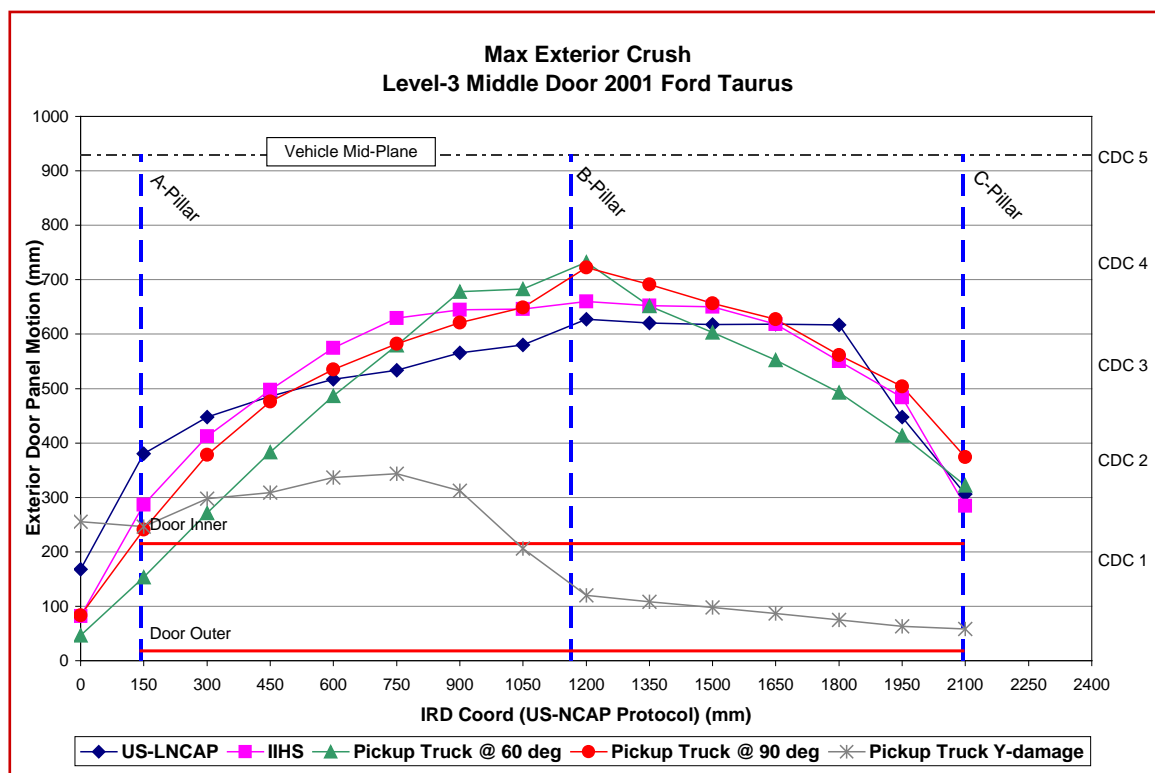


Figure 6.1.2: Max Crush at Mid-door

6.1.3 IIHS Crash Test Deformations vs. Model Results

The crush measures from the above impact configurations are shown in Figure 6.1.2. The impact configuration with the pick-up truck produced the max exterior crush at the windowsill. The extent of damage was about CDC 3.8. Except for the Y-impact configuration the other 4 cases produces similar crush characteristics.

The crush measures from the US-LNCAAP simulation were compared to the test data available from NHTSA. The FE model yields a softer response compared to the test data. The model needs to be further validated and the front seat models needs to be included to obtain better correlation with the test data. However, the results are considered to be useful for comparing the damage patterns.

The IIHS database of side crash tests was examined to determine crush profiles of vehicles tested. The data on the following 12 vehicles were available: Honda Accord, Nissan Altima, Toyota Camry, Subaru Forrester, Mitsubishi Galant, Saturn L series, Chevy Malibu, Mazda 6, Volvo S40, Saab 9-3, Hyundai Sonata, and Dodge Stratus.

A plot of the average deformation at the mid level of the door for the 12 vehicles is shown in Figure 6.1.3 as the plot in blue. The average delta-V of these tests was 23.km/h. The average CDC extent of deformation was 2.2. The pink plot shows the FEM simulation for the IIHS barrier impact with a Ford Taurus at a delta-V of 25.8 km/h.

The higher deformation in the FEM simulation is partially due to the elastic component of deformation that is present in the FEM results but not in the IIHS test results. After the test there is a spring-back of the door structure. There may also be differences due to the higher delta-V for the FEM test. Finally, the model may not account for some of the structural interactions including seat and floorboard interactions.

Figure 6.1.3 provides two adjustments to the FEM model. The red curve adjusts the FEM deflection for spring-back. Scaling the FEM curve by a factor of 0.7, as shown in the light blue curve, brings the FEM model close to the IIHS average deformation pattern.

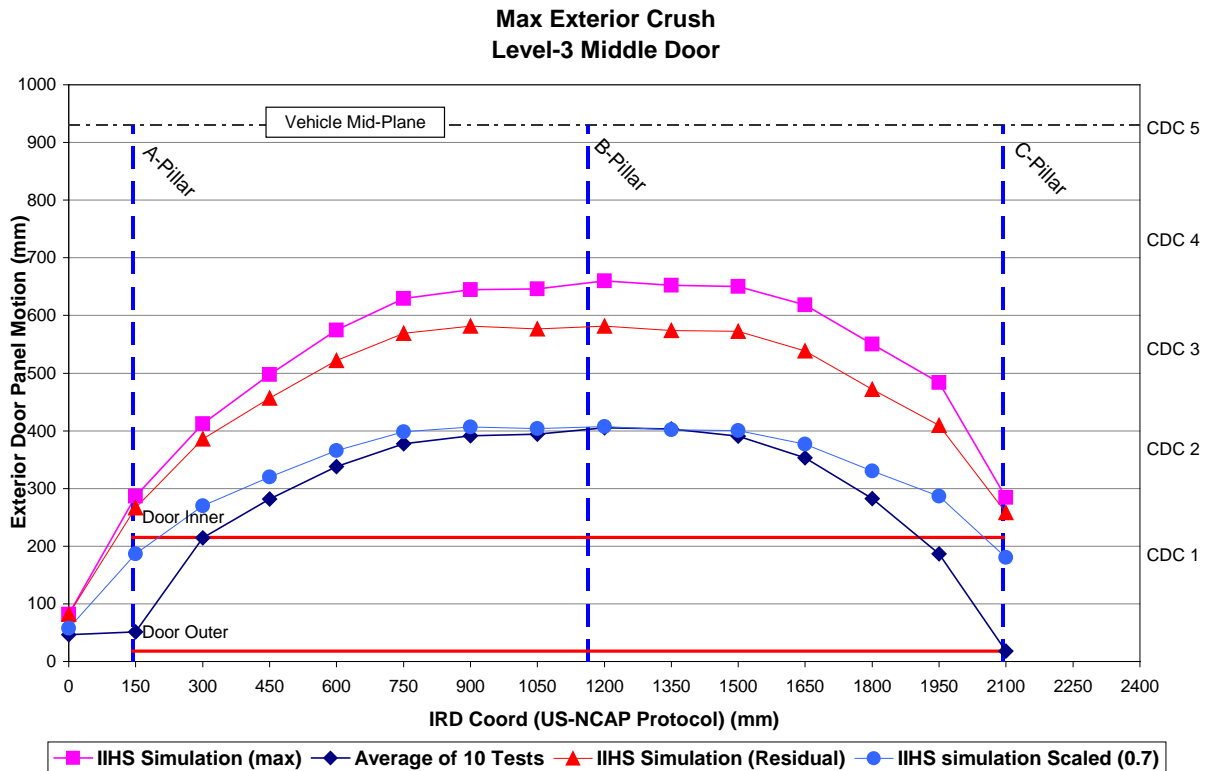


Figure 6.1.3: Side deformation: Average of 12 IIHS Tests with Delta-V of 23.6 km/h and predictions from FEM Model with a Delta-V of 25.6 km/h; Adjustments to FEM model for Spring-back

6.1.4 Discussion

Figure 6.1.3 shows a comparison of the residual deformation typical of IIHS tests and the deformation predicted by the Taurus model. The predicted shape of the deformation matches the test data. However, the extent of deformation predicted by the model is higher. This result suggests the need for further validation of the model to predict the extent of damage. However, the model is assumed to be useful in predicting the shape of the damage.

The shape of the damage predicted by the model for the IIHS test was generally similar in shape and extent to the damage produced by a pickup impacting the occupant compartment. Both the NCAP test and the Y damage test produced less damage to the front door than the IIHS test or the pickup impacts with the occupant compartment. This observation indicates that the IIHS barrier is the most suitable for simulating vehicle impacts to the front door of the occupant compartment.

As reported in Chapter 2, the average CDC extent of damage for far-side occupants who sustain AIS 3+ injuries is 3.6. The average CDC extent of damage produced in the IIHS tests plotted in Figure 6.1.3 is 2.0. This difference suggests that the far-side test speed should be higher than the near-side test speed used by IIHS.

The maximum deformation for the pickup impact was within 230 cm of the centreline of the Taurus. This produced an extent of damage of approximately 3.6. The Y-damage impact produced a lower extent of damage than that produced by the central impacts.

6.1.5 Conclusions

The Finite Element Models indicate that the IIHS barrier produced similar damage on a Taurus patterns to those produced by a full size pickup truck. The NHTSA barrier and the Y damage test produced less damage to the Taurus front door than the IIHS barrier.

The average CDC extent of damage produced in actual IIHS crash tests is considerably less than the average extent of damage to vehicles with far-side occupants injured at the AIS 3+ severity. Further work is needed to validate the FEM model at the higher crash severities that cause serious injuries in far-side crashes.

6.2 HUMAN FACET MODEL VALIDATION AND DUMMY EVALUATION

6.2.1 Introduction

The objective of this research was to use either of the two MADYMO human models provided by TNO – finite-element and faceted – to create a model that accurately simulates occupant motion in far-side impacts. This model will then be used as the baseline for future modelling. This task provided a comparison of the kinematics of dummy and human models in the far-side crash environment. The research is documented in more detail in reports listed in the Reference section [Alonso, 2004].

To date, anthropomorphic test devices (ATD's) have not been designed with consideration for human motion in far-side impacts. Thus leaving the question whether ATD's designed for frontal impacts or near-side crashes can adequately be used to model human motion in far-side. Previous tests with a BioSID dummy confirmed that the dummy does not suitably model the human motion, especially with consideration to the spine, since it is rather rigid. This was compared with a similar test with a human cadaver in far-side. (Fildes et al., ICROBI, 2002). Figure 6.2.1 illustrates these MADYMO dummies compared with a cadaver test.

From top left to top right, the dummies are Hybrid III, BioSID, and EuroSID 1. The bottom left and centre are EuroSID 2 and SID2s, respectively. These dummy models were exposed to a crash pulse from a 2000 Taurus side impact NCAP test at 62 km/h. The cadaver video, at the bottom right, shows the head excursion of the dummy does not nearly match that of the cadaver in relation to the passenger seat. This cadaver test was exposed to a slightly higher speed of 65 km/h.

In addition to the ATD MADYMO models, TNO provides two human cadaver models. One model was based on finite elements and the other used faceted surfaces. These two models were examined for suitability in far-side impacts.

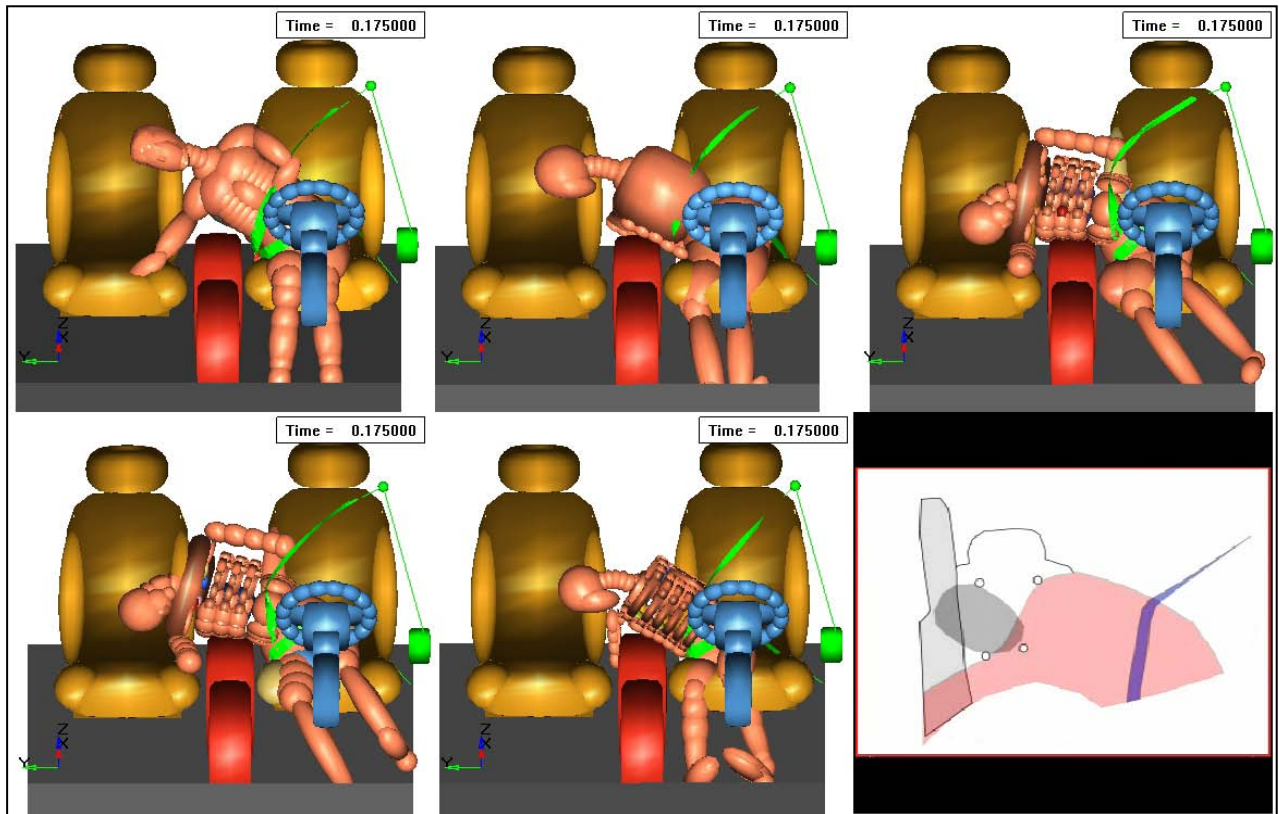


Figure 6.2.1: Dummy Models in Far-side with Cadaver Comparison - Hybrid III, BioSID, EuroSID 1, EuroSID2 and SID2s

6.2.2 Results

The TNO human finite element model proved to be difficult to use. First, the dummy cannot be initially positioned - the finite elements are fixed and validated in a certain position. Secondly, the runtime for the computer was extraordinary by MADYMO standards. It took a multi-processor machine 36 hours to run on 4 processors simultaneously. Finally, the model consistently went mathematically unstable. The meshed surfaces experienced extensive deformation causing the nodes to become chaotic and difficult to calculate further. The model could not run to completion. Figure 6.2.2 shows the human finite element simulation with theoretical centre console pelvis support.

By examining this figure, one must question the biofidelity of this model for far-side. The pelvis translation shown in the model is perhaps unrealistic. Also, the human model displayed extensive intrusion into the body, which a true human is unlikely to react in such a way with respect to the pelvis. It is noted that the model was developed and tested preliminarily for frontal impacts.

Conversely, the TNO human facet model showed promise when modelling a far-side crash. This model is simpler than the finite element model. It assumes rigid bodies surrounded by fixed nodes creating a faceted surface. Further, advantageous to this model is the representation of a flexible spine by modelling each vertebra with individual rigid bodies. Also, it provided flexibility in initial positioning by rotating joints for the knees, hips, shoulders, elbows, etc.

Some modifications were made to the model in order to make the human properly react with the seat belts. It is difficult for MADYMO to mathematically calculate a facet to facet surface contact. The quantity and penetration of nodal surface into nodal surface is difficult to resolve. Therefore, additional ellipsoids were added to the human underneath the skin layer. These ellipsoids surrounded the same rigid bodies that the facets do, except are used for the belt contact surfaces instead of the

facets. Ellipsoids were added for the rigid bodies making the pelvis, abdomen, shoulders, and upper arms. Besides the seat belt contacts, these ellipsoids are inconsequential to the rest of the model.

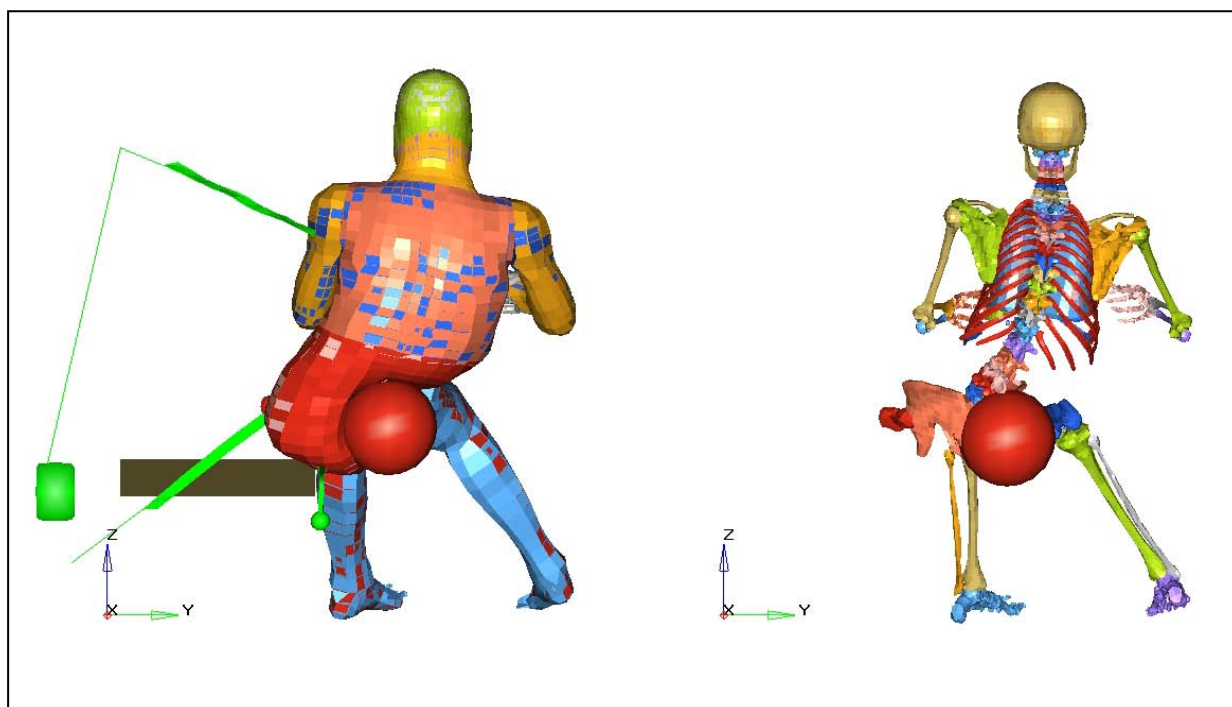


Figure 6.2.2: Human Finite Element Simulation

Upon placing the human facet model into the interior of the vehicle, positioning it properly, and defining the contact functions; the model duplicated the motion of the cadaver quite well. The excursion and upper body motion of the two were similar. Figure 6.2.3 shows the two synchronized at discrete time steps.

The crash pulse recorded during the cadaver test was used as the input for the MADYMO model. This pulse measured the lateral acceleration of the Holden Commodore as it was struck on the far-side.

One difference between the two models is noted in the shoulder belt. In the MADYMO model, the shoulder belt easily falls off the occupant. In the cadaver, some light friction keeps the belt on the occupant. In the MADYMO model, it is difficult to model friction between two faceted surfaces, which may explain this.

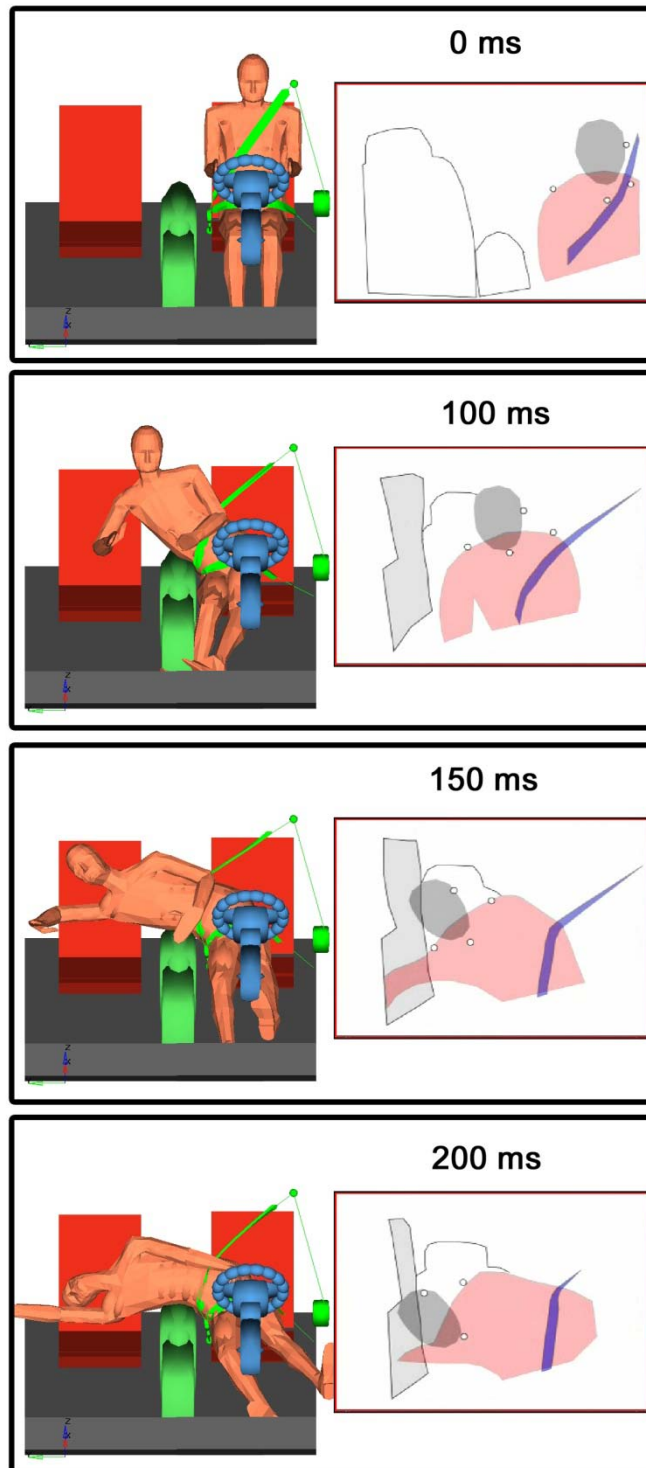


Figure 6.2.3: Human Facet Model with Cadaver Comparison

To further examine the human facet model, a direct comparison with a Hybrid III MADYMO model was made. A pulse from an IIHS barrier test was used to excite both models simultaneously. Figure 6.2.4 shows snap shots of the two at 0, 100, and 150 milliseconds.

Human Facet MADYMO Model vs Hybrid III MADYMO Model - IIHS Pulse

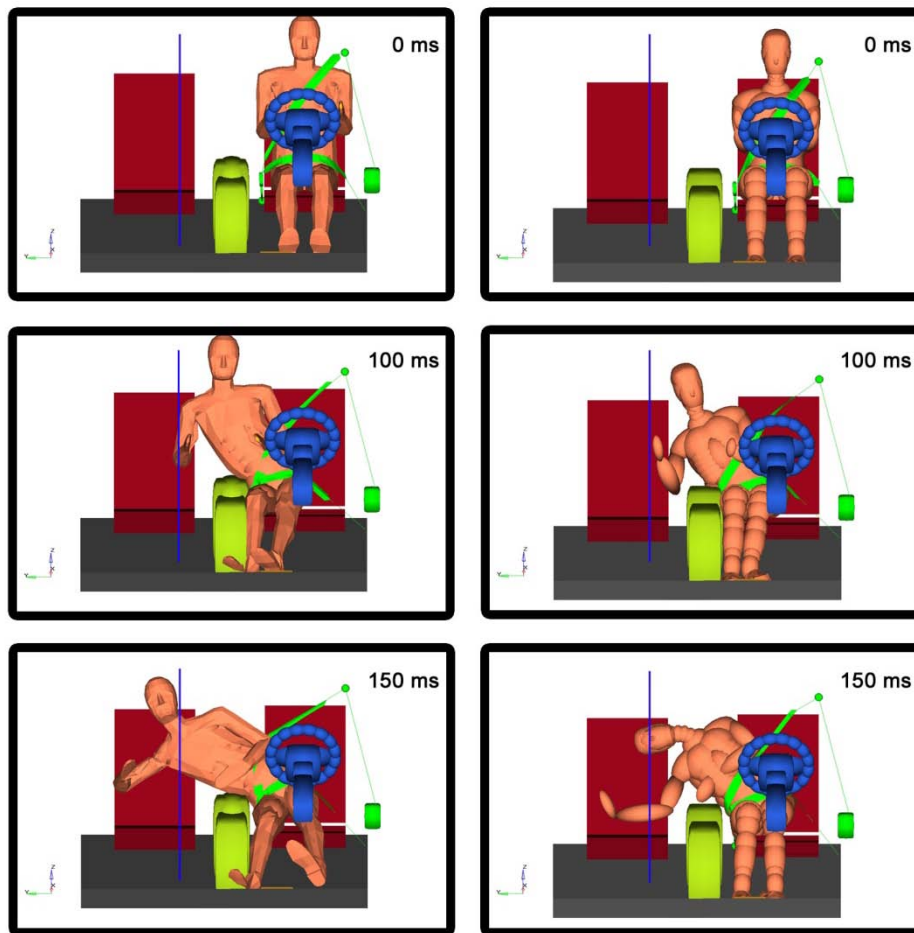


Figure 6.2.4: Human Facet MADYMO Model vs. Hybrid III MADYMO Model

In Figure 6.2.4, the vertical line through the passenger seat estimates the maximum intrusion distance from the impact. This estimation comes from a finite element vehicle model conducted at the GWU – National Crash Analysis Centre (Digges et al, AAAM, 2005). The difference between the human facet model and Hybrid III is clear when examining the occupant excursion towards the impact. The head location for the human facet model is similar to a cadaver test while the Hybrid III model produces quite different results..

6.2.3 Conclusions

Using visual approximations, the human facet model moved similarly to a human cadaver test under the same impact configuration. Using this single test as a benchmark, comfort was gained in this model – it moved more similar to the human than any crash dummy or other computer model did. In contrast the human finite element MADYMO model seemed not to be too realistic, and it was difficult to use. As shown in Figures 1 and 4, the MADYMO dummy models (Hybrid III, BioSID, EuroSID 1, EuroSID2, or SID2s) did not accurately reflect the motion of a human cadaver under the same impact configurations as a cadaver test.

In the future, this model should be refined and correlated to more cadaver tests. Parameters such as chest and head acceleration plots should be examined more closely and checked for correctness.

6.3 EFFECT OF SLED TEST PARAMETERS ON DUMMY KINEMATICS

6.3.1 Introduction

The objective of this task is to use the MADYMO computer simulation tool to examine the effects of the crash pulse and the centre console height on occupant motion in far-side impacts. The research is documented in more detail in reports listed in the Reference section [Alonso, 2004].

When examining occupant motion in far-side impacts, it is apparent that few countermeasures exist to limit motion towards the far-side surface. Occupant head strikes to the far-side surface (a-pillar, door, roof, or b-pillar) are observed in real world crash investigations. This is also confirmed in cadaver testing with full vehicle to vehicle collisions.

For belted occupants, which this study limits itself to, the lap portion of a 3-point seatbelt helps to keep the occupant's pelvis in the seat. However, the shoulder belt provides little resistance for the upper body, while the lap portion keeps the pelvis in place. The centre console also prevents the pelvis and abdomen from translating towards the impact. However, the size, shape, and even presence of a console vary among vehicle models.

Another objective was to use the MADYMO computer simulation tool to determine whether a square acceleration pulse of equal energy to a peaked crash pulse is suitable for far-side cadaver Hyge sled tests.

The Hyge sled at Medical College of Wisconsin was designed to run square shaped deceleration profiles. This sled will be used for future far-side human cadaver or dummy experiments. A previous cadaver test for far-side utilized a full-vehicle - Holden Commodore. This vehicle was struck on the far-side according to ECE 95 protocol. The test produced a multi-peaked acceleration pulse, as measured in full-vehicle crashes (Fildes et al., ICROBI, 2002).

6.3.2 Methods

A previous Task with MADYMO modelling, reported in Section 2, found the TNO human facet model placed inside a simplified vehicle model visually correlated rather well to a similar cadaver test. This grossly validated model served as the foundation for the centre console experiment. The model contained an occupant seated in the normal driving position with a steering wheel, centre console, transmission tunnel, and a 3 point belt system.

The lateral acceleration pulse from the cadaver test performed by Fildes et al. with a Holden Commodore was used as the input for each run (Fildes et al IRCOBI 2002). Only the y-direction acceleration was considered, ignoring x, z, roll, pitch, and yaw accelerations. As part of the study, the square sled pulse of the MCW sled was scaled to provide the same energy as the Holden crash pulse. Ten different levels for the centre console were chosen. First, the centre console was made flush with the driver and passenger seats. Each iteration of the model raised the centre console by 25 mm (approximately 1 inch). The centre console started out as flush then moved up by one inch until standing 10 inches above the seats.

6.3.3 Results

The vehicle crash pulse in Figure 6.3.1 was applied to the human facet model and the height of the centre console was varied. The combined forces placed on the centre console for each iteration of console height was determined. Figure 6.2.2 shows the peak force for each centre console height.

The two curves from Figure 6.3.1 were used as the input for a MADYMO model with the TNO human faceted occupant. The model was only accelerated in the y-direction (lateral) according to the curves. Any accelerations in the x or z directions were ignored, in addition to not accounting for vehicle roll, pitch, and yaw. Both simulations were run from 0 to 200 milliseconds. For any time beyond 170ms, the acceleration was assumed to be 0 m/s^2 .

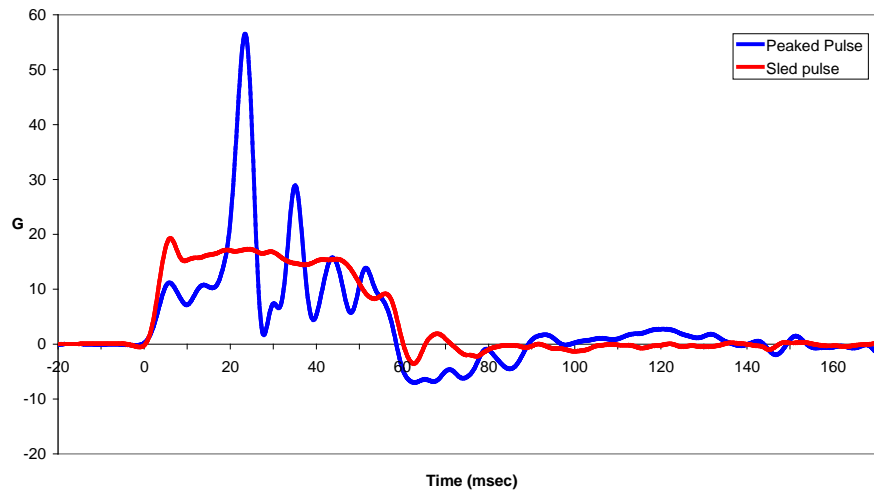


Figure 6.3.1: Peaked and Square Lateral Acceleration

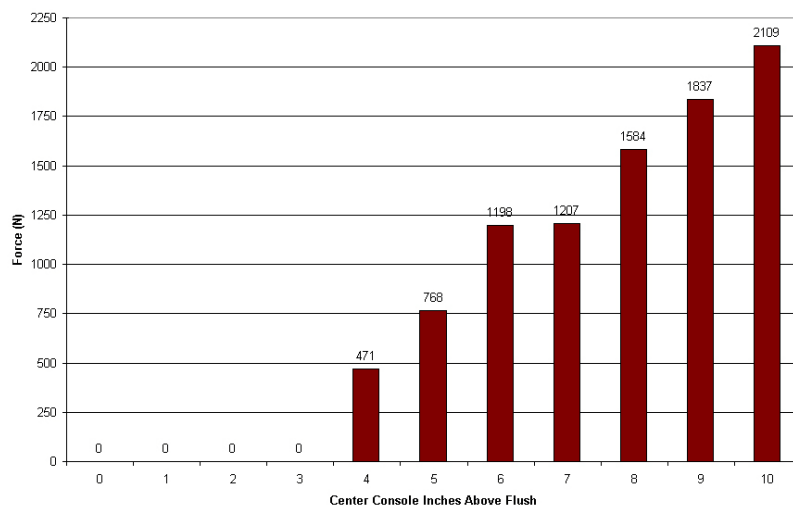


Figure 6.3.2: Centre Console to Occupant Peak Force

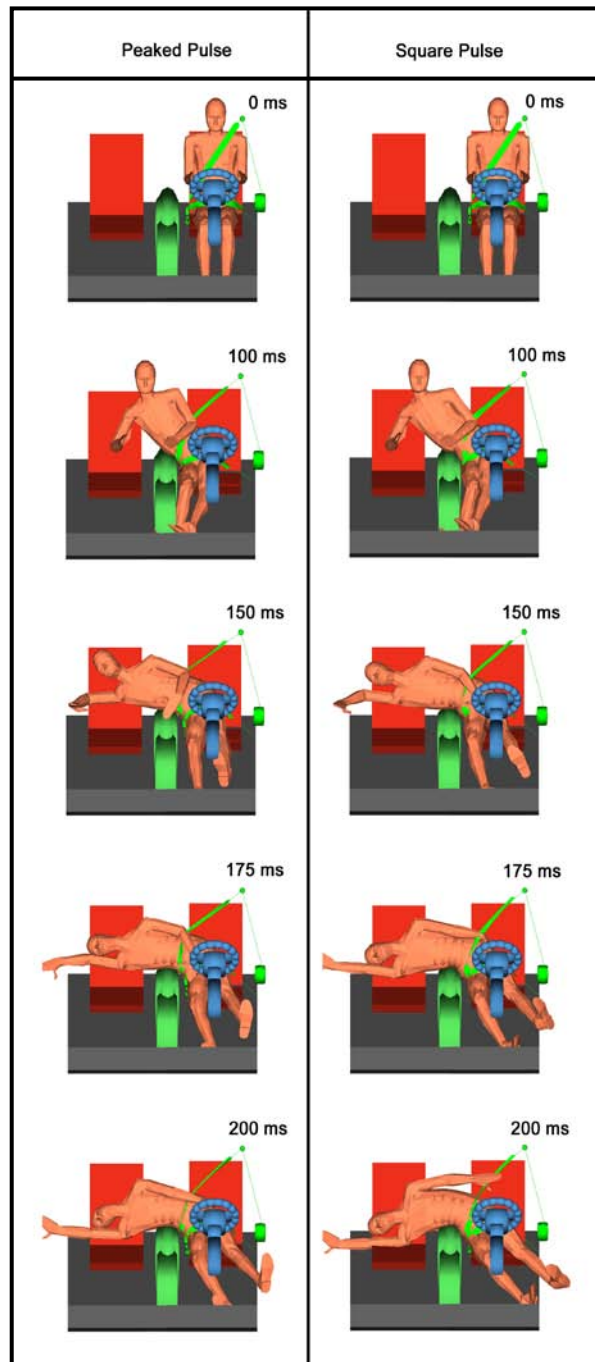


Figure 6.3.3: Human Facet Model with Peaked and Square Pulses

Figure 6.3.2 contains snapshots of the vehicle and sled pulse animations simultaneously. The model predicted the occupant excursion in a square wave impact was slightly greater than the excursion in a peaked wave impact, this is demonstrated in the snapshot at 175ms. Also, the occupant's reaction to the peaked pulse is delayed to that of the square pulse. .

6.3.4 Conclusions

The model predicts that the height of the centre console changed the occupant excursion slightly, perhaps not as much as would be expected. The modelling conducted in this section showed that a square wave sled test pulse can produce similar occupant kinematics to the desired car-to-car pulse.

The centre console height on the sled should be less than 12.8cm (8 inches) in order to separate the pelvic loading from rib loading.

The plots for the lap belt force numbers are inconclusive at this point. The human facet model used has not been correlated to a test and the forces have not been checked for correctness. From the plot in figure 6.2.3, it can be seen that the magnitudes of the belt forces did not change significantly as the centre console height changed, especially within the first 60 milliseconds. This could be interpreted that the lap belt holds the restrains the pelvis regardless of centre console height. Beyond this, though, the plot traces move erratically. This is when the pelvis moves upward over the centre console, which changes as the centre console changes.

In examining the consequence of different crash pulses, there were differences in excursion distance and time delay. However, the motion of the two human models remains remarkably similar based on these results from MADYMO modelling. Nearly the same result was achieved between the two with acceleration pulses of equal energy. Similar peak acceleration magnitudes of the head, chest, and pelvis were produced. The square pulse was considered to be satisfactory for simulating a far-side crash.

6.4 VARIATIONS OF DUMMIES AND COUNTERMEASURES

6.4.1 Introduction

Collisions occurring on the far-side of the vehicle to the occupant position account for a significant portion of automotive fatalities and HARM annually. All side impacts generally account for 35% of road trauma (Fildes 2002). Of these side-impact injuries, those resulting from impacts on the far-side of the vehicle account for 40% of HARM (Fildes, Digges, etc.). Despite these statistics, most research and regulations to date for side-impacts are dedicated to near-side, without further understanding of injury mechanisms of far-side.

Impacts on the far-side are most commonly characterized by a head injury and fewer chest and abdominal injuries (Fildes 1994). These outcomes stem from occupants excursion out of the seat and contacting the far-side door, impacting vehicle or object, or occupant (Fildes 1994). This same excursion and occupant kinematics are not seen in near-side impacts due to the nature of the event.

Since most side impact research and regulations are focused on near-side impacts, side-impact dummies are designed to consider injury criteria and biofidelic requirements of near-side hits. These are characterized by broad intruding impacts to one side of the body. Conversely, far-side is marked by excursion out of the seat and towards source of impact. Typical modern vehicle interior arrangements are limited in the ability to hold the occupant in place during this situation and thus results in upper torso movement and spinal bending. In contrast, the occupant usually absorbs near-side impacts in the ribs and hips. The stark differences in these two side-impact scenarios places the suitability of current side-impact ATDs for far-side impact testing into question.

This section of the report seeks to further evaluate the available dummy models using computer simulations to assess dummy responses to typical countermeasures in far-side crashes. For thoroughness, multiple angles and multiples speeds were used in the simulations. Additional details on this research are reported in the Reference section [Alonso, 2007].

6.4.2 Methodology

The model work commenced with a previous MADYMO model designed primarily for frontal impacts. It contained a Hybrid III crash test dummy seated inside a full vehicle interior. From this, any vehicle acceleration could be applied linearly in the x, y, or z-axis directions, concurrently with rotational accelerations around the three axes. Contact interactions and force deflection functions

between the dummy and vehicle interior were previously defined in the model. The first far-side simulations began by applying y-axis acceleration pulses for a side impact test to this same model.

Upon deleting the Hybrid III dummy from the model, the remaining vehicle interior was used as the basis of future simulations with other dummy models. The original model was written in MADYMO Version 5.4 and converted to MADYMO 6.0.1 in XML computer language. All further modelling conducted in MADYMO 6.0.1 table format.

Five dummy models in total were analyzed, they were:

- (1) Hybrid III; (2) BioSID; (3) EuroSID I; (4) EuroSID II, and (5) SID2s.

With these dummy models, five restraint configurations were simulated:

- (1) Baseline (just vehicle interior); (2) Reverse belts; (3) Base with chest airbag; (4) Base with shoulder airbag, and (5) Base with chest and shoulder airbag.

The five dummies and five restraint configurations were subjected to both a lateral and a 45 degree crash pulse. This totaled 50 simulations for the dummies. The human facet model was also subjected to the simulation matrix.

Figure 6.4.1 shows each dummy's prediction of neck injury for the air bag configurations. Three metrics were used: F_z , neck tension and compression; F_y , neck shear force; and M_x , the bending moment about x-axis. All these measurements were taken at the upper and lower bodies of the neck. The graphs display the peak forces and moments for each measurement. The vertical axis represents the percent value of the injury assessment reference value.

6.4.3 Discussion

For each of the simulations in the configuration with only a standard 3-point belt, it was seen that occupant excursion existed towards the passenger seat, but did not reach the door. Although the five dummies reacted similarly, differences still existed. For example, the BioSID, with a rigid spine was not able to bend easily around the centre console, transmitting more load onto the neck. Conversely, the Hybrid III with the exact same neck contained lower forces. The more flexible spine of the Hybrid III allowed it to bend and thus decrease neck forces.

To assess the dummies' suitability for far-side testing, additional countermeasures were introduced to reduce occupant excursion. The countermeasures were: chest and shoulder airbags and a 3-point seatbelt in the reverse direction. Each limited occupant excursion, however, exposed more unique possibilities of injuries.

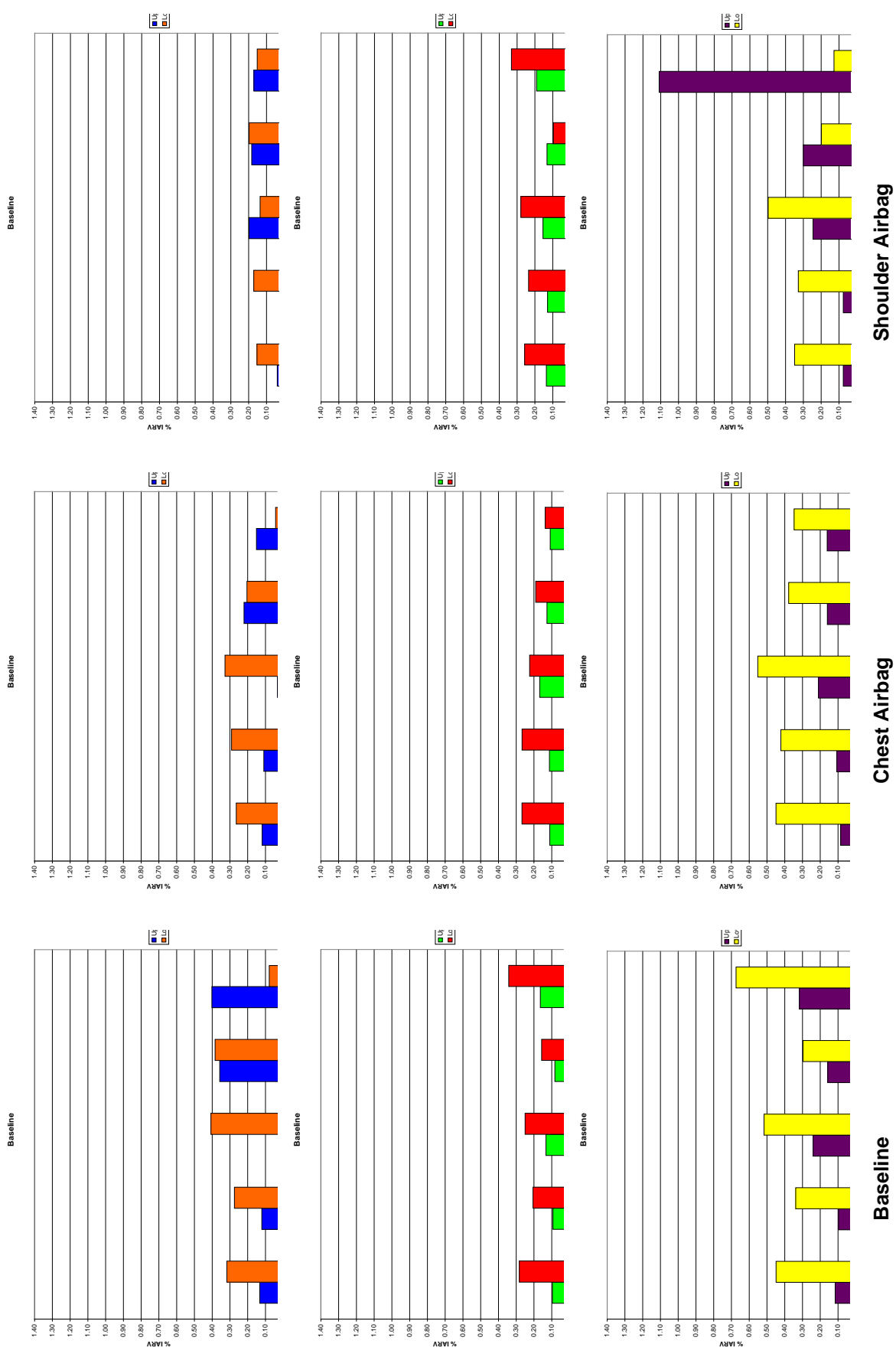


Figure 6.4.1. Neck Output

A chest airbag prevented some excursion, but not nearly as much as the shoulder bag or reverse belt. However, it restrained each dummy in the rib region, which introduces the potential for rib injuries.

The shoulder airbag restrained each dummy at the top of the torso. This was effective at preventing occupant excursion, however, it left the head unrestrained. By restraining the upper body and leaving the head unrestrained additional load was transmitted to the neck. For this countermeasure, the Hybrid III neck measurements were close to the injury value, but still below the injury threshold.

The chest and shoulder bags together acted similarly to the shoulder bag alone. This situation looked much like a near-side impact and contact with a door. Again, the head was unrestrained and put additional stress on the neck.

The SID2s was the only odd sized dummy used. The EuroSID I and II, BioSID, and Hybrid III are all based on a 50th percentile male. The SID2s, based on a smaller individual, exposed the vulnerability of the chest and shoulder bags to smaller sized occupants. The SID2s struck the chest bag with its shoulder and the shoulder bag with its head/neck. Positioning of these bags may be difficult for oversize and undersized occupants. Additionally, the chest and shoulder bags showed possible weaknesses of the countermeasures for elderly occupants with weak bones. The chest bag put nearly all forces into the rib areas, and the shoulder bag onto bones of the shoulder.

The reverse 3-point belt is a simple and cheap method of restraining an occupant for far-side collisions. The simulations demonstrated the effectiveness of such a countermeasure. All ATDs were prevented from moving over the centre console, by loading the neck and shoulder. Although effective at restraining motion using the neck, this sensitive area of the body can lead to further injuries. MADYMO was able to show significantly higher neck load forces for this situation, many beyond injury thresholds.

6.4.4 Conclusions

Side-impact dummies, designed primarily to test for occupant injuries on the near-side are limited in their ability to emulate occupant kinematics for a far-side impact. A Hybrid III test device, designed primarily for frontal impacts, is limited in its ability to test for far-side impacts. Based on historical crash data, the leading cause of injury in side-impacts on the far-side is head strikes with the opposite side hard vehicle surfaces. The occupant kinematics that led to this result were reproduced with a post mortem human subject (PMHS). The PMHS, seated in the vehicle, moved out of its seat and contacted the far-side B-pillar when its vehicle was impacted on the far-side.

Computer simulations offer an easy way to test additional dummies and circumstances. Five anthropomorphic test devices (ATDs) were simulated in MADYMO for far-side impacts and all failed to produce desired kinematics.

Despite the short-comings of the dummies for reproducing far-side kinematics, the reaction of these dummies in MADYMO to certain countermeasures offers some insight into future studies. A reverse 3-point seatbelt effectively restrained the occupant. However, it significantly increased neck force levels.

Chest and shoulder airbags contained the occupant and prevented excursion. However, these countermeasures left the head and neck unrestrained and an awkward movement of the head resulted. In addition, the use of a petite dummy showed that positioning of these airbags for different size occupants may be difficult.

6.5 SLED TEST CONFIGURATIONS FOR THE FAR-SIDE CRASH ENVIRONMENT

6.5.1 Introduction

In order to develop countermeasures for occupants seated on the non-stuck side of a vehicle it is necessary to specify the sled test procedures to evaluate the safety performance. To date there have been very few crash tests with dummies on the far-side of the crash. The primary purpose of this study is to develop sled tests that mimics the far-side crash environment. The crash orientations selected for this study include crash tests of vehicles that undergo significant yaw during the event. A successful duplication of occupant motion in far-side crashes will prove that a sled test is an effective, cost-efficient means of testing and developing safety countermeasures for far-side occupants.

This research applies finite element vehicle modelling and MADYMO occupant modelling to determine the sled test conditions required to simulate crash environments that produce significant numbers of AIS 3+ injuries to far-side occupants. Of particular interest are angular crashes and crashes that produce vehicle rotation that could influence occupant kinematics. The SNCAP test was included in the study because the striking barrier's direction of travel is 63 degrees relative to the centreline of the struck vehicle.

The following crash modes were modeled in this study: The NHTSA Test 4660 is discussed in this summary. The other results are contained in the paper documenting the research [Cuadrado 2008].

- SNCAP Crash Test
- Y Damage Crash Test
- 40% Overlap 30° Corner Impact Crash Test (NHTSA Test 4660)

6.5.2 Background

The crash environment that produces injuries in far-side impacts has been studied by others [Gabler 2005, Digges 2001]. A large number of crashes that produce serious injuries occur in configurations that produce rotation of the impacted vehicle. To date, the countermeasures being evaluated in sled tests that do not consider the complications created by vehicle rotation [Bostrom 2003]. A requirement exists for appropriate sled test configurations to permit the economical development of effective far-side countermeasures. Initial considerations of the sled test requirements for crashes with rotation have been published by Smyth [2007]. The present study is based on a thesis for a Master's degree at the George Washington University [Cuadrado, 2008]. The thesis contains additional simulations based on finite element models of vehicle-to-vehicle crashes and in-depth evaluations of the requirements for a sled crash pulse.

The change in velocity, or delta-V, is a metric frequently used by researchers and experts to define crash severity and determine injury causation [Palmer 2006]. Numerous studies have analysed the relationships between the vehicle delta-V, occupant delta-V, and occupant injury [Marine 1998, Buhdorf 1996, Roberts 1993]. For cases with negligible vehicle rotation, the occupant delta-V is similar to that of the vehicle [Cheng 1989]. However, the delta-V must be calculated for every position within the vehicle if it rotates to account for the change in angular velocity and angular displacement [Fay 1996]. Taking the rotational component into consideration means that the total delta-V for occupants on one side of the vehicle will be reduced while increasing the total delta-V for occupants on the other side of the vehicle [Fay 1996]. This fact is pertinent in understanding the differences in the crash environment between near and far-side occupants.

Another important consideration is that near-side occupants contact the inside of the vehicle within 50 ms of the initial impact while far-side occupants can strike the interior as late as 180 ms after impact [Solinski 1997]. This is particularly significant in side collisions. Near-side passengers are commonly struck by the intruding interior while far-side occupants have sufficient interior space to permit more of the crash energy to be absorbed by restraint systems before contact with the vehicle interior occurs. In addition, the longer "ride down" time for far-side occupants permits more time for a rotating vehicle to move relative to the occupant. Consequently, the influence of the vehicle's motion and intrusion will be different for far-side occupants.

6.5.3 Methodology

The kinematics of far-side occupants exposed to impacts that involve vehicle rotation are largely unknown. As of 2007 there are over 5000 crash tests in the National Highway Traffic Safety Administration (NHTSA) database, but only three tests were found to have been performed with a far-side dummy. These tests were unable to be used in this study because they were not instrumented with accelerometers in the lateral direction and poor video quality prevented accurate yaw data to be obtained through video analysis. In addition, US Government research has not conducted crash tests in configurations that are responsible for most of the far-side injuries. Consequently, the far-side occupant motion in a crash test configuration must be determined in order to design a sled test for each considered case. The cases chosen in this study were based on three full-scale crash tests that were available in the GW film library. None of these crash tests contained a dummy on the far-side of the vehicle.

The methodology involved running the MADYMO model in two steps [MADYMO 2004]. The MADYMO human facet model was selected based on the validation of the model for far-side occupant simulations by Alonso [2005] and summarized in Sections 3 and 4 of this Section.

In the first step, the actual vehicle acceleration and yaw experienced by the subject vehicle in each crash test were used to create the acceleration environment for a MADYMO model to determine the motion that a far-side occupant would undergo in each crash mode. The computer model permits the vehicle to undergo both linear and angular accelerations that vary with time. Consequently the actual rotation of the vehicle can be simulated. However, it is assumed that the sled angle will remain constant. The challenge was to determine the appropriate sled angle to simulate the far-side crash environments represented by injury producing events.

The second step was to determine a sled test with a constant angle of rotation that best simulates the far-side occupant motion and contacts. In this step, runs with different sled angles were conducted and the far-side occupant motion was compared with the response in the crash test from step one.

The input variables of the sled test model were altered until the occupant motion matched that of the crash test model. The reference condition for the evaluation of occupant motion was the occupant restrained only by a lap belt. The objective was to match the trajectory of the head as closely as possible to the occupant in the crash pulse model. The lap belt configuration was chosen to maximize the amount of distance the occupant's head would travel unimpeded. Errors that may be indistinguishable when comparing 3-point belted occupants will be exacerbated due to the longer travel distance. The proper configuration was then simulated and compared for occupants using 3-point belt restraints. The final sled test configuration can then be used in an actual sled test to mimic the occupant motion of a far-side occupant exposed to the original crash environment.

The dummy model seating position was determined from the 2000 Ford Taurus SNCAP NHTSA Test Report (Test No. 3263). Although more far-side accidents occur with an occupant in the driver seating position, the passenger position was chosen to allow for a greater travel distance before interacting with the vehicle instrument panel.

In this study, the sled angle is defined as the angle that the buck is rotated with respect to its position in the crash pulse tests. The pulse is applied to the buck in the negative x-direction of the global coordinate system. The sled angle for a frontal impact test is 0° and is 90° for a side impact test. The initial sled angle for each pulse was set to the impact angle between the bullet vehicle/barrier and the longitudinal axis of the target vehicle. The simulations were then run using the baseline vehicle crash pulse. The sled angle and pulse were then adjusted on a trial and error basis until the timing and contact locations of the sled test occupant matched that of the crash pulse model.

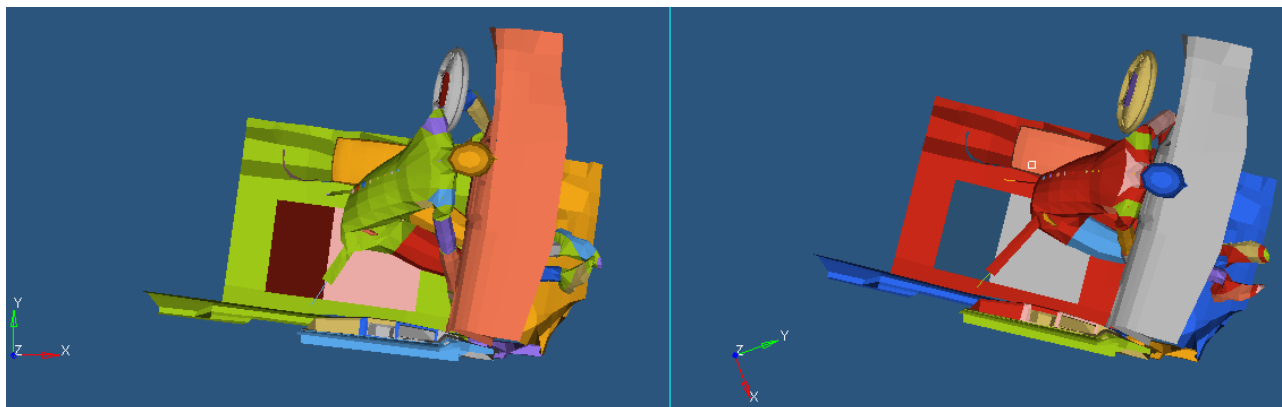


Figure 6.5.1. Comparison of 30° Corner Impact Crash Pulse Test (left) to Initial Sled Test (right)

Results from sled test simulations revealed that the angle between the occupant's torso and the instrument panel significantly differed between the crash pulse model and sled test model (see Fig 6.5.1). This difference is only noted in crashes where vehicle yaw was a factor. Therefore, the difference was attributed to the rotation of the vehicle relative to the occupant.

In order to deal with crashes in which the vehicle rotates relative to the occupant, the dashboard on the sled was rotated. This technique created a sled buck with the seat and floorboard in the coordinate system of the crash tests' initial position and an instrument panel in the coordinate system of the crash tests' final position. This sled modification allowed for the vehicle yaw to be considered (see Figure 6.5.2).

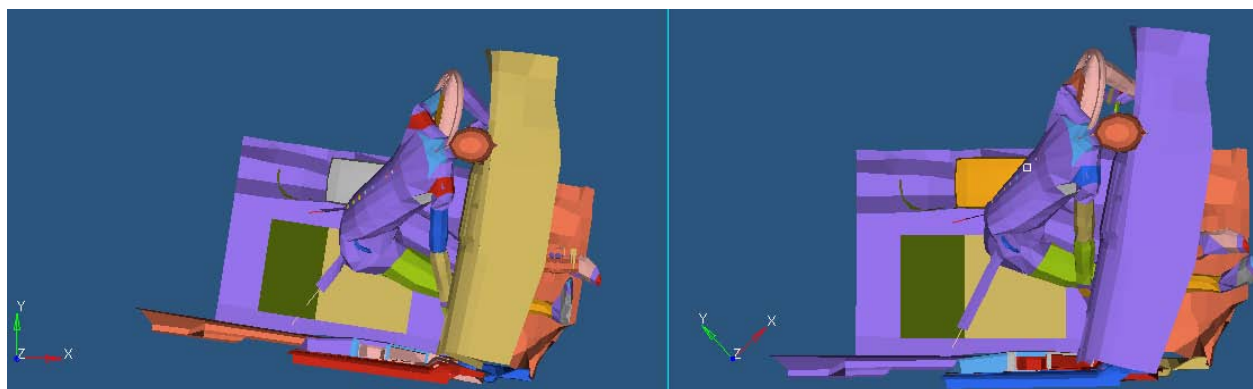


Figure 6.5.2. Comparison of 30° Corner Impact Crash Pulse Test (left) to Initial Sled Test (right) with Rotated Instrument Panel

6.5.4 Simulations

The sled test configurations are defined by the following parameters: pulse shape, pulse magnitude, pulse duration, sled angle, and instrument panel angle. Three crash test cases are presented in detail to demonstrate the process used to determine the proper sled configuration. The cases to follow will concentrate on the appropriate sled angle and instrument panel angle. A discussion of the crash pulses can be found in the documentation for the complete study [Cuadrado 2008].

The available crash tests did not have a dummy located in the far-side seating position. Consequently, the motion of the far-side occupant was simulated using the MADYMO human facet model. The simulation was accomplished by applying the vehicle acceleration pulse measured at the occupant

location during the actual crash. This simulation was called “Pulse” because the actual crash pulse was applied to the simulation

Two belt configurations were simulated. These configurations were lap belt only and conventional three point lap and shoulder belt. In the baseline simulations, the far-side occupant was restrained by a lap belt only. This belt configuration was chosen to provide the most extreme upper body excursion for a restrained occupant. This configuration also represented a worst-case scenario in the event the shoulder belt had no influence on the kinematics.

The kinematics obtained from the lap belt “Pulse” simulations formed the basis for judging the suitability of a sled configuration to provide the same general motion and upper body contact locations. The sled test was simulated applying a constant direction acceleration pulse that was representative of the crash to an occupant compartment configuration that was rotated relative to the direction of travel. The simulations of the sled configurations were labelled “Sled”.

It was found that in some crashes, the rotation of the vehicle relative to the occupant was sufficient to require that the dashboard be rotated as well as the sled angle. The kinematics of the far-side occupant restrained by a lap belt was compared with the kinematics from the “Pulse” simulation. The sled and dashboard angles were adjusted until agreement was reached. After agreement of the lap belt configurations, the “Pulse” and “Sled” simulations with three point belts were compared.

6.5.5 Simulation Results

Table 6.5.1 presents the final sled and instrument panel angle for 3 different tests modelled in this study. The details of these simulations are included in the paper that documents the study [Cuadradro, 2008]. Although the moving barrier in the SNCAP test had a direction of travel 63 degrees to the struck vehicle centrelines, the appropriate sled angle was almost 90 degrees (87°). The Y damage tests had the same sled angle (87°), but required a rotated interior that resulted in the greatest total angle of 95.4°.

The instrument panel angle is equal to the vehicle rotation when the event is considered ‘over’ in each case. For this reason, it is dependent upon the location that the force of impact acts and the moment that it places on the vehicle with respect to the vehicle’s centre of gravity. This effect is observed by comparing the SNCAP and Y damage tests, which both contact the side of the vehicle. The MDB in the SNCAP test contacts the subject vehicle near its centre causing the PDOF to pass near the vehicle centre of gravity. The bullet vehicle in the Y damage test contacts the target vehicle in the front of the vehicle creating the 8.4° of rotation observed in the test. It follows that the amount of energy transmitted by the bullet vehicle in a Y damage crash configuration could influence the sled configuration.

Table 6.5.1. Summary of Sled and Instrument Panel (IP) Angle

TEST CONFIGURATION	TEST IMPACT ANGLE	SLED ANGLE	IP ANGLE	TOTAL ANGLE
63° SNCAP – 25.8 k/hr	90°	87°	0.0°	87.0°
90° Y Damage ~ 26 k/hr	90°	87°	8.4°	95.4°
30° Corner Impact - 57.6 k/hr	30°	43°	8.5°	51.5°

The total angle for each test configuration is composed of the sled angle, or angle of the sled buck, and the instrument panel angle, which is equal to the amount of rotation experienced by the vehicle during the event. An increase in the impact angle of the bullet vehicle to the target vehicle typically increases the sled angle, but a direct correlation can not be made between the two angles.

For the three cases simulated, the occupant kinematics of the sled tests accurately mimicked the occupants of their corresponding crash tests. The sled test configuration determined from the lap belt tests was also found to be the proper configuration for occupants wearing 3-point belt restraints

The accuracy of the sled test occupant excursion is greatly dependent upon the amount of vehicle rotation in the crash test. This is seen in the Head Excursion Cross Plots as the sled tests occupants move in a relatively linear motion while the vehicle rotates underneath the crash tests occupants. The Head PDOF plots reiterate these findings as the Sled curves remains relatively constant and the Pulse curves change dependent on the amount of vehicle rotation. In all cases the Head PDOF of the Sled and Pulse curves are nearly identical when the event is considered 'over' for the crash mode.

6.5.6 Conclusions

The results from this study show that a sled test can effectively mimic the kinematic response of a far-side occupant in the side and corner impacts for which there was crash test data. The impact angle, initial vehicle velocities, delta-V, and impact location are all important factors in developing a proper sled test configuration. However, no direct correlations were able to be determined between a single variable and the sled pulse or correct sled or instrument panel angle to be used in the test configuration. Of equal importance to each of these variables is how the structure of each vehicle interacts with one another. This interaction is highly dependent upon the previously mentioned variables but can drastically change with small variations in the impact conditions.

Although the results from this study conclude that crashes are too complicated to correlate a single input variable to the sled configuration, certain sled configurations may accurately represent a wide range of crash environments. For example, a sled test angle of 87 degrees appeared to be appropriate for both the SNCAP and the Y-damage test conditions that were simulated. The use of the approach documented by this paper will provide a basis for determining the best sled configuration to mimic any far-side crash condition.

7 COMPUTER MODEL DEVELOPMENT

AUTHORS: Clay Douglas, Brian Fildes, Tom Gibson & Peter Hillard

7.0 INTRODUCTION

In current vehicles, the primary form of restraint for a far-side occupant is the outboard mounted three-point (lap-sash) seatbelt. However, it has been recognised that this design does not always provide sufficient thoracic restraint in far-side impacts. In the early 1990's, Mackay et al. (1993) observed that of those far-side occupants sustaining AIS 2 head injuries, 35% experienced excursion from the shoulder section of the seat belt. A similar finding was reported more recently Gabler et al. (2005), where he observed that 32% of the AIS 2+ head injuries could be attributed to contact with the right interior, b-pillar and roof. In order to be subjected to impacts from these contact sources, it is likely that the occupant slipped out of the shoulder portion of the seatbelt. Another finding by Gabler and colleagues was that the seat belt was the cause of 86% and 24% of AIS 2+ abdominal and chest injuries respectively sustained in far-side crashes (Gabler et al., 2005). There have been few laboratory tests investigating the problem of seatbelt performance in far-side impacts (Adomeit et al., 1988; Horsch, 1980; Kent et al., 2003; Törnvall et al., 2005), primarily due to the lack of government regulations and consumer tests. Another issue which has not yet been analysed is the role of seat back contour and its effect on lateral restraint.

Due to the lack of far-side impact regulations, no ATD has been designed specifically for far-side impacts. It has been proposed that the WorldSID is the best of the available ATDs for this impact configuration, but it still exhibits certain limitations (Fildes et al., 2002). In his comparison of ThorNT and WorldSID against PMHS in a series of far-side impacts, Pintar concluded that both types of ATDs had limitations (Pintar et al., 2008). WorldSID appeared to operate better in lateral impacts and in cases where plate-type countermeasures are used, whereas Thor-NT was better in oblique impacts and evaluating belt-type countermeasures. The results from both the WorldSID and the Thor-NT were implicated by the performance of the thorax-abdomen regions, which were not capable of accurately measuring deflection.

While there may not be a well accepted physical ATD for far-side impacts, there is potential to use computer models to further investigate occupant dynamics and countermeasures. The TNO Human Facet Model (HFM) has been proposed as the best model available far-side impact analysis (Alonso et al., 2008). Alonso and colleagues compared the BioSID, EuroSID II, SID-II, TNO Human FE Model and the HFM through simulating a simplified far-side impact modelled on physical test results from Fildes et al., (2002). Despite the simplified approach, it was clear that from the models investigated, only the HFM was suitable for use in far-side crash simulations. The TNO HFM is a multibody model consisting of rigid and flexible bodies connected by a series of joints whose exterior contact surface is made up of facets (Figure 7.1). While the model does not strictly use the finite element method, it provides an increased level of sophistication compared to earlier ellipsoid models.

In terms of occupant biofidelity under impact loadings, the HFM has been partially validated for frontal, rear and lateral impacts (TNO, 2005). De Lange et al. (2005) demonstrated the most complete validation of the HFM thus far showing that in lateral impacts the model compares well to the most advanced side-impact ATD, the WorldSID (8.6 compared to 8.0). In these lateral impacts, De Lange and colleagues used simulations based on physical requirements from ISO-TR9890. This demonstrated the model's lateral biofidelity for the head, neck, thorax, abdomen and pelvis. The primary aim of this aspect of the collaborative project was to develop and validate an occupant model for far-side impacts. This model was then designed to be capable of predicting trends in occupant response when subjected to various impact configurations.

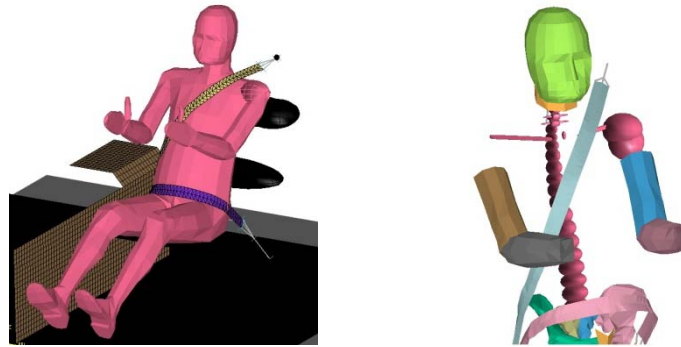


Figure 7.1. The modified TNO Human Facet Model in a sled set-up (left) and the model without thorax elements present, but with spine and shoulder ellipsoids present (right).

7.1 TESTS CONDUCTED AND RESULTS

The version of the TNO Human Facet Model used in this study is that modified and described in Douglas et al. (2008). The model runs in MADYMO Version 6.2.2. All mathematical models were created to geometrically match physical testing. The HFM was exercised through a series of pendulum, quasi-static rig, sled and full-vehicle tests with the results compared to volunteers, PMHS and ATDs where available.

All channels are filtered according to SAE-J211. Thoracic and abdomen deflections were measured at the site of impact using the displacement of the deformable bodies which are pre-existing in the HFM (DISVEL output files). The HFM has four sets of deformable bodies located on the front and lateral sides. All HFM accelerations and contact forces were derived from the LINACC and CNTFRC outputs files in the MADYMO.

7.1.1 Quasi-static far-side tests

These tests aimed to characterise the influence of belt geometry and pretension on the belt to shoulder-complex interaction in a lateral far-side impact. This was achieved using a test rig that rotated the subject in the frontal plane, about an axis running horizontal to the ground through their thorax. When rotated 90°, the subject experienced a 1g lateral force. The subject was seated normally in a Volvo V80 seat with the belt in the driver's position (Figure 7.2). The seat x-position (fore/aft) was instrumented such that 5 positions: 0, 60, 120, 180, and 240 could be determined. These positions (measured in millimetres from most-rearward) represented 0%, 25%, 50%, 85%, and 100% forward.

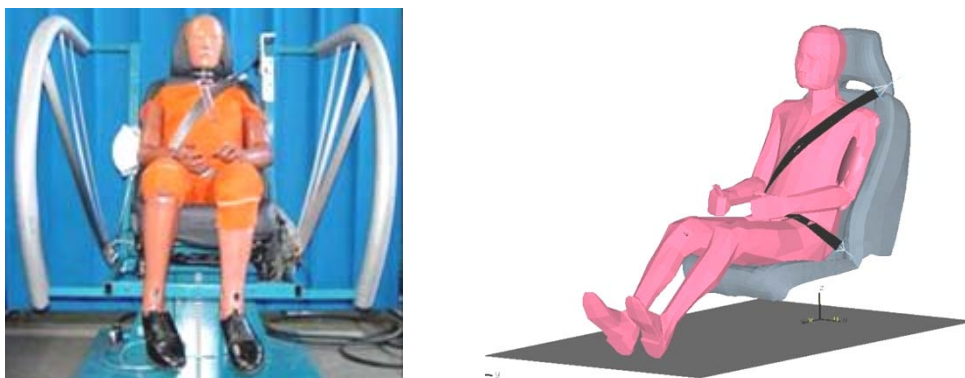


Figure 7.2. Rotating quasi-static rig: the actual rig (left) and the simulated rig (right).

Three subjects were put through the entire matrix of tests: a Hybrid III 50th percentile male; a Hybrid III 50th percentile male with a spring-spine (as seen in Boström et al., 2005); and a mid-sized male volunteer (V1) (180cm, 80kg). The Spring-spine was added to the Hybrid III ATD to allow the spine to shear, bend and elongate. A second volunteer (V2) with broader shoulders and greater chest depth was exposed only to the X=120mm, 0N pretension configuration to highlight the difference body size had on the resulting restraint. V1's shoulder breadth was approximately 480mm, whereas V2's was 560mm. The shoulder breadth of the human model was approximately 460mm.

The only measurement from the physical quasi-static tests was whether the seat belt slipped off the shoulder or not. Slip was deemed to have occurred if the belt slipped off the shoulder and loaded the upper arm. Five physical tests were conducted with each subject at the same configuration. As such, the percentage of times belt slip occurred for each configuration was determined. As the model's shoulder was not standard, shoulder anteroposterior (AP) thickness was varied to quantify the model's sensitivity to this dimension. The standard AP thickness used was 106mm, which represents a 50th percentile male (Tilley et al., 2002). Here, shoulder AP thickness was increased to 116mm and also decreased to 82mm to replicate dimensions for 99th and 1st percentile males respectively (Tilley et al., 2002). The results from the four rearmost D-ring positions are shown (Table 1). For V1, the most-forward D-ring (X=0mm) gave the same results as X=60mm. Hence those results are not shown.

Table 7.1. Quasi-static test results at 1g. The numbers represent the proportion of time slip occurred at that configuration while the shading represents cases that match V1's response.

VOLUNTEER 1 (V1)			
D-ring Pos.	0N	100-150N	200-250N
60	100	100	100
120	100	100	20
180	100	0	0
240	100	0	0

HYBRID III SPRING-SPINE			
D-ring Pos.	0N	100-150N	200-250N
60	100	60	0
120	100	0	0
180	0	0	0
240	0	0	0

HUMAN MODEL			
D-ring Pos.	0N	125N	225N
60	100	100	100
120	100	100	0
180	100	0	0
240	100	0	0

HYBRID III			
D-ring Pos.	0N	100-150N	200-250N
60	60	0	0
120	0	0	0
180	0	0	0
240	0	0	0

The results from the volunteer tests indicated that a trend exists between moving the D-ring rearward, increasing pretension, and thus, an increased likelihood of the belt engaging the shoulder. A visual example of subjects in cases of belt slip and shoulder or thorax engagement can be seen in Figure 7.3. The results also highlighted that the model correctly predicted the binary outcomes from the mid-sized volunteer tests, in addition to the trend observed between D-ring position, pretension and belt slip. The only difference being the case of X=120mm, 200-250N, where the model was not able to predict a 20% likelihood of slip. This model was only capable of predicting 0% or 100% likelihood, as the input parameters are fixed for a given configuration. In the physical testing, some minor differences in test setup may have been present. Hence the reason for completing five tests at any one configuration.

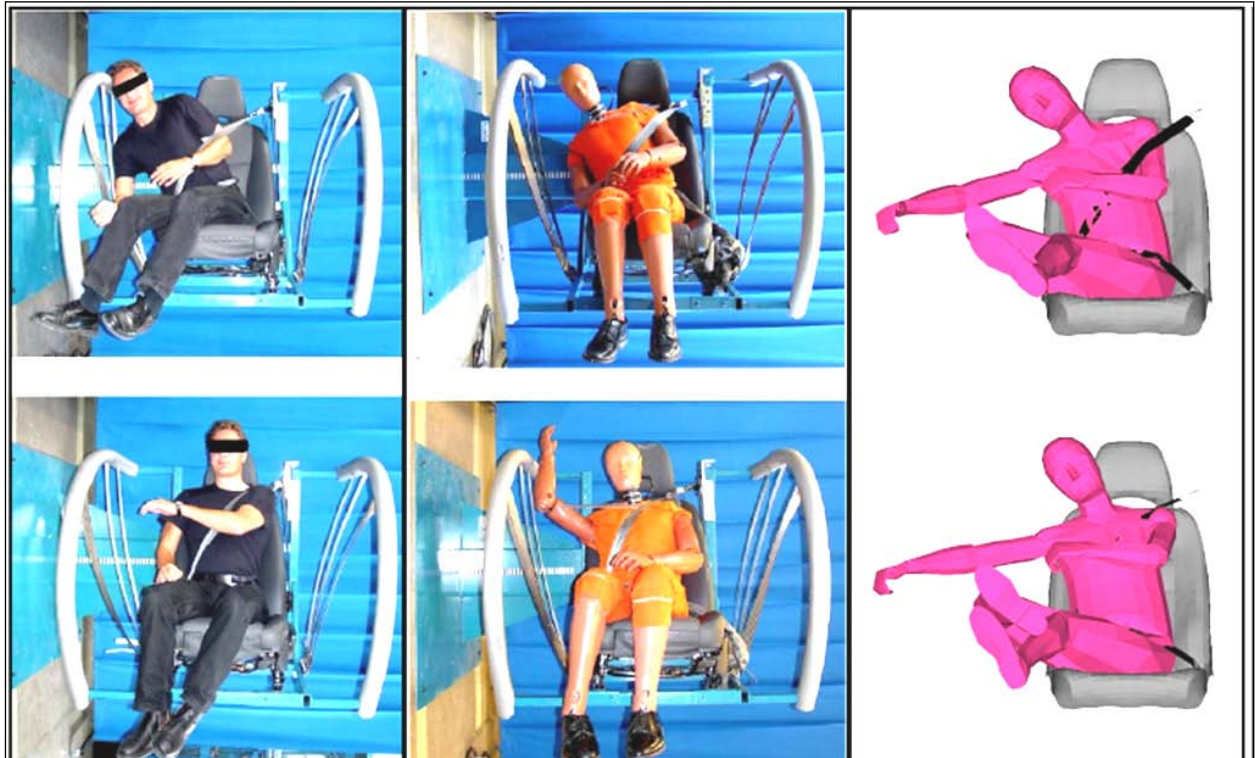


Figure 7.3. Volunteer 1 (left), Hybrid III Spring-Spine (centre) and Human model (right). Cases indicative of belt slip are seen on top, with cases engaging the shoulder or thorax on the bottom.

In addition to the slip or no-slip condition, model T1 lateral (Y) displacements were plotted to quantify the effect of D-ring position and pretension on the thorax lateral displacement (Figure 7.4). The results indicated that the belt slipping (or not slipping) off the shoulder is a crucial factor influencing the magnitude of thorax lateral displacement. For cases where the belt slips off the shoulder, T1 displacements average 138mm, whereas when the belt engages the shoulder the average displacement is 126mm. This only equates to an average 9% reduction in T1 lateral displacement. It should be noted however that the maximum displacements for cases with slip occurred approximately 200ms earlier than those with engagement.

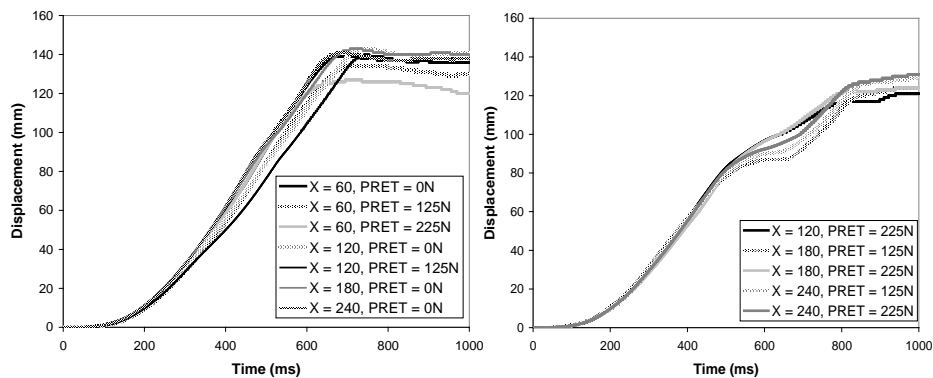


Figure 7.4. T1 lateral displacement versus time for cases with belt slip (left) and those engaging the shoulder (right).

As previously mentioned, V2 was only tested in the X=120mm, 0N pretension case. At that configuration, no belt slip was observed for the larger occupant. Despite this only being a single configuration, it suggests that anthropometry plays a major role in governing restraint. It also implies

that outboard mounted three-point belts may better restrain larger occupants in far-side impacts. Due to this effect, it was expected that varying the model's shoulder AP thickness would affect belt to shoulder interaction. Results suggest that this dimension is an important factor in governing restraint (Table 7.2). Specifically, that an increased shoulder thickness increased the likelihood of the shoulder engaging the belt and vice versa. Other factors such as shoulder breadth and chest depth may also be contributors, however this was not possible to vary with the model at hand. Hence, thus far, all these results suggest is that the model is sensitive to shoulder AP thickness. Further investigations should be carried out with more volunteers in an attempt to better quantify this relationship.

Table 7.2. Sensitivity of model to shoulder AP thickness.

HUMAN MODEL (1% SHOULDER)				HUMAN MODEL (99% SHOULDER))			
D-ring	0N	125N	225N	D-ring	0N	125N	225N
60	Y	Y	Y	60	Y	Y	Y
120	Y	Y	Y	120	Y	N	N
180	Y	N	N	180	N	N	N
240	Y	N	N	240	N	N	N

HUMAN MODEL (50% SHOULDER)			
D-ring	0N	125N	225N
60	Y	Y	Y
120	Y	Y	N
180	Y	N	N
240	Y	N	N

7.1.2 Pendulum tests

In far-side crashes, occupants commonly sustain oblique impacts to the thorax and abdomen region either caused by contact with rigid objects or the seat belt. For this reason, pendulum impacts previously conducted by Viano et al (1989) were simulated. In Viano's work, impacts were concentrated not only to the upper abdomen but also the pelvis and thorax. Subjects were impacted more than once, however impacts were never focussed on the same side and body region more than once. PMHSs in many cases sustained severe skeletal damage. The pendulum used was a 23.4kg (60lb) mass accelerated to speeds of approximately 4.3, 6.8 and 9.5 m/s. The results were subsequently scaled to these three test speeds. For the purposes of this study, we focussed on the results of upper abdomen impacts. Impacts to the thorax were previously demonstrated by De Lange et al., (2005) as they form part of ISO-TR9890. Upper abdomen impacts were focused at the height of the xiphoid process incoming at an angle of 60 degrees (from frontal), focussing at the spine. The HFM was positioned and impacted by a pendulum at 4.3, 6.8 and 9.5 m/s, as described in Viano (1989). Model Force-Time and Force-Deflection characteristics for the upper abdomen are reported and compared to PMHS corridors.

Images of the model setup and impact in the pendulum tests can be seen in Figure 7.5. The results from the pendulum test simulations (Figure 7.6) indicate that the HFM force-time responses for all three impact speeds fit within the corridors defined by Viano (1989). Upper abdomen force-deflection curves on the other hand do not closely match those of the PMHSs. The model's thoracic region appears stiffer than the PMHSs, particularly at lower impact severities. Generally, the deflections observed in the PMHS tests exceed that observed by the HFM by at least a factor of two for a given impact severity.

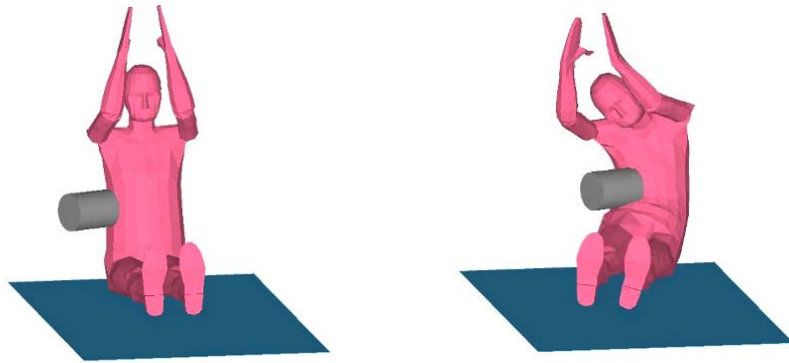


Figure 7.5. Images from the pendulum impact simulations.

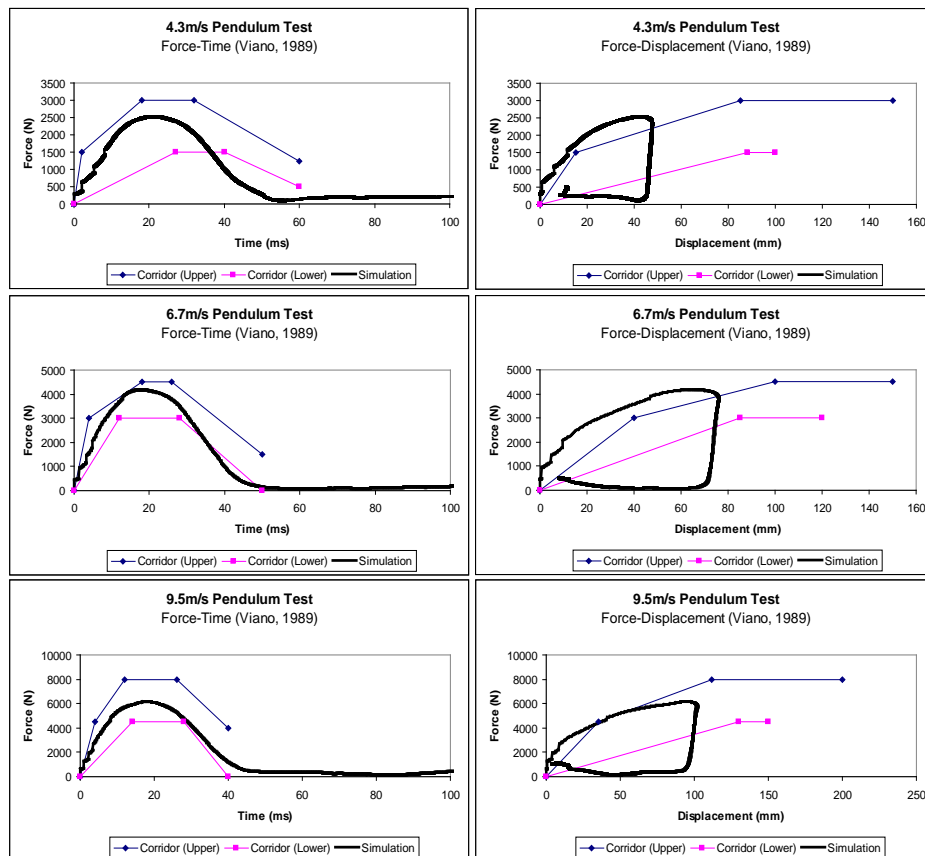


Figure 7.6. Force-time/force-deflection responses of pendulum impact test simulations (Viano, 1989).

7.1.3 Pelvic Offset Sled Tests

Far-side impact data suggests that during a crash, contact between the pelvis and centre console is made prior to any thoracic or head impact – a similar interaction as seen in the pelvic offset tests. As a result of these similarities, sled tests previously conducted by Pintar et al., (1998) were simulated. These tests were originally conducted for the NHTSA in lieu of changes to near-side impact regulation FMVSS 214. Sled tests were conducted in a variety of configurations with a flat wall and pelvic offset condition, either padded with 110mm of paper honeycomb cardboard (PHC) or not padded. Two speeds were selected, 6.8m/s and 9.5m/s for the tests with PMHSs and ATDs (SID and EuroSID). While the pelvic offset tests were originally conducted to identify if there was any benefit/disbenefit of pre-loading the pelvis in a near-side impact, they also provide an interesting source of data for far-side impacts.

The HFM model was exercised in rigid pelvic offset tests conducted at 6.8m/s. Model responses for Pelvis, T12, T1 accelerations in addition to thorax and abdomen deflection are reported and compared against PMHS corridors. Images of the model setup and impact in the sled tests can be seen in Figure 7.7. The results illustrate that the HFM provides a reasonable prediction of PMHS kinematics. While the magnitude of peak forces and accelerations are generally close to that seen in the PMHS results, there is difference between the phasing of the upper body responses of the HFM and PMHSs. This was attributed to differences in shoulder breadth and arm position of the HFM and PMHS.

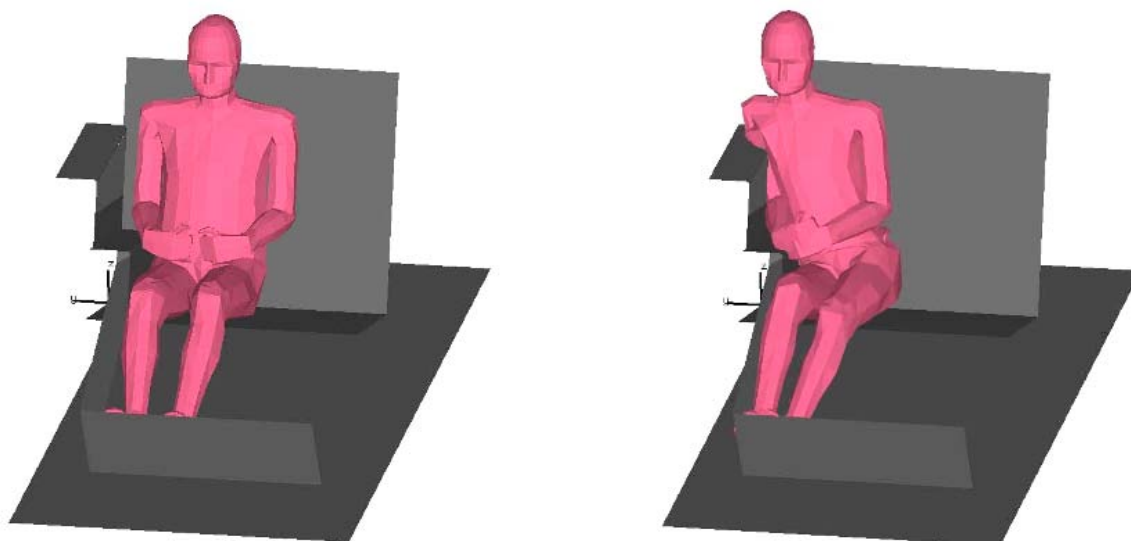


Figure 7.7. Images from pelvic-offset simulations.

7.1.4 Full Vehicle Crash Test

A full-scale crash was conducted by Fildes et al. (2002) to better understand occupant kinematics in a far-side impact (Figure 7.8). A PMHS was positioned in the driver's seat of a large passenger sedan which was impacted by an ECE-R95 MDB at 65km/h. As anecdotally seen in the real-world, the belted PMHS managed to traverse from the driver's side of the vehicle across to the passenger side and strike its head on the b-pillar. Subsequent full-vehicle and sled tests were conducted to further evaluate the potential performance of the existing ATDs in a far-side impact.

The vehicle interior geometry was generated from the pre-deformed buck used in the sled tests by Fildes et al. (2002). Sled pulse and PMHS response were also generated from the published data (Fildes et al., 2002). Model responses are reported for Pelvis, T12, T1 accelerations, Spinal Elongation, Head Lateral Excursion, HIC and Lap Belt Load and are compared to PMHS results.

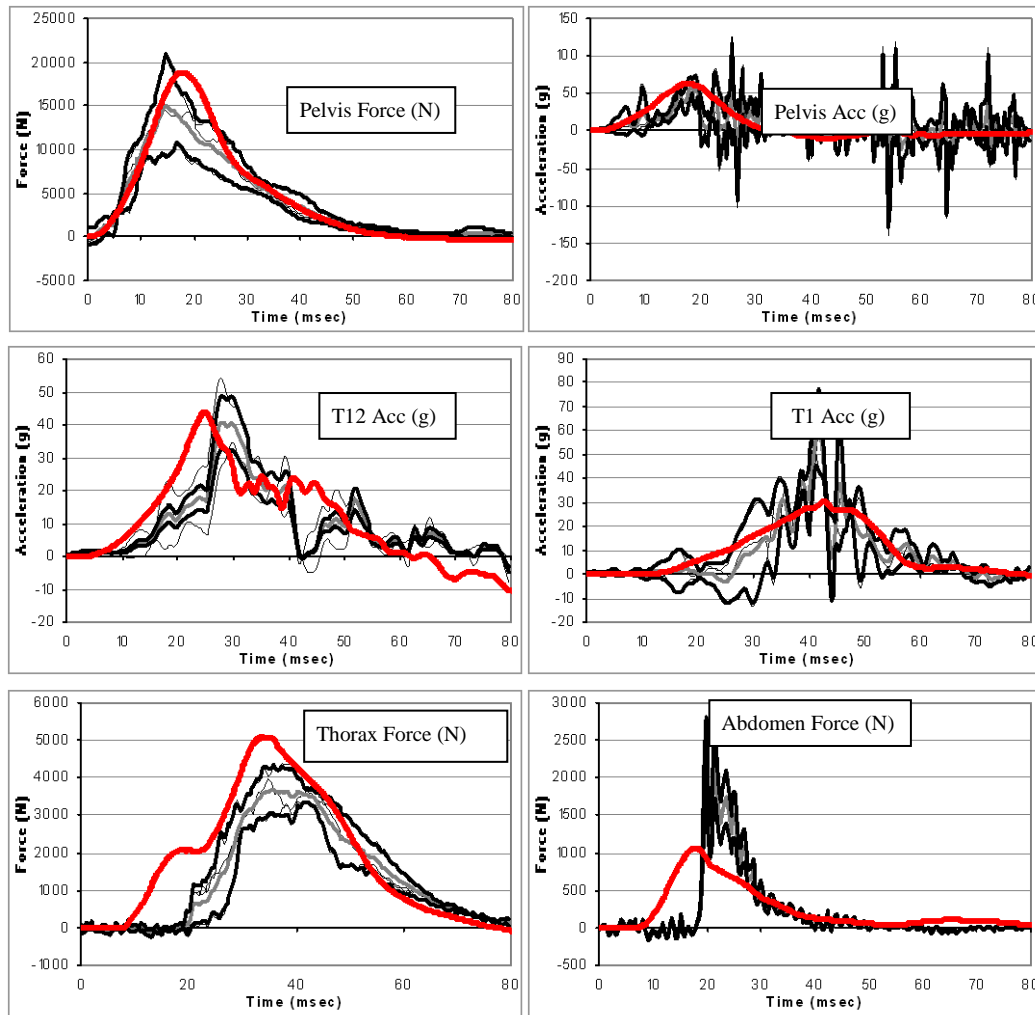


Figure 7.8. Pelvic Offset Simulations (Red) and PMHS (Corridors)



Figure 7.9. Far-side test buck (left) created from the PMHS full-scale test (right)

Images of the model setup and impact in the full-scale test simulation can be seen in Figure 7.10. The HFM (a) slips out of the belt and (b) achieves a head impact against the intruded vehicle structure, both similar to that seen with the PMHS in the full-vehicle test. Quantifiable results shown in Table 7.3 indicate that the HFM reasonably predicts PMHS kinematic response in the full-scale test. Specifically, it is able to generate pelvis and lower spinal kinematics quite well, in addition to matching the magnitudes of lap belt load and head lateral excursion.

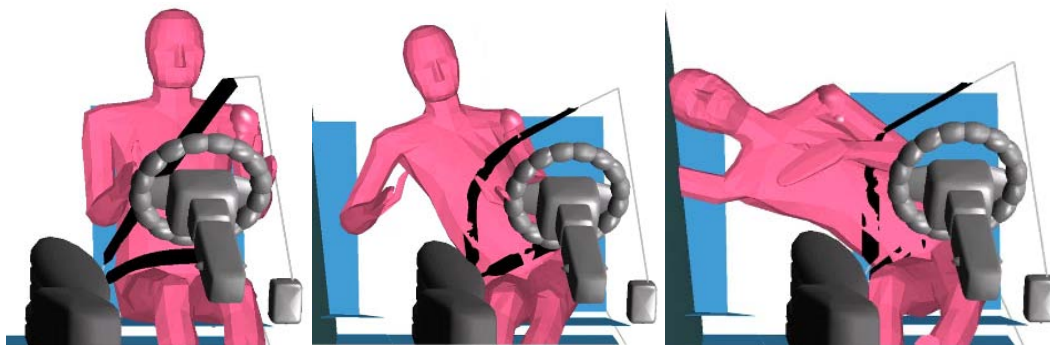


Figure 7.10. Images from full-scale test simulations

While HIC levels are lower than that experienced in the physical test, a head strike was still achieved. Generating a head strike with similar severity was going to be difficult given the limitations in replicating local contour variations of the tested vehicles b-pillar and door with a simplified MADYMO model that only included static intrusion not dynamic (see Table 7.3).

Table 7.3. Peak Results from PMHS Test Compared to HFM

Measure	PMHS	Model
HIC	600	208
Head Y Displacement (mm)	670	621
T1 Y Acceleration (g)	-12	-7
T12 Y Acceleration (g)	-23	-21
Spine Elongation (mm)	70	50
Pelvis Y Acceleration (g)	-30	-28
Lap Belt Load (N)	1037	1153

7.1.5 Far-Side Sled Tests

Shoulder belt forces and head displacements from far-side sled tests conducted with unembalmed PMHS and WorldSID ATD were used as means of model validation and comparison in this first phase of impact (Tables 7.4 and 7.5). Impacts at 60° (30° from lateral) and 90° (pure lateral) were conducted at 30km/h (19mph) using a unique far-side impact buck which included, as a standard configuration, a centre console and outboard three-point belt system (Figure 7.11) [Pintar et al. 2006]. Impact speed was chosen based on median delta-v estimations by Gabler et al. (2005b) for occupants sustaining AIS3+ injuries in far-side crashes. The effects of adjacent occupants, airbags and intrusion were not considered in these particular sled tests.

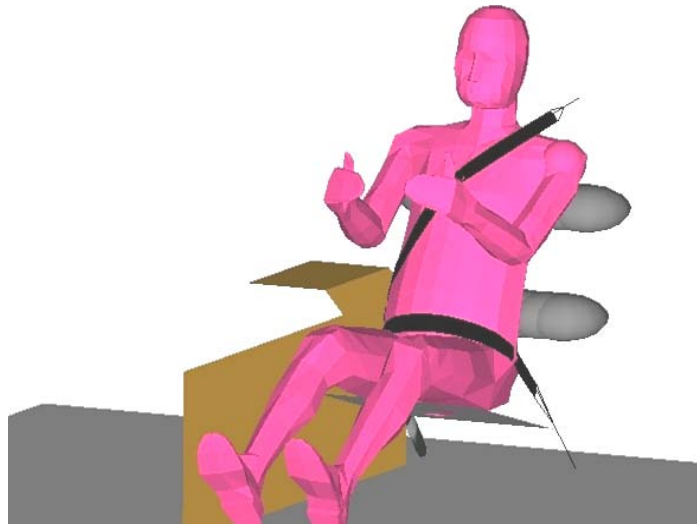


Figure 7.11. Human model in simulated far-side buck.

Table 7.4. Sled test matrix.

Test	Impact Direction	D-Ring Position	Pretension	Test Subjects
1	90	Forward	0N	PMHS 1, WorldSID
2	90	Middle	100N	PMHS 2, WorldSID
3	60	Middle	0N	PMHS 3, WorldSID

Table 7.5. PMHS sex, age and anthropometry.

PMHS	Sex (M/F)	Age (Years)	Height (m)	Weight (kg)
1	F	74	1.60	70
2	M	80	1.73	67
3	M	81	1.75	70

For this study, three configurations of impact angle, seat belt geometry and pretension were investigated (Table 7.4). The D-ring positions were not arbitrary but meant to replicate realistic real-world belt positions at average and extreme conditions. As a realistic worst-case scenario for the shoulder and thorax escaping the belt, a 90° impact with a forward mounted D-ring (located 120mm above and 30mm rear of the shoulder) was performed. A second 90° test was conducted with a mid mounted D-ring (located 120mm above and 90mm rear of the shoulder) and 100N of pretension applied. This middle position was deemed to be an average D-ring location for a B-pillar mounted belt. A third test was conducted at 60° (middle D-ring) to investigate model behaviour in angled far-side impacts.

For Test 1 (Forward D-ring, 90°, No pretension), all test subjects (PMHS, WorldSID and Model) slipped out of the shoulder portion of the seat belt (Figure 7.12). In all cases, the belt provided restraint via loading the thorax in the early phases of impact, however this was more prominent in the model. The belt subsequently slipped past the shoulder and got caught on the upper arm near the elbow (Belt force-time traces found in Pintar 2008, Task 2 Final Report; Appendix).

The resulting lateral (Y) head displacements for all test subjects were similar (within 5%) (Figure 7.13). In contrast to the physical test results, the Model spent in excess of 100ms at 95% of maximum displacement, whereas the PMHS and WorldSID only spent 60ms and 65 ms respectively. This was related to the human model continuing to slip and not rebound as quickly as the PMHS and WorldSID.

This being partly related to the model's slightly lower lateral velocity compared to both PMHS and WorldSID.

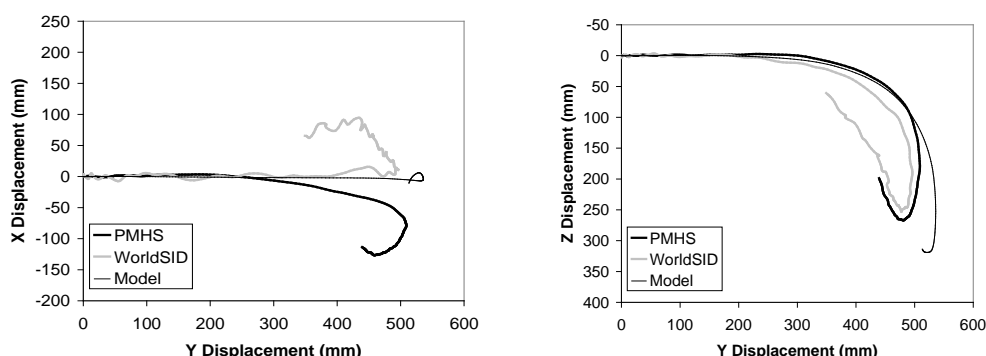


Figure 7.12. Head Trajectories in Test 1: 90° far-side test with Forward D-Ring and No pretension. Transverse plane (left) and Coronal Plane (right), 0-240ms shown.

For Test 2 (Middle D-ring, 90°, 100N pretension), the shoulder-complex of all test subjects engaged the seat belt. Both WorldSID and the Model predicted the peak magnitude of shoulder belt force very well (within 4%), however this peak was delayed 10-12ms compared to the PMHS test (Table 7.6).

For Test 1 – 90° Fwd D-ring 0N Pretension. Test 2 - 90° Mid D-ring 100N Pretension. Test 3 - 60° Mid D-ring 0N Pretension.

Table 7.6. Peak shoulder belt force and timing for test subjects.

	TEST 1		TEST 2		TEST 3	
	Peak Force (N)	Timing (ms)	Peak Force (N)	Timing (ms)	Peak Force (N)	Timing (ms)
PMHS	2410	89	2982	96	3808	101
WorldSID	1700	99	2806	106	3030	98
Model	2629	99	2927	108	2867	96

The magnitude of head lateral displacement for all three subjects in Test 2 was within 6%, despite the Model and WorldSID reaching these maxima up to 10ms later than the PMHS (Figure 7.13). The Model did however predict less inferior (Z) motion than both WorldSID and the PMHS. In the AP (X) direction, WorldSID moved very little, whereas the Model and PMHS showed posterior rebound.

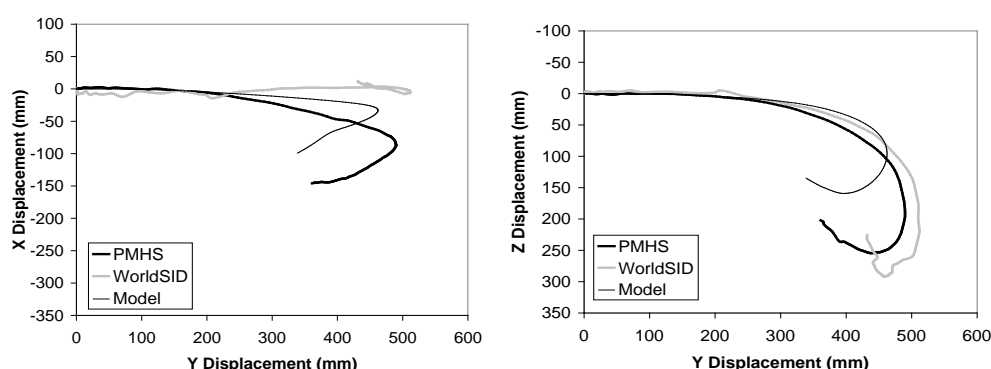


Figure 7.13. Head Trajectories in Test 2: 90° far-side test with Middle D-Ring and 100N pretension. Transverse plane - Left and Coronal Plane – Right. (0 - 190ms shown).

For Test 3 (Middle D-ring, 60°, No pretension), the PMHS and WorldSID engaged the belt at the shoulder and then subsequently slipped out. The Model on the other hand did not engage the belt at the shoulder, instead hooking on the upper arm. Despite the difference in loading locations, the shoulder belt force magnitude was similar for both WorldSID and the Model, however the PMHS loading was much higher (see Table 7.6).

As can be seen in Figure 7.14, despite the difference in shoulder belt loading locations, the PMHS, WorldSID and Model head coronal trajectories are similar. In the transverse plane, variations are observed between human surrogate head displacements. This observed difference is explained by the way in which all three human surrogates interacted with the shoulder belt. For the model, the belt slipping off the shoulder allowed more anterior motion to be achieved.

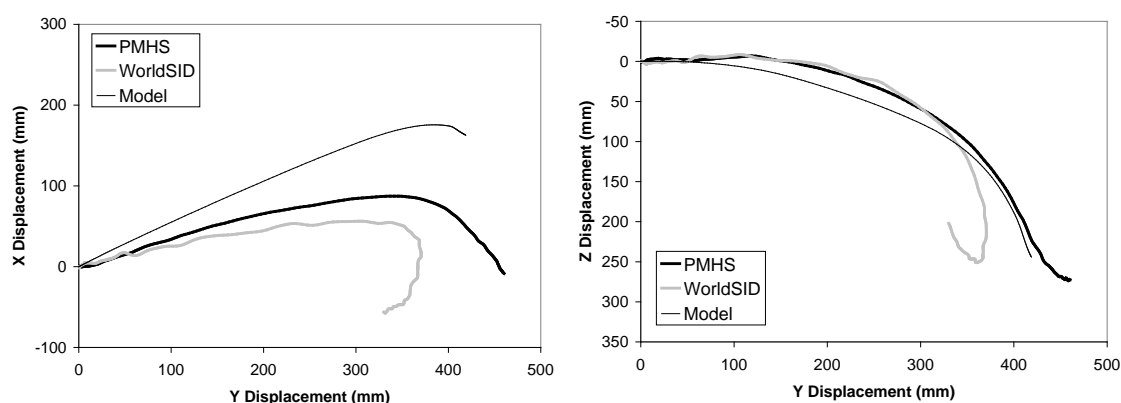


Figure 7.14. Head Trajectories in Test 3: 60° far-side test with Middle D-Ring and no pretension. Transverse plane - Left and Coronal Plane – Right. (0 - 190ms shown).

In light of these results, it appears that the human model is generally capable of mimicking events seen in the sled tests. It should be noted that these impacts only represent one PMHS for each configuration. As already mentioned in the quasi-static tests, the fact that anthropometry of the model and PMHS are not the same makes it difficult to draw definite conclusions pertaining to model biofidelity. Furthermore, since factors such as airbags, adjacent occupants and intrusion were not simulated, the head excursions reported only reflect what is seen in cases where these factors are not influential. When those factors are present, issues of model rebound after maximum excursion are of less significance.

7.1.6 Parameter Study

Two separate parameter studies were conducted to investigate the effect of D-ring position, pretension levels and impact direction on occupant-to-seat belt interaction (Table 7.8). Vehicle interior geometry was identical that used in the far-side sled tests previously described. D-rings located in the forward and middle positions were as previously described. High and low D-rings were located 90mm rear of shoulder and 0mm and 150mm above the shoulder respectively [Pintar et al., 2006]. The low D-ring position was aimed to replicate a vehicle with a seat-mounted retractor. The high belt position was the realistic worst-case position for neck loading (if positioned inboard).

Table 7.8. Parameter study matrix.

	D-ring position(s)	Pretension Levels	Impact Directions
Study A	Fwd, High, Mid, Low	0N, 100N, 200N	60, 90
Study B	Middle	0N, 100N	30, 40, 50, 60, 70, 80, 90

Study A investigated the effect of 4 D-ring positions and three pretension levels on whether the belt slipped off the shoulder and the resulting head trajectory (assuming no adjacent occupants, airbags or intrusion). This was performed for both 60° and 90° impacts (Figures 7.15 and 7.16). Head displacements in the coronal (YZ) plane were focused on.

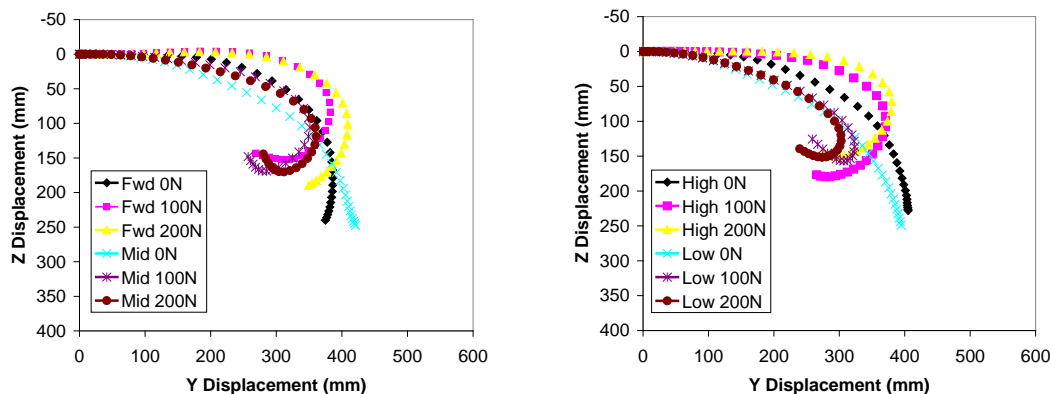


Figure 7.15. Head coronal plane trajectories in 60° far-side impacts with varying D-ring positions and pretension levels (0-190ms shown).

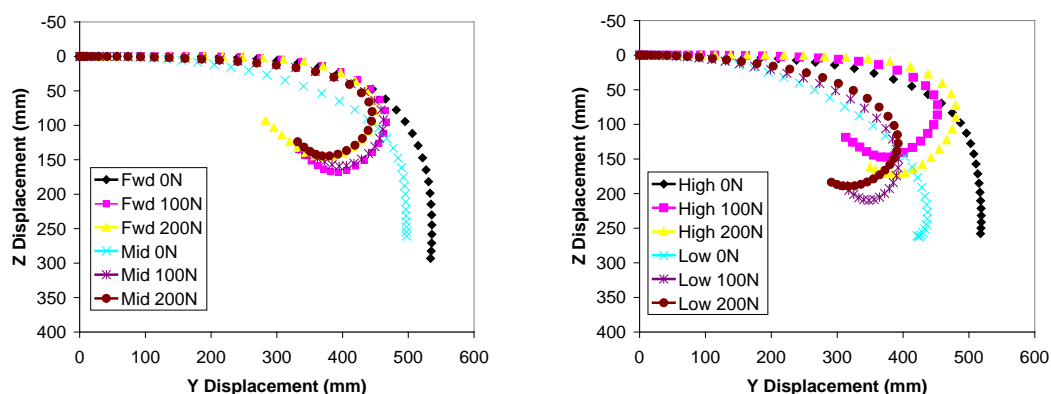


Figure 7.16. Head coronal plane trajectories in 90° far-side impacts with varying D-ring positions and pretension levels (0-190ms shown).

It was firstly observed that the belt slipped off the shoulder in all 60 and 90 degree impacts without pretension, regardless of D-ring location. When pretension was added, regardless of severity, the belt did not slip off the shoulder. Additionally, these results suggest lower or more rearward D-rings and the addition of pretension reduce lateral head excursion in both 60 and 90-degree impacts.

Study B investigated the effect of impact direction and pretension on occupant-to-belt interaction and the resulting head trajectory. Head trajectories in the transverse and coronal planes can be seen in Figures 7.18 and 7.19. Results indicated that the model's shoulder escaped the belt at impact angles greater than 40° when no pretension was used. When pretension was used, the belt restrained the shoulder in all cases and generally reduced lateral displacement. Furthermore, these results indicate that if no pretension is applied, head lateral excursion is similar for impact angles 80° to 90°. The addition of pretension was shown to generally reduce head inferior (Z) motion as impact angle increases from 30° to 90°.

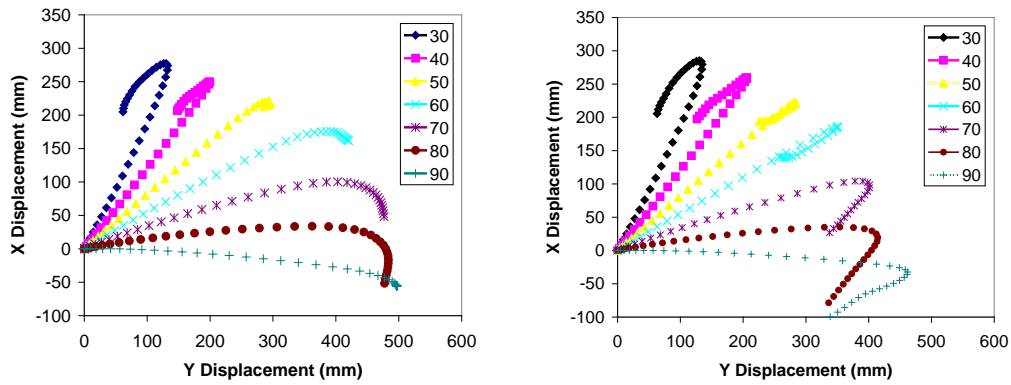


Figure 7.18. Head transverse plane trajectories in 30° – 90° impacts without pretension (left) and with 100N of pretension (right).

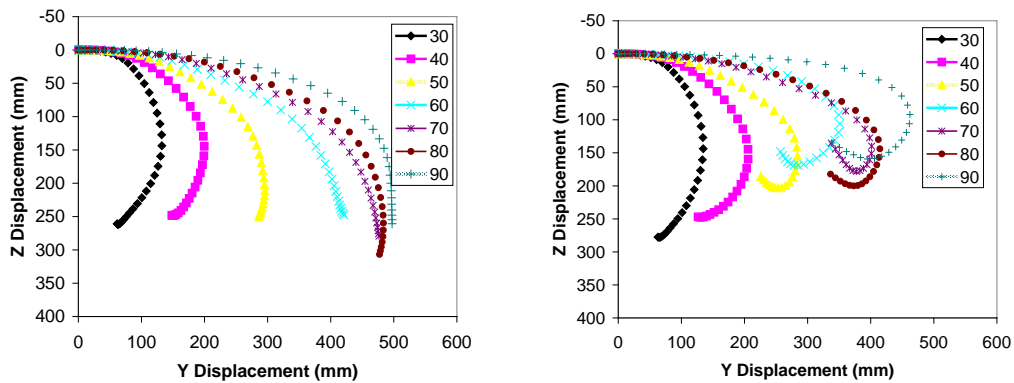


Figure 7.19. Head coronal plane trajectories in 30° – 90° impacts without pretension (left) and with 100N of pretension (right).

7.2 DISCUSSION

The primary aim of this work was to develop and validate an occupant model for use in far-side impacts. This firstly involved demonstrating that the model was generally capable of mimicking human-like motion in far-side impacts and then drilling down further to identify the models capabilities and weaknesses. This chapter is a collection of the work that has been undertaken thus far on this task to develop a far-side model.

As previously described, a far-side occupant model is unique in terms of its biofidelity and use requirements. Where the frontal impact ATD (Hybrid III) needs to be operational both in belted and unbelted impacts, a far-side model needs to be operational in both no countermeasure, and countermeasure situations. In a current vehicle, it is reasonable to suggest that a far-side model would be expected to slip out of the shoulder belt and shift laterally towards the vehicle's nearside and potentially impact the intruding door. In contrast, the model also needs to work in situations where devices such as Autoliv's inboard side airbag are present. It is arguable that for these particular impacts, a near-side dummy such as WorldSID will be capable. However, should belt type countermeasures be used in the vehicle, WorldSID may not be the most suitable dummy and the likes of THOR may be more indicative of human response. Again, this highlights the benefit and potential cost effectiveness of having a computer model of a far-side occupant that can achieve both these tasks.

The HFM's ability to mimic near-side biofidelity requirements (ISO-TR9890) was demonstrated by De Lange et al., (2005). It was shown that the HFM's lateral biofidelity on a subsystem level was good (8.6/10), almost as good as the best performing dedicated side impact dummy, WorldSID (8.0/10). While ISO-TR9890 is a near-side impact dummy standard, the lateral biofidelity of any side impact model on a subsystem level should largely be the same. ISO-TR9890 defines subsystem biofidelity requirements of the head, neck, thorax, abdomen and pelvis. Using those biofidelity predictors, associated injury criteria would be based on measures such as Head (HIC), Neck (Bending and Tension), Thorax and Abdomen (Deflection) and Pelvis (Force and Acceleration). The HFM is capable of measuring all these biofidelity requirements and injury criteria.

Generally speaking, the main differences between near and far-side crashes are that in a far-side impact: (1) the thorax and shoulder interact with the sash belt more; (2) the thorax is seen to shear away from the pelvis after impact with the centre console; and (3) the occupant can achieve large lateral excursions.

Addressing the issue of sash belt to thorax and shoulder interaction, quasi-static and dynamic far-side impacts (2.4 and 2.5) looked at the influence of belt geometry and pretension on restraint provided by the seat belt. In the 1g quasi-static tests, the human model was able to demonstrate both of the critical findings from the volunteer tests. Firstly, thorax lateral restraint is dependent on seat belt geometry and level of pretension applied to the belt. Specifically, the seat belt is less likely to slip off the shoulder with a more rearward D-ring and increasing levels of pretension. However, modelling suggested that once the belt engages (or slips off) the shoulder, the effect of D-ring position and pretension is negligible.

Secondly, the relationship between the shoulder engaging the belt (or slipping) and seat belt geometry and pretension is highly dependent on human anthropometry. Only two volunteers were needed to demonstrate the uniqueness of humans in this sense. While the modelling only focused on a single parameter change (shoulder AP thickness), it was able to replicate the same trend as seen in the volunteer tests. Specifically, a person with greater shoulder depth is less likely to slip out of the shoulder belt.

In Parameter Study A, it was shown that without pretension in 60 and 90-degree impacts, the belt is likely to slip off the shoulder regardless of D-ring position. The addition of pretension facilitated the shoulder engaging the belt in all cases, with the effect of pretension level being minor. Furthermore, as seen in the quasi-static tests, D-ring position generally has little effect on lateral displacement once the belt has either slipped off or engaged the shoulder. Results did however suggest that a low D-ring yields lower lateral displacements.

The concept of a low D-ring decreasing lateral restraint contradicts previous work by Rains et al. (1998) who claimed that raising the D-ring reduced lateral excursion in far-side rollover tests. However Rains et al. based their conclusions on results from a Hybrid III ATD, which this paper has already shown is not capable of accurately mimicking seat belt to shoulder-complex interaction.

Whilst lowering a D-ring and applying pretension seem relatively simple methods of increasing lateral restraint, due care must be taken regarding the use of a low positioned D-ring. In severe frontal impacts, such a design may potentially increase restraint to the upper torso, causing the kyphotic thoracic spine to straighten and press on the thoracolumbar spine, resulting in anterior wedge fractures [99nd Pratima,1983]. Despite this model not being validated for severe vertical loading, some spinal compression was observed in these far-side impacts. Further research should be undertaken to ensure that such a design is not going to have adverse effects on other body regions.

In Parameter Study B, the influence of impact direction and pretension on occupant-to-seat belt interaction was estimated. When no pretension was used, the model's shoulder did not escape the belt until impact angles exceeded 40 degrees (from frontal). This result agrees with previous findings by Adomeit et al. (1988) and Horsch (1980). Interestingly though, despite the difference in shoulder belt loading locations for the PMHS and Model in the 60 degree impacts, the resulting lateral head excursion was similar. Further research needs to be conducted to better understand this shoulder to belt interaction in far-side oblique impacts. The reason for this is that evidence already suggests that 60-degree impacts are the most important far-side crashes to understand (Gabler et al., 2005b). Results

also indicated that when the impact angle is between 80 and 90-degrees, lateral head excursion is similar. This suggests that the shoulder portion of the seat belt provides very little thoracic restraint at these angles compared to more frontal impacts.

In addition to the work on belt interaction, it was important to determine if the model's thorax could mimic the loading observed in far-side impacts – namely the shearing away from the pelvis and also oblique loading to the upper abdomen. This was achieved through simulating pelvic offset and pendulum tests.

As previously shown, pendulum impacts were conducted with the upper abdomen of the HFM at 60 degrees from frontal. These impacts were chosen to highlight whether the HFM was capable of measuring deflection in an oblique direction. This is critically important as oblique angled far-side impacts are more common and injurious than purely lateral impacts. The loading to the abdomen and thorax in those cases generally comes from loading due to the sash belt, adjacent seat, intruded structures and adjacent occupants.

The results of this study showed that while the HFM is capable of measuring upper abdomen deflection in the frontal and lateral directions, it could not replicate the large deflections seen by Viano (1989). While deflection is generally considered a good measure of thoracic injury and matching PMHS results is considered essential for model validation, the deflection seen in Viano's data is very large. The PMHS used in those tests were impacted multiple times, and as such this may have affected the result. ISO-TR9890 uses the force-time responses for the upper-thorax. As such, since the lower-thorax force-time responses match within the corridors, the biofidelity of the model in that region appears reasonable.

Within this study the performance of the HFM in a pelvic offset sled test was also considered. These tests were chosen to highlight whether the HFM was capable of simulating a thoracic impact subsequent to pelvis impact. The results of this study showed that the model was capable of replicating pelvis, T1 and T12 accelerations. There were differences observed in terms of phasing, however this issue was primarily attributed to differences in shoulder breadths of HFM and PMHS. Simulated sled tests using a flat-wall instead of a pelvic offset condition are also considered useful for characterising lateral biofidelity. Such tests were simulated by De Lange et al., (2005) whereby Wayne State University (Heidelberg type) flat-wall tests were reconstructed.

While the pendulum and pelvic offset tests proved useful in evaluating whether the HFM was capable of far-side-type loading, it was important to demonstrate that the whole body kinematics are also well predicted by the model. Hence the unique full-vehicle far-side PMHS test conducted by Fildes et al., (2002) was simulated. While the results generally compared favourably to the PMHS, it is important to note that the PMHS results represent a single cadaver. As such, those results are only indicative of what may be representative of humans in far-side impacts. The authors of this study are well aware of this limitation. As such results were shown to demonstrate that model response was cadaver-like, and not necessarily representative of a large sample of humans. Two important factors likely to influence results include differences in anthropometry and muscle tone between PMHS and HFM. In addition, the model was approximated from the vehicle used and only static intrusion was modelled rather than dynamic. Nevertheless, the results demonstrated by the HFM highlight that it is capable of mimicking human-like or cadaver-like kinematics in a full-vehicle far-side impact.

With the HFM being shown to be a reasonable predictor of kinematics and kinetics in far-side impacts, it could be used for initial development tests for far-side countermeasures. While physical countermeasures will always need to be tested and optimised with federalised dummies (where possible) using a computer model such as the HFM may provide insight into design features required that will not be captured by the physical dummies. Already, it has been shown that the HFM was capable of producing human-like kinematics in far-side impacts from 30-90 degrees. Furthermore, as the HFM has been shown to be able to replicate belt-to-shoulder interaction well based on both impact angle, pretension and belt position, using a computer model provides a unique tool to identify these worst case scenarios and then run the physical tests.

While it has been demonstrated that the TNO Human Facet Model can meet the biofidelity and performance requirements outlined in this study, it is important to note that more in-depth far-side PMHS laboratory tests with PMHS need to be conducted. Such tests should aim to establish biofidelity corridors for models and ATDs. The study by Pintar et al., (2008) provided a baseline for how one might conduct a far-side sled test and what results you would expect to see. However, more tests need to be conducted in the same impact configuration to determine biofidelity corridors.

In light of the limitations of this study, it is hypothesized that introducing methods that encourage the belt to engage the shoulder will reduce both the likelihood and severity of head and thorax contacts with intruding structures or other occupants. However, further research needs to be conducted taking these additional factors into consideration. Additionally, the influence of both driver and passenger airbags in angled far-side impacts needs to be explored.

7.3 CONCLUSION

This work has highlighted that the modified version of the TNO Human Facet Model shows good biofidelity compared to PMHS results from quasi-static, pelvic offset tests, sled tests, pendulum tests and a full-scale far-side crash test. The model's primary limitation is that its thorax is less capable of matching the severity of deflection observed in the PMHS pendulum tests.

In addition, this work has quantified some of the factors influencing occupant-to-seat belt interaction in far-side impacts. Results from both quasi-static and dynamic tests indicate that lower positioned D-rings with the addition of pretension offer potential benefit in far-side impacts. Specifically by increasing the likelihood of the shoulder engaging the seat belt. It was also observed that occupants are likely to escape the shoulder portion of the belt at far-side impact angles greater than 40 degrees from frontal when no pretension is used. The addition of pretension allowed the shoulder to engage the belt in all impacts from 30 to 90 degrees.

This body of work on model validation is not yet complete. It is the task of the author Clay Douglas to complete this work for submission of his PhD thesis. This is expected to occur during 2009. Final results will be available at that time.

8 COUNTERMEASURES BENEFITS ANALYSIS

AUTHORS: Ola Bostrom, H. Clay Gabler, Kennerly Digges, Brian Fildes & Clay Douglas

8.0 FAR SIDE COUNTERMEASURES

Throughout this report, the conventional three-point belt has been the baseline countermeasure for preventing far side occupant injuries.. In some configurations of belt slack and geometry, the three-point belt-restrained far side occupants are primarily restrained only by the lap portion of the belt. Sled tests and full scale crash tests (Digges and Dalmotas, 2001; Fildes et al., 2002; Bostrom et al., 2003) have shown that, in a side impact, the far side occupant may slide out of the seat belt and flail toward the struck side of the vehicle. In real world crashes, the occupant then may collide with the surfaces or objects on the nearside including the intruded nearside door, the adjacent seat, and the nearside occupant.

Several far side impact injury countermeasures, for three-point belted occupants, have been proposed and evaluated. The countermeasures include belt pretensioning (Stolinski et al., 1999; Douglas et al., 2008), the side support airbag (SSA) (Bostrom and Haland, 2005), reversed geometry shoulder belts (Bostrom et al., 2005), criss-cross shoulder belts (Bostrom and Haland, 2005), the V-shaped 4-point belt (Rouhana et al., 2003 and 2006), inflatable curtains (Kahane, 2008) and even an adjacent occupant (Frampton et al, 1998). Table 8.1 (from Bostrom et al., 2008) lists most of the proposed countermeasures including references.

Table 8.1. List, feature, examples, test specifications and references of examples of concepts of far side countermeasures.

Countermeasure	Feature	Examples	Δv , angle, dummy	Reference
Belt pretensioner	Reduce slack and tighten the belt by various degrees	Pyrotechnical and electrical retractor, buckle and latch plate pretensioners	30 km/h, 30-90 deg, Numerical model of human	Douglas et al 2008
Inboard side support	Restrain the occupant from moving inboard	Side support airbags, side support wings	24 km/h, 60&90 deg, BioSID spring spine	Bostrom and Haland, 2005
Altered 3-point belt geometry	Restrain the occupant from moving inboard	Criss-cross, reversible 3-point, rucksack-belt, V-shaped 4-point belt (V4)	24 km/h, 60&90 deg, BioSID spring spine	Bostrom and Haland, 2005
			About 24 km/h (FMVSS214) Post-Mortem Human Subjects	Rouhana et al 2006
			30 km/h, 90 deg, Thor	Bostrom et al 2008
Nearside head and thorax airbags	Provide cushioning between deformed struck side and occupant	Head and thorax airbags, inflatable curtain, window bags	50 km/h, 90 deg, WorldSID	Bostrom et al 2008

Adelta-Vanced belt systems such as criss-cross belts, V-shaped 4-point (V-4) belts or rucksack belts, shown in Figure 8.1, would benefit not only far side struck occupants, but occupants subjected to frontal impacts as well. In a frontal impact, the more symmetrical, thoracic loading provided by these belt systems may help to reduce thoracic injuries (Bostrom and Haland, 2005; Rouhana et al, 2003). It is important though to design these belts not to cause new injury patterns such as neck injuries. Research is underway to gauge the potential for any restraint to cause neck injuries (Fildes et al 2005).



Figure 8.1. Three versions of altered 3-point belt geometry, criss cross, V4 and rucksack (from Bostrom et al 2008).

Seat belt systems, which improve restraint of the far side occupant, may also benefit the nearside occupant. In a side crash where there are two adjacent front seat occupants, the nearside occupant may be struck on one side by the deformed side structure and on the opposite side by the adjacent, far side, occupant.

It is critical to understand that median injury test conditions may represent only a minimal injury risk. Consequently, tests conducted under these conditions may result in low injury assessment outcomes. Injury incidence is a result of both exposure and risk. For this reason it is crucial to determine exposure and risk as a function of crash severity to compute the opportunities of countermeasures.

8.1 COUNTERMEASURE TESTS

Sled tests to evaluate countermeasure performance in far side crashes were conducted by Autoliv. Typical dummy kinematics are shown in Figure 8.2 [Bostrom, 2005], Figure 8.3 [Bostrom, 2008] and Figure 8.4 [Bostrom, 2008]. The dummies in these figures were BioSID with spring spine, a Thor and a WorldSID.



Figure 8.2. Photographs taken at 1, 85 and 150 ms - side support airbag test with a BioSID spring spine at 90 degrees and delta-V 24 km/h.



Figure 8.3. Photographs at 1, 85 and 150 ms from tests with a Thor restrained by an extra belt (no load limiting) at 90 degrees and delta-V 30 km/h.



Figure 8.4. Photographs at 1, 50 and 100 ms from tests with a belted WorldSID interacting with an inflatable curtain at 90 degrees and delta-V 50 km/h.

Real-life crash analysis indicates that occupants on the struck side of a vehicle may also be injured by contact with an adjacent occupant in the same seating row. The injury consequences of occupant-to-occupant impacts can be severe, and sometimes fatal. With the support and assistance of the program Newland et al. (2008) investigated the risk of such impacts by analysing real life crashes and also evaluated the feasibility of potential countermeasures by conducting and analysing six full scale side impacts where both front seat row seats were occupied with dummies. Examples of dummy interaction in two crash simulations are shown in Figures 8.5 and 8.6.

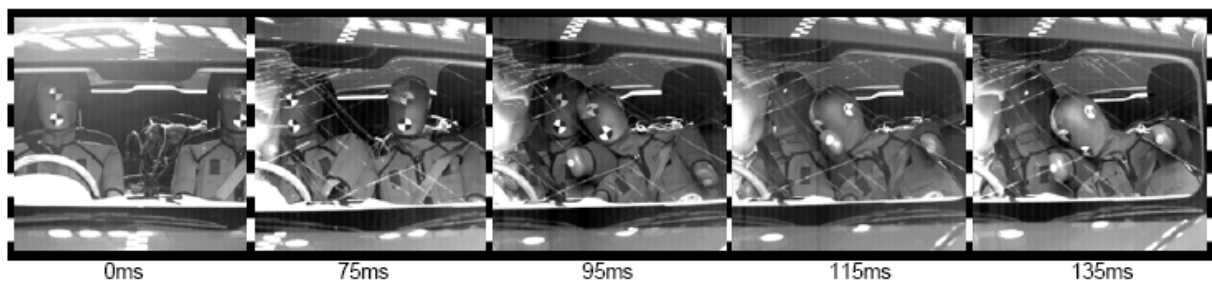


Figure 8.5. Two belted WorldSID dummies interacting in a pole impact. The dummy interaction started after the critical (in terms of injury values) near side occupant interaction with the side interior. The HIC exceeded 8000 for both dummies. From Newland et al 2008.



Figure 8.6. Two belted WorldSID dummies interacting in a pole impact where side support airbags were present in-between the dummies. No injurious head contact occurred. (from Newland et al 2008)

The field crash analysis suggested that the risk of injury to a driver seated on the non-struck side in a side impact crash is likely to be increased by the presence of an adjacent front seat occupant. Moreover, the side support airbag (altered seat belts were not tested) was shown to be effective in preventing interaction injury in the vehicle-to-pole test.

8.2 INJURY REDUCTION ANALYSIS

Within the programme, Bostrom et al estimated the injury reduction opportunities of altered seat belts, side support airbags and inflatable side curtains for belted far side occupants in planar side impact crashes [Bolstrom, 2008]. The analysis was based on real life crash analysis and mechanical simulations of occupant motion.

Head or thorax injuries caused by contact with the struck side are the dominant type of injury among belted far side occupants in planar side impacts. In contrast to the situation in belted nearside and frontal impacts, the injury mechanism seems to be bimodal in that the occupant may or may not reach the opposite side of the car. Although over half of all serious injuries take place for delta-V below 30 km/h (Gabler et al, 2005), the risk of a serious head/thorax injury is small (3%). A full-scale replication of a delta-V 30 km/h far side impact crash is likely to reveal dummy readings indicating only a small risk of serious or fatal injury.

Nevertheless, the countermeasures evaluated in this study, do, to various degrees, either restrain a belted far side occupant from colliding with the struck side or cushion the struck side in planar side impacts, therefore, the potential opportunity is considerable. The opportunities of three promising conceptual countermeasures are summarized in Table 8.2

Table 8.2. Estimated opportunity of far side countermeasures mitigating AIS3+ and fatalities at the delta-V threshold

Conceptual countermeasure	Delta-V threshold (km/h)	Far side AIS3+	Far side Fatalities
Altered seat belt (4-point), side support airbags	0-30	715 (57%)	83 (18%)
Side curtain	30-50	350 (28%)	136 (30%)

Other injuries, such as injuries caused by the countermeasure or extremity injuries (majority of the remaining), were not addressed in this study. Also not addressed was the opportunity of the evaluated countermeasures to protect nearside occupants (7% of all far side occupant head injuries were caused by occupant-to-occupant interaction) or to protect occupants exposed to other crash circumstances such as rollover, oblique or high-speed frontal crashes.

8.3 CONCLUSIONS

A countermeasure 100% effective in reducing the risk of a serious or fatal head and thorax injury up to a delta-V of 20 km/h would potentially reduce the number of serious injuries by 18%. If the effectiveness extended to 30 km/h, the injury reduction would increase to 57%. According to the crash test results shown or referred to in this study, side support airbags with modified 3-point belt geometry could constitute such a countermeasure. Any possible injuries induced by these countermeasures were disregarded as there is no evidence yet to support such an event. The crash test results further suggest that an inflatable curtain, with suitable coverage area and stand-up time, would also be desirable.

9 GENERAL DISCUSSION & COMMENTS

AUTHORS: Kennerly Digges & Brian Fildes

9.0 INTRODUCTION

The ARC Far Side Impact Collaborative Research Project followed on from earlier research conducted at the Monash University Accident Research Centre for General Motors Holden in Australia. In a 1995 study, Dr. Fildes observed that, in Australia, serious head injuries were more frequent among occupants exposed to far-side crashes than near-side crashes [Fildes, 1995]. Later in the USA, Dr. Digges conducted crash tests of vehicles with far-side dummies and found that conventional three-point safety belts provided very little restraint for the upper body [Digges, 2001]. In an examination of US accident data, he found that in far-side crashes, the unfavourable safety belt geometry produced chest and abdominal injuries in relatively low severity crashes.

Head injuries were frequent in higher severity crashes. Since there were no existing standards, qualified dummies or accepted test procedures for far-side crashes, this unique safety improvement opportunity was selected for a joint collaborative research project. The objective was to provide the technology base to permit the development and test of countermeasures for far-side crashes. To accomplish this objective, a number of tasks were defined and teams of researchers with international recognition were invited to participate on a cost sharing basis. Industrial partners were invited to participate and contribute funding to the project. The George Washington University contributed a substantial amount of funding by way of a grant received from the Ford Motor Company. The Australian Research Council in Australia approved a project proposal and provided overall funding and sponsorship of the project, along with additional funds from GMH and Autoliv Sweden. A list of the participants is included in the Acknowledgements Section.

To meet the research objectives it was necessary to develop the technical basis for the crash dummies, injury criteria, and test procedures to be used in evaluating far-side countermeasures. The development of test procedures required an understanding of the crash environment that produces serious injuries in far-side crashes. The development of suitable dummies required a comprehensive test program that subjected both dummies and cadavers to far-side crashes. The injury criteria research required additional research to understand the injury mechanism for carotid arteries. In order to develop countermeasures and assess benefits, validated computer simulations needed to be developed. Finally, methods of conducting benefits analyses of generic countermeasures also required research effort.

The research involved the following projects:

- Definition of the far-side injury environment and the opportunities for injury reduction
- Development of representative test conditions and injury criteria for use with far-side test dummies. The development of injury criteria required research to understand the nature of injuries to the carotid artery from shoulder belt loading of the neck.
- Development and validation of computer human models for use in the evaluation of far-side countermeasures.
- Assessment of the occupant kinematics representative far-side crashes that produce injury and of the dummies available for the evaluation of far-side countermeasures. Occupant kinematics were assessed by a comprehensive biomechanical test program of post mortem human subjects (PMHS).
- Assessment of the opportunities for injury reduction based on generic countermeasures

The organization of the Far Side Impact Collaborative Research Project has been described in Chapter 1 and by Fildes (2005). It involved the assembly of a research team from industry, government and academia in Australia, Europe, and the United States. The research team has developed a technology base of far-side dummies, injury criteria, computer models, and representative test environments that can be used to evaluate countermeasures for far-side crash protection. This final chapter provides an overview of the results of the extensive and innovative research program.

9.1 DEFINITION OF THE FAR-SIDE INJURY ENVIRONMENT

In the US, the National Highway Traffic Safety Administration (NHTSA) maintains the NASS/CDS database of vehicle crashes in the United States. The NASS/CDS is a stratified sample of light vehicles involved in highway crashes that were reported by the police and involved sufficient damage that one vehicle was towed from the crash scene. In Australia, too, the Monash University Accident Research Centre collects in-depth crash investigations using a stratified and weighted sample (MIDS) and these data were also available for analysis in this study [Gabler, Fitzharris, Scully et al 2005b].

In the NASS/CDS data query, far-side occupants in planar crashes were defined as drivers in vehicles with right side damage or right front passengers in vehicles with left side damage. Drivers in rollovers that were passenger side leading were classified as being in far-side rollovers. The converse was true for passengers. Each NASS/CDS case contained a weighting factor that is used by the NHTSA to extrapolate the individual cases to the national numbers. The distributions to follow are based on the NASS/CDS weighted events. The MIDS data in Australia is also similarly weighted for representativeness.

Table 9.1 shows the annual distribution of MAIS 3 and greater injuries by belt use, crash direction and crash mode, using at least nine years of data for years prior to 2004 [Digges, 2006].

Table 9.1: Annual MAIS 3+ Injuries from NASS/CDS in Near-side and Far-side Crashes by Crash Type and Direction

Crash Type/ Belt Use	Planar	Roll	Total
Far-side Belted	2,166	3,540	5,706
Far-side Unbelted	5,095	6,325	11,420
Far-side Total	7,261	9,865	17,126
Near-side Belted	7,360	3,532	10,892
Near-side Unbelted	6,714	5,551	12,265
Near-side Total	14,074	9,083	23,157
Near-side/Far-side Total	21,335	18,948	40,283
% Due to Far-side	34%	52%	43%

These data in Table 9.1 shows that about 43% of the MAIS 3+ injuries in side crashes and rollovers occur in far-side crashes. More than half of the MAIS 3+ injuries in rollover are in far-side rolls.

An in depth analysis of the crash environment for belted occupants in far-side crashes was presented in a earlier papers [Gabler, SAE 2005 and ESV 2005]. The analysis indicated that for belted occupants with MAIS 3+ injuries, the 50% median crash severity was a lateral delta-V of 28 km/h and an extent of damage of 3.6 as measured by the CDC scale [SAE Standard J224, Collision Deformation Classification]. The most frequent damage area for seriously injured belted occupants was the front 2/3 of the vehicle (42%), followed by the rear 2/3 (21%). The most frequent principal direction of force (PDOF) was 60° (60%), followed by 90° (24%). The head and chest were the most frequently injured body regions, each at about 40% [Gabler 2008]. The injuring contacts that most frequently

caused chest injury were the struck-side interior (23.6%), the belt or buckle (21.4%) and the seat back (20.9%) [Fildes, 2007]

9.2 TEST CONDITIONS AND INJURY CRITERIA

Finite element vehicle models were used to compare the damage patterns induced in a 2004 Taurus when impacted in the side by a GMC 1500 pickup truck at a crash severity of 28 km/h lateral delta-V [Mohan, 2005, Digges, 2005]. The 60 degree impact produced an extent of damage CDC 4. The 90 degree impact produced a CDC extent of damage of 3.6. The FEM Taurus model was impacted by both NHTSA and the IIHS barrier at a lateral delta-V equivalent to 28 km/h. The IIHS barrier produced a damage pattern that closely duplicated the pattern of the pickup truck at 90 degrees but produced the maximum damage at the same location as the pickup test at 60 degrees. Since the IIHS barrier and test condition is generally accepted as a de facto standard, the IIHS barrier impact was established as the baseline for assessing the performance of available dummies based on MADYMO computer modelling. However, the test speed was increased to produce a lateral delta-V of 28 km/h.

The MADYMO human facet model was initially validated for the far-side crash condition by duplicating the far-side PMHS test reported by Fildes [2002]. The model validation was reported in a separate paper [Alonso, 2005]. The model was then used to evaluate occupant kinematics when subjected to a 28 km/h delta-V pulse that approximates the one produced by the IIHS barrier [Alonso, 2007]. The human facet model was also used to evaluate the consequence of variations in crash pulse and in generic countermeasures. The MADYMO human facet model was considered to be a good tool for assessing the influence of countermeasures on occupant kinematics in far-side crashes [Alonso 2007].

The accuracy of the seat belt to shoulder interaction for the MADYMO human facet model was evaluated by Douglas [ESV 2007 and AAAM 2007]. The shoulder complex of the model was modified to better duplicate the belt interaction. Validation of the model was based on low severity human volunteer tests and higher severity PMHS tests involving varying belt configurations and levels of pretension.

Initially, a range of current side impact test dummies (BioSID, BioSID_Mod, EuroSID1, and WorldSID) were compared with a single PMHS test to evaluate their potential to represent a human in a far side crash [Fildes 2002, Bostrom 2003]. Subsequently, the MADYMO computer models of the existing adult side and frontal dummies were compared with the human facet model [Alonso, 2007]. The dummy models evaluated included the following: Hybrid III, Biosid, Eurosid 1, Eurosid 2 and SID2S. It was evident from the evaluation that none of the standard dummies possessed the kinematics to duplicate the motion observed in either the initial PMHS test or the MADYMO human facet model. Consequently, these dummies were eliminated from further testing. The WorldSID and the THOR-NT were subsequently selected as the best candidates for a far-side dummy. Sled testing indicated that the BioSID with a modified spine and shoulder unit did provide reasonable human-like kinematics [Fildes 2002, Bolstrom 2003]. However, this modified dummy was not a serious contender given its pure research status.

The WorldSID Working Group has proposed injury criteria for use when the dummy is subjected to near-side impacts. Many of the injury measures are also applicable to far-side impacts. The WorldSID criteria that are applicable to far-side impacts have been summarized and criteria needed for the evaluation of far-side countermeasures has been added in the Task V Report prepared for the project [Gibson and Morgan 2008]. The Task 5 Report contains the available injury risk functions for the head and face, neck, spine, shoulder, thorax, abdomen, pelvis, lower extremities and upper extremities. It contains proposed injury risk curves for head, neck (skeletal), spine, chest, abdomen, pelvis, lower extremities and upper extremities.

One of the injury measures currently missing from dummy measurements is the criteria for injury to the soft tissues of the neck. Of particular concern is the injury to the carotid artery from direct or induced loading by the shoulder belt or by other countermeasures. This issue was attacked by teams from Autoliv, Medical College of Wisconsin, and Wake Forrest-Virginia Tech. Tests of carotid artery specimens found that the pinching mechanism of injury was difficult to produce. The failure mode of

the carotid artery when subjected to simulated loading from the seat belt tended to be tension rather than pinching. The tension failures occurred as a result of a longitudinal stretching of the artery. This result suggests that when the belt loads the neck, the artery on the opposite side is more vulnerable to injury than the near side artery that is pinched by the belt. This observation was confirmed by tests on cadavers in four-point belts conducted by Ford. The results from this task were reported in a series of papers [Stemper, IRCOB 2005, J. Bio., 2005, Bio. Sci. Inst., 2005, IRCOB 2006, J. Trauma, 2007, Annals Bio.Eng., 2007, J. Bio, 2007, and Gayzik, AAAM, 2006 and Bio. Sci. Inst., 2006].

9.3 OCCUPANT KINEMATICS AND AVAILABLE DUMMIES

A review of the crash test films available at the NHTSA/FHWA Crash Film Library found only one documented test of a far-side crash. In this crash the crash direction was 90 degrees and the delta-V was approximately 15 Km/h. The dummy slid out of the shoulder belt. Six far-side crashes were subsequently conducted and documented [Digges, 2001]. In this series of tests, angle of impact was 60 degrees and the delta-V was 40 km/h. The tests evaluated variations in shoulder belt tension and latch plate design. In all configurations, the Hybrid III dummy slid out of the shoulder belt. These tests suggested that additional countermeasures would be necessary to limit the excursion of the upper body.

Fildes [2002] reported on efforts to develop a dummy for use in far-side impacts. He found that existing dummies lacked the flexibility in the spine to duplicate the kinematics of a baseline PHMS test. In a later paper, Fildes reported better results based on limited testing of a BioSID dummy in which the spine had been replaced with a coil spring [Fildes 2003]. He recommended continuing research to develop a dummy and injury criteria so that countermeasures could be specified and evaluated.

9.4 THE BIOMECHANICAL TEST PROGRAM

Under the Far Side Impact Collaborative Research Program, a series of PMHS tests was conducted by the research staff at The Medical College of Wisconsin [Pintar, 2006, 2007]. The purpose of the PMHS tests was to assess the kinematics that needed to be reproduced in a dummy. The development of injury criteria was not a requirement. A test program that involved 18 different test configurations was conducted. Each test condition was run first with a PHMS and then the WorldSID and THOR-NT dummies were subjected to the same test condition. The test variations included test impact angle (60 and 90 degrees), test speed (11 and 30 km/h), shoulder belt type (inboard and outboard anchorages), centre support (chest and shoulder load paths), shoulder belt tension, and shoulder belt anchorage location (high, low, mid and forward).

Both the WorldSID and the THOR-NT response in far side impacts compared favorably to the PMHS responses. The WorldSID performed somewhat better in the 90deg tests while the THOR-NT was better in the 60deg tests. However, both dummies closely mimicked the head trajectory of the PMHS subjects in the testing conditions to which they were subjected. The greatest limitation of the dummies was the location of the chest deflection instrumentation. Some relocation of the chest instrumentation would be required in order to accurately measure this parameter in far-side crashes. The test results have been reported by Pintar (2007) who concludes, "The THOR and WorldSID dummies demonstrate adequate biofidelity to develop countermeasures in this (far-side) crash mode". [Pintar, 2007].

9.5 CRASH TESTS WITH BOTH NEAR SIDE AND FAR SIDE DUMMIES

A supplementary research program of crash testing was conducted by The Australian Federal Office of Road Safety with the partnership of the Hyundai Motor Company, Transport Canada, the New-South Wales Roads and Traffic Authority and Va. Tech/Wake Forest. A series of six tests were conducted with

an objective of evaluating occupant-to-occupant contact. Three of the tests were impacts with a moving deformable barrier and three were impacts with poles [Newland, 2008].

A moving deformable barrier side impact test at 65 km/h with WorldSID dummies in both the near-side and far-side front seat locations indicated that interaction between the dummies occurred at about 90 ms [Newland, 2008]. In this test, the belt restraint system allowed the dummy to slip out of the belt. The interaction between the dummies was late enough so that it did not influence the interaction of the near-side dummy with the near-side countermeasures. The interaction was also late enough to permit the far-side dummy to slip out of the shoulder belt.

These tests indicated that interaction between dummies does occur. However, the presence of the far-side dummy did not influence the injury measures of the near-side dummy in the near-side impact. This result suggests that a far-side dummy could be incorporated in tests for near-side occupant protection without influencing the injury measurements from the near-side impact.

The incorporation of a far-side dummy in crash tests that rate vehicles for near-side protection has been proposed [Digges, 2009].

9.6 COUNTERMEASURES AND INJURY REDUCTION ANALYSIS

Sled tests and computer simulations were conducted to evaluate the performance of altered 3-point belt geometry, side support air bags and air curtains. Crash tests and sled test results have been published [Bolstrom 2005, 2008; Newland 2008]. Computer simulations of safety belt performance in far-side crashes have also been published [Douglas 2008, Digges 2009, and Eschmedia 2009].

A countermeasure 100% effective in reducing the risk of a serious or fatal head and thorax injury up to a Delta-V of 20 and 30 km/h would potentially reduce the number of serious injuries by 18% and 57% respectively. According to crash tests shown or referred to in this study side support airbags and altered 3-point belt geometry could constitute such countermeasures. Possible injuries being induced by these countermeasures were disregarded.

A countermeasure 100% effective in reducing the risk of fatality in far side impacts for Delta-V between 30 and 50 km/h would reduce the number of fatalities by 30%. According to crash tests shown in this paper and a recently published benefit analysis, an inflatable curtain, with suitable coverage area and stand-up time, could constitute such a countermeasure.

9.7 CONCLUSIONS

The far-side crash environment that produces 50% of the MAIS 3+F injuries for belted adult occupants in planar crashes is as follows: (1) Lateral Delta-V = 28 km/h and (2) CDC Extent of Damage = 3.6. This crash environment was reproduced by a simulated crash of a full size Chevrolet pickup into a Ford Taurus using finite element models. The damage pattern was found to be generally similar to that produced by the IIHS barrier. However, it was necessary to impact the vehicle far-side at a higher delta-V than specified in the IIHS test for near-side safety ratings.

The MADYMO human facet model was shown to accurately duplicate the human kinematics when applied to an available test of a PMHS in a far-side impact. Further improvements in the model shoulder to belt interaction has been accomplished, based on human volunteer testing at low severity far-side impacts and PMHS testing in more severe impacts. The modified MADYMO human facet model offers a basis for evaluating human kinematics when exposed to far side impacts. Consequently, the model should be useful for evaluating design variables in far-side safety systems. The MADYMO models of the Hybrid III, Biosid, Eurosid 1, Eurosid 2 and SID2S were found to produce kinematics that did not duplicate the human response. Research to apply computer models to assess countermeasures is underway and will be reported when completed.

The WorldSID and the THOR-NT both demonstrated a high degree of biofidelity in 18 tests that were representative of a large range of far-side crashes. Either dummy appears to be a satisfactory

measuring device with regard to its kinematic response. However, changes in the location of the chest instrumentation would be required to obtain accurate readings of the maximum chest deflection. The available injury risk functions to be used with the WorldSID has been collected from the literature and summarized in a report developed under the project.

Crash tests conducted by FORS Australia indicate that a far-side dummy could be incorporated in tests for near-side occupant protection without influencing the injury measurements from the near-side impact.

Sled tests and computer simulations indicate that countermeasures such as altered 3-point belt geometry, side support air bags and air curtains offer substantial opportunities for injury reduction in far-side crashes. Serious injury reduction opportunity in the order of 57% was estimated for improved belts and side support air bags. Air curtains designed for far-side crashes offer a fatality reduction opportunity of 30%.

All technical impediments to the crash test and evaluation of far-side countermeasures have now been removed by the research conducted under the ARC Far Side Impact Collaborative Research Project.

There continue to be a large number of injuries that occur in far-side planar crashes and rollovers. A number of countermeasures have been demonstrated that could mitigate the injury producing environment of far-side crashes. There is at present no marketing incentive for introducing far-side countermeasures. The absence of regulatory and consumer information tests of far-side safety is now the major impediment to improved safety.

Improved safety features in far-side crashes offer a large opportunity for reducing motor vehicle casualties. The research cited in this paper provides the technical basis for evaluating and developing far-side countermeasures. A program of consumer information is now required to encourage far-side crash protection improvements. Ultimately, minimum safety standards should be adopted.

10 REFERENCES

- Adomeit, D., Goegler, H., Vu Han, V. (1988) Expected Belt-Specific Injury Patterns Dependent on the Angle of Impact. 3rd International Conference on Impact Trauma, International Research Council on Biokinetics of Impacts. pp. 242-250.
- AIS (Abbreviated Injury Scale) 1990 Revision, Update 98. Association for the Advancement of Automotive Medicine (AAAM), Des Plaines, Illinois (1998).
- Alliance (1999). Comments to the National Highway Traffic Safety Administration on Supplementary Notice of Proposed Rulemaking FMVSS 208, Occupant Protection – Annex 2, Dummy Response Limits for FMVSS 208 Compliance Testing, Alliance of Automobile Manufacturers, Dec 23, 1999.
- Alonso, B., Digges, K., and Morgan, R. (2007) Far-side Vehicle Simulations with MADYMO, SAE 2007-01-0378, April 2007.
- Alonso, B. (2005) Centre Console Height Study, Report written to George Washington University – National Crash Analysis Centre, April, 2005.
- Alonso, B. (2004 a) MADYMO Human Facet Model Validation for Far-side, Report written to George Washington University – National Crash Analysis Centre, October 2004.
- Alonso, B. (2004 b) Far-side Impact Simulations with MADYMO, Report written to George Washington University – National Crash Analysis Centre, October 2004.
- Alonso, B. (Nov 2004) Suitability of Square Acceleration Profile for Far-Side Impact Testing Report written to George Washington University – National Crash Analysis Centre, November 2004.
- Augenstein J, Perdeck E, Martin P, Bowen J, Stratton T, Horton T, Singer M, Digges K, Steps J. (2000) Injuries to restrained occupants in far-side crashes. 44th Annual Proceedings, Association for the Advancement of Automotive Medicine, Barrington, IL pp 58-66.
- Banglmaier RF, Rouhana SW, Beillas P, Yang KH. (2003) Lower extremity injuries in lateral impact: A retrospective study. 48th Annual Proceedings, Association for the Advancement of Automotive Medicine, Barrington, IL pp 425-444.
- Begeman P. and Pratima K. (1999). Bending strength of the human cadaveric forearm due to lateral loads, Paper 99sc24, Proceedings of the 43rd Stapp car conference, San Diego, California.
- Biffl, W. L., Moore, E. E., Offner, P. J. and Burch, J. M. (2001) Blunt carotid and vertebral arterial injuries. World J Surg, Vol. 25, pp. 1036-43 (2001).
- Bolte, J.H., Hines, M.H. *et al.* (2000). Shoulder response characteristics and injury due to lateral glenohumeral joint impacts. 44th Stapp.
- Boström O., Gabler, H., Digges, K., Fildes, B., and Sunnevang, C. (2008) Injury reduction opportunities of far-side impact countermeasures, Proceedings of the 52nd AAAM, pp.289-300.
- Boström, O., Haland, Y., Soderstrom, P. (2005) Seat integrated 3-point belt with reversed geometry and an inboard torso side-support airbag for improved protection in rollover. Proceedings of the 19th International Conference on Enhanced Safety of Vehicles.
- Bostrom, O., Fildes, B., Morris, A., Sparke, L., Smith, S., and Judd, R. (2003) A cost effective far side crash simulation, UCrash 8 (3) pp. 307-313, 2003.
- Bostrom, O., Haland, Y. (2003) Benefits of a 3+2 point belt system and an inboard torso side support in frontal, far-side, and rollover crashes. 18th ESV conference proceedings, Nagoya, Japan.
- Brown, T., *et al.* (1957). Some mechanical tests on the lumbosacral spine with particular reference to the intervertebral disks. J. Bone and Joint Surg. 39-A(5), pp: 1135-1164.
- Bundorf, R.(1996) Analysis and Calculation of Delta-V from Crash Test Data, SAE Paper 960899, 1996.

- Cavanaugh, J.M., Zhu, Y., Huang, Y., King, A.I. (1993) Injury and response of the thorax in side impact cadaveric tests. SAE Paper 933127.
- Cesari, D, Ramet, M, Herry, HD. (1988) Injury mechanisms in side impact. Proc.22nd Stapp Car Conference, pp. 431–448, Ann Arbor, Michigan, USA.
- Chandler, R.F. and Gowdy, R.V. (1983) “Human Exposure to Impact with Two Point (Lapbelt) and Three Point (Lapbelt: and Diagonal Shoulder Belt) Restraint Systems.” Memorandum No. AAC-119-83-7; Protection and Survival Laboratory, Civil Aeromedical Institute, Mike Monroney Aeronautical Centre, Federal Aviation Administration, Oklahoma City, Oklahoma 73125.
- Cheng, P. and Guenther, D., (1989), Effects of change in angular velocity of a vehicle on the change in velocity experienced by an occupant during a crash environment and the localized delta V concept, SAE Paper No. 890636.
- Chipman, M. L. (2004) Side impact crashes--factors affecting incidence and severity: review of the literature. Traffic Injury Prevention. Vol 5, No 1, pp. 68-85 (2004).
- Cuadrado, J. (2008) Comparison of crash pulses and sled responses for far-side impact, Master’s Thesis The George Washington University, March 6, 2008.
- Demetropoulos, C. (1998). Mechanical properties of the cadaveric and hybrid II Lumbar spines. Proceedings of the 42nd Stapp car crash conference, SAE paper number 983160. pp: 1-10.
- Digges, K., Alonso, B., Cuadrado, J., and Mohan, P., Task 5 Report: test procedures - crash tests and sled tests for the far-side, June, 2009; 32 pages.
- Digges, K., Echemendia, C., Fildes, B., and Pintar, F.(2009) A safety rating for far-side crashes, Paper Number 09-0217, Proceedings of the 21st ESV Conference, June 2009.
- Digges, K., Gabler, H. (2006) Opportunities for reducing casualties in far-side crashes. SAE World Congress Meeting (2006-01-0450), Warrendale, PA, SP-1998.
- Digges K., Gabler H, Mohan P, Alonso B. (2005) Characteristics of the injury environment in far-side crashes. 49th Annual Proceedings, Association for the Advancement of Automotive Medicine, Barrington, IL pp 185-198.
- Digges, K. and Dalmotas, D.(2001) Injuries to restrained occupants in far-side crashes, Proceedings of the Seventeenth International Conference on Enhanced Safety of Vehicles, Amsterdam, Netherlands.
- Douglas C, Fildes B, Gibson T, Boström O, Pintar F. Modelling the seat belt to shoulder-complex interaction in far-side crashes” Proceedings of the 20th International Conference on Enhanced Safety of Vehicles. Paper No. 08-0296; 2008.
- Douglas, C., Fildes, B., Gibson, T., Bostrom , O., and Pintar, F. (2007) Factors influencing occupant to seat belt interaction in far side crashes, 51th Proceedings of the Association for the Advancement of Automotive Medicine”, pp. 319-342, October 2007.
- Duma, S, *et al.* (2006). Biomechanical response of the lumbar spine in dynamic compression. biomedical sciences instrumentation symposium. 42, pp: 476-481.
- Duma, S., Santiago, A., Cormier, J., Yoganandan, N., and Pintar, F. (2008) Humerus and forearm bending fracture injury risk functions for the 50th percentile male, Centre for Injury Biomechanics Report No. 2008-010, June 2008.
- Echemendia, C. (2009) PMHS far-side sled test validation with MADYMO, Report to the National Crash Analysis Centre, GW University, March 2009.
- Fay, R., Raney, A., and Robinette, R. (1996) The effect of vehicle rotation on the occupants’ delta V, SAE Paper 960649.
- Federal Aviation Administration (1996). Dynamic evaluation of seat restraint systems and occupant protection on transportation airplanes. Adelta-Visory Circular Number: 25.562-1A.

- Fildes, B., Bostrom O., Sparke L., Pintar F., and Yoganadan, N.,(2006) The influence of a flexible lumbar spine in far-side impact testing, *International Journal of Crashworthiness*, Vol 11, No 3, pp. 273-280, 2006.
- Fildes B, Bostrom O, Haland Y and Sparke L. (2003) Countermeasures to address far side crashes: first results. *Proceedings of the Nineteenth International Conference on Enhanced Safety of Vehicles*, Paper No. 05-0448-O, Nagoya; 2003.
- Fildes, B., Fitzharris, M., Logan, D. and Gabler, H.C.(2005) Side impact crashes and countermeasures, *Proceedings of the Fourth International Forum of Automotive Traffic Safety*, Changsha, China
- Fildes, B., Linder, A., Douglas, C., Digges, K., Morgan, R., Pintar, F., Yoganadan, N., Gabler, H.C., Duma, S., Stitzel, J., Bostrom, O., Sparke, L., Smith, S., and Newland, C. (2005) Occupant protection in far-side crashes. *Proceedings of the Nineteenth International Conference on Enhanced Safety of Vehicles*. Washington, DC, USA (2005)
- Fildes, BN, Sparke, LJ, Bostrom, O, Pintar, FA, Yoganandan, N, Morris, AP. (2002) Suitability of current side-impact test dummies in far-side impacts. *Proceedings IRCOBI*, 19th International Conference on the Biomechanics of Impact, Lyon, France pp 43-56.
- Fildes, B., Digges, K., Carr, D., Dyte, D., and Vulcan, P., (1995) “Side impact regulation benefits”, prepared by Monash University Accident Research Centre, Federal Office of Road Safety Report CR154, June 1995.
- Frampton, RJ, Brown, R, Thomas, P, Fay, P. (1998). The Importance of non-struck side occupants in side collisions. *42nd Annual Proceedings, Association for the Advancement of Automotive Medicine*, Barrington, IL pp 303-320.
- Franklyn, M, Fitzharris, M, Yang, K, Frampton, R, Morris, A, Fildes, B. (2002) Aortic injuries in side impacts: A preliminary analysis. *46th Annual Proceedings, Association for the Advancement of Automotive Medicine*, Barrington, IL pp 1-12.
- Gabler, C., Fitzharris, M., Scully, J., Fildes, B., Digges, K., Sparke, L., (2008) Task 1Report: Injury and harm analysis final report”, February 2008; 30 pages
- Gabler, H, Digges K., Fildes, B., and Sparke, L. (2005a). Side impact injury risk for belted far side passenger vehicle occupants, *SAE World Congress*, paper # 2005-01-0288, Society of Automotive Engineers, Warrendale, PA.
- Gabler H, Fitzharris M, Scully J, Fildes B, Digges K, Sparke L. (2005b) Far-side impact injury risk for belted occupants in Australia and the United States. *Proceedings of the 19th International Conference on Enhanced Safety of Vehicles*.
- Gabler, H., and Hollowell, W. (1998) The aggressivity of light trucks and vans in traffic crashes, *SAE Transactions, Journal of Passenger Cars*. Section 6, v.108, Paper No. 980908.
- Gayzik, F. Tan, J. Duma, S and Stitzel, J. (2006) Mesh development for a finite element model of the carotid artery, *Biomedical Sciences Instrumentation Rocky Mountain Bioengineering Symposium*, Terre Haute, IN, 2006, pp. 188-192.
- Gennarelli, T., Pintar, F., Yoganandan, N. (2003) Biomechanical tolerances for diffuse brain injury and a hypothesis for genotypic variability in response to trauma, *Proceedings of the AAAM*. Lisbon, Portugal.
- Gibson. T., Morgan, R., Duma, S., and Kemper, A., “Task 5 Report: injury criteria”, September, 2007, 52 pages.
- Gibson, T., Benetatos, E., Newstead, S., and Fildes, B., (2001a) Improved side impact protection: The Development of Injury Assessment Functions,” *Proceedings of the 18th ESV Conference*, June 2001.
- Gibson T., Fildes B., Deery H., Sparke L., Benetatos E., Fitzharris M., McLean J. and Vulcan P. (2001b) Improved side impact protection: a review of injury patterns, injury tolerance and ATD measurement capabilities. *Monash University Accident Research Centre Report No. 148*.

- Gibson T, Benetatos E and Newstead S (2001c): "Lateral Injury Assessment Functions for Use with the Biosid.", Monash University Accident Research Centre Report.
- Guerra, R.C.(2004) A refined methodology for vehicle finite element modelling incorporating robust capabilities, fine uniform mesh, and comprehensive interior, A Thesis for the School of Engineering and Applied Science of The George Washington University, August 13, 2004.
- Haffner, M., Eppinger, R., Rangarajan, N., Shams, T., Artis, M. and Beach, D., (2001) Foundations and elements of the NHTSA Thor Alpha ATD design, Proceedings of the 18th ESV Conference, June 2001.
- Haland Y, Lovsund P, Nygren A. (1990). Estimation of fatalities and disabilities in car-to-car side impacts: An evaluation of different risk factors. 34th Annual Proceedings, Association for the Advancement of Automotive Medicine, Barrington, IL pp. 285-288.
- Hansson, T, *et al.* (1979). The bone mineral content and ultimate compressive strength of lumbar vertebrae. *Spine* 5(1), pp: 46-55.
- Haneline, M., Croft, A., and Frishberg, B. (2003) Association of internal carotid artery dissection and chiropractic manipulation, *Neurologist*, vol. 9, pp. 35-44, Jan 2003.
- Haneline, M., and Lewkovich, G. (2005) An analysis of the etiology of cervical artery dissections: 1994 to 2003," *Journal of Manipulative and Physiological Therapeutics*, vol. 28, pp. 618-622, 2005.
- Hardy, W., Schneider, L., Rouhana, S.. (2001) Abdominal impact response to rigid-bar, seatbelt, and airbag loading. *Stapp Car Crash Journal* 45:1-31.
- Hautmann, E., Scherer, R., Akiyama, A., Page, M., Xu, L., Kostyniuk, G., Sakurai, M., Bortenschlager, K., Harigae, T. and Tylko, S., (2003) Updated biofidelity rating of the revised WorldSID prototype dummy," 18th ESV Proceedings, Nagoya, Japan.
- Horsch JD., Schneider DC., Kroell CK. & Raasch FD. (1979). Response of belt restrained subjects in simulated lateral impact, Paper 791005, Society of Automotive Engineers Inc.
- Horsch, J. (1980) Occupant dynamics as a function of impact angle and belt restraint. Proceedings of the 24th Stapp Car Crash Conference, SAE Paper 801310, pp. 418–438.
- Hutton, W, *et al.* (1979). The compressive strength of lumbar vertebrae, *J. Anatomy*, 129(4), pp: 753-8.
- IIHS (1998). Crash Compatibility: How Vehicle Type, Weight Affect Outcomes", Insurance Institute for Highway Safety Status Report, 33(1).
- IIHS (2004). "Side Impact Crashworthiness Evaluation: Guidelines for rating injury measures (Version II)", Insurance Institute for Highway Safety, April 2004.
- ISO TC 22/SC 12/WG6 N 613, "Road Vehicles – Injury Risk Curves to Evaluate Occupant Protection in Side Impact," 29 March 2005.
- ISO/TC22/SC12/WG6, (2004): "WorldSID injury risk curves." Document N602 prepared by LAB.
- ISO/TC22/SC12/WG6 (1999) Document N: Draft Technical Report (DTR-7861) Road Vehicle-Injury Risk Curves to Evaluate Occupant Protection in Simulated Frontal Collisions.
- ISO/TR 9790 (1999): Road Vehicles – Anthropomorphic side impact dummy – Lateral impact response requirements to assess the biofidelity of the dummy.
- Ivarsson J, Lessley D, Kerrigan J, Bhalla K, Bose D, Crandall J, and Kent R (2004): "Dynamic Response Corridors and Injury Thresholds of the Pedestrian Lower Extremities" IRCOB.
- Kahane C. (2008) An Evaluation of Side Impact Protection FMVSS 214 TTI (D) Improvements and side air bags. Report No. DOT HS 810 848. National Highway Traffic Safety Administration. January 2008.
- Kazarian, L and Graves, G (1977). Compressive strength characteristics of the human vertebrae centrum. *Spine* 2(1), pp: 1-14.

- Kennedy, E.A., Hurst, W.J., Stitzel, J.D., Cormier, J.M., Hansen, G.A., Smith, E.P., and Duma, S.M., (2004) "Lateral and Posterior Dynamic Bending of the Mid-Shaft Femur: Fracture Risk Curves for the Adult Population," Proceedings of the STAPP Car Crash Conference.
- Kemper, A. and Duma, S. (2006) Failure properties of the human thoracolumbar spine applicable to far-side automotive impacts, Centre for Injury Biomechanics, Report No. 2006-100, June 2006.
- Kerrigan J, Drinkwater D, Kam C, Murphy D, Ivarsson B, Crandall J, and Patrie, J (2004): "Tolerance of the Human Leg and Thigh in Dynamic Latero-Medial Bending." Proceedings of the ICRASH Conference.
- Kikuchi, Ono and Nakamura (1982): "Human Head Tolerance to Lateral Impact Deduced from Experimental Head Injuries Using Primates." Proceedings of the 1982 ESV Conference.
- Konosu A, Issiki T, and Tanahashi M (2005): "Development Of A Pedestrian Lower Extremity Protection Car Using A Biofidelic Flexible Pedestrian Legform Impactor." Proceedings of the ICRASH Conference.
- Kent, R., Lessley, D., Sherwood, C. (2004). Thoracic response to dynamic, non-impact loading from a hub, distributed belt, diagonal belt, and double diagonal belts. *Stapp Car Crash Journal* 48: 495-519.
- Kent R., Shaw G., Lessley D., Crandall .J, Svensson M. (2003) Comparison of belted Hybrid III, THOR, and cadaver thoracic responses in oblique frontal and full frontal sled tests, SAE Paper 2003-01-0160.
- Kerrigan J, Drinkwater D, Kam C, Murphy D, Ivarsson B, Crandall J, and Patrie, J (2004): Tolerance of the human leg and thigh in dynamic latero-medial bending, Proceedings of the ICRASH Conference.
- Kildare, S.(2005) Report on the progress of work on the development of finite element models of the FMVSS 214 and IIHS side impact barriers, GW Report, January, 2005.
- Kikuchi, Ono and Nakamura (1982): "Human Head Tolerance to Lateral Impact Deduced from Experimental Head Injuries Using Primates." Proceedings of the 1982 ESV Conference.
- Kleinberger, M. (1993) Application of finite element techniques to the study of cervical spine mechanics, 38th Strapp Car Crash Conference: SAE, Warrendale, PA.
- Kuppa, S (2004) Injury criteria for side impact dummies, National Highway Traffic Safety Administration, U. S. Department of Transportation Report.
- Lambert, C. Gayzik, S., and Stitzel, J. (2008) Characterization of the carotid and adjacent anatomy using non-contrast CT for biomechanical model development, *Biomed Sci Instrum*, vol. 43, pp. 330-5, 2008.
- Lund A (2003): "Recommended Procedures for Evaluating Occupant Risk from Deploying Side Airbags." Technical Working Group.
- Mackay, GM., Parkin, S., Hill, J., Munns, JAR. (1991) Restrained occupants on the non-struck side in lateral collisions, 35th Annual Proceedings, Association for the Advancement of Automotive Medicine, Barrington, IL pp 119-132.
- Mackay G, Hill J, Parkin S, Munns J. (1993) Restrained Occupants on the non-struck side in lateral collisions. *Accident Analysis and Prevention*. Vol. 25, No. 2, pp. 148-152; 1993.
- MADYMO V6.2 Theory Manual, TNO MADYMO BV, 2004.
- Malliaris AC, Hitchcock R, Hedlund J. (1982) A search for priorities in crash protection. SAE International paper #820242. Society of Automotive Engineers, Warrendale, PA.
- Maltese, MR., Eppinger, RH., Rhule, HH., Donnelly, BR., Pintar, FA., Yoganandan, N. (2002) Response corridors of human surrogates in lateral impacts. *Stapp Car Crash Journal* 46:321-351.
- Marine, M. and Werner, S. (1998) Delta-V analysis from crash test data for vehicles with post-impact yaw motion," SAE Paper No. 980219.
- Margulies SS, and Thibault LE, (1992): "A Proposed Tolerance Criterion for Diffuse Axonal Injury in Man," *J. Biomech*, 25(8) 1992: 917-23.

- McLean AJ. (1996) "Brain injury without head impact?" In Bandak FB, Eppinger RH, Ommaya AK eds. *Traumatic Brain Injury*. Larchmount, NY: Mary Ann Liebert Inc.
- McLean AJ., Fildes BN., Kloeden CN, Digges KH, Anderson RWG, Moore VM. & Simpson DA, (1997). Prevention of Head Injuries to Car Occupants: An Investigation of Interior Padding Options, Report CR 160, Federal Office of Road Safety, Commonwealth Department of Transport, Canberra, Australia.
- Meaney D, Thibault L, Gennarelli T. (1994) "Rotational brain injury tolerance criteria as a function of vehicle crash parameters." IRCOBI. Lyon, France.
- Mertz H, Irwin A, and Prasad P (2003): "Biomechanical and Scaling Basis for Frontal and Side Impact Injury Assessment Reference Values." Proceedings of the STAPP Car Crash Conference.
- Messerer, O (1880). *Über elasticität und festigkeit der menschlichen knochen*. Stuttgart, J.G. Cottaschen Buchhandeling.
- Melvin, JW, Gideon T. (2004) Biomechanical principles of racecar seat design for side impact protection. SAE International, paper #2004-01-3515. Society of Automotive Engineers. Warrendale, PA.
- Mertz, H., Prasad, P. & Irwin, AL. (1997). Injury risk curves for children and adults in frontal and rear collisions, SAE Paper No. 973318. Society of Automotive Engineers. Warrendale, PA
- Mertz, H., Irwin, A., and Prasad, P. (2003): "Biomechanical and scaling basis for frontal and side impact injury assessment reference values." Proceedings of the STAPP Car Crash Conference.
- Mohan, P. (2005) Crush comparison in side impacts, Report to George Washington University, June 20, 2005.
- Morris A, Hassan A, Mackay M, et al. (1993) "Head injuries in lateral impact collisions." Proceedings of IRCOBI.
- Myklebust, J (1989). Experimental spinal trauma studies in human and monkey cadavers. Proceedings of the 27th Stapp car crash conference, SAE paper number 831614. pp: 149-161.
- Newman JA, Shewchenko N, Welbourne E (2000). "A Proposed New Biomechanical Head Injury Assessment Function - The Maximum Power Index." Proceedings of the 44th Stapp Car Crash Conference.
- Ommaya A (1988). "Mechanisms and Preventative Management of Head Injuries: A Paradigm for Injury Control." The George Snively Memorial Lecture given at the 32nd AAAM.
- Ono, K., "Current Status on Human Impact Tolerance, Clinical and Biomechanical," Frontiers in Head and Neck Trauma, ISO Press, 1998.
- Palmer, S. (2006) NHTSA's final ruling for automotive EDRs will revolutionize auto insurance, Injury Sciences, LLC., 2006.
- Patrick L. (1965). Human tolerance to impact: basis for safety design, paper 650171, Society of Automotive Engineers, New York.
- Perry, O (1957). Fracture of the vertebral end-plate in the lumbar spine. *Acta Orthop. Scand.* 25 (suppl.), pp: 2-101.
- Pintar F. (1986). The biomechanics of spinal elements, Doctoral Dissertation, Marquette University, Milwaukee, WI.
- Pintar, F., Moore, J., Yoganandan , N., Stemper, B., Digges, K., Bostrom , O., Rouhana , S., Smith, S., Fildes, B., "Task 2 Report: Biomechanical test program final report," October, 2008; 55 pages.
- Pintar FA, Yoganandan N, Baisden J. (2005) Characterizing occipital condyle loads under high-speed head rotation. *Stapp Car Crash Journal* 49:33-48.
- Pintar F, Yoganandan N, Hines M, Maltese M, McFadden J, Saul R, Eppinger R, Khaewpong N, Kleinberger M. (2008) Chestband analysis of human tolerance to side impact. Proceedings of 41st Stapp Car Crash Conference, pp. 63–84; 1998

- Pintar, F. Yoganandan, N., Stemper, J., Bostrom, O., Rouhana, S., Digges, K. and Fildes, B. (2008) Comparison of PMHS, WorldSID, and THOR-NT responses in simulated far side impact, *Stapp Car Crash J*, vol. 51, pp. 313-60, Oct 2008.
- Pintar, F., Yoganandan, N., Stemper, B., Boström, O., Rouhana, S., Smith, S., Sparke, L., Fildes, B., Digges, K. (2006) WorldSID assessment of far side impact countermeasures. *Proceedings of the 50th Annual Conference, Association for the Advancement of Automotive Medicine*; pp 189-209.
- Roberts, V. and Compton, C. (1993) Relationship between Delta V and injury, *SAE Paper 930311*.
- Rouhana, S, Elhagediab, A., Chapp J. (1998) A high-speed sensor for measuring chest deflection in crash test dummies. *Proceedings of 16th International Technical Conference on Enhanced Safety of Vehicles*, Technical Paper No. 98-S9-O-15, Windsor, Canada.
- Rouhana SW, Kankanala SV, Prasad P, Rupp JD, Jeffreys TA, Schneider LW. (2006) Biomechanics of 4-Point seat belt systems in far-side impacts. *Stapp Car Crash Journal*, 50:268-298.
- G. S. Rozycki, L. Tremblay, D. V. Feliciano, K. Tchorz, A. Hattaway, J. Fountain, and B. J. Pettitt, (2002) A prospective study for the detection of vascular injury in adult and pediatric patients with cervicothoracic seat belt signs, *J Trauma*, vol. 52, pp. 618-23; discussion 623-4, Apr 2002.
- SAE Standard J224, Collision Deformation Classification (1980).
- Scherer R, Cesari D, Uchimura T, Kostyniuk G, Page M, Asakawa K, Hautmann E, Bortenschlager K, Sakurai M, and Harigae T (2001): Design and evaluation of the worldsid prototype dummy, *Proceedings of the 18th ESV Conference*, June 2001.
- Schievink, W. (2001) Spontaneous dissection of the carotid and vertebral arteries," *N Engl J Med*, vol. 344, pp. 898-906, Mar 22 2001.
- Schievink, W., Mokri, B., and O'Fallon, W. (1994) Recurrent spontaneous cervical-artery dissection," *N Engl J Med*, vol. 330, pp. 393-8, Feb 10 1994.
- Sinson, G., Yoganandan, N., Pintar, F., Morgan, R., Maiman, D., Brasel, K., Gennarelli, T. (2003) Carotid artery trauma in motor vehicle crashes: Investigation of the local tensile loading mechanism. *Proceedings IRCOBI, 20th International Conference on the Biomechanics of Impact*, Lyon, France pp 208-216.
- Sonoda, T (1962). Studies on the strength for compression, tension, and torsion of human vertebrae column. *J. Kyoto Pref. Med. Univ.* 71, pp: 659-702.
- Smyth, B and Smith J. (2007) Developing a sled test from crash test data, *SAE Paper 2007-01-0711*.
- Stemper B.D., Stineman M. R., Yoganandan N., Pintar F. A., Sinson G. P., and Gennarelli T. A. (2005) Mechanical characterization of internal layer failure in the human carotid artery, in *IRCOBI*, Prague, Czech Republic, 2005, pp. 269-288.
- Stemper BD, Yoganandan N, Pintar FA. (2008) Mechanics of arterial subfailure with increasing loading rate. *Journal of Biomechanics* 40(8):1806-1812.
- Stolinski, R, Grzebieta, RH, Fildes BN, Judd R, Wawrzynczak J, Gray I, McGrath P, and Case M. (1999) Response of far-side occupants in car-to-car impacts with standard and modified restraint systems using Hybrid III and US- SID. *SAE paper 1999-01-1321*.
- Summers, S., Prasad, A., Hollowell, W.T., (2001) NHTSA's research program for vehicle aggressivity and fleet compatibility", *Proceedings of the Seventeenth International Conference on Enhanced Safety of Vehicles*, Paper no. 249.
- Sundararajan, S (2005). Characteristics of PMHS lumbar motion segments in lateral shear. *Proceedings of the 49th Stapp car crash conference*, pp: 367-379.
- Thomas, P., and Frampton, R. (1999) Large and small cars in real-world crashes—patterns of use, collision types and injury outcomes. In: *Proceedings of the 43rd Annual Meeting of the Association for the Advancement of Automotive Medicine*, Barcelona (Sitges), Spain, 20–21 September 1999. Des Plaines, Ill: Association for the Advancement of Automotive Medicine; pp.101–118.

- TNO. MADYMO human models manual. Version 6.3. (2005) TNO Automotive, Delft, The Netherlands, December 2005.
- Törnqvall F, Svensson M, Davidsson J, Flögard A, Kallieris D, Haland Y. (2005) Frontal impact dummy kinematics in oblique frontal collisions: evaluation against post mortem human subject test data, *Traffic Injury Prevention*, 6:340–350.
- Viano D., Fan A., Ueno K., Walilko T., Cavanaugh J & King A. (1995). Biofidelity and injury assessment in EuroSID 1 and BioSID, Paper 952731, Proceedings of the 39th Stapp car conference, pp 307-325, Warrendale, PA.
- Yoganandan, N, *et al.* (1988). Biomechanical investigations of the human thoracolumbar spine. SAE technical paper number 881331. pp: 1-9.
- Yoganandan N, Zhang J, Pintar FA, Liu YK. (2006) Lightweight low-profile nine-accelerometer package to obtain head angular accelerations in short-duration impacts. *Journal of Biomechanics* 39:1348-1354.
- Yoganandan, N., Pintar, F.A., Gennarelli, T.A., Maltese, M.R., Eppinger, R.H. (2002) Biofidelity evaluation of recent side impact dummies. IRCOBI Conference. September 2002.
- Yoganandan N, Pintar FA, Gennarelli TA, Maltese MR. (2000) Patterns of abdominal injuries in frontal and side impacts. 44th Annual Proceedings, Association for the Advancement of Automotive Medicine, Barrington, IL. pp 18-36.

APPENDIX 1 LIST OF REPORTS CREATED DURING THIS PROJECT

Task 1 – Injury and HARM Analysis (Chapter 2)

Gabler, C., Fitzharris, M., Scully, J., Fildes, B., Digges, K., Sparke, L., “Task 1 Report: Injury and Harm Analysis Final Report”, February 2008; 30 pages

Fildes, B., Fitzharris, M., Gabler, H., Digges, K., and Smith, S., “Chest and Abdominal Injuries in Far-side Crashes”, Paper, 07-0384, *20th ESV Conference*, June 2007.

Digges, K., Gabler, H., “Opportunities for Reducing Casualties in Far-side Crashes”, SAE 2006-01-0450, April 2006.

Fildes, B., Linder, A., Douglas, K., Digges, K., Morgan, R., Pintar, F., Yoganandan, Y., Gabler, C., Duma, S., Stitzel, J., Bostrom, O., Sparke, L., Smith, S., Newland, C., “Occupant Protection in Far-side Crashes”, Paper 05-0299, *19th ESV Conference*, June 2005.

Gabler, C., Fitzharris, M., Scully, J., Fildes, B., Digges, K., Sparke, L., “Far-side Impact Risk for Belted Occupants in Australia and the United States”, Paper 05-0420, *19th ESV Conference*, June 2005.

Gabler, H., Digges, K., Fildes, B., and Sparks, L., “Side Impact Injury Risk for Belted Far-side Passenger Vehicle Occupants”, SAE 2005-01-0287, April 2005.

Tasks 2 and 4 – Biomechanical Test Programme & Dummies (Chapter 3)

Pintar, F., Moore, J., Yoganandan, N., Stemper, B., Digges, K., Bostrom, O., Rouhana, S., Smith, S., Fildes, B., “Task 2 Report: Biomechanical Test Program Final Report,” October, 2008; 55 pages.

Pintar, F., Yoganandan, N., Stemper, J., Bostrom, O., Rouhana, S., Digges, K. and Fildes, B. (2008) Comparison of PMHS, WorldSID, and THOR-NT Responses in Simulated Far-side Impact”, *Stapp Car Crash J*, vol. 51, pp. 313-60, Oct 2008; 58 pages.

Pintar, F., Yoganandan, N., Stemper, B., Bostrom, O., Rouhana, S., Smith, S., Digges, K., Fildes, B., “Far Side Impact Response and Dummy Biofidelity”, *Proceedings of the 2007 Stapp Car Crash Conference*, October, 2007.

Fildes, B., Bostrom O., Sparke L., Pintar F., and Yoganandan, N., “The Influence of a Flexible Lumbar Spine in Far-side Impact Testing”, *International Journal of Crashworthiness*, Vol 11, No 3, pp. 273-280, 2006.

Task 3 –Soft Tissue Injury to the Neck (Chapter 4)

Stemper, B., Stineman, M., Yoganandan, N., and Pintar, F., “Subcatastrophic Failure Characteristics of the Porcine Descending Aorta”, *Biomedical Science Instrumentation*, 41:110-115, 2005.

Stemper, B., Yoganandan, N., Pintar, F., “Methodology to Study Intimal Failure Mechanics in Human Internal Carotid Arteries”, *Journal of Biomechanics*, 38(12):2491-2496, 2005.

Stemper, B., Stineman, M., Yoganandan, N., Pintar, F., Sinson, G., Gennarelli, T., “Mechanical Characterization of Intimal Layer Failure in the Human Carotid Artery”, *Proceedings of the 2005 IRCOB Conference*, p.269-277, September 21-23, 2005.

Gayzik F, Tan J, Duma S & Stitzel J. Mesh development for a finite element model of the carotid artery, *Biomedical Sciences Instrumentation*, 42: 19-24, 2006

Stemper, B., Stineman, M., Yoganandan, N., Gennarelli, T., and Pintar, F. “Effect of Common Experimental Storage Techniques on Arterial Biomechanics”, *Proceedings of the 2006 IRCOB Conference*, p.417-420, September 20-22, 2006.

Gayzik, S., Bostrom, O., Örtengren, P., Duma, S., and Stitzel, J., “An Experimental and Computational Study of Blunt Artery Injury”, *50th Proceedings of the Association for the Advancement of Automotive Medicine*, p13-34, October 2006.

Stemper, B., Yoganandan, N., Sinson, G., Gennarelli, A., Stineman, M., and Pintar F., “Biomechanical Characterization of Internal Layer Subfailure in Blunt Arterial Injury”, *Annals of Biomedical Engineering*, Vol.35, No.2, p. 285-291, February 2007.

Stemper, B., Yoganandan, N., Pintar, F., and Brasel, K., “Multiple Subfailure Characterize Blunt Aortic Injury”, *Journal of Trauma*, Volume 62 Number 5, p.1171-1174 May 2007.

Stemper, B., Yoganandan, N., and Pintar, F., “Mechanics of Subcatastrophic and Ultimate Arterial Failure as a Function of Loading Rate”, *Journal of Biomechanics*, 40(2007) 1860-1812, 2007.

Task 5 – Test Procedures and Injury Criteria (Chapters 5 and 6)

Digges, K., Gabler, H., Mohan, P., and Alonso, B., “Characteristics of the Injury Environment in Far-Side Crashes”, *49th Proceedings of the Association for the Advancement of Automotive Medicine*, p185-214, September 2005.

Alonso, B., Digges, K., and Morgan, R., “Far-side Vehicle Simulations with MADYMO”, SAE 2007-01-0378, April 2007.

Gibson, T., Morgan, R., Duma, S., and Kemper, A., “Task 5 Report: Test Procedures - Injury Criteria”, September, 2007, 52 pages

Digges, K., Alonso, B., Cudradro, J., and Mohan, P., “Task 5 Report: Test Procedures - Crash Tests and Sled Tests for the Far-side”, June, 2009; 32 pages.

Digges, K., Echemendia, C., Fildes, B., and Pintar, F., A Safety Rating For Far-Side Crashes, Paper Number 09-0217, Proceedings of the 21st ESV Conference, June 2009.

Task 6 – Computer Model Development (Chapter 7)

Douglas, B., Fildes, B., Gibson, T., Bostrom, O., and Pintar, F., “Modelling the Seat Belt to Shoulder-Complex Interaction in Far Side Crashes”, Paper, 07-0296, *20th ESV Conference*, June 2007.

Douglas, B., Fildes, B., Gibson, T., Bostrom, O., and Pintar, F., “Factors Influencing Occupant to Seat Belt Interaction in Far Side Crashes”, *51th Proceedings of the Association for the Advancement of Automotive Medicine*, p319-342, October 2007.

Douglas C., Fildes B. & Gibson T. (2010). Development of an occupant model for far-side vehicle crashes, *Int. J. Vehicle Safety*, (in Press)

Task 7 –Countermeasures Benefits Analysis (Chapter 9)

Digges K, and Fildes B, The Technology Base for Far side Occupant Protection, Paper F2008-08-131, International Federation of Automotive Engineering Societies, FISITA 2008 World Automotive Congress in Munich, September 2008.

Bostrom O, Gabler H, Digges K, Fildes B, Sunnevang C, Opportunities of Far side Impact Countermeasures, *Proceedings of the 52nd Association for the Advancement of Automotive Medicine Conference*, October 2008.

Newland C, Belcher T, Bostrom O, Gabler H, Cha J-G, Wong H-L, Tylko S, Dal Nevo R, Occupant-to-Occupant Interaction and Impact Injury Risk in Side Impact Crashes, *Stapp Car Crash Journal*, Vol. 52, November 2008.